CONSTRUCTION OF HIGHLY STABLE METAL-ORGANIC FRAMEWORKS WITH MULTIPLE FUNCTIONALITIES

A Dissertation

by

YUJIA SUN

Submitted to the Office of Graduate and Professional Studies of
Texas A&M University
in partial fulfillment of the requirements for the degree of

DOCTOR OF PHILOSOPHY

Chair of Committee,	Hong-Cai Zhou
Co-Chair of Committee,	Abraham Clearfield
Committee Members,	Paul Lindahl
	Jaime Grunlan
Head of Department,	Simon North

December 2018

Major Subject: Chemistry

ABSTRACT

Metal-organic frameworks (MOFs) are a class of newly emerged crystalline porous materials consisting of metal ions or clusters and organic linkers. Through judicious choice of inorganic joints and organic struts, the structure, porosity and functionality of MOFs can be tuned. However, the lack of high stability of most of the reported MOFs as well as limited methods to introduce multiple functionalities into the framework hinders the exploration of MOFs towards a wide variety of potential applications. The main goal of this research is to develop synthetic strategies to construct MOFs with high stability and multiple functionalities.

Firstly, a brief introduction of MOFs was provided, focusing on strategies to increase their stability and introduce functionalities.

Secondly, a facile one-pot synthetic strategy was developed to introduce porphyrin into highly stable UiO-66 homogeneously. The crystal structure, morphology, and ultrahigh chemical stability of UiO-66 were well maintained in the functionalized MOFs. In addition, the amount of integrated porphyrin can be gradually tuned.

Thirdly, a general in situ secondary ligand incorporation (ISLI) strategy was investigated to synthesize multivariate UiO series of MOFs. Both experimental and computational studies were carried out to understand the chemistry behind this strategy.

Fourthly, ISLI strategy was further applied in highly stable Zr-MOFs constructed from multitopic ligands to incorporate multiple functionalities.

Fifthly, a porphyrin and pyrene-based mixed-ligand MOF with high stability and novel topology was synthesized. This MOF provides an ideal platform for further functionalization and exploration of new structures.

In summary, different strategies were investigated to construct highly stable MOFs with the incorporation of multiple functionalities. These studies provide useful tools to explore stable MOFs with desired multifunctionality for potential applications.

DEDICATION

To my family and friends for their love and support

ACKNOWLEDGEMENTS

I would like to thank my graduate advisor and committee chair, Dr. Hong-Cai Zhou, and my committee co-chair, Dr. Abraham Clearfield, as well as my committee members, Dr. Paul Lindahl and Dr. Jaime Grunlan for their guidance and support throughout the course of this research.

I feel grateful to all the group members, especially Dr. Dawei Feng for his advice and suggestions during my graduate research.

Thanks also go to the collaborators especially Dr. Xiaodong Zou and Dr. Zhehao Huang from Stockholm University for help in the structural analysis, and Dr. Pengru Huang from Guilin University of Electronic Technology for help in the computational work.

Thanks also go to my friends and colleagues and the department faculty and staff for making my time at Texas A&M University a great experience.

Finally, I want to thank my parents for their support and encouragement and my fiancé for his patience and love.

CONTRIBUTORS AND FUNDING SOURCES

This work was supervised by a dissertation committee consisting of Professor Hong-Cai Zhou, Professor Abraham Clearfield, Professor Paul Lindahl of the Department of Chemistry, and Professor Jaime Grunlan of the Department of Mechanical Engineering.

The computational work depicted in Chapter III was conducted in part by Dr. Pengru Huang from Guilin University of Electronic Technology. And the structural analysis in Chapter V was conducted in part by Dr. Zhehao Huang from Stockholm University

All other work conducted for the dissertation was completed independently by the student.

This research was supported as part of the Center for Gas Separations Relevant to Clean Energy Technologies, an Energy Frontier Research Center funded by the U.S. Department of Energy, Office of Science, and Office of Basic Energy Sciences under Award Number DE-SC0001015, and by part of The Welch Foundation under Award Number A-1725.

NOMENCLATURE

2-D	2-Dimensional
3-D	3-Dimensional
ABTS	2,2'-Azino-Bis(3-Ethylbenzothiazoline-6-Sulphonic acid)
AcOH	Acetic Acid
BDC	Terephthalate
BET	Brunauer, Emmett and Teller
BTC	Benzene-1,3,5-Tricarboxylate
cRED	Continuous Rotation Electron Diffraction
CsF	Cesium Fluoride
DEF	*N*,*N*-Diethylformamide
DFT	Density Functional Theory
DMA	*N*,*N*-Dimethylacetylamide
DME	1,2-Dimethoxyethane
DMF	*N*,*N*-Dimethylformamide
DMSO	Dimethyl Sulfoxide
DOBDC	2,5-Dihydroxyterephthalic Acid
EA	Elemental Analysis
EDS	Energy Dispersive X-Ray Spectroscopy
FT-IR	Fourier Transform-Infrared Spectroscopy
H_2AZDC	Azobenzene-4,4'-Dicarboxylic Acid

H_2BDC	Terephthalic Acid
H_2BPDC	4,4'-Biphenyldicarboxylic Acid
H_2BPYDC	2,2'-Bipyridne-5,5'-Dicarboxylic Acid
H_4BTeC	1,2,4,5-Benzenetetracarboxylic Acid
H_2EDDB	4,4’-(Ethyne-1,2-Diyl)dibenzoic Acid
H_4ETTC	4',4''',4'''',4'''''-(Ethene-1,1,2,2-Tetrayl)tetrakis(([1,1'-Biphenyl]-4-Carboxylic Acid))
H_2NDC	2,6-Naphthalene-Dicarboxylic Acid
H_4TBAPy	1,3,6,8-Tetrakis(p-Benzoic Acid)pyrene
H_4TCPB	1,2,4,5-Tetrakis(4-Carboxyphenyl)benzene
H_2TPDC-4Me	2',3',5',6'-Tetramethyl-(1,1':4',1''-Terphenyl)-4,4''-Dicarboxylic Acid
HKUST	Hong Kong University of Science and Technology
LMOF	Luminescent Metal-Organic Framework
MeOH	Methanol
MIL	Materials from Institut Lavoisier
MOF	Metal-Organic Framework
MTV-MOFs	Multivariate MOFs
NDC	2,6-Naphthalenedicarboxylate
NH_2-BDC	2-Aminoterephthalic Acid
NMR	Nuclear Magnetic Resonance
NU	Northwestern University

ICP	Inductively Coupled Plasma
ISLI	In Situ Secondary Ligand Incorporation
PCN	Porous Coordination Network
PCP	Porous Coordination Polymer
$Pd(PPh_3)_4$	Tetrakis(triphenylphosphine)palladium(0)
PSM	Post-Synthetic Modification
PXRD	Powder X-Ray Diffraction
SALI	Solvent-Assisted Ligand Incorporation
SBU	Secondary Building Unit
SEM	Scanning Electron Microscopic
TCPP	Tetrakis(4-Carboxyphenyl)porphyrin
TBPP	Tetrakis(4-Bromophenyl)porphyrin
TEM	Transmission Electron Microscopy
TGA	Thermogravimetric Analysis
THF	Tetrahydrofuran
UiO	Universitetet i Oslo

TABLE OF CONTENTS

LIST OF FIGURES

Page

Page

LIST OF TABLES

LIST OF SCHEMES

CHAPTER I

INTRODUCTION *

In the past two decades, metal-organic frameworks (MOFs) have emerged as a new class of highly ordered porous materials.[1-3] MOFs are constructed from inorganic nodes and organic linkers (Figure I-1). Due to the modular nature of MOFs, their structure, porosity and functionality can be tuned on the atomic level, which attracted growing attention for applying MOFs in many areas, including gas storage,[4-7] gas separation,[8-9] catalysis,[10-14] sensing,[15-18] light harvesting,[19] and biomedicine.[20-21]

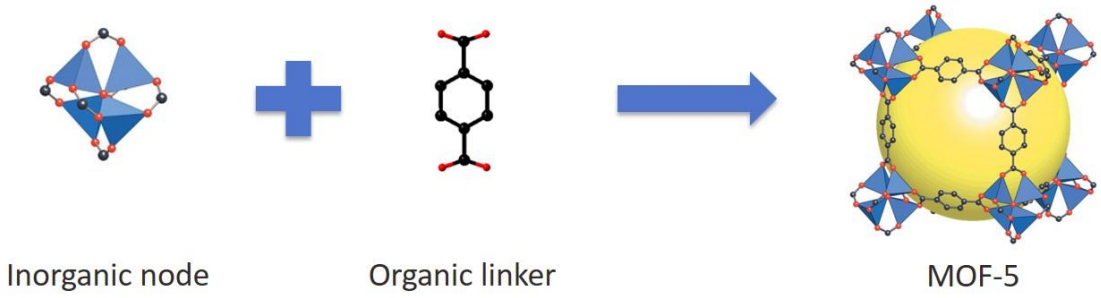

Figure I-1. Schematic representation of the synthesis of MOF-5.

MOFs with high stability are greatly desired to guarantee their structural integrity during the application process.[22] However, large numbers of the reported MOFs are constructed from low valent metal (e.g. Cu^{2+}, Zn^{2+}, and Mn^{2+}) clusters and carboxylate

* Reproduced with permission from: Helm, L.; Merbach, E. A., "Applications of advanced experimental techniques: high pressure NMR and computer simulations" *J. Chem. Soc., Dalton Trans.*, **2002**, *5*, 633–641. Copyright 2002 by Royal Society of Chemistry; Deng, H.; Doonan, C. J.; Furukawa, H.; Ferreira, R. B.; Towne, J.; Knobler, C. B.; Wang, B.; Yaghi, O. M., "Multiple Functional Groups of Varying Ratios in Metal-Organic Frameworks" *Science*, **2010,** *327*, 846-850. Copyright 2010 by American Association for the Advancement of Science.

organic ligands, and thus these MOFs suffer from weak stability.[23-24] This is because of the labile bonds formed between relatively soft Lewis acidic species (metal clusters) and hard Lewis basic species (carboxylate ligands), which have weak stabilization energy and undergo fast dissociation process in various conditions (e.g. moisture, acid, and base) (Figure I-2).[25] To address this issue, many MOFs with high valent metal (e.g. Al^{3+}, Fe^{3+}, Zr^{4+}) clusters have been synthesized and studied in recent years.[26-30]

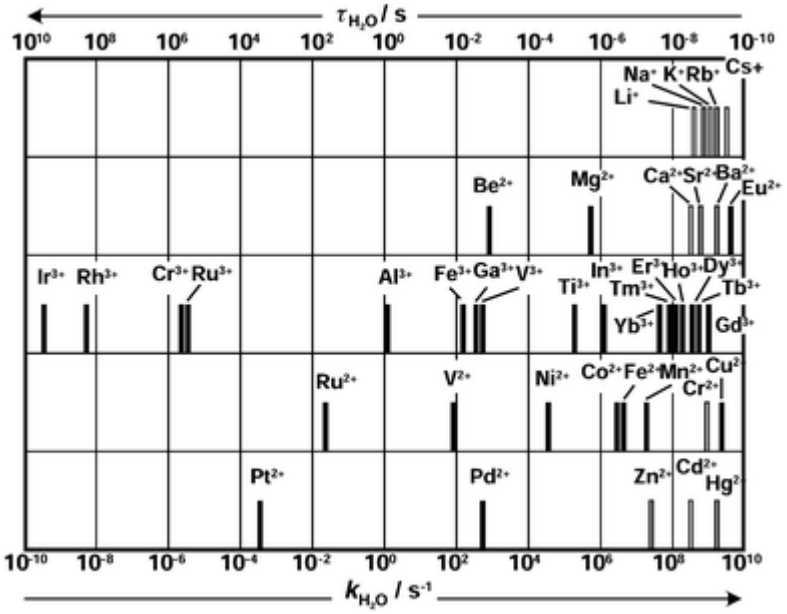

Figure I-2. Aqua exchange rate for various metal cations.

In addition to the robustness, MOFs with various functionalities are highly desired since the properties of MOFs are significantly influenced by the functionality incorporated in the framework. For example, MOF-74 functionalized with amino groups shows increased CO_2 uptake,[31] UiO-67 modified with transition metals can catalyze organic transformations,[32] and LMOF-241 containing luminescent ligands can be used as

a chemical sensor.[33] Compared to mono-functionalized MOFs, MOFs with multiple functionalities are of particular interest to explore the advanced applications of MOFs (e.g. gas storage, gas separation, and catalysis) taking advantage of the synergistic effects.[34-37]

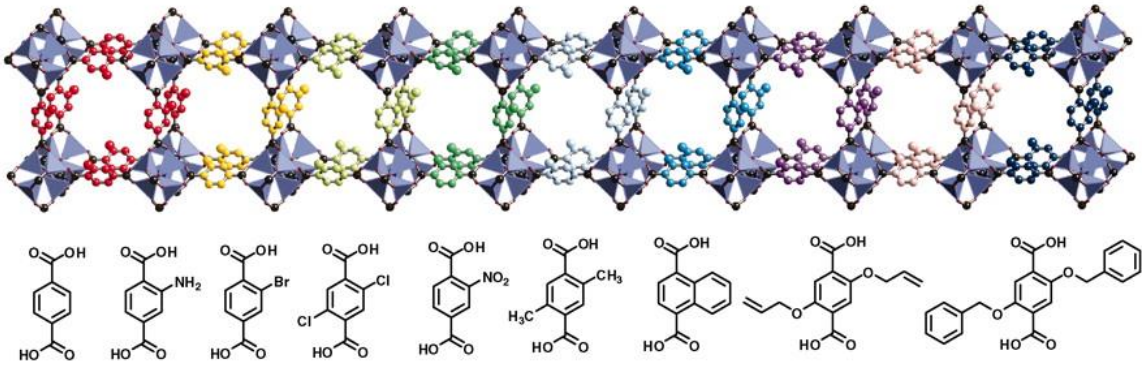

Figure I-3. Schematic illustration of MTV-MOF-5.

In recent years, tremendous efforts have been investigated to synthesize multifunctional MOFs.[38-42] For instance, Yaghi's group reported the synthesis of multivariate MOF-5 (MTV-MOF-5) by mixing terephthalic acid (H_2BDC) and its derivatives (Figure I-3).[43] MOF-5 has been successfully modified with up to eight different functional groups by this mixed-ligand strategy. Significantly, incorporation of multiple functionalities leads to dramatically increased CO_2/CO selectivity compared to corresponding mono-functionalized MOFs. Although this strategy is straightforward and beneficial to preserve the structural integrity of the framework, it requires the use of ligands with the same length, geometry, and connectivity, which restricts the variety of the functionality that can be introduced into the framework. In addition, MOF-5 contains Cu^{2+} paddlewheel clusters, and thus it is sensitive to the moisture, acidic and basic

conditions. So far, several pillar-layered MOFs synthesized by mixing a ditopic ligand and a tetratopic ligand have been reported.[44] However, the majority of these MOFs suffer from weak stability. There are still many challenges in synthesizing multifunctional MOFs by conventional one-pot reactions: (1) stability issue; (2) limited variety of functionalities; (3) random distribution of each functionality; and (4) formation of mixed phases.

Therefore, exploration of methods to synthesize stable and multifunctional MOFs that take advantage of one-pot synthesis while overcoming the limitations of the traditional mixed-ligand strategy is of great importance. In this thesis, highly stable MOFs, especially Zr-MOFs, were synthesized and studied. Ligands of different length, geometry, and connectivity were used to functionalize a series of Zr-MOFs by in situ secondary ligand incorporation (ISLI) strategy. The crystal structure, morphology, and ultrahigh chemical stability of the parent Zr-MOF were well maintained after functionalization while the amount of functionality can be tuned gradually. The synthetic conditions (e.g. linker ratio, and the amount of modulating reagent) were carefully adjusted to control the growth of the multicomponent MOF towards a single phase. Unlike random distribution of each functionality by ISLI, through a thermodynamically controlled synthesis, a mixed-ligand MOF with a new topology was obtained. Each component can be located precisely and the presence of coordinatively available metal clusters allows for further functionalization. Strategies discussed in this thesis are facile and provide different routes to synthesize multifunctional MOFs with high stability for various potential applications.

CHAPTER II

CONSTRUCTION OF MULTIVARIATE UIO-66 THROUGH AN IN SITU ONE-POT SYNTHETIC APPROACH [*]

2.1 Introduction

In recent years, Zr-MOFs have been widely studied due to significantly improved stability compared to Zn/Cu/Cd-based MOFs.[45-51] As a prototype of Zr-MOF, UiO-66 is constructed from Zr_6 clusters and 1,4-benzenedicarboxylate (BDC) ligands that are commercially available.[45] Studies showed that UiO-66 has a decomposition temperature above 500 °C and its crystallinity is well preserved even under harsh chemical conditions and high external pressures.[28, 52] The ideal structure of UiO-66 is a 2,12-connected network with **fcu-a** topology. Upon connectivity reduction, UiO-66 can be tolerant to several sub-networks, such as **reo-a**, **bcu-a**, and **hxg-a** networks, as well as defects.[53-56] As a result, the generated available coordination sites on Zr_6 clusters make it possible for other functionalities to connect to UiO-66. Despite versatile symmetry and connectivity of Zr_6 clusters, the majority of the UiO-66 reported so far only contain BDC ligand and/or its derivatives, which limits the variety of functionality that can be incorporated into the framework.

As one of the most important functionalities, porphyrins possess many functional properties that can be utilized for a series of applications, such as sensors,[57-59] solar

[*] This chapter is reproduced with permission from Sun, Y.; Sun, L.; Feng, D.; Zhou, H.-C. "An in situ one-pot synthetic approach towards multivariate Zr-MOFs" *Angew. Chem. Int. Ed.*, **2016**, *55*, 6471-6475. Copyright 2016 by WILEY-VCH Verlag GmbH & Co. KGaA, Weinheim.

cells,[60-63] biomimetic catalysis,[64-66] and cancer therapy.[20, 67-68] The chemical and physical properties of porphyrins can be modified at the molecular level, providing potentials for investigating advanced applications of porphyrins.[69] Particularly, MOFs are a class of promising materials to fix porphyrins. This is because MOFs can prevent the formation of catalytically inactive porphyrin dimers due to aggregation, enhancing the lifetime of porphyrin catalysts.[34, 70-72]

Therefore, it is of great importance to incorporate porphyrin into UiO-66. Taking advantage of the coordinatively available sites on Zr_6 clusters, ligands of different length, geometry, and connectivity were used in a one-pot reaction towards porphyrin-functionalized UiO-66. The crystal structure, morphology and ultrahigh chemical stability of UiO-66 were well maintained. Moreover, the amount of integrated porphyrin can be gradually adjusted. Upon various combinations of BDC derivatives and porphyrin species, UiO-66 with various functionalities were synthesized successfully.

2.2 Experimental Section

Materials and Instrumentation. Methyl 4-formylbenzoate was purchased from Oakwood Products, Inc. Pyrrole, propionic acid, N,N-dimethylformamide (DMF), benzoic acid, acetone, zirconium(IV) chloride, iron(II) chloride tetrahydrate ($FeCl_2 \cdot 4H_2O$), manganese(II) chloride tetrahydrate ($MnCl_2 \cdot 4H_2O$), nickel(II) chloride hexahydrate ($NiCl_2 \cdot 6H_2O$), cobalt(II) chloride hexahydrate ($CoCl_2 \cdot 6H_2O$), copper(II) chloride tetrahydrate ($CuCl_2 \cdot 4H_2O$), and zinc(II) chloride ($ZnCl_2$, anhydrous) were purchased from Alfa Aesar. Terephthalic acid (H_2BDC), 2-aminoterephthalic acid (NH_2-BDC), 2,5-dihydroxyterephthalic acid (DOBDC), 1,2,4,5-benzenetetracarboxylic acid

(H_4BTeC) were purchased from Sigma-Aldrich. Tetrakis(4-carboxyphenyl)porphyrin (H_2TCPP) were purchased from Frontier Scientific. Tetrakis(4-methylphenyl)porphyrin, [5,10,15,20-tetrakis(4-carboxyphenyl)porphyrinato]-Mn(III) chloride (MnTCPPCl), [5,10,15,20-tetrakis(4-carboxyphenyl)porphyrinato]-Fe(III) chloride (FeTCPPCl), [5,10,15,20-tetrakis(4-carboxyphenyl)porphyrinato]-Zn(II) (ZnTCPP), [5,10,15,20-tetrakis(4-carboxyphenyl)porphyrinato]-Ni(II) (NiTCPP), [5,10,15,20-tetrakis(4-carboxyphenyl)porphyrinato]-Co(II) (CoTCPP), and [5,10,15,20-tetrakis(4-carboxyphenyl)porphyrinato]-Cu(II) (CuTCPP) were synthesized according to the procedure in previous reports with slight modifications.[73] 2-Azido terephthalic acid was synthesized according to the procedure in the literature.[74] All commercial chemicals were used without further purification unless otherwise mentioned.

Powder X-ray diffraction (PXRD) was carried out with a BRUKER D8-Focus Bragg−Brentano X-ray powder diffractometer equipped with a Cu-sealed tube (λ = 1.54178) at 40 kV and 40 mA. Thermogravimetric analysis (TGA) were conducted on a Shimadzu TGA-50 thermogravimetric analyzer from room temperature to 700 °C at a ramp rate of 2 °C/min in a flowing nitrogen atmosphere. Nuclear magnetic resonance (NMR) spectra were collected on a Mercury 300 spectrometer. The UV-vis absorption spectra were recorded on a Shimadzu UV-2450 spectrophotometer. N_2 adsorption-desorption isotherms were measured by using a Micrometritics ASAP 2420 system at 77 K. Sample was activated by solvent exchange (in several cycles using fresh acetone), followed by degassing at elevated temperature (100 °C) for 3 h. Elemental microanalyses (EA) were performed on vario EL cube – Elementar. Scanning electron

microscope (SEM) analysis was performed on QUANTA 450 FEG and energy dispersive X-ray spectroscopy (EDS) analysis was carried out by X-Max20 with Oxford EDS system equipped with X-ray mapping.

Synthesis of Porphyrin Ligands (MTCPP). Porphyrin ligands with different metals in the center (MTCPP) were synthesized according to following synthetic routes:

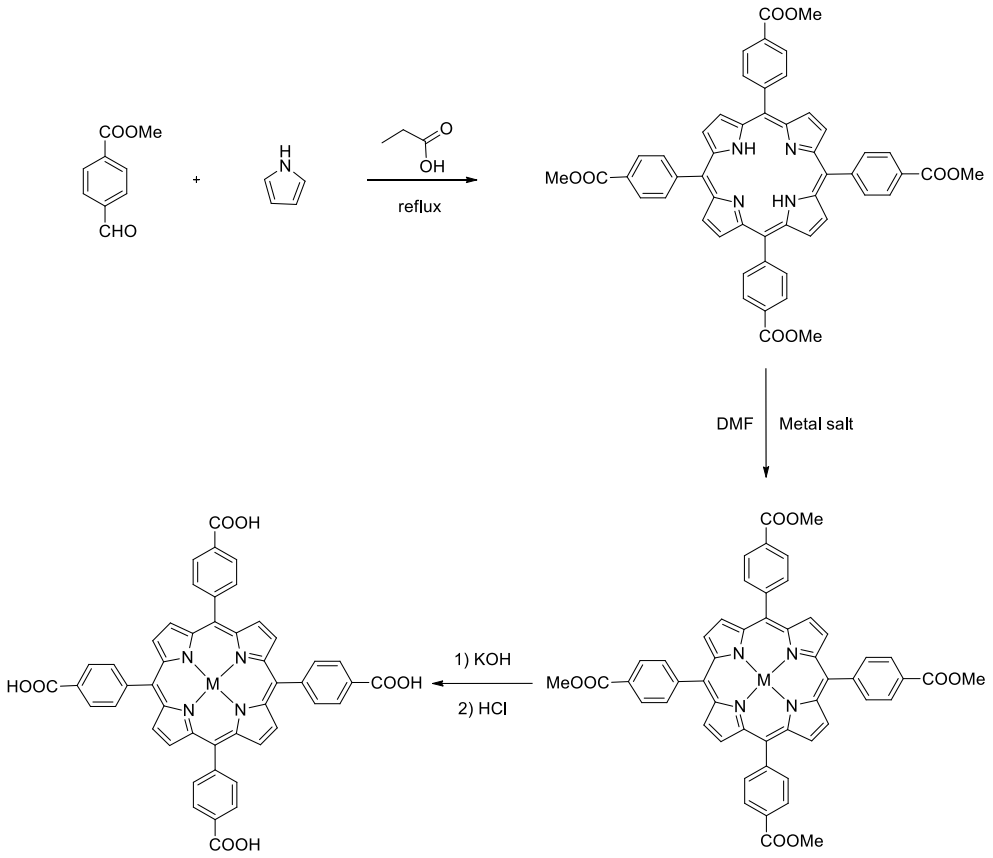

Scheme II-1. Synthetic routes for MTCPP ligands.

Synthesis of 5,10,15,20-Tetrakis(4-Methoxycarbonylphenyl)porphyrin (TPPCOOMe). To propionic acid (100 mL) in a 500 mL three-necked flask were added pyrrole (3.0 g, 0.043 mol) and methyl p-formylbenzoate (6.9 g, 0.042 mol). Then the

solution was refluxed for 12 h in darkness. After the reaction mixture was cooled to room temperature, crystals were collected by suction-filtration to afford purple crystals (1.9 g, 2.24 mmol, 21%). ^{1}H NMR (300 MHz, $CDCl_3$), δ 8.81 (s, 8H), 8.43 (d, 8H), 8.28 (d, 8H), 4.11 (s, 12H), 2.83 (s, 2H).

Synthesis of [5,10,15,20-Tetrakis(4-Methoxycarbonylphenyl)porphyrinato]-Ni(II). A solution of TPPCOOMe (0.854 g, 1.0 mmol) and $NiCl_2 \cdot 6H_2O$ (3.1 g, 12.8 mmol) in 100 mL of DMF was refluxed for 6 h. After the mixture was cooled to room temperature, 150 mL of H_2O was added. The resultant precipitate was filtered and washed with 50 mL of H_2O for two times. The obtained solid was dissolved in $CHCl_3$, followed by washing three times with 1 M HCl and twice with water. The organic layer was dried over anhydrous magnesium sulfate and evaporated to afford quantitative crimson crystals.

Synthesis of [5,10,15,20-Tetrakis(4-Methoxycarbonylphenyl)porphyrinato]-Fe(III) Chloride. A solution of TPPCOOMe (0.854 g, 1.0 mmol) and $FeCl_2 \cdot 4H_2O$ (2.5 g, 12.8 mmol) in 100 mL of DMF was refluxed for 6 h. After the mixture was cooled to room temperature, 150 mL of H_2O was added. The resultant precipitate was filtered and washed with 50 mL of H_2O for two times. The obtained solid was dissolved in $CHCl_3$, followed by washing three times with 1 M HCl and twice with water. The organic layer was dried over anhydrous magnesium sulfate and evaporated to afford quantitative dark brown crystals.

Synthesis of [5,10,15,20-Tetrakis(4-Methoxycarbonylphenyl)porphyrinato]-Mn(III) Chloride. A solution of TPPCOOMe (0.854 g, 1.0 mmol) and $MnCl_2 \cdot 4H_2O$

(2.5 g, 12.8 mmol) in 100 mL of DMF was refluxed for 6 h. After the mixture was cooled to room temperature, 150 mL of H_2O was added. The resultant precipitate was filtered and washed with 50 mL of H_2O for two times. The obtained solid was dissolved in $CHCl_3$, followed by washing three times with water. The organic layer was dried over anhydrous magnesium sulfate and evaporated to afford quantitative dark green crystals.

Synthesis of [5,10,15,20-Tetrakis(4-Methoxycarbonylphenyl)porphyrinato]-Cu(II). A solution of TPPCOOMe (0.854 g, 1.0 mmol) and $CuCl_2 \cdot 2H_2O$ (2.2g, 12.8 mmol) in 100 mL of DMF was refluxed for 6 h. After the mixture was cooled to room temperature, 150 mL of H_2O was added. The resultant precipitate was filtered and washed with 50 mL of H_2O for two times. The obtained solid was dissolved in $CHCl_3$, followed by washing three times with water. The organic layer was dried over anhydrous magnesium sulfate and evaporated to afford quantitative dark red crystals.

Synthesis of [5,10,15,20-Tetrakis(4-Methoxycarbonylphenyl)porphyrinato]-Zn(II). A solution of TPPCOOMe (0.854 g, 1.0 mmol) and $ZnCl_2$ (1.75 g, 12.8 mmol) in 100 mL of DMF was refluxed for 6 h. After the mixture was cooled to room temperature, 150 mL of H_2O was added. The resultant precipitate was filtered and washed with 50 mL of H_2O for two times. The obtained solid was dissolved in $CHCl_3$, followed by washing three times with water. The organic layer was dried over anhydrous magnesium sulfate and evaporated to afford quantitative violet crystals.

Synthesis of [5,10,15,20-Tetrakis(4-Methoxycarbonylphenyl)porphyrinato]-Co(II). A solution of TPPCOOMe (0.854 g, 1.0 mmol) and $CoCl_2 \cdot 6H_2O$ (3.1 g, 12.8 mmol) in 100 mL of DMF was refluxed for 6 h. After the mixture was cooled to room

temperature, 150 mL of H_2O was added. The resultant precipitate was filtered and washed with 50 mL of H_2O for two times. The obtained solid was dissolved in $CHCl_3$, followed by washing three times with water. The organic layer was dried over anhydrous magnesium sulfate and evaporated to afford quantitative red crystals.

Synthesis of [5,10,15,20-Tetrakis(4-Carboxyphenyl)porphyrinato]-Ni(II) (NiTCPP). The obtained corresponding ester (0.75 g) was stirred in THF (25 mL) and MeOH (25 mL) mixed solvent, to which a solution of KOH (2.63 g, 46.95 mmol) in H_2O (25 mL) was added. The mixture was then refluxed for 12 h. After cooling down to room temperature, THF and MeOH were evaporated under vacuum. Additional water was added to the resulting water phase and the mixture was heated until the solid was fully dissolved, then the homogeneous solution was acidified with 1 M HCl until no further precipitate was detected. The crimson solid was collected by filtration, washed with water and dried in vacuum.

Synthesis of [5,10,15,20-Tetrakis(4-Carboxyphenyl)porphyrinato]-Fe(III) Chloride (FeTCPPCl). The obtained corresponding ester (0.75 g) was stirred in THF (25 mL) and MeOH (25 mL) mixed solvent, to which a solution of KOH (2.63 g, 46.95 mmol) in H_2O (25 mL) was added. The mixture was then refluxed for 12 h. After cooling down to room temperature, THF and MeOH were evaporated under vacuum. Additional water was added to the resulting water phase and the mixture was heated until the solid was fully dissolved, then the homogeneous solution was acidified with 1 M HCl until no further precipitate was detected. The brown solid was collected by filtration, washed with water and dried in vacuum.

Synthesis of [5,10,15,20-Tetrakis(4-Carboxyphenyl)porphyrinato]-Mn (III) Chloride (MnTCPPCl). The obtained corresponding ester (0.75 g) was stirred in THF (25 mL) and MeOH (25 mL) mixed solvent, to which a solution of KOH (2.63 g, 46.95 mmol) in H_2O (25 mL) was added. The mixture was then refluxed for 12 h. After cooling down to room temperature, THF and MeOH were evaporated under vacuum. Additional water was added to the resulting water phase and the mixture was heated until the solid was fully dissolved, then the homogeneous solution was acidified with 1 M HCl until no further precipitate was detected. The dark green solid was collected by filtration, washed with water and dried in vacuum.

Synthesis of [5,10,15,20-Tetrakis(4-Carboxyphenyl)porphyrinato]-Cu(II) (CuTCPP). The obtained corresponding ester (0.75 g) was stirred in THF (25 mL) and MeOH (25 mL) mixed solvent, to which a solution of KOH (2.63 g, 46.95 mmol) in H_2O (25 mL) was added. The mixture was then refluxed for 12 h. After cooling down to room temperature, THF and MeOH were evaporated under vacuum. Additional water was added to the resulting water phase and the mixture was heated until the solid was fully dissolved, then the homogeneous solution was acidified with 1 M HCl until no further precipitate was detected. The dark red solid was collected by filtration, washed with water and dried in vacuum.

Synthesis of [5,10,15,20-Tetrakis(4-Carboxyphenyl)porphyrinato]-Zn(II) (ZnTCPP). The obtained corresponding ester (0.75 g) was stirred in THF (25 mL) and MeOH (25 mL) mixed solvent, to which a solution of KOH (2.63 g, 46.95 mmol) in H_2O (25 mL) was added. The mixture was then refluxed for 12 h. After cooling down to room

temperature, THF and MeOH were evaporated under vacuum. Additional water was added to the resulting water phase and the mixture was heated until the solid was fully dissolved, then the homogeneous solution was acidified with 1 M HCl until no further precipitate was detected. The violet solid was collected by filtration, washed with water and dried in vacuum.

Synthesis of [5,10,15,20-Tetrakis(4-Carboxyphenyl)porphyrinato]-Co(II) (CoTCPP). The obtained corresponding ester (0.75 g) was stirred in THF (25 mL) and MeOH (25 mL) mixed solvent, to which a solution of KOH (2.63 g, 46.95 mmol) in H_2O (25 mL) was added. The mixture was then refluxed for 12 h. After cooling down to room temperature, THF and MeOH were evaporated under vacuum. Additional water was added to the resulting water phase and the mixture was heated until the solid was fully dissolved, then the homogeneous solution was acidified with 1 M HCl until no further precipitate was detected. The red solid was collected by filtration, washed with water and dried in vacuum.

Synthesis of NiTCPP⊂UiO-66. $ZrCl_4$ (30 mg, 0.129 mmol), H_2BDC (20 mg, 0.120 mmol), NiTCPP (10 mg, 0.012 mmol) and benzoic acid (600 mg, 4.918 mmol) in 2 mL of DMF were ultrasonically dissolved in a Pyrex vial. The mixture was heated in an oven at 130 °C for 12 h. After cooling down to room temperature, red precipitates were collected by centrifugation. The solids were washed with DMF three times to remove unreacted precursors, and then solvent-exchanged with acetone three times. The resulting red powder was obtained by centrifugation, and dried in an oven at 80 °C.

Synthesis of UiO-66. $ZrCl_4$ (30 mg, 0.129 mmol), H_2BDC (20 mg, 0.120 mmol)

and benzoic acid (600 mg, 4.918 mmol) in 2 mL of DMF were ultrasonically dissolved in a Pyrex vial. The mixture was heated in an oven at 130 °C for 12 h. After cooling down to room temperature, white precipitates were collected by centrifugation. The solids were washed with DMF three times to remove unreacted precursors, and then solvent-exchanged with acetone three times. The resulting white powder was obtained by centrifugation, and dried in an oven at 80 °C.

Synthesis of NiTCPP⊂UiO-66-NH_2. $ZrCl_4$ (30 mg, 0.129 mmol), NH_2-BDC (20 mg, 0.110 mmol), NiTCPP (10 mg, 0.012 mmol) and benzoic acid (600 mg, 4.918 mmol) in 2 mL of DMF were ultrasonically dissolved in a Pyrex vial. The mixture was heated in an oven at 120 °C for 12 h. After cooling down to room temperature, red precipitates were collected by centrifugation. The solids were washed with DMF three times to remove unreacted precursors, and then solvent-exchanged with acetone three times. The resulting red powder was obtained by centrifugation, and dried in an oven at 80 °C.

Synthesis of UiO-66-NH_2-S1. $ZrCl_4$ (30 mg, 0.129 mmol), NH_2-BDC (20 mg, 0.110 mmol) and benzoic acid (600 mg, 4.918 mmol) in 2 mL of DMF were ultrasonically dissolved in a Pyrex vial. The mixture was heated in an oven at 120 °C for 12 h. After cooling down to room temperature, white precipitates were collected by centrifugation. The solids were washed with DMF three times to remove unreacted precursors, and then solvent-exchanged with acetone three times. The resulting powder was obtained by centrifugation, and dried in an oven at 80 °C.

Synthesis of FeTCPPCl⊂UiO-66-NH_2. $ZrCl_4$ (30 mg, 0.129 mmol), NH_2-BDC

(20 mg, 0.110 mmol), FeTCPPCl (10 mg, 0.011 mmol) and benzoic acid (600 mg, 4.918 mmol) in 2 mL of DMF were ultrasonically dissolved in a Pyrex vial. The mixture was heated in an oven at 120 °C for 12 h. After cooling down to room temperature, brown precipitates were collected by centrifugation. The solids were washed with DMF three times to remove unreacted precursors, and then solvent-exchanged with acetone three times. The resulting brown powder was obtained by centrifugation, and dried in an oven at 80 °C.

Synthesis of MnTCPPCl⊂UiO-66-NH_2. $ZrCl_4$ (30 mg, 0.129 mmol), NH_2-BDC (30 mg, 0.166 mmol), MnTCPPCl (10 mg, 0.011 mmol) and benzoic acid (500 mg, 4.098 mmol) in 2 mL of DMF were ultrasonically dissolved in a Pyrex vial. The mixture was heated in an oven at 120 °C for 12 h. After cooling down to room temperature, dark green precipitates were collected by centrifugation. The solids were washed with DMF three times to remove unreacted precursors, and then solvent-exchanged with acetone three times. The resulting dark green powder was obtained by centrifugation, and dried in an oven at 80 °C.

Synthesis of CuTCPP⊂UiO-66-NH_2. $ZrCl_4$ (30 mg, 0.129 mmol), NH_2-BDC (30 mg, 0.166 mmol), CuTCPP (10 mg, 0.012 mmol) and benzoic acid (500 mg, 4.098 mmol) in 2 mL of DMF were ultrasonically dissolved in a Pyrex vial. The mixture was heated in an oven at 120 °C for 12 h. After cooling down to room temperature, dark green precipitates were collected by centrifugation. The solids were washed with DMF three times to remove unreacted precursors, and then solvent-exchanged with acetone three times. The resulting powder was obtained by centrifugation, and dried in an oven

at 80 °C.

Synthesis of ZnTCPP⊂UiO-66-NH_2. $ZrCl_4$ (30 mg, 0.129 mmol), NH_2-BDC (30 mg, 0.166 mmol), ZnTCPP (10 mg, 0.012 mmol) and benzoic acid (500 mg, 4.098 mmol) in 2 mL of DMF were ultrasonically dissolved in a Pyrex vial. The mixture was heated in an oven at 120 °C for 12 h. After cooling down to room temperature, dark green precipitates were collected by centrifugation. The solids were washed with DMF three times to remove unreacted precursors, and then solvent-exchanged with acetone three times. The resulting powder was obtained by centrifugation, and dried in an oven at 80 °C.

Synthesis of H_2TCPP⊂UiO-66-NH_2. $ZrCl_4$ (30 mg, 0.129 mmol), NH_2-BDC (30 mg, 0.166 mmol), H_2TCPP (10 mg, 0.013 mmol) and benzoic acid (500 mg, 4.098 mmol) in 2 mL of DMF were ultrasonically dissolved in a Pyrex vial. The mixture was heated in an oven at 120 °C for 12 h. After cooling down to room temperature, dark green precipitates were collected by centrifugation. The solids were washed with DMF three times to remove unreacted precursors, and then solvent-exchanged with acetone three times. The resulting powder was obtained by centrifugation, and dried in an oven at 80 °C.

Synthesis of CoTCPP⊂UiO-66-NH_2. $ZrCl_4$ (30 mg, 0.129 mmol), NH_2-BDC (30 mg, 0.166 mmol), CoTCPP (10 mg, 0.012 mmol) and benzoic acid (500 mg, 4.098 mmol) in 2 mL of DMF were ultrasonically dissolved in a Pyrex vial. The mixture was heated in an oven at 120 °C for 12 h. After cooling down to room temperature, dark green precipitates were collected by centrifugation. The solids were washed with DMF

three times to remove unreacted precursors, and then solvent-exchanged with acetone three times. The resulting powder was obtained by centrifugation, and dried in an oven at 80 °C.

Synthesis of FeTCPPCl⊂UiO-66. $ZrCl_4$ (30 mg, 0.129 mmol), H_2BDC (30 mg, 0.181 mmol), FeTCPPCl (10 mg, 0.011 mmol) and benzoic acid (500 mg, 4.098 mmol) in 2 mL of DMF were ultrasonically dissolved in a Pyrex vial. The mixture was heated in an oven at 130 °C for 12 h. After cooling down to room temperature, brown precipitates were collected by centrifugation. The solids were washed with DMF three times to remove unreacted precursors, and then solvent-exchanged with acetone three times. The resulting brown powder was obtained by centrifugation, and dried in an oven at 80 °C.

Synthesis of MnTCPPCl⊂UiO-66. $ZrCl_4$ (30 mg, 0.129 mmol), H_2BDC (50 mg, 0.301 mmol), MnTCPPCl (10 mg, 0.011 mmol) and benzoic acid (500 mg, 4.098 mmol) in 2 mL of DMF were ultrasonically dissolved in a Pyrex vial. The mixture was heated in an oven at 130 °C for 12 h. After cooling down to room temperature, dark green precipitates were collected by centrifugation. The solids were washed with DMF three times to remove unreacted precursors, and then solvent-exchanged with acetone three times. The resulting dark green powder was obtained by centrifugation, and dried in an oven at 80 °C.

Synthesis of CuTCPP⊂UiO-66. $ZrCl_4$ (30 mg, 0.129 mmol), H_2BDC (30 mg, 0.181 mmol), CuTCPP (10 mg, 0.012 mmol) and benzoic acid (500 mg, 4.098 mmol) in 2 mL of DMF were ultrasonically dissolved in a Pyrex vial. The mixture was heated in

an oven at 130 °C for 12 h. After cooling down to room temperature, brown precipitates were collected by centrifugation. The solids were washed with DMF three times to remove unreacted precursors, and then solvent-exchanged with acetone three times. The resulting powder was obtained by centrifugation, and dried in an oven at 80 °C.

Synthesis of ZnTCPP⊂UiO-66. $ZrCl_4$ (30 mg, 0.129 mmol), H_2BDC (30 mg, 0.181 mmol), ZnTCPP (10 mg, 0.012 mmol) and benzoic acid (500 mg, 4.098 mmol) in 2 mL of DMF were ultrasonically dissolved in a Pyrex vial. The mixture was heated in an oven at 130 °C for 12 h. After cooling down to room temperature, brown precipitates were collected by centrifugation. The solids were washed with DMF three times to remove unreacted precursors, and then solvent-exchanged with acetone three times. The resulting powder was obtained by centrifugation, and dried in an oven at 80 °C.

Synthesis of H_2TCPP⊂UiO-66. $ZrCl_4$ (30 mg, 0.129 mmol), H_2BDC (30 mg, 0.181 mmol), H_2TCPP (10 mg, 0.013 mmol) and benzoic acid (500 mg, 4.098 mmol) in 2 mL of DMF were ultrasonically dissolved in a Pyrex vial. The mixture was heated in an oven at 130 °C for 12 h. After cooling down to room temperature, brown precipitates were collected by centrifugation. The solids were washed with DMF three times to remove unreacted precursors, and then solvent-exchanged with acetone three times. The resulting powder was obtained by centrifugation, and dried in an oven at 80 °C.

Synthesis of CoTCPP⊂UiO-66. $ZrCl_4$ (30 mg, 0.129 mmol), H_2BDC (30 mg, 0.181 mmol), CoTCPP (10 mg, 0.012 mmol) and benzoic acid (500 mg, 4.098 mmol) in 2 mL of DMF were ultrasonically dissolved in a Pyrex vial. The mixture was heated in an oven at 130 °C for 12 h. After cooling down to room temperature, brown precipitates

were collected by centrifugation. The solids were washed with DMF three times to remove unreacted precursors, and then solvent-exchanged with acetone three times. The resulting powder was obtained by centrifugation, and dried in an oven at 80 °C.

Synthesis of NiTCPP⊂UiO-66-2,5-(OH)$_2$. $ZrCl_4$ (30 mg, 0.129 mmol), DOBDC (60 mg, 0.303 mmol), NiTCPP (10 mg, 0.012 mmol) and benzoic acid (320 mg, 2.623 mmol) in 2 mL of DMF and 1 d H_2O were ultrasonically dissolved in a Pyrex vial. The mixture was heated in an oven at 105 °C for 12 h. After cooling down to room temperature, red precipitates were collected by centrifugation. The solids were washed with DMF three times to remove unreacted precursors, and then solvent-exchanged with acetone three times. The resulting red powder was obtained by centrifugation, and dried in an oven at 80 °C.

Synthesis of FeTCPPCl⊂UiO-66-2,5-(OH)$_2$. $ZrCl_4$ (30 mg, 0.129 mmol), DOBDC (60 mg, 0.303 mmol), FeTCPPCl (10 mg, 0.011 mmol) and benzoic acid (320 mg, 2.623 mmol) in 2 mL of DMF and 1 d H_2O were ultrasonically dissolved in a Pyrex vial. The mixture was heated in an oven at 105 °C for 12 h. After cooling down to room temperature, red precipitates were collected by centrifugation. The solids were washed with DMF three times to remove unreacted precursors, and then solvent-exchanged with acetone three times. The resulting powder was obtained by centrifugation, and dried in an oven at 80 °C.

Synthesis of MnTCPPCl⊂UiO-66-2,5-(OH)$_2$. $ZrCl_4$ (30 mg, 0.129 mmol), DOBDC (60 mg, 0.303 mmol), MnTCPPCl (10 mg, 0.011 mmol) and benzoic acid (320 mg, 2.623 mmol) in 2 mL of DMF and 1 d H_2O were ultrasonically dissolved in a Pyrex

vial. The mixture was heated in an oven at 105 °C for 12 h. After cooling down to room temperature, red precipitates were collected by centrifugation. The solids were washed with DMF three times to remove unreacted precursors, and then solvent-exchanged with acetone three times. The resulting powder was obtained by centrifugation, and dried in an oven at 80 °C.

Synthesis of CuTCPP⊂UiO-66-2,5-(OH)$_2$. $ZrCl_4$ (30 mg, 0.129 mmol), DOBDC (60 mg, 0.303 mmol), CuTCPP (10 mg, 0.012 mmol) and benzoic acid (320 mg, 2.623 mmol) in 2 mL of DMF and 1 d H_2O were ultrasonically dissolved in a Pyrex vial. The mixture was heated in an oven at 105 °C for 12 h. After cooling down to room temperature, red precipitates were collected by centrifugation. The solids were washed with DMF three times to remove unreacted precursors, and then solvent-exchanged with acetone three times. The resulting powder was obtained by centrifugation, and dried in an oven at 80 °C.

Synthesis of H_2TCPP⊂UiO-66-2,5-(OH)$_2$. $ZrCl_4$ (30 mg, 0.129 mmol), DOBDC (60 mg, 0.303 mmol), H_2TCPP (10 mg, 0.013 mmol) and benzoic acid (320 mg, 2.623 mmol) in 2 mL of DMF and 1 d H_2O were ultrasonically dissolved in a Pyrex vial. The mixture was heated in an oven at 105 °C for 12 h. After cooling down to room temperature, red precipitates were collected by centrifugation. The solids were washed with DMF three times to remove unreacted precursors, and then solvent-exchanged with acetone three times. The resulting powder was obtained by centrifugation, and dried in an oven at 80 °C.

Synthesis of ZnTCPP⊂UiO-66-2,5-(OH)$_2$. $ZrCl_4$ (30 mg, 0.129 mmol),

DOBDC (60 mg, 0.303 mmol), ZnTCPP (10 mg, 0.012 mmol) and benzoic acid (320 mg, 2.623 mmol) in 2 mL of DMF and 1 d H_2O were ultrasonically dissolved in a Pyrex vial. The mixture was heated in an oven at 105 °C for 12 h. After cooling down to room temperature, red precipitates were collected by centrifugation. The solids were washed with DMF three times to remove unreacted precursors, and then solvent-exchanged with acetone three times. The resulting powder was obtained by centrifugation, and dried in an oven at 80 °C.

Synthesis of CoTCPP⊂UiO-66-2,5-$(OH)_2$. $ZrCl_4$ (30 mg, 0.129 mmol), DOBDC (60 mg, 0.303 mmol), CoTCPP (10 mg, 0.012 mmol) and benzoic acid (320 mg, 2.623 mmol) in 2 mL of DMF and 1 d H_2O were ultrasonically dissolved in a Pyrex vial. The mixture was heated in an oven at 105 °C for 12 h. After cooling down to room temperature, red precipitates were collected by centrifugation. The solids were washed with DMF three times to remove unreacted precursors, and then solvent-exchanged with acetone three times. The resulting powder was obtained by centrifugation, and dried in an oven at 80 °C.

Synthesis of NiTCPP⊂UiO-66-2,5-$(CH_3)_2$. $ZrCl_4$ (20 mg, 0.086 mmol), 2,5-dimethylterephthalic acid (50 mg, 0.258 mmol), NiTCPP (10 mg, 0.012 mmol) and benzoic acid (250 mg, 2.049 mmol) in 2 mL of DMF were ultrasonically dissolved in a Pyrex vial. The mixture was heated in an oven at 135 °C for 12 h. After cooling down to room temperature, red precipitates were collected by centrifugation. The solids were washed with DMF three times to remove unreacted precursors, and then solvent-exchanged with acetone three times. The resulting red powder was obtained by

centrifugation, and dried in an oven at 80 °C.

Synthesis of FeTCPPCl⊂UiO-66-2,5-$(CH_3)_2$. $ZrCl_4$ (20 mg, 0.086 mmol), 2,5-dimethylterephthalic acid (50 mg, 0.258 mmol), FeTCPPCl (10 mg, 0.011 mmol) and benzoic acid (250 mg, 2.049 mmol) in 2 mL of DMF were ultrasonically dissolved in a Pyrex vial. The mixture was heated in an oven at 135 °C for 12 h. After cooling down to room temperature, red precipitates were collected by centrifugation. The solids were washed with DMF three times to remove unreacted precursors, and then solvent-exchanged with acetone three times. The resulting powder was obtained by centrifugation, and dried in an oven at 80 °C.

Synthesis of MnTCPPCl⊂UiO-66-2,5-$(CH_3)_2$. $ZrCl_4$ (20 mg, 0.086 mmol), 2,5-dimethylterephthalic acid (50 mg, 0.258 mmol), MnTCPPCl (10 mg, 0.011 mmol) and benzoic acid (250 mg, 2.049 mmol) in 2 mL of DMF were ultrasonically dissolved in a Pyrex vial. The mixture was heated in an oven at 135 °C for 12 h. After cooling down to room temperature, red precipitates were collected by centrifugation. The solids were washed with DMF three times to remove unreacted precursors, and then solvent-exchanged with acetone three times. The resulting powder was obtained by centrifugation, and dried in an oven at 80 °C.

Synthesis of CuTCPP⊂UiO-66-2,5-$(CH_3)_2$. $ZrCl_4$ (20 mg, 0.086 mmol), 2,5-dimethylterephthalic acid (50 mg, 0.258 mmol), CuTCPP (10 mg, 0.012 mmol) and benzoic acid (250 mg, 2.049 mmol) in 2 mL of DMF were ultrasonically dissolved in a Pyrex vial. The mixture was heated in an oven at 135 °C for 12 h. After cooling down to room temperature, red precipitates were collected by centrifugation. The solids were

washed with DMF three times to remove unreacted precursors, and then solvent-exchanged with acetone three times. The resulting powder was obtained by centrifugation, and dried in an oven at 80 °C.

Synthesis of H_2TCPP⊂UiO-66-2,5-$(CH_3)_2$. $ZrCl_4$ (20 mg, 0.086 mmol), 2,5-dimethylterephthalic acid (50 mg, 0.258 mmol), H_2TCPP (10 mg, 0.013 mmol) and benzoic acid (250 mg, 2.049 mmol) in 2 mL of DMF were ultrasonically dissolved in a Pyrex vial. The mixture was heated in an oven at 135 °C for 12 h. After cooling down to room temperature, red precipitates were collected by centrifugation. The solids were washed with DMF three times to remove unreacted precursors, and then solvent-exchanged with acetone three times. The resulting powder was obtained by centrifugation, and dried in an oven at 80 °C.

Synthesis of ZnTCPP⊂UiO-66-2,5-$(CH_3)_2$. $ZrCl_4$ (20 mg, 0.086 mmol), 2,5-dimethylterephthalic acid (50 mg, 0.258 mmol), ZnTCPP (10 mg, 0.012 mmol) and benzoic acid (250 mg, 2.049 mmol) in 2 mL of DMF were ultrasonically dissolved in a Pyrex vial. The mixture was heated in an oven at 135 °C for 12 h. After cooling down to room temperature, red precipitates were collected by centrifugation. The solids were washed with DMF three times to remove unreacted precursors, and then solvent-exchanged with acetone three times. The resulting powder was obtained by centrifugation, and dried in an oven at 80 °C.

Synthesis of CoTCPP⊂UiO-66-2,5-$(CH_3)_2$. $ZrCl_4$ (20 mg, 0.086 mmol), 2,5-dimethylterephthalic acid (50 mg, 0.258 mmol), CoTCPP (10 mg, 0.012 mmol) and benzoic acid (250 mg, 2.049 mmol) in 2 mL of DMF were ultrasonically dissolved in a

Pyrex vial. The mixture was heated in an oven at 135 °C for 12 h. After cooling down to room temperature, red precipitates were collected by centrifugation. The solids were washed with DMF three times to remove unreacted precursors, and then solvent-exchanged with acetone three times. The resulting powder was obtained by centrifugation, and dried in an oven at 80 °C.

Synthesis of NiTCPP⊂UiO-66-SO_3H. $ZrCl_4$ (20 mg, 0.086 mmol), monosodium salt of 2-sulfonyl terephthalic acid (60 mg, 0.224 mmol) and NiTCPP (10 mg, 0.012 mmol) in 0.7 mL of acetic acid and 2 mL of DMF were ultrasonically dissolved in a Pyrex vial. The mixture was heated in an oven at 120 °C for 12 h. After cooling down to room temperature, red precipitates were collected by centrifugation. The solids were washed with DMF three times to remove unreacted precursors, washed with H_2O twice to remove salts, and then solvent-exchanged with acetone three times. The resulting red powder was obtained by centrifugation, and dried in an oven at 80 °C.

Synthesis of FeTCPPCl⊂UiO-66-SO_3H. $ZrCl_4$ (20 mg, 0.086 mmol), monosodium salt of 2-sulfonyl terephthalic acid (60 mg, 0.224 mmol) and FeTCPPCl (10 mg, 0.011 mmol) in 0.7 mL of acetic acid and 2 mL of DMF were ultrasonically dissolved in a Pyrex vial. The mixture was heated in an oven at 120 °C for 12 h. After cooling down to room temperature, red precipitates were collected by centrifugation. The solids were washed with DMF three times to remove unreacted precursors, washed with H_2O twice to remove salts, and then solvent-exchanged with acetone three times. The resulting powder was obtained by centrifugation, and dried in an oven at 80 °C.

Synthesis of MnTCPPCl⊂UiO-66-SO_3H. $ZrCl_4$ (30 mg, 0.129 mmol),

monosodium salt of 2-sulfonyl terephthalic acid (80 mg, 0.298 mmol) and MnTCPPCl (5 mg, 0.006 mmol) in 0.7 mL of acetic acid and 2 mL of DMF were ultrasonically dissolved in a Pyrex vial. The mixture was heated in an oven at 120 °C for 12 h. After cooling down to room temperature, dark green precipitates were collected by centrifugation. The solids were washed with DMF three times to remove unreacted precursors, washed with H_2O twice to remove salts, and then solvent-exchanged with acetone three times. The resulting dark green powder was obtained by centrifugation, and dried in an oven at 80 °C.

Synthesis of CuTCPP⊂UiO-66-SO_3H. $ZrCl_4$ (30 mg, 0.129 mmol), monosodium salt of 2-sulfonyl terephthalic acid (80 mg, 0.298 mmol) and CuTCPP (5 mg, 0.006 mmol) in 0.7 mL of acetic acid and 2 mL of DMF were ultrasonically dissolved in a Pyrex vial. The mixture was heated in an oven at 120 °C for 12 h. After cooling down to room temperature, dark green precipitates were collected by centrifugation. The solids were washed with DMF three times to remove unreacted precursors, washed with H_2O twice to remove salts, and then solvent-exchanged with acetone three times. The resulting powder was obtained by centrifugation, and dried in an oven at 80 °C.

Synthesis of H_2CPP⊂UiO-66-SO_3H. $ZrCl_4$ (30 mg, 0.129 mmol), monosodium salt of 2-sulfonyl terephthalic acid (80 mg, 0.298 mmol) and H_2TCPP (5 mg, 0.006 mmol) in 0.7 mL of acetic acid and 2 mL of DMF were ultrasonically dissolved in a Pyrex vial. The mixture was heated in an oven at 120 °C for 12 h. After cooling down to room temperature, dark green precipitates were collected by centrifugation. The solids

were washed with DMF three times to remove unreacted precursors, washed with H_2O twice to remove salts, and then solvent-exchanged with acetone three times. The resulting powder was obtained by centrifugation, and dried in an oven at 80 °C.

Synthesis of ZnTCPP⊂UiO-66-SO_3H. $ZrCl_4$ (30 mg, 0.129 mmol), monosodium salt of 2-sulfonyl terephthalic acid (80 mg, 0.298 mmol) and ZnTCPP (5 mg, 0.006 mmol) in 0.7 mL of acetic acid and 2 mL of DMF were ultrasonically dissolved in a Pyrex vial. The mixture was heated in an oven at 120 °C for 12 h. After cooling down to room temperature, dark green precipitates were collected by centrifugation. The solids were washed with DMF three times to remove unreacted precursors, washed with H_2O twice to remove salts, and then solvent-exchanged with acetone three times. The resulting powder was obtained by centrifugation, and dried in an oven at 80 °C.

Synthesis of CoTCPP⊂UiO-66-SO_3H. $ZrCl_4$ (30 mg, 0.129 mmol), monosodium salt of 2-sulfonyl terephthalic acid (80 mg, 0.298 mmol) and CoTCPP (5 mg, 0.006 mmol) in 0.7 mL of acetic acid and 2 mL of DMF were ultrasonically dissolved in a Pyrex vial. The mixture was heated in an oven at 120 °C for 12 h. After cooling down to room temperature, dark green precipitates were collected by centrifugation. The solids were washed with DMF three times to remove unreacted precursors, washed with H_2O twice to remove salts, and then solvent-exchanged with acetone three times. The resulting powder was obtained by centrifugation, and dried in an oven at 80 °C.

Synthesis of NiTCPP⊂UiO-66-2,5-$(COOH)_2$. $ZrCl_4$ (100 mg, 0.429 mmol),

H_4BTeC (120 mg, 0.472 mmol) and NiTCPP (10 mg, 0.012 mmol) in 0.3 mL of TFA, 0.1 mL of H_2O and 2 mL of DMF were ultrasonically dissolved in a Pyrex vial. The mixture was heated in an oven at 135 °C for 10 h. After cooling down to room temperature, red precipitates were collected by centrifugation. The solids were washed with DMF three times to remove unreacted precursors, and then solvent-exchanged with acetone three times. The resulting red powder was obtained by centrifugation, and dried in an oven at 80 °C.

Synthesis of FeTCPPCl⊂UiO-66-2,5-(COOH)$_2$. $ZrCl_4$ (100 mg, 0.429 mmol), H_4BTeC (120 mg, 0.472 mmol) and FeTCPPCl (10 mg, 0.011 mmol) in 0.3 mL of TFA, 0.1 mL of H_2O and 2 mL of DMF were ultrasonically dissolved in a Pyrex vial. The mixture was heated in an oven at 135 °C for 10 h. After cooling down to room temperature, red precipitates were collected by centrifugation. The solids were washed with DMF three times to remove unreacted precursors, and then solvent-exchanged with acetone three times. The resulting powder was obtained by centrifugation, and dried in an oven at 80 °C.

Synthesis of MnTCPPCl⊂UiO-66-2,5-(COOH)$_2$. $ZrCl_4$ (100 mg, 0.429 mmol), H_4BTeC (120 mg, 0.472 mmol) and MnTCPPCl (5 mg, 0.006 mmol) in 0.3 mL of TFA, 0.1 mL of H_2O and 2 mL of DMF were ultrasonically dissolved in a Pyrex vial. The mixture was heated in an oven at 135 °C for 10 h. After cooling down to room temperature, red precipitates were collected by centrifugation. The solids were washed with DMF three times to remove unreacted precursors, and then solvent-exchanged with acetone three times. The resulting powder was obtained by centrifugation, and dried in

an oven at 80 °C.

Synthesis of CuTCPP⊂UiO-66-2,5-(COOH)$_2$. $ZrCl_4$ (100 mg, 0.429 mmol), H_4BTeC (120 mg, 0.472 mmol) and CuTCPP (5 mg, 0.006 mmol) in 0.3 mL of TFA, 0.1 mL of H_2O and 2 mL of DMF were ultrasonically dissolved in a Pyrex vial. The mixture was heated in an oven at 135 °C for 10 h. After cooling down to room temperature, red precipitates were collected by centrifugation. The solids were washed with DMF three times to remove unreacted precursors, and then solvent-exchanged with acetone three times. The resulting powder was obtained by centrifugation, and dried in an oven at 80 °C.

Synthesis of H_2TCPP⊂UiO-66-2,5-(COOH)$_2$. $ZrCl_4$ (100 mg, 0.429 mmol), H_4BTeC (120 mg, 0.472 mmol) and H_2TCPP (5 mg, 0.006 mmol) in 0.3 mL of TFA, 0.1 mL of H_2O and 2 mL of DMF were ultrasonically dissolved in a Pyrex vial. The mixture was heated in an oven at 135 °C for 10 h. After cooling down to room temperature, red precipitates were collected by centrifugation. The solids were washed with DMF three times to remove unreacted precursors, and then solvent-exchanged with acetone three times. The resulting powder was obtained by centrifugation, and dried in an oven at 80 °C.

Synthesis of ZnTCPP⊂UiO-66-2,5-(COOH)$_2$. $ZrCl_4$ (100 mg, 0.429 mmol), H_4BTeC (120 mg, 0.472 mmol) and ZnTCPP (5 mg, 0.006 mmol) in 0.3 mL of TFA, 0.1 mL of H_2O and 2 mL of DMF were ultrasonically dissolved in a Pyrex vial. The mixture was heated in an oven at 135 °C for 10 h. After cooling down to room temperature, red precipitates were collected by centrifugation. The solids were washed with DMF three

times to remove unreacted precursors, and then solvent-exchanged with acetone three times. The resulting powder was obtained by centrifugation, and dried in an oven at 80 °C.

Synthesis of CoTCPP⊂UiO-66-2,5-(COOH)$_2$. $ZrCl_4$ (100 mg, 0.429 mmol), H_4BTeC (120 mg, 0.472 mmol) and CoTCPP (10 mg, 0.012 mmol) in 0.3 mL of TFA, 0.1 mL of H_2O and 2 mL of DMF were ultrasonically dissolved in a Pyrex vial. The mixture was heated in an oven at 135 °C for 10 h. After cooling down to room temperature, red precipitates were collected by centrifugation. The solids were washed with DMF three times to remove unreacted precursors, and then solvent-exchanged with acetone three times. The resulting powder was obtained by centrifugation, and dried in an oven at 80 °C.

Synthesis of NiTCPP⊂UiO-66-N$_3$. $ZrCl_4$ (20 mg, 0.086 mmol), 2-azido terephthalic acid (40 mg, 0.193 mmol), NiTCPP (10 mg, 0.012 mmol) and benzoic acid (320 mg, 2.623 mmol) in 2 mL of DMF were ultrasonically dissolved in a Pyrex vial. The mixture was heated in an oven at 120 °C for 12 h. After cooling down to room temperature, red precipitates were collected by centrifugation. The solids were washed with DMF three times to remove unreacted precursors, and then solvent-exchanged with acetone three times. The resulting red powder was obtained by centrifugation, and dried in an oven at 80 °C.

Synthesis of FeTCPPCl⊂UiO-66-N$_3$. $ZrCl_4$ (20 mg, 0.086 mmol), 2-azido terephthalic acid (40 mg, 0.193 mmol), FeTCPPCl (10 mg, 0.011 mmol) and benzoic acid (320 mg, 2.623 mmol) in 2 mL of DMF were ultrasonically dissolved in a Pyrex

vial. The mixture was heated in an oven at 120 °C for 12 h. After cooling down to room temperature, red precipitates were collected by centrifugation. The solids were washed with DMF three times to remove unreacted precursors, and then solvent-exchanged with acetone three times. The resulting powder was obtained by centrifugation, and dried in an oven at 80 °C.

Synthesis of MnTCPPCl⊂UiO-66-N_3. $ZrCl_4$ (20 mg, 0.086 mmol), 2-azido terephthalic acid (40 mg, 0.193 mmol), MnTCPPCl (10 mg, 0.011 mmol) and benzoic acid (320 mg, 2.623 mmol) in 2 mL of DMF were ultrasonically dissolved in a Pyrex vial. The mixture was heated in an oven at 120 °C for 12 h. After cooling down to room temperature, red precipitates were collected by centrifugation. The solids were washed with DMF three times to remove unreacted precursors, and then solvent-exchanged with acetone three times. The resulting powder was obtained by centrifugation, and dried in an oven at 80 °C.

Synthesis of CuTCPP⊂UiO-66-N_3. $ZrCl_4$ (20 mg, 0.086 mmol), 2-azido terephthalic acid (40 mg, 0.193 mmol), CuTCPP (10 mg, 0.012 mmol) and benzoic acid (320 mg, 2.623 mmol) in 2 mL of DMF were ultrasonically dissolved in a Pyrex vial. The mixture was heated in an oven at 120 °C for 12 h. After cooling down to room temperature, red precipitates were collected by centrifugation. The solids were washed with DMF three times to remove unreacted precursors, and then solvent-exchanged with acetone three times. The resulting powder was obtained by centrifugation, and dried in an oven at 80 °C.

Synthesis of H_2TCPP⊂UiO-66-N_3. $ZrCl_4$ (20 mg, 0.086 mmol), 2-azido

terephthalic acid (40 mg, 0.193 mmol), H_2TCPP (10 mg, 0.013 mmol) and benzoic acid (320 mg, 2.623 mmol) in 2 mL of DMF were ultrasonically dissolved in a Pyrex vial. The mixture was heated in an oven at 120 °C for 12 h. After cooling down to room temperature, red precipitates were collected by centrifugation. The solids were washed with DMF three times to remove unreacted precursors, and then solvent-exchanged with acetone three times. The resulting powder was obtained by centrifugation, and dried in an oven at 80 °C.

Synthesis of ZnTCPP⊂UiO-66-N_3. $ZrCl_4$ (20 mg, 0.086 mmol), 2-azido terephthalic acid (40 mg, 0.193 mmol), ZnTCPP (10 mg, 0.012 mmol) and benzoic acid (320 mg, 2.623 mmol) in 2 mL of DMF were ultrasonically dissolved in a Pyrex vial. The mixture was heated in an oven at 120 °C for 12 h. After cooling down to room temperature, red precipitates were collected by centrifugation. The solids were washed with DMF three times to remove unreacted precursors, and then solvent-exchanged with acetone three times. The resulting powder was obtained by centrifugation, and dried in an oven at 80 °C.

Synthesis of CoTCPP⊂UiO-66-N_3. $ZrCl_4$ (20 mg, 0.086 mmol), 2-azido terephthalic acid (40 mg, 0.193 mmol), CoTCPP (10 mg, 0.012 mmol) and benzoic acid (320 mg, 2.623 mmol) in 2 mL of DMF were ultrasonically dissolved in a Pyrex vial. The mixture was heated in an oven at 120 °C for 12 h. After cooling down to room temperature, red precipitates were collected by centrifugation. The solids were washed with DMF three times to remove unreacted precursors, and then solvent-exchanged with acetone three times. The resulting powder was obtained by centrifugation, and dried in

an oven at 80 °C.

Synthesis of TBPP⊂UiO-66. $ZrCl_4$ (30 mg, 0.129 mmol), H_2BDC (20 mg, 0.120 mmol), TBPP (10 mg, 0.010 mmol) and benzoic acid (600 mg, 4.918 mmol) in 2 mL of DMF were ultrasonically dissolved in a Pyrex vial. The mixture was heated in an oven at 130 °C for 12 h. After cooling down to room temperature, red precipitates were collected by centrifugation. The solids were washed with DMF three times to remove unreacted precursors, and then solvent-exchanged with acetone three times. The resulting powder was obtained by centrifugation, and dried in an oven at 80 °C.

Synthesis of PP⊂UiO-66. $ZrCl_4$ (30 mg, 0.129 mmol), H_2BDC (20 mg, 0.120 mmol), protoporphyrin IX (PP) (15 mg, 0.027 mmol) and benzoic acid (600 mg, 4.918 mmol) in 2 mL of DMF were ultrasonically dissolved in a Pyrex vial. The mixture was heated in an oven at 130 °C for 12 h. After cooling down to room temperature, red precipitates were collected by centrifugation. The solids were washed with DMF three times to remove unreacted precursors, and then solvent-exchanged with acetone three times. The resulting powder was centrifuged, and dried in an oven at 80 °C.

Synthesis of CoTCP⊂UiO-66. $ZrCl_4$ (30 mg, 0.129 mmol), BDC (30 mg, 0.180 mmol), CoTCP (5 mg, 0.004 mmol) and benzoic acid (500 mg, 4.098 mmol) in 2 mL of DMF were ultrasonically dissolved in a Pyrex vial. The mixture was heated in an oven at 135 °C for 20 h. After cooling down to room temperature, the precipitates were collected by centrifugation. The solids were washed with DMF three times to remove unreacted precursors, and then solvent-exchanged with acetone three times. The resulting light-yellow powder was obtained by centrifugation, and dried in an oven at 80 °C.

Synthesis of BBA⊂UiO-66. $ZrCl_4$ (30 mg, 0.129 mmol), BDC (20 mg, 0.120 mmol), 4-bromobenzoic acid (BBA, 10 mg, 0.050 mmol) and benzoic acid (500 mg, 4.098 mmol) in 2 mL of DMF were ultrasonically dissolved in a Pyrex vial. The mixture was heated in an oven at 135 °C for 20 h. After cooling down to room temperature, the precipitates were collected by centrifugation. The solids were washed with DMF three times to remove unreacted precursors, and then solvent-exchanged with acetone three times. The resulting white powder was obtained by centrifugation, and dried in an oven at 80 °C.

^{1}H NMR Spectroscopy of Digested NiTCPP⊂UiO-66. Approximately 15 mg of dried MOF sample was digested in 5 mL 16% HF solution. The tube was them immersed in boiling water to evaporate HF. The dried product was dissolved in DMSO-d_6 for ^{1}H NMR test. BDC δ: 8.00 (s, 4H). NiTCPP δ: 8.13 (d, J = 7.8 Hz, 8H), 8.30 (d, J = 8.2 Hz, 8H), 8.75 (s, 8H). Molar ratio based on integration of the peaks: NiTCPP: BDC = 0.07: 1.

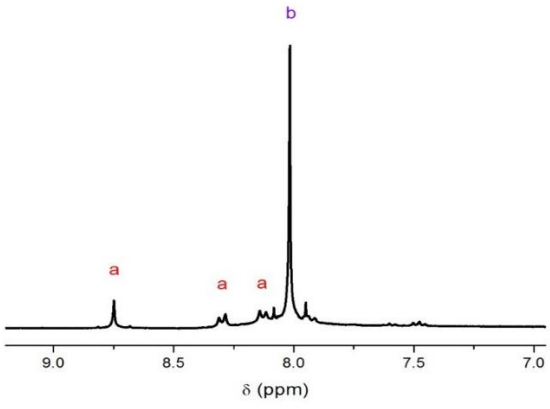

Figure II-1. ^{1}H NMR spectrum used to determine the ratio of (a) NiTCPP and (b) BDC in NiTCPP⊂UiO-66.

^{1}H NMR Spectroscopy of Digested NiTCPP⊂UiO-66-NH_2. Approximately 15 mg of dried MOF sample was digested in 5 mL 16% HF solution. The tube was them immersed in boiling water to evaporate HF. The dried product was dissolved in DMSO-d_6 for ^{1}H NMR test. NH_2-BDC δ: 6.99 (d, J = 8.3 Hz, 1H), 7.36 (s, 1H), 7.75 (d, J = 8.3 Hz, 1H). NiTCPP δ: 8.13 (d, J = 8.2 Hz, 8H), 8.30 (d, J = 8.0 Hz, 8H), 8.75 (s, 8H). Molar ratio based on integration of the peaks: NiTCPP: NH_2-BDC = 0.07: 1.

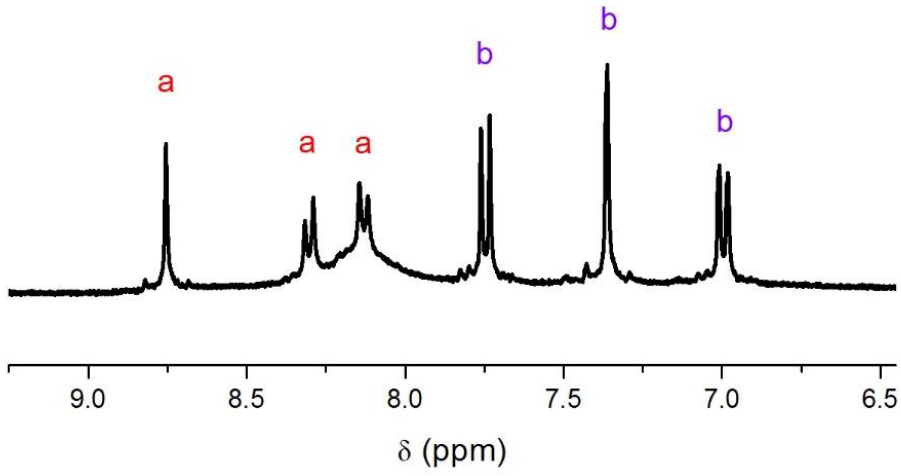

Figure II-2. ^{1}H NMR spectrum used to determine the ratio of (a) NiTCPP and (b) NH_2-BDC in NiTCPP⊂UiO-66-NH_2**.**

2.3 Results and Discussion

Functionalization of UiO-66 through a One-Pot Synthesis. Solvothermal reaction of $ZrCl_4$, H_2BDC, and benzoic acid (BA) in N,N-dimethylformamide (DMF) at 130 ℃ for 12 hours yielded white powders of UiO-66 (Figure II-3a). And solvothermal reaction of $ZrCl_4$, H_2BDC, [5,10,15,20-tetrakis(4-carboxyphenyl)porphyrinato]-Ni(II) (NiTCPP), and BA in DMF at 130 ℃ for 12 hours yielded red powders of

NiTCPP⊂UiO-66. The products remained red after washing with DMF and acetone (Figure II-3a), indicating the presence of NiTCPP, and displayed powder x-ray diffraction (PXRD) patterns consistent with that of phase-pure UiO-66 (Figure II-3b).

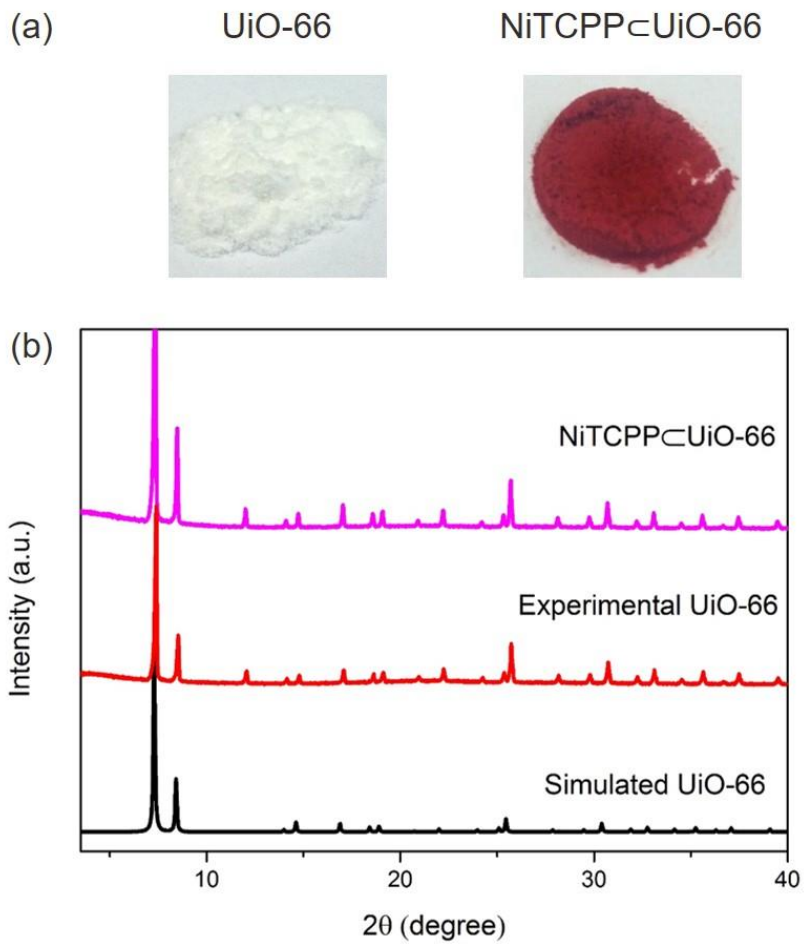

Figure II-3. (a) Photographs of UiO-66 (white) and NiTCPP⊂UiO-66 (red). (b) The PXRD patterns for UiO-66 and NiTCPP⊂UiO-66.

Scanning electron microscopy (SEM) results also confirmed that NiTCPP⊂UiO-66 was phase pure, which showed that the powders were octahedral microcrystals with an even distribution in size (Figure II-4a). The elemental mappings of a single crystal

obtained from energy dispersive X-ray spectroscopy (EDS) demonstrated an even distribution of all the elements (Figure II-4b), especially Zr and Ni, implying that UiO-66 was successfully functionalized with NiTCPP.

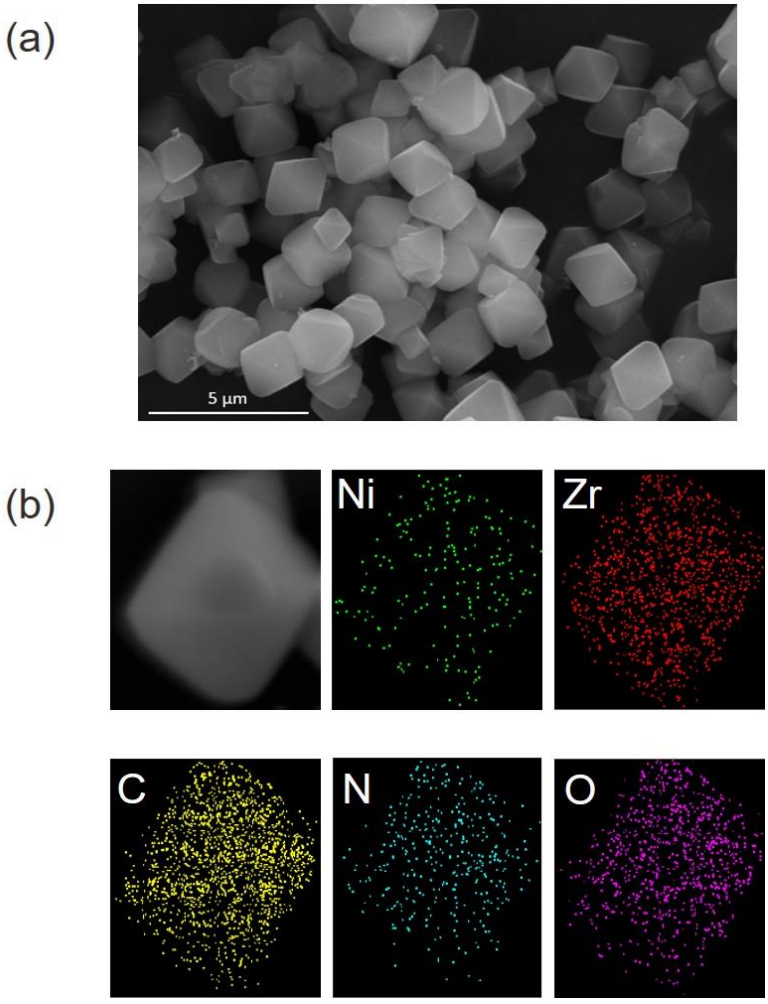

Figure II-4. (a) SEM image of NiTCPP⊂UiO-66. Scale bar: 5 µm. (b) SEM image of a NiTCPP⊂UiO-66 single crystal and the corresponding elemental EDS-mappings.

To assess the permanent porosity of NiTCPP⊂UiO-66, the samples were activated directly upon removal of the solvent and carried out N_2 uptake experiments at 77 K (Figure II-5). Type I isotherms that are typical for microporous solids were

acquired. After functionalization with NiTCPP, the samples showed N_2 uptake of around 260 cm^3 g^{-1} at 1 bar, which is lower than that of the parent MOF (UiO-66) (Figure II-5). The decrease of N_2 uptake confirmed the functionalization of UiO-66 with NiTCPP.

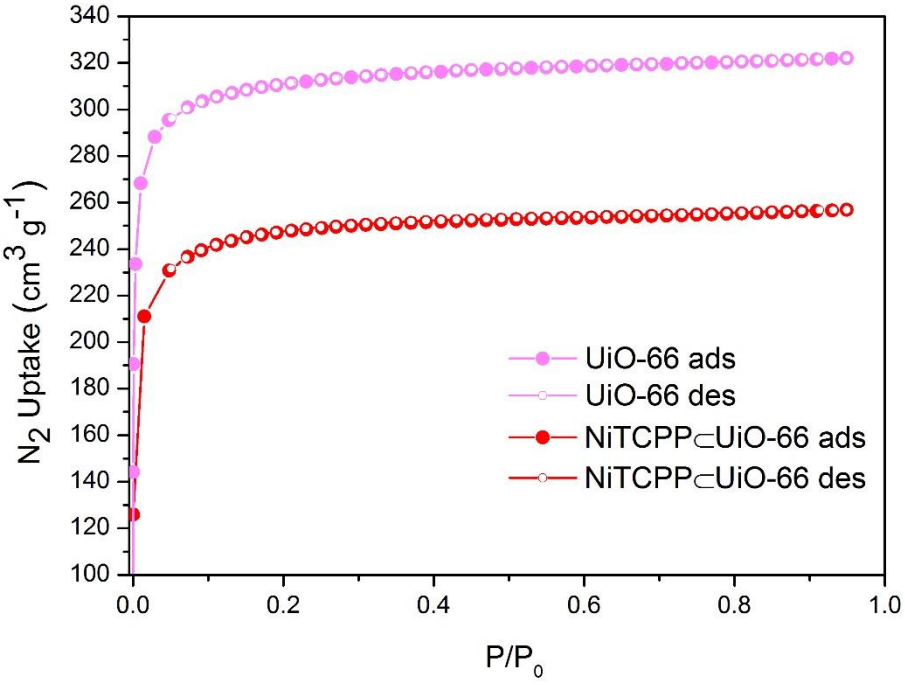

Figure II-5. N_2 adsorption/desorption isotherms of UiO-66 and NiTCPP⊂UiO-66 at 77 K.

Quantitative Analysis. The amount of NiTCPP in the sample was determined by ^1H NMR analysis and EDS analysis. According to EDS analysis, the atomic ratio of Ni to Zr in NiTCPP⊂UiO-66 was calculated to be about 0.05: 1 (Figure II-6, and Table II-1). Since each Zr_6 cluster in UiO-66 is coordinated to a maximum of twelve BDC linkers while each BDC linker is bonded to two Zr_6 clusters, the molar ratio of Zr to BDC in UiO-66 is 1: 1 in theory, which suggests that the atomic ratio of Ni to Zr should be the

same as the molar ratio of NiTCPP to BDC. However, after the samples were digested in HF and dissolved in DMSO-d_6 for ^{1}H NMR test, the integration results from ^{1}H NMR spectra showed that the molar ratio of NiTCPP to BDC was around 0.07: 1 (Figure II-1). Such discrepancy can be ascribed to two aspects. First, UiO-66 generally contains missing-linker defects in the presence of modulating reagent, which results in a lower molar ratio of BDC to Zr compared to that in an ideal crystal without structural defects. Second, NiTCPP in NiTCPP⊂UiO-66 may compete with BDC to coordinate to Zr_6 clusters and therefore leads to further elimination of BDC in the framework. As a result, the atomic ratio of Ni to Zr calculated from EDS data was lower than the molar ratio of NiTCPP to BDC obtained from ^{1}H NMR spectra.

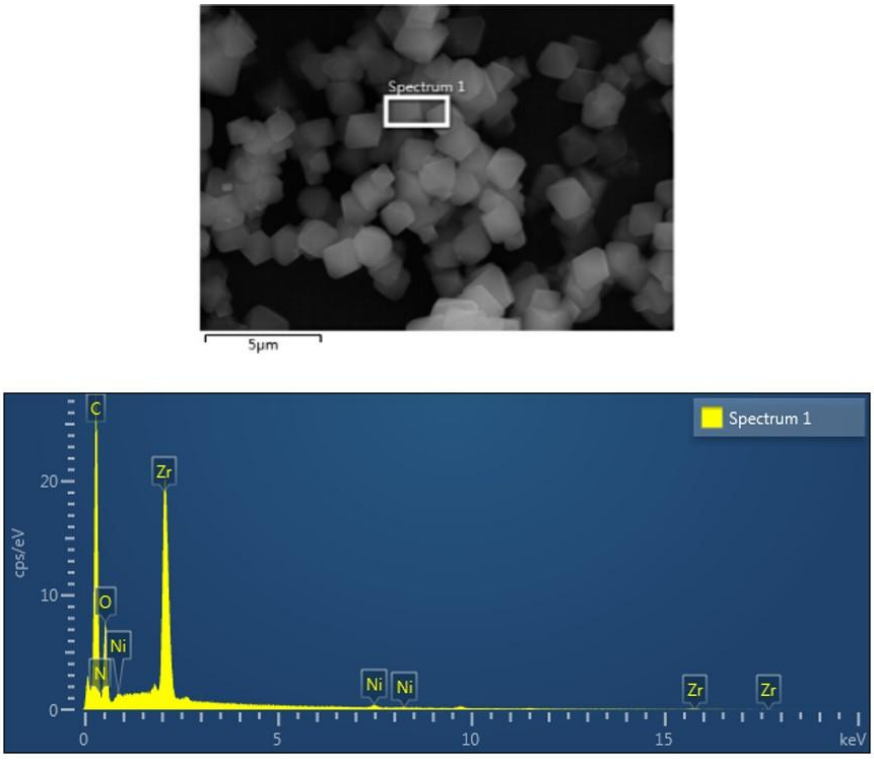

Figure II-6. SEM/EDS analysis for NiTCPP⊂UiO-66.

Table II-1. The atomic ratio of Ni to Zr in NiTCPP⊂UiO-66 obtained from EDS analysis

	Trial 1		Trial 2		Trial 3	
Element	Weight%	Atomic%	Weight%	Atomic%	Weight%	Atomic%
Ni	0.51	0.13	0.41	0.10	0.57	0.15
Zr	17.03	2.86	13.63	2.23	18.53	3.14
	Average Ni: Zr ratio = 0.046: 1					

Calculation of Plausible Chemical Formula. The plausible chemical formula of the obtained sample was calculated based on the EDS data and ^{1}H NMR data. According to EDS data and ^{1}H NMR data, the ratio of Ni to Zr as well as NiTCPP ligand to BDC ligand can be calculated, respectively. And the preliminary chemical formula of the sample can be written as $Zr_6O_4(OH)_4(BDC)_{3.73}(NiTCPP)_{0.28}$. Next, additional hydroxide anions were added to keep the charge balance, which has been reported by Yaghi's group to achieve the charge balance of UiO-66 with defects.[75] Finally, the plausible chemical formula of the synthesized NiTCPP⊂UiO-66 sample can be expressed as $Zr_6O_4(OH)_8(BDC)_{3.73}(NiTCPP)_{0.28}$ (C: 32.6%, H: 1.9%, N: 1.0% were calculated from the calculated chemical formula while C: 32.6%, H: 2.0%, N: 1.2% were obtained from the elemental analysis).

Tune the Amount of Introduced Porphyrin. In the next step, different amounts of NiTCPP were used for the synthesis of NiTCPP⊂UiO-66 and the atomic ratio of Ni to Zr in the product was tested. As shown in Figure II-7, the amount of incorporated

NiTCPP can be gradually increased by increasing the amount of NiTCPP ligand used in the synthesis. This provides possibilities to optimize the performance of the MOF when it is related to the concentration of the functionality.

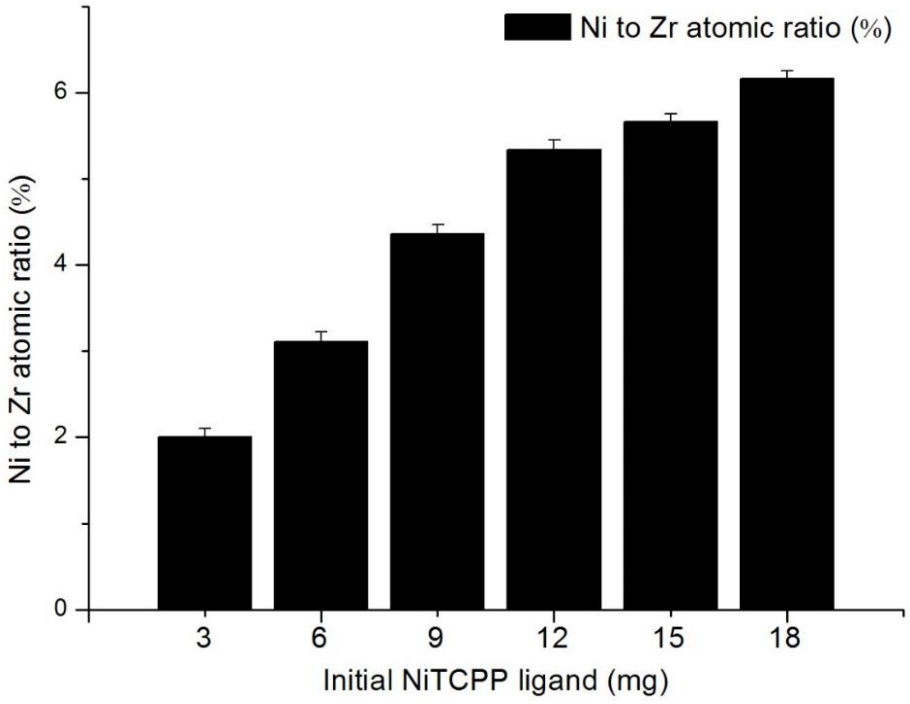

Figure II-7. The atomic ratio of Ni to Zr in NiTCPP⊂UiO-66 under different synthetic conditions.

When the amount of NiTCPP added in the system increased to a certain value, some new peaks appeared in the PXRD pattern of the product, indicating the formation of impure phases along with the UiO-66 phase (Figure II-8). This result shows that UiO-66 has a certain range of tolarence to NiTCPP ligands. As a result, the synthetic

conditions (e.g. the ratio of the ligands) should be carefully selected to guaratee the phase purity of the product.

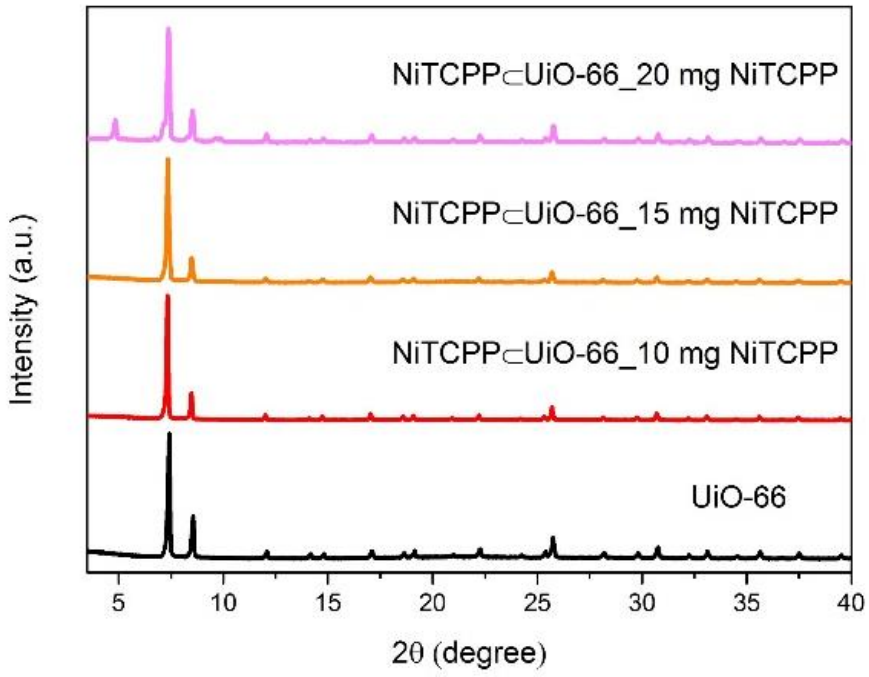

Figure II-8. The PXRD patterns of different products synthesized with different amounts of NiTCPP added in the system.

Stability Tests. Since many studies have shown that UiO-66 has very high thermal and chemical stability, we carried out experiments to study the stability of obtained porphyrin-functionalized UiO-66. About 10.0 mg of the sample was heated on the Shimadzu TGA-50 instrument from room temperature to 700 °C at a ramp rate of 2 °C/min under nitrogen flow of 25 mL/min. The decomposition of material was observed at around 400 °C (Figure II-9), showing high thermal stability of NiTCPP⊂UiO-66.

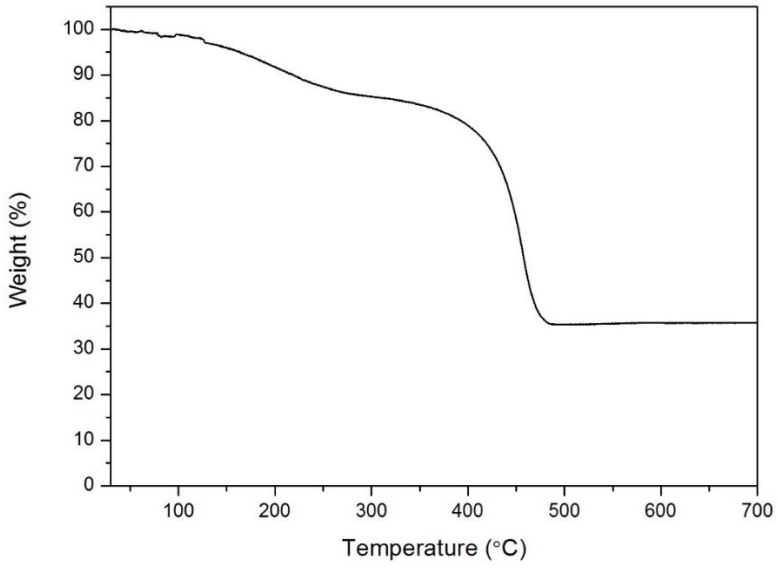

Figure II-9. The TGA analysis of NiTCPP⊂UiO-66.

The chemical stability of NiTCPP⊂UiO-66 was investigated by immersing 100 mg of samples in aqueous solutions with a series of conditions (1 M HCl, 2 M HCl, 6 M HCl, deionized water, and 1 mM NaOH). The solutions stayed colorless after these treatments, suggesting no leaching of NiTCPP under these conditions. In addition, their PXRD patterns remained intact (Figure II-10a), indicating that no framework collapse or phase transition occurred during the stability test. More importantly, the N_2 adsorption isotherms of these samples after the treatment further demonstrated that NiTCPP⊂UiO-66 was stable under these harsh conditions (Figure II-10b). These stability tests confirmed that the MOFs maintained the stability of UiO-66 after functionalized with NiTCPP. Therefore, the high stability of UiO-66 and was maintained very well by

applying our method to functionalize the MOF, which is promising for MOFs functionalization towards applications.

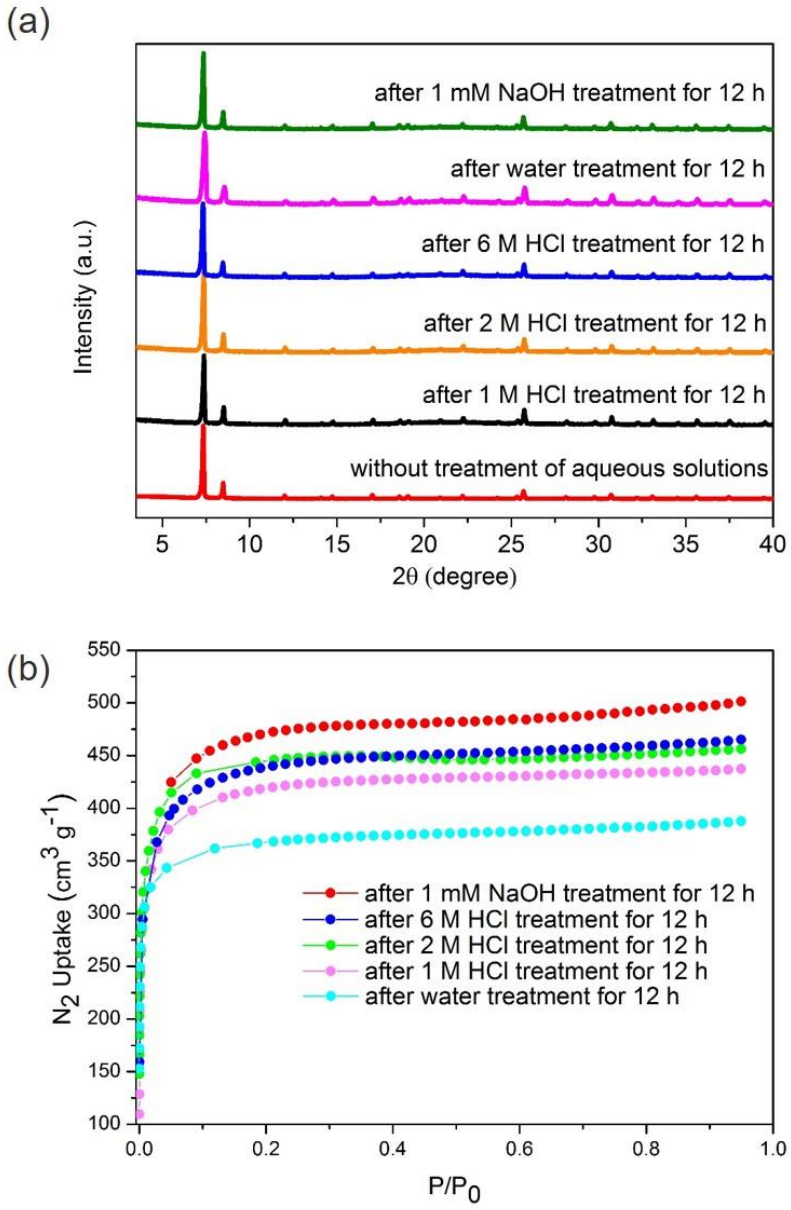

Figure II-10. (a) PXRD patterns for NiTCPP⊂UiO-66 before and after treatment with different aqueous conditions. (b) N_2 adsorption isotherms of NiTCPP⊂UiO-66 at 77 K, 1atm before and after treatment with different aqueous conditions.

The chemical stability of NiTCPP⊂UiO-66 was further compared with two reported porphyrin MOFs (PCN-222 and PPF-5). PPF-5 has a pillar-layered structure, which makes it possible to incorporate additional functionality through the pillars.[44] Therefore, PPF-5 provides an interesting platform to investigate the advanced applications of porphyrins. On the other hand, PCN-222 contains a single type of porphyrin ligand and exhibits relatively higher chemical stability than PPF-5.[73] However, after immersing PCN-222 in 1 mM NaOH for 12 h, its change in PXRD pattern demonstrated that the crystallinity was lost under this base condition (Figure II-11). For PPF-5, the framework collapsed even in 0.1 mM NaOH aqueous solution (Figure II-11). These results showed that NiTCPP⊂UiO-66 synthesized by our method was chemically more stable than PCN-222 and PPF-5.

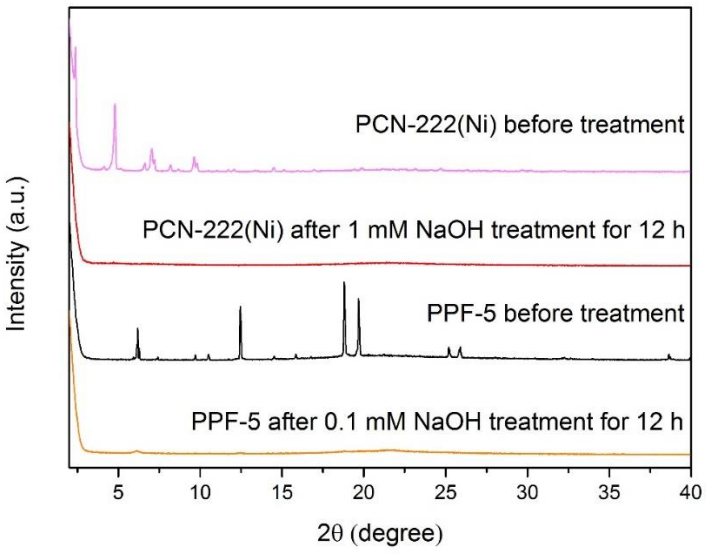

Figure II-11. PXRD patterns for PCN-222(Ni) and PPF-5 before and after the treatment of NaOH aqueous solutions.

Control Experiments. To investigate wheather the porphyrin functionality was only attached on the surface of UiO-66 instead of integrated in the framework, UiO-66 was synthesized under the same condition as NiTCPP⊂UiO-66, except that no NiTCPP was added in the system. Then, the obtained UiO-66 and NiTCPP was mixed in DMF solution for 12 h. The obtained powders with light pink color exhibited the PXRD pattern similar to that of UiO-66, indicating that the framework was well maintained after the PSM process (Figure II-12). However, the amount of NiTCPP was too small to be tested by ^{1}H NMR experiment, suggesting that the light color is most likely because of the attachment of NiTCPP on the surface of UiO-66.

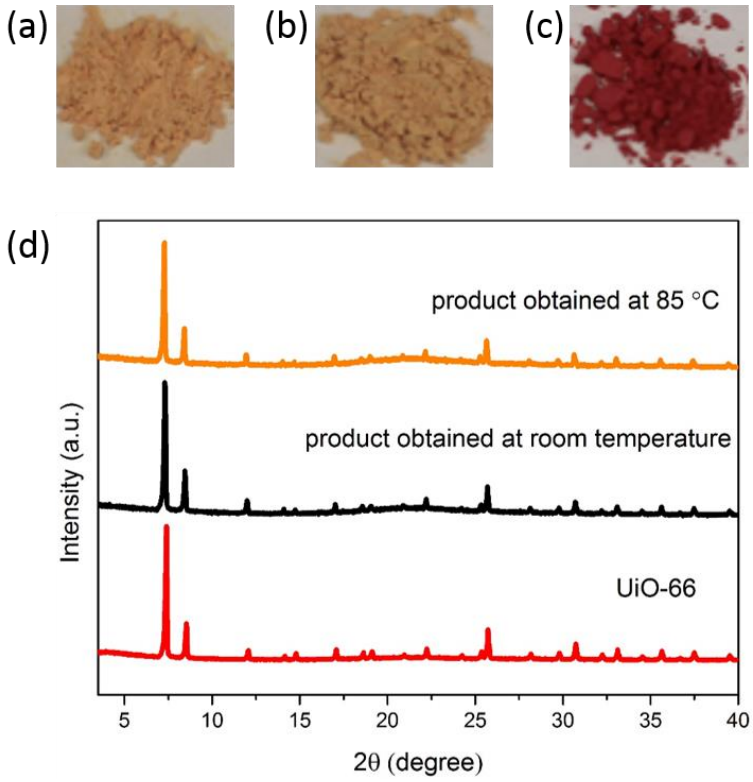

Figure II-12. Photographs of products obtained by (a) PSM at room temperature; (b) PSM at 85 °C, and (c) one-pot synthesis. (d) Their corresponding PXRD patterns.

In order to understand the different products obtianed by our one-pot synthesis and PSM process,[76] the structure of UiO-66 and the size of porphyrin ligand were analyzed. UiO-66 contains smaller pores with a diameter of 7.5 Å (Figure II-13a) and larger pores with a diameter of 12 Å (Figure II-13b). On the other hand, NiTCPP ligand has a square shape with 20 Å in the length of the diagonal (Figure II-13c). Due to larger size of NiTCPP ligand, it it difficult diffuse into the framework of UiO-66 during PSM process. Compared with PSM method, our one-pot synthesis can greatly avoid the size limitation of UiO-66 for NiTCPP incorporation. In addition, the small pore windows will prevent the leaching of NiTCPP ligand after its incorporation, which is much like a "ship in a bottle".

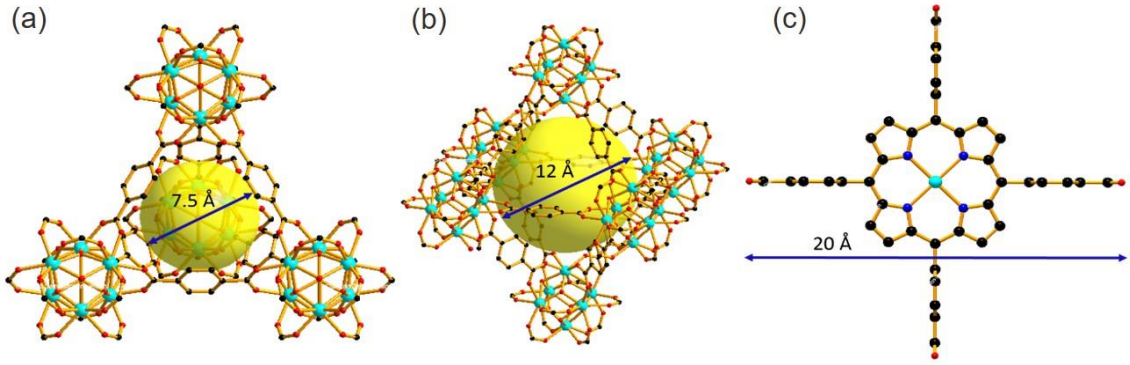

Figure II-13. (a) The tetrahedral pore and (b) the octahedral pore in UiO-66. (c) The structure of NiTCPP ligand.

In the next step, a control experiment was designed to study whether NiTCPP was introduced through connecting to the Zr_6 cluster or just trapped inside the pore of UiO-66. After replacing NiTCPP with [5,10,15,20-tetrakis(4-

bromophenyl)porphyrinato]-Ni(II) (NiTBPP), white powders were obtained (Figure II-14b) instead of red powders when using NiTCPP for the synthesis (Figure II-14a). Despite similar size of NiTBPP and NiTCPP, the difficulty in introducing NiTBPP into the framework of UiO-66 excluded the possibility that NiTCPP was purely trapped in the pore, indicating that the carboxylates on NiTCPP ligand most likely participated the coordination during the formation of UiO-66.

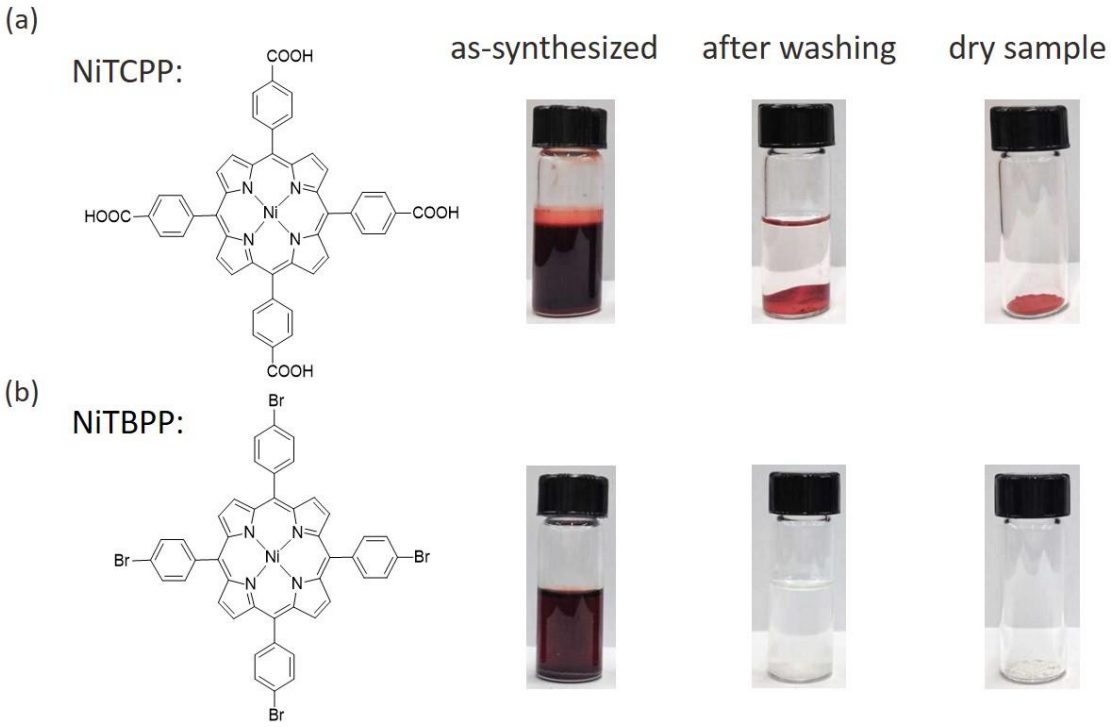

Figure II-14. Photographs of the products obtained by using (a) NiTCPP and (b) NiTBPP for the functionalization of UiO-66.

After carrying out above experiments, we tried to understand the chemistry behind our method and explain these results from both thermodynamic and kinetic perspectives. Since the concentration of BDC was much higher than NiTCPP in the

reaction system, the nucleation of UiO-66 was dominating. However, NiTCPP in the system can compete with BDC to connect to the Zr_6 cluster during the nucleation process of UiO-66 and thus participate in its growth, creating some defects in the framework. Due to high symmetry and connectivity of the Zr_6 cluster, the framework of UiO-66 remained intact even after partially occupied by NiTCPP ligand. On the other hand, the initial nucleation of possible impurity phases (e.g. porphyrin MOFs) took longer time due to very low concentration of NiTCPP. Moreover, the nucleation of UiO-66 consumed Zr species and further inbibited the formation of impurities. Therefore, UiO-66 functionalized with NiTCPP while maintaining the phase purity was obtained by our one-pot synthetic approach (Figure II-15).

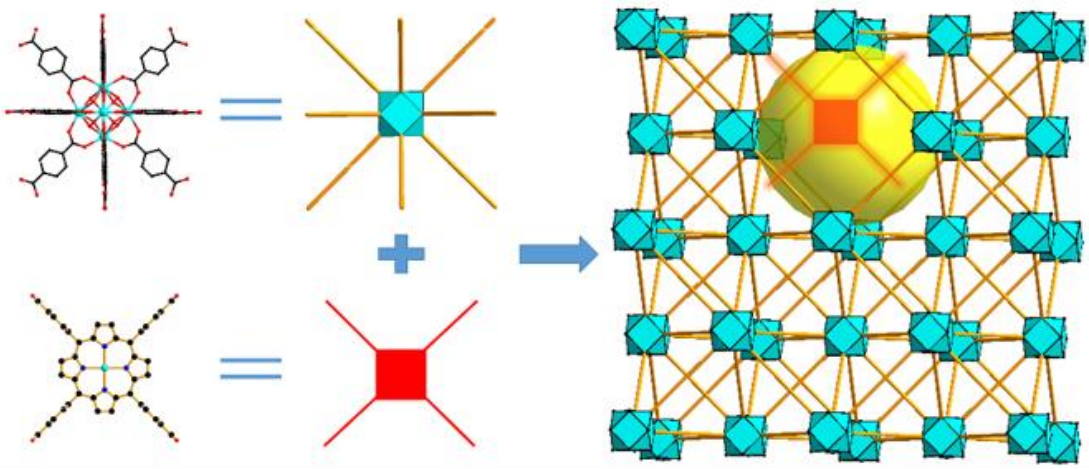

Figure II-15. Schematic illustration of UiO-66 functionalized with NiTCPP through one-pot reactions**.**

Functionalization of UiO-66 with Various Porphyrin Ligands. Next, this method was applied to modify UiO-66 with other functionalities by using porphyrin

ligands with different metals in the middle (e.g. Fe, Mn, Cu, Zn, and Co) for the synthesis. Powders with different colors were obtained (Figure II-16a), which exhibited PXRD patterns in consistent with that of pristine UiO-66 (Figure II-16b).

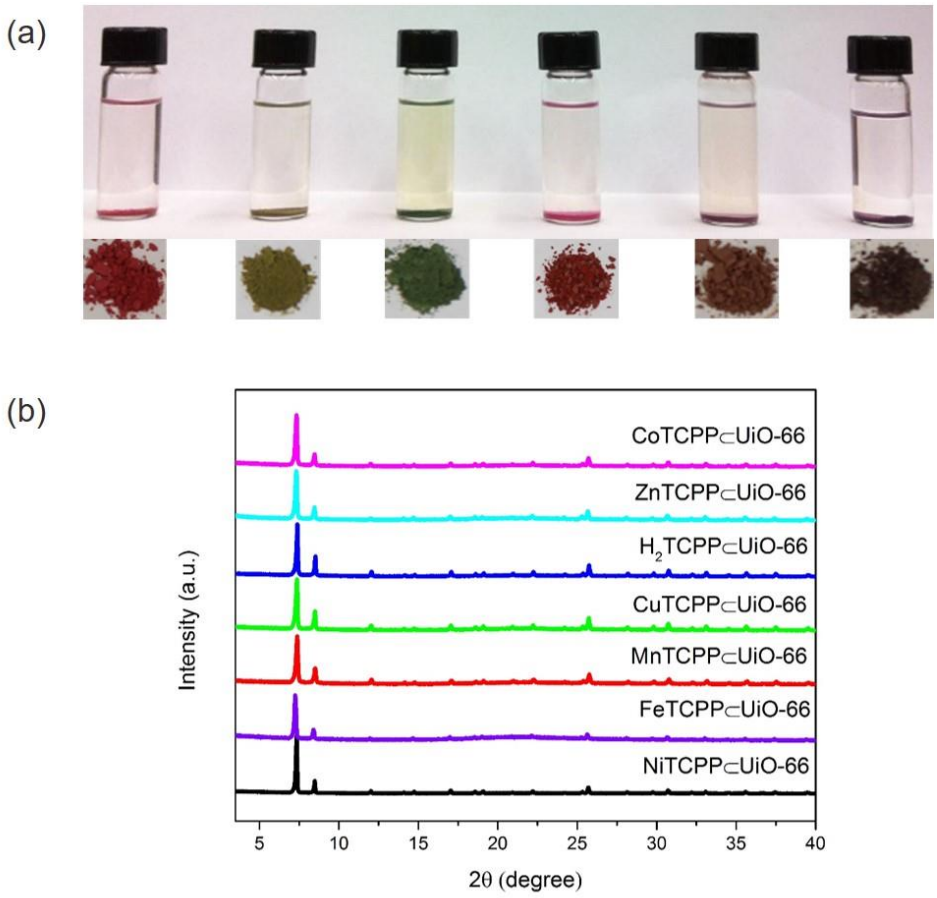

Figure II-16. (a) Photographs of NiTCPP⊂UiO-66, FeTCPPCl⊂UiO-66, MnTCPPCl⊂UiO-66, CuTCPP⊂UiO-66, H_2TCPP⊂UiO-66, and ZnTCPP⊂UiO-66 from left to right. (b) PXRD patterns of NiTCPP⊂UiO-66, FeTCPPCl⊂UiO-66, MnTCPPCl⊂UiO-66, CuTCPP⊂UiO-66, H_2TCPP⊂UiO-66, ZnTCPP⊂UiO-66, and CoTCPP⊂UiO-66 from left to right.

Introduction of a Secondary Functionality. After functionalizing UiO-66 with different porphyrins successfully, we tried to introduce a secondary functionality into

UiO-66 through this one-pot synthetic strategy. Firstly, the amino group was selected as a candidate because many studies have shown that MOFs functionalizaed with amino groups exhibit many interesting features, including increased CO_2 uptake,[77-78] CO_2 selectivity over N_2 and CH_4,[79-82] and catalytic activity.[83] Moreover, amino groups can undergo various organic transformation reactions, which is useful for studying MOF applications.[84-85] By replacing BDC with NH_2-BDC for the synthesis, red powders of NiTCPP⊂UiO-66-NH_2 was synthesized and characterized. The phase purity of the product was verified by PXRD (Figure II-20a) and SEM (Figure II-17a). An even distribution of all the elements was shown by EDS mappings of a single crystal (Figure II-17b).

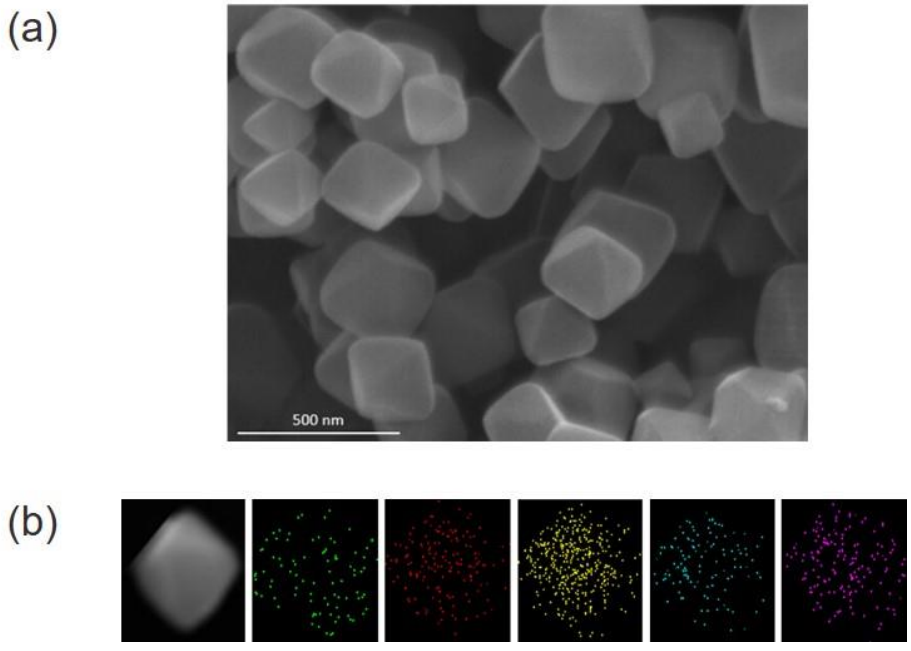

Figure II-17. (a) SEM image of NiTCPP⊂UiO-66-NH2. (b) SEM image of NiTCPP⊂UiO-66-NH2 single crystal and EDS mappings of element Ni, Zr, C, N, O from left to right.

The product exhibited N_2 uptake of about 250 cm^3 g^{-1} at 77 K, 1 bar (Figure II-18a). TGA analysis showed that the sample was stable up to 360 °C (Figure II-18b). Moreover, the sample was stable in a series of aqueous solutions (e.g. 6 M HCl and 10 mM NaOH), which was indicated by the PXRD patterns (Figure II-18c) and N_2 adsorption isotherms (Figure II-18d) obtained in the chemical stability tests. These results confirmed that the stability of UiO-66 was well maintained after incorporation of a secondary functionality (amino group) into the framework.

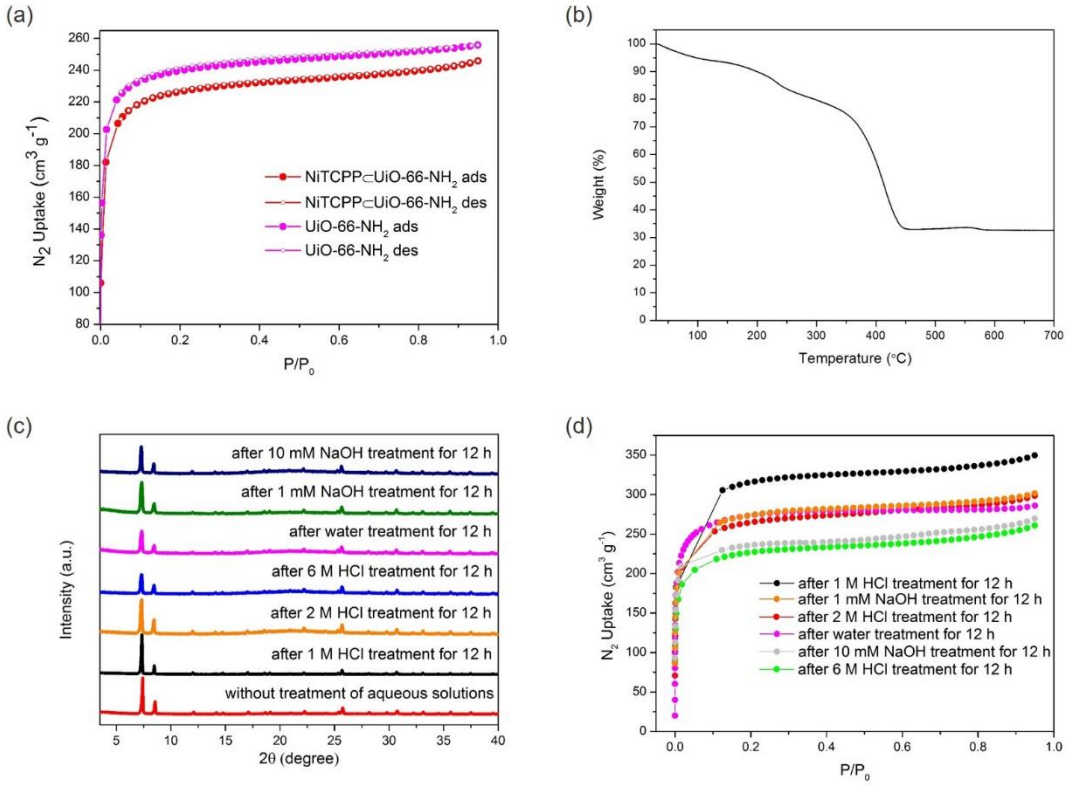

Figure II-18. (a) N_2 adsorption isotherms. (b) TGA analysis of NiTCPP⊂UiO-66-NH_2. (c) PXRD patterns and (d) N_2 adsorption isotherms of NiTCPP⊂UiO-66-NH_2 after treatment with different aqueous solutions.

Construction of Multivariate UiO-66. One of the major advantages of MOFs over other conventional porous materials is the synthetic versatility arises from choosing diverse organic ligands for the synthesis. Given that, a series of functionalities were selected to incorporate into UiO-66 by our one-pot synthetic strategy. Through the combination of porphyrin moieties with different metals in the center (e.g. Ni, Fe, Mn, Cu, Zn, and Co) as well as BDC and its derivatives (e.g. hydroxyl group, methyl group, sulfonic group, carboxyl group, and azide group) (Figure II-19), UiO-66 functionalized with various functionalities were synthesized successfully, including X⊂UiO-66, X⊂UiO-66-NH_2, X⊂UiO-66-2,5-$(OH)_2$, X⊂UiO-66-2,5-$(CH_3)_2$, X⊂UiO-66-SO_3H, X⊂UiO-66-2,5-$(COOH)_2$, and X⊂UiO-66-N_3 (X = NiTCPP, FeTCPPCl, MnTCPPCl, CuTCPP, H_2TCPP, ZnTCPP, and CoTCPP) (Figure II-20). The PXRD patterns of these products remained the same as that of pristine UiO-66 (Figure II-21).

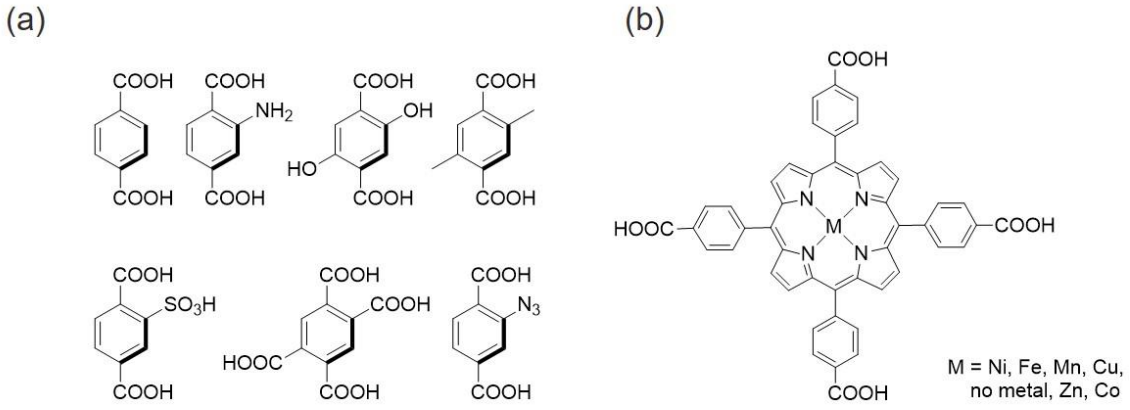

Figure II-19. Chemical structures of (a) BDC moieties and (b) porphyrin moieties selected for synthesizing UiO-66 with multiple functionalities.

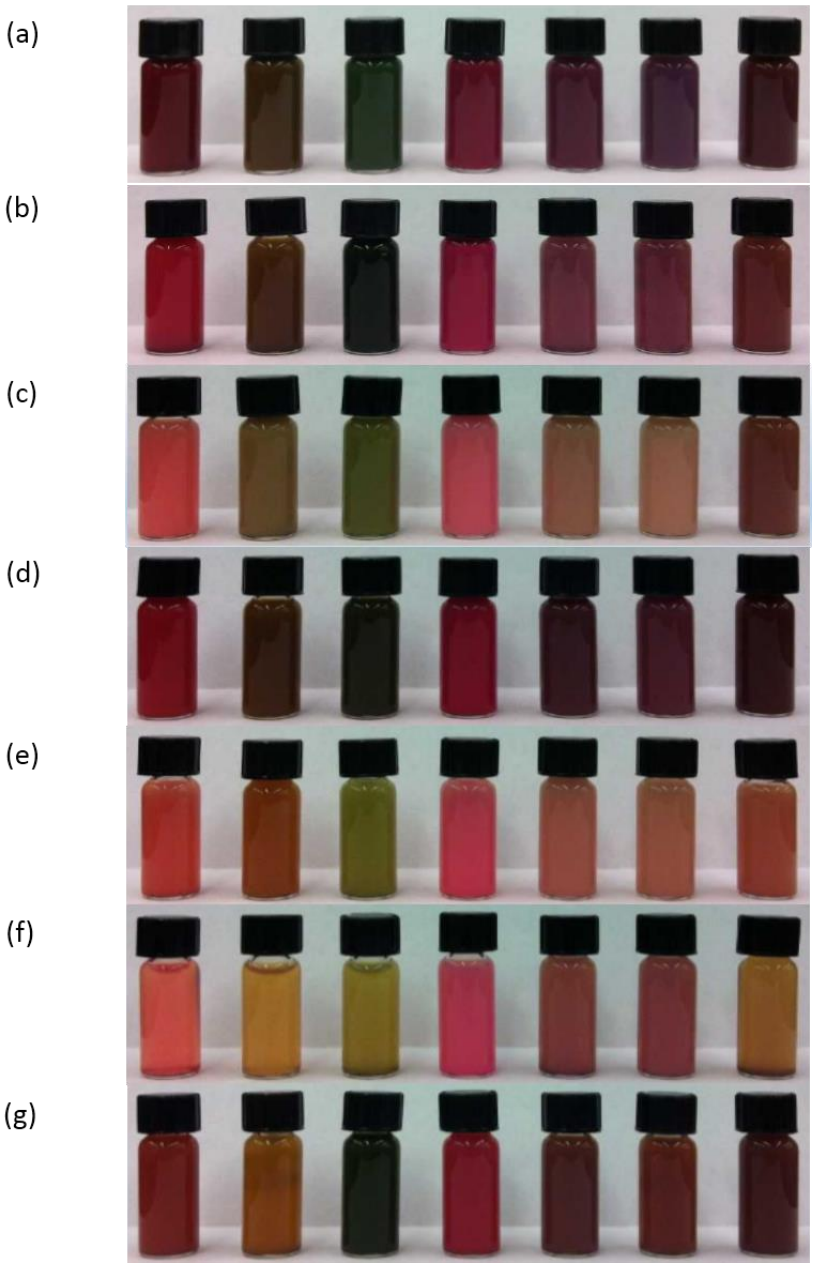

Figure II-20. Photographs of (a) X⊂UiO-66, (b) X⊂UiO-66-NH_2, (c) X⊂UiO-66-2,5-$(OH)_2$, (d) X⊂UiO-66-2,5-$(CH_3)_2$, (e) X⊂UiO-66-SO_3H, (f) X⊂UiO-66-2,5-$(COOH)_2$, and (g) X⊂UiO-66-N_3 (X = NiTCPP, FeTCPPCl, MnTCPPCl, CuTCPP, H_2TCPP, ZnTCPP, and CoTCPP from left to right).

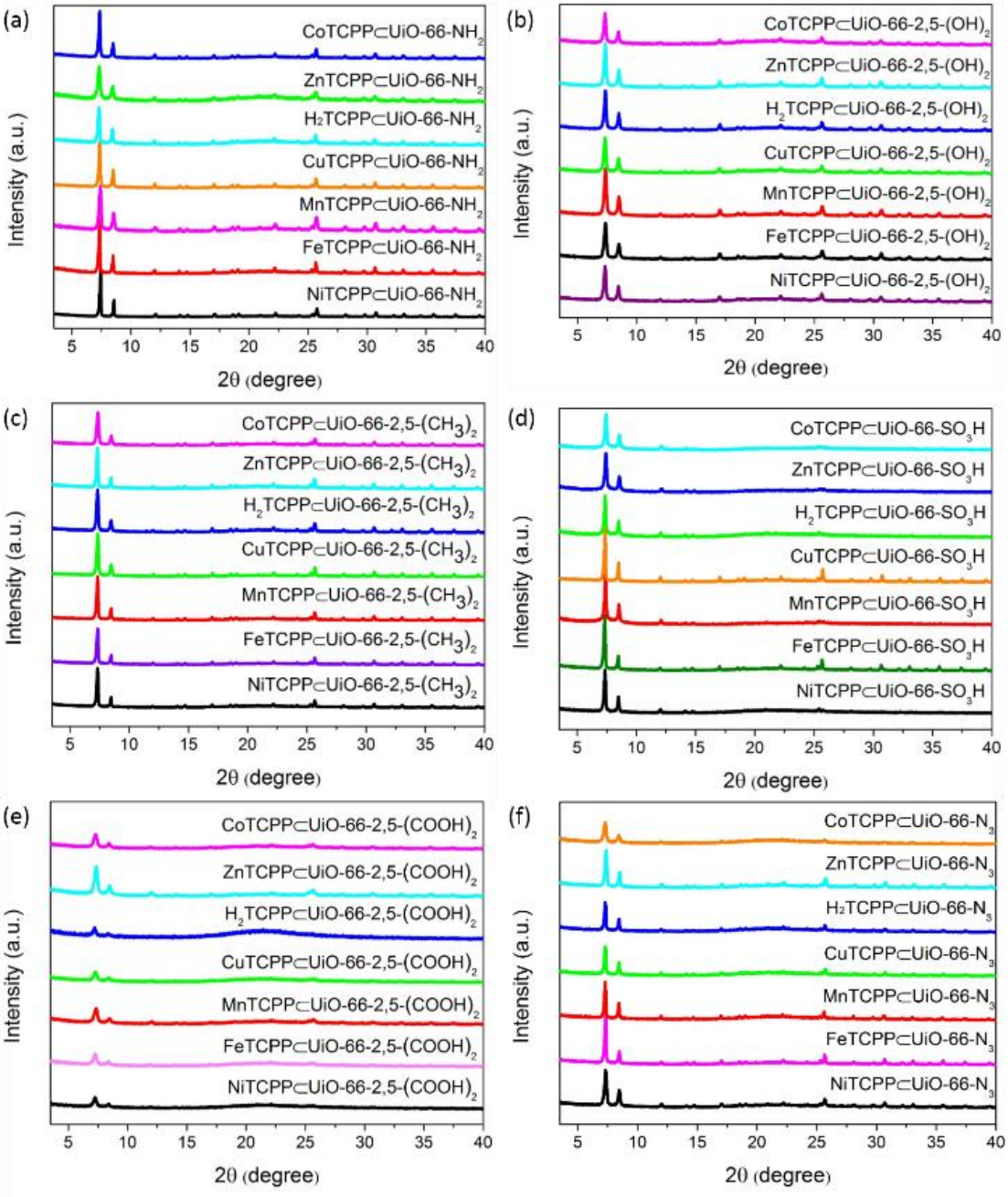

Figure II-21. The PXRD patterns for (a) X⊂UiO-66-NH_2, (b) X⊂UiO-66-2,5-$(OH)_2$, (c) X⊂UiO-66-2,5-$(CH_3)_2$, (d) X⊂UiO-66-SO_3H, (e) X⊂UiO-66-2,5-$(COOH)_2$, and (f) X⊂UiO-66-N_3 (X = NiTCPP, FeTCPP, MnTCPP, CuTCPP, H_2TCPP, ZnTCPP, and CoTCPP).

2.4 Conclusions

A facile one-pot synthetic strategy was demonstrated to synthesize stable UiO-66 with multiple functionalities by mixing ditopic BDC ligands and tetratopic porphyrin ligands. Compared to conventional mixed ligand strategy, ligands of different length, geometry, and connectivity were used in a one-pot synthesis, and the crystal structure, morphology, and ultrahigh chemical and thermal stability of UiO-66 were well preserved after functionalization. The amount of integrated porphyrin can be gradually tuned by changing the amount of porphyrin used for the synthesis. Due to size limitation, incorporation of porphyrin into UiO-66 by PSM method cannot be achieved. Taking advantage of the synthetic versatility, 49 MOFs with multiple functionalities were synthesized through mixing various porphyrin moieties and BDC derivatives. This synthetic strategy combines the framework robustness of UiO-66 as well as the desired functionalities, which allows for further investigation of the chemistry within the framework. Therefore, this strategy provides a facile route to multi-functionalize stable MOFs for a wide scope of potential applications.

CHAPTER III

IN SITU SECONDARY LIGAND INCORPORATION STRATEGY TOWARDS MULTIFUNCTIONAL UIO SERIES OF MOFS

3.1 Introduction

Generally, MOFs are synthesized by the solvothermal reaction of inorganic metal salts and organic ligands in the organic solvent.[39, 86] Carboxylic acids are one of the most commonly used organic ligands to coordinate to the metal clusters to form an ordered porous structure. However, it is very difficult to control the growth of MOFs during the solvothermal reaction process, which gives rise to many problems: (i) hard to predict the structure of the MOF product; (ii) formation of MOFs containing mixed phases; (iii) formation of polycrystalline or even amorphous products. To address these issues, the reaction conditions have to be carefully adjusted, including the organic solvent, reaction temperature, reaction time, reaction pressure, the concentration of each component, the ratio of metal species to the organic ligands, and even the anions of the metal salts.[87] Therefore, it is very time-consuming and tedious to optimize this series of reaction parameters.

To solve this problem, a method called “reticular synthesis” have been reported in recent years, which could help tune the MOF structure and pore size systematically and thus eliminate unnecessary investigations to save a tremendous amount of time and effort. [1, 88-91] By using the same inorganic metal species and the organic ligand of the same shape and connectivity but different length, a new MOF with a similar structure

but different pore size can be synthesized. For example, MOF-5 is constructed from Zn_4O clusters and ditopic BDC ligands. By replacing the BDC ligand with a longer ditopic 2,6-naphthalenedicarboxylate (NDC) ligand, IRMOF-8 with the structure similar to MOF-5 but contains larger pores have been synthesized.[4]

For highly stable Zr-MOFs, application of reticular chemistry to synthesize MOFs have also been reported so far. For example, UiO-66 contains 12-connected Zr_6 clusters and ditopic BDC ligands. By using longer ditopic 4,4'-biphenyldicarboxylate (BPDC) ligand, UiO-67 isostructural to UiO-66 have been obtained.[46] From UiO-66 to UiO-67, the size of tetrahedral pores and octahedral pores increased from 7.5 Å to 12 Å, and 12 Å to 16 Å, respectively. Although reticular synthesis provides a useful tool to investigate highly stable Zr-MOFs of UiO-typed structures, the presence of only a single ligand in these Zr-MOFs limits the functionality that can be incorporated into the framework.[46, 92-96]

In this work, taking advantage of the reticular chemistry, porphyrin ligands have been introduced into highly stable UiO series of MOFs (e.g. UiO-66, UiO-67, and UiO-68) by in situ secondary ligand incorporation (ISLI) strategy. The amount of incorporated porphyrin can be gradually adjusted. And the original crystal structure, morphology, and high chemical stability of the parent Zr-MOFs were well preserved after mixing ditopic ligands and tetratopic ligands to functionalize these MOFs. The reaction conditions (e.g. the amount of organic ligands and acid) were carefully selected to control the reaction towards formation of single-phased UiO series of MOFs with incorporated functionality. Moreover, both experimental and computational studies were

carried out to investigate the thermodynamic and kinetic aspects of the ISLI strategy.

3.2 Experimental Section

Materials and Instrumentation. Commercially available reagents and solvents were used as received without further purification. Tetrakis(4-carboxyphenyl)porphyrin (H_2TCPP), [5,10,15,20-tetrakis(4-carboxyphenyl)porphyrinato]-Mn(III) chloride (MnTCPPCl), [5,10,15,20-tetrakis(4-carboxyphenyl)porphyrinato]-Fe(III) chloride (FeTCPPCl), [5,10,15,20-tetrakis(4-carboxyphenyl)porphyrinato]-Zn(II) (ZnTCPP), [5,10,15,20-tetrakis(4-carboxyphenyl)porphyrinato]-Ni(II) (NiTCPP), [5,10,15,20-tetrakis(4-carboxyphenyl)porphyrinato]-Co(II) (CoTCPP), [5,10,15,20-tetrakis(4-carboxyphenyl)porphyrinato]-Cu(II) (CuTCPP) were synthesized according to the procedure in previous reports with slight modifications.[73]

Powder X-ray diffraction (PXRD) experiment was carried out with a BRUKER D8-Focus Bragg−Brentano X-ray powder diffractometer equipped with a Cu-sealed tube (λ = 1.54178) at 40 kV and 40 mA. Thermogravimetric analysis (TGA) were conducted on a Shimadzu TGA-50 thermogravimetric analyzer at a ramp rate of 2 °C/min in a flowing nitrogen atmosphere. Nuclear magnetic resonance (NMR) spectra were collected on a Mercury 300 spectrometer. Inductively coupled plasma (ICP) tests were conducted on a Perkin Elmer Optima 8000 ICP spectrometer. N_2 adsorption-desorption isotherms were measured on a Micrometritics ASAP 2020 system at 77 K. The sample was activated by solvent exchange (in several cycles using fresh acetone), followed by degassing at elevated temperature (100 °C) for 5 h. Scanning electron microscope (SEM) analysis was performed on QUANTA 450 FEG and energy dispersive X-ray

spectroscopy (EDS) analysis was carried out by X-Max20 with Oxford EDS system equipped with X-ray mapping.

Synthesis of Azobenzene-4,4'-Dicarboxylic Acid (H_2AZDC). As shown in Scheme III-1, azobenzene-4,4'-dicarboxylic acid (H_2AZDC) was synthesized according to the reference.[97] 4-Nitrobenzoic acid (10.0 g, 59.9 mmol) and 50 mL water were added to a three-neck round-bottom flask attached to a reflux condenser. A 5.6 M solution of sodium hydroxide was slowly added (150 mL total) to the reaction flask and the resulting solution was heated to 50 °C. Next, a hot glucose solution (61.5 g in 200 mL water) was slowly added to the reaction that was kept at a constant 50 °C. Airflow was continuously passed through the solution. Orange precipitate formed initially, and the solution's color gradually turned brown upon more addition of glucose. The solution was left to react at 50 °C overnight, which resulted in a dark-colored solution with noticeable precipitate the following day. The reaction mixture was subsequently filtered. The solid was then dissolved in water and acidified with concentrated HCl to afford an orange precipitate. The final product was filtered once again, washed with copious amounts of water, and dried at 60 °C to yield azobenzene-4,4'-dicarboxylic acid (H_2AZDC) (6.8 g, 85%). ^{1}H NMR (DMSO-d_6, 300 MHz): δ 8.01-8.03 (d, 4H), δ 8.16-8.18 (d, 4H), δ 13.21 (brs, 2H).

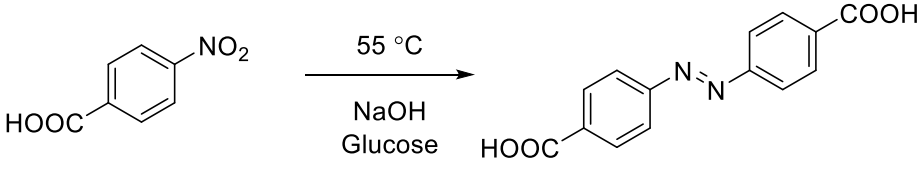

Scheme III-1. Synthesis of H_2AZDC ligand**.**

Synthesis of 4,4'-(Ethyne-1,2-Diyl)dibenzoic Acid (H_2EDDB). As shown in Scheme III-2, 4,4'-(ethyne-1,2-diyl)dibenzoic acid (H_2EDDB) was synthesized according to the reference.[98]

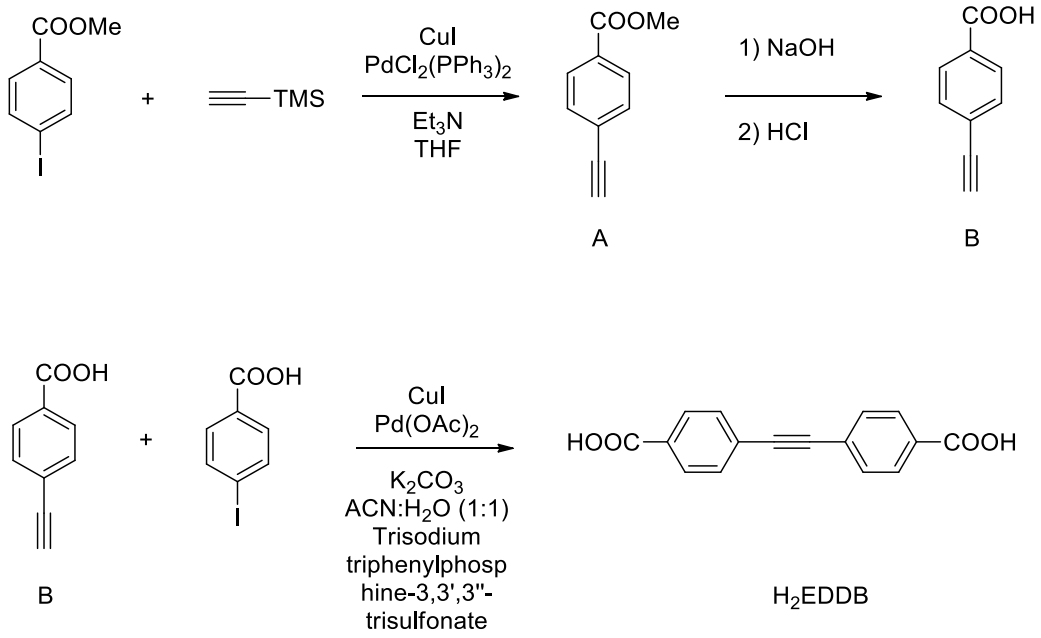

Scheme III-2. Synthesis of H_2EDDB ligand**.**

Synthesis of A: methyl-4-iodobenzoate (2.6 g, 10 mmol) and $PdCl_2(PPh_3)_2$ (0.14 g, 2 mol%) were placed in a two-necked flask and purged with N_2. THF (20 mL) was purged with N_2 and added via syringe. The reaction mixture was stirred until all solids had dissolved. Trimethylsilylacetylene (1.8 mL, 12.5 mmol) and triethylamine (1.7 mL, 12.5 mmol) were added, followed by copper(I) iodide (0.076 g, 4 mol%). The reaction mixture was stirred under N_2 for 4 h at room temperature, before being transferred to a

round-bottomed flask. The THF was almost completely removed by rotary evaporation and hexane (50 mL) was added to the remaining mixture. Solid $Et_3N{\cdot}HI$ was removed by filtration through Celite, which was washed with hexane (3 × 25 mL). The filtrate and washings were then transferred to a separating funnel and washed with water (50 mL). The hexane layer was collected, dried with sodium sulfate and decanted into a round-bottomed flask. The hexane was removed by rotary evaporation and methanol (20 mL) was added to re-dissolve the remaining solid. K_2CO_3 (0.15 g) was then added and the reaction mixture was stirred for 90 min at room temperature. The methanol was almost completely removed by rotary evaporation and water (50 mL) was added to the remaining mixture. The product was extracted from this mixture with diethyl ether (3 × 30 mL). The organic extracts were washed with water (3 × 30 mL), followed by brine (20 mL). The organic extracts were collected, dried with sodium sulfate and decanted into a round-bottomed flask. The diethyl ether was removed by rotary evaporation and the remaining solid was purified on a silica column, yielding methyl-4-ethynylbenzoate as a pale orange powder (1.5 g, 98%). ^{1}H NMR ($CDCl_3$, 300 MHz), δ 3.23 (s, 1H), 3.92 (s, 3H), 7.55 (d, 2H), 7.99 (d, 2H).

Synthesis of B: methyl-4-ethynylbenzoate (1.43 g, 8.9 mmol), 1M aqueous sodium hydroxide (10.3 mL, 10.3 mmol) and 1:1 of methanol:THF (20 mL) were added to a round bottomed flask and stirred for 2 h at room temperature. The solvents were removed by rotary evaporation and water (50 mL) was added to the remaining solid. The mixture was filtered through Celite and washed through with water. The filtrate was transferred to a conical flask and acidified with 1M HCl to precipitate the product, which

was isolated by filtration and washed with water (3 × 30 mL). The solid was dried, yielding 4-ethynylbenzoic acid as a pale orange powder with a 98% yield.

Synthesis of H_2EDDB: 4-ethynylbenzoic acid (0.410 g, 2.8 mmol), 4-iodobenzoic acid (0.690 g, 2.8 mmol), K_2CO_3 (1.16 g, 8.4 mmol), $Pd(OAc)_2$ (0.032 g, 5mol%) and trisodium triphenylphosphine-3,3',3''-trisulfonate (0.350 g, 25 mol%) were placed in a two-necked flask and purged with N_2. A 1:1 mixture of acetonitrile and water (100 mL) was purged with nitrogen and added via syringe. The reaction mixture was stirred until all solids had dissolved. The mixture was then heated to 50 °C in an oil bath. Copper(I) iodide (0.053 g, 10 mol%) was added and the mixture was stirred under N_2 for 24 h at 50 °C. The solvent was removed under vacuum and water (100 mL) added. The solution was filtered to remove any unwanted copper iodide or copper compounds that may have been formed. The filtrate was transferred to a conical flask and acidified with 1M HCl to precipitate the product. The solid was separated by filtration and the product washed with water (3 × 50 mL). The isolated solid was then re-dissolved in hot DMF and filtered hot, then washed with further DMF. The filtrate was allowed to cool, and the product precipitated on cooling as a white powdery solid with a 90% yield. ^{1}H NMR ($CDCl_3$, 300 MHz), δ 7.52 (d, 4H), 7.93 (d, 4H).

Synthesis of 2',3',5',6'-Tetramethyl-(1,1':4',1''-Terphenyl)-4,4''-Dicarboxylic Acid (H_2TPDC-4Me). As shown in Scheme III-3, 2',3',5',6'-tetramethyl-(1,1':4',1''-terphenyl)-4,4''-dicarboxylic acid (H_2TPDC-4Me) was synthesized according to the reference.[99]

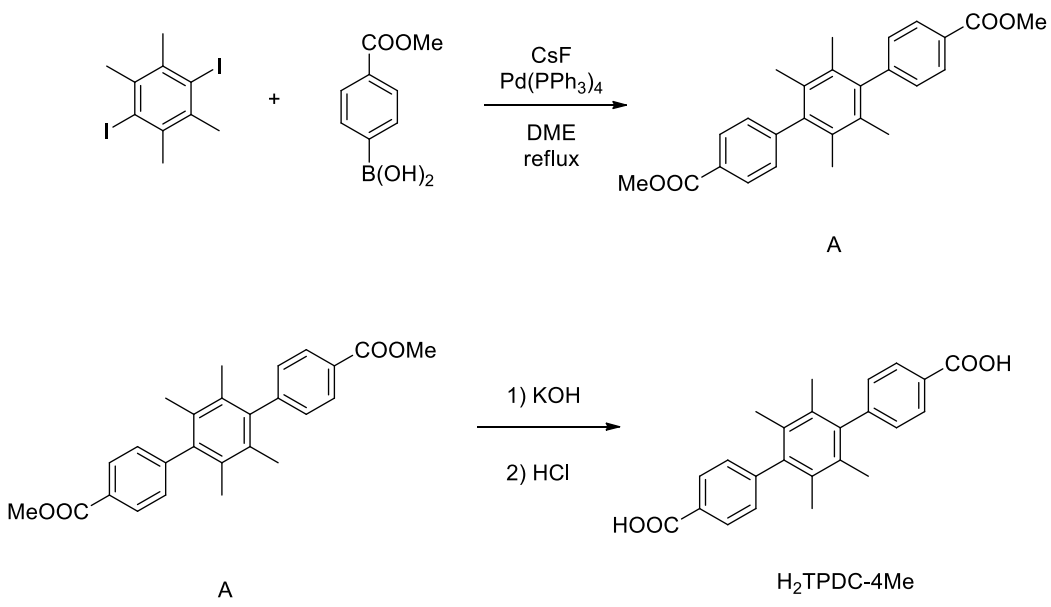

Scheme III-3. Synthesis of H_2TPDC-4Me ligand**.**

Synthesis of A: dimethyl ether (DME, 100 mL) was bubbled with nitrogen for around 30 min. Then DME was introduced into a nitrogen-protected round bottom flask containing solid mixtures of 1,4-diiodo-2,3,5,6-tetramethylbenzene (1.0 g, 2.59 mmol), 4-methoxyl carbonylphenylboronic acid (1.12 g, 6.24 mmol), cesium fluoride (CsF) (2.37 g, 15.6 mmol) and tetrakis (triphenylphosphine) palladium ($Pd(PPh_3)_4$) (0.3 g, 0.26 mmol). The mixtures were allowed to reflux for 3 days under nitrogen protection. After cooling to room temperature, the solvent was evaporated under vacuum. The residue was washed with a large amount of water followed by acetone. After removing the solvent, the residue was purified with column chromatography (silica gel, CH_2Cl_2) to give the 0.85 g ester as a white solid. ^{1}H NMR ($CDCl_3$, 300 MHz), δ 1.93 (s, 12H), 3.97 (s, 6H), 7.28 (d, 4H), 8.14 (d, 4H).

Synthesis of B: The obtained product A (0.63 g, 1.57 mmol) was stirred in THF (25 mL) and MeOH (25 mL) mixed solvent, to which a solution of KOH (2.63 g, 46.95 mmol) in H_2O (25 mL) was introduced and the mixture was refluxed for 12 h. After cooling down to room temperature, THF and MeOH were evaporated under vacuum. Additional water was added to the resulting water phase and the mixtures were heated until the solid was fully dissolved, then the homogeneous solution was acidified with diluted HCl until no further precipitate was detected (pH $\approx$ 2-3). Finally, 0.5 g of white solid H_2TPDC-4Me was collected by filtration, washing with water and drying in vacuum. ^{1}H NMR (DMSO, 300 MHz), δ 1.87 (s, 12H), 7.29 (d, 4H), 8.05 (d, 4H), 12.98 (s, 2H).

Synthesis of Compound 1. $ZrOCl_2 \cdot 8H_2O$ (32.2 mg, 0.100 mmol), H_2BDC (16.6 mg, 0.100 mmol), and benzoic acid (600 mg. 4.913 mmol) in 2 mL of DMF were ultrasonically dissolved in a Pyrex vial. The mixture was heated in an oven at 120 °C for 22 h. After cooling down to room temperature, the precipitates were collected by centrifugation. The solids were washed with DMF three times to remove unreacted precursors, and then solvent-exchanged with acetone three times. The resulting powder was obtained by centrifugation, and dried in an oven at 80 °C.

Synthesis of NiTCPP⊂Compound 1. $ZrOCl_2 \cdot 8H_2O$ (32.2 mg, 0.100 mmol), H_2BDC (16.6 mg, 0.100 mmol), NiTCPP (3.0 mg, 0.004 mmol) and benzoic acid (600 mg. 4.913 mmol) in 2 mL of DMF were ultrasonically dissolved in a Pyrex vial. The mixture was heated in an oven at 120 °C for 22 h. After cooling down to room temperature, the precipitates were collected by centrifugation. The solids were washed

with DMF three times to remove unreacted precursors, and then solvent-exchanged with acetone three times. The resulting powder was obtained by centrifugation, and dried in an oven at 80 °C.

Synthesis of Compound 2. $ZrOCl_2 \cdot 8H_2O$ (32.2 mg, 0.100 mmol), H_2NDC (21.6 mg, 0.100 mmol), and benzoic acid (220 mg. 1.801 mmol) in 2 mL of DMF were ultrasonically dissolved in a Pyrex vial. The mixture was heated in an oven at 120 °C for 22 h. After cooling down to room temperature, the precipitates were collected by centrifugation. The solids were washed with DMF three times to remove unreacted precursors, and then solvent-exchanged with acetone three times. The resulting powder was obtained by centrifugation, and dried in an oven at 80 °C.

Synthesis of NiTCPP⊂Compound 2. $ZrOCl_2 \cdot 8H_2O$ (32.2 mg, 0.100 mmol), H_2NDC (21.6 mg, 0.100 mmol), NiTCPP (3.0 mg, 0.004 mmol) and benzoic acid (220 mg. 1.801 mmol) in 2 mL of DMF were ultrasonically dissolved in a Pyrex vial. The mixture was heated in an oven at 120 °C for 22 h. After cooling down to room temperature, the precipitates were collected by centrifugation. The solids were washed with DMF three times to remove unreacted precursors, and then solvent-exchanged with acetone three times. The resulting powder was obtained by centrifugation, and dried in an oven at 80 °C.

Synthesis of Compound 3. $ZrOCl_2 \cdot 8H_2O$ (32.2 mg, 0.100 mmol), H_2BPDC (24.2 mg, 0.100 mmol), and benzoic acid (300 mg, 2.457 mmol) in 2 mL of DMF were ultrasonically dissolved in a Pyrex vial. The mixture was heated in an oven at 120 °C for 22 h. After cooling down to room temperature, the precipitates were collected by

centrifugation. The solids were washed with DMF three times to remove unreacted precursors, and then solvent-exchanged with acetone three times. The resulting powder was obtained by centrifugation, and dried in an oven at 80 °C.

Synthesis of NiTCPP⊂Compound 3. $ZrOCl_2 \cdot 8H_2O$ (32.2 mg, 0.100 mmol), H_2BPDC (24.2 mg, 0.100 mmol), NiTCPP (3.0 mg, 0.004 mmol) and benzoic acid (300 mg, 2.457 mmol) in 2 mL of DMF were ultrasonically dissolved in a Pyrex vial. The mixture was heated in an oven at 120 °C for 22 h. After cooling down to room temperature, the precipitates were collected by centrifugation. The solids were washed with DMF three times to remove unreacted precursors, and then solvent-exchanged with acetone three times. The resulting powder was obtained by centrifugation, and dried in an oven at 80 °C.

Synthesis of Compound 4. $ZrOCl_2 \cdot 8H_2O$ (32.2 mg, 0.100 mmol), H_2AZDC (27.0 mg, 0.100 mmol), and benzoic acid (300 mg, 2.457 mmol) in 2 mL of DMF were ultrasonically dissolved in a Pyrex vial. The mixture was heated in an oven at 120 °C for 22 h. After cooling down to room temperature, the precipitates were collected by centrifugation. The solids were washed with DMF three times to remove unreacted precursors, and then solvent-exchanged with acetone three times. The resulting powder was obtained by centrifugation, and dried in an oven at 80 °C.

Synthesis of NiTCPP⊂Compound 4. $ZrOCl_2 \cdot 8H_2O$ (32.2 mg, 0.100 mmol), H_2AZDC (27.0 mg, 0.100 mmol), NiTCPP (2.5 mg, 0.003 mmol) and benzoic acid (300 mg, 2.457 mmol) in 2 mL of DMF were ultrasonically dissolved in a Pyrex vial. The mixture was heated in an oven at 120 °C for 22 h. After cooling down to room

temperature, the precipitates were collected by centrifugation. The solids were washed with DMF three times to remove unreacted precursors, and then solvent-exchanged with acetone three times. The resulting powder was obtained by centrifugation, and dried in an oven at 80 °C.

Synthesis of Compound 5. $ZrOCl_2 \cdot 8H_2O$ (32.2 mg, 0.100 mmol), H_2EDDB (26.6 mg, 0.100 mmol), and benzoic acid (170 mg, 1.392 mmol) in 2 mL of DMF were ultrasonically dissolved in a Pyrex vial. The mixture was heated in an oven at 120 °C for 22 h. After cooling down to room temperature, the precipitates were collected by centrifugation. The solids were washed with DMF three times to remove unreacted precursors, and then solvent-exchanged with acetone three times. The resulting powder was obtained by centrifugation, and dried in an oven at 80 °C.

Synthesis of NiTCPP⊂Compound 5. $ZrOCl_2 \cdot 8H_2O$ (32.2 mg, 0.100 mmol), H_2EDDB (26.6 mg, 0.100 mmol), NiTCPP (3.0 mg, 0.004 mmol) and benzoic acid (170 mg, 1.392 mmol) in 2 mL of DMF were ultrasonically dissolved in a Pyrex vial. The mixture was heated in an oven at 120 °C for 22 h. After cooling down to room temperature, the precipitates were collected by centrifugation. The solids were washed with DMF three times to remove unreacted precursors, and then solvent-exchanged with acetone three times. The resulting powder was obtained by centrifugation, and dried in an oven at 80 °C.

Synthesis of Compound 6. $ZrOCl_2 \cdot 8H_2O$ (32.2 mg, 0.100 mmol), H_2TPDC-4Me (37.4 mg, 0.100 mmol), and benzoic acid (250 mg, 2.047 mmol) in 2 mL of DMF were ultrasonically dissolved in a Pyrex vial. The mixture was heated in an oven at 120 °C for

22 h. After cooling down to room temperature, the precipitates were collected by centrifugation. The solids were washed with DMF three times to remove unreacted precursors, and then solvent-exchanged with acetone three times. The resulting powder was obtained by centrifugation, and dried in an oven at 80 °C.

Synthesis of NiTCPP⊂Compound 6. $ZrOCl_2 \cdot 8H_2O$ (32.2 mg, 0.100 mmol), H_2TPDC-4Me (37.4 mg, 0.100 mmol), NiTCPP (3.0 mg, 0.004 mmol) and benzoic acid (250 mg, 2.047 mmol) in 2 mL of DMF were ultrasonically dissolved in a Pyrex vial. The mixture was heated in an oven at 120 °C for 22 h. After cooling down to room temperature, the precipitates were collected by centrifugation. The solids were washed with DMF three times to remove unreacted precursors, and then solvent-exchanged with acetone three times. The resulting powder was obtained by centrifugation, and dried in an oven at 80 °C.

Synthesis of NiTCPP⊂UiO-67-2NO$_2$. $ZrOCl_2 \cdot 8H_2O$ (32.2 mg, 0.100 mmol), H_2BPDC-2NO_2 (35.0 mg, 0.105 mmol), NiTCPP (2.0 mg, 0.002 mmol) and benzoic acid (300 mg, 2.457 mmol) in 2 mL of DMF were ultrasonically dissolved in a Pyrex vial. The mixture was heated in an oven at 120 °C for 22 h. After cooling down to room temperature, the precipitates were collected by centrifugation. The solids were washed with DMF three times to remove unreacted precursors, and then solvent-exchanged with acetone three times. The resulting powder was obtained by centrifugation, and dried in an oven at 80 °C.

Synthesis of NiTCPP⊂UiO-67-2OH. $ZrOCl_2 \cdot 8H_2O$ (32.2 mg, 0.100 mmol), H_2BPDC-2OH (34.0 mg, 0.124 mmol), NiTCPP (2.0 mg, 0.002 mmol) and benzoic acid

(300 mg, 2.457 mmol) in 2 mL of DMF were ultrasonically dissolved in a Pyrex vial. The mixture was heated in an oven at 120 °C for 22 h. After cooling down to room temperature, the precipitates were collected by centrifugation. The solids were washed with DMF three times to remove unreacted precursors, and then solvent-exchanged with acetone three times. The resulting powder was obtained by centrifugation, and dried in an oven at 80 °C.

Synthesis of NiTCPP⊂UiO-67-2I. $ZrOCl_2 \cdot 8H_2O$ (32.2 mg, 0.100 mmol), H_2BPDC-2I (50.0 mg, 0.101 mmol), NiTCPP (2.0 mg, 0.002 mmol) and benzoic acid (550 mg, 4.504 mmol) in 2 mL of DMF were ultrasonically dissolved in a Pyrex vial. The mixture was heated in an oven at 120 °C for 22 h. After cooling down to room temperature, the precipitates were collected by centrifugation. The solids were washed with DMF three times to remove unreacted precursors, and then solvent-exchanged with acetone three times. The resulting powder was obtained by centrifugation, and dried in an oven at 80 °C.

Synthesis of NiTCPP⊂UiO-67-2OMe. $ZrOCl_2 \cdot 8H_2O$ (32.2 mg, 0.100 mmol), H_2BPDC-2OMe (35.0 mg, 0.116 mmol), NiTCPP (2.0 mg, 0.002 mmol) and benzoic acid (450 mg, 3.685 mmol) in 2 mL of DMF were ultrasonically dissolved in a Pyrex vial. The mixture was heated in an oven at 120 °C for 22 h. After cooling down to room temperature, the precipitates were collected by centrifugation. The solids were washed with DMF three times to remove unreacted precursors, and then solvent-exchanged with acetone three times. The resulting powder was obtained by centrifugation, and dried in an oven at 80 °C.

Synthesis of NiTCPP⊂UiO-67(BPyDC). $ZrOCl_2 \cdot 8H_2O$ (32.2 mg, 0.100 mmol), H_2BPyDC (24.4 mg, 0.100 mmol), NiTCPP (2.5 mg, 0.003 mmol) and benzoic acid (350 mg, 2.866 mmol) in 2 mL of DMF were ultrasonically dissolved in a Pyrex vial. The mixture was heated in an oven at 120 °C for 22 h. After cooling down to room temperature, the precipitates were collected by centrifugation. The solids were washed with DMF three times to remove unreacted precursors, and then solvent-exchanged with acetone three times. The resulting powder was obtained by centrifugation, and dried in an oven at 80 °C.

PSM of UiO-67 with MnTCPPCl. $ZrOCl_2 \cdot 8H_2O$ (32.2 mg, 0.100 mmol), H_2BPDC (24.2 mg, 0.100 mmol) and benzoic acid (300 mg, 2.457 mmol) in 2 mL of DMF were ultrasonically dissolved in a Pyrex vial. The mixture was heated in an oven at 120 °C for 22 h. After cooling down to room temperature, the precipitates were collected by centrifugation. The solids were washed with DMF three times to remove unreacted precursors, and then solvent-exchanged with acetone three times. The resulting powder was obtained by centrifugation, and dried in an oven at 80 °C. The synthesized UiO-67 was immersed in 5 mL DMF solution of MnTCPPCl (3 mg, 0.004 mmol) in an oven at 120 °C for 12 h. Then the solids were washed with DMF three times to remove unreacted precursors, and then solvent-exchanged with acetone three times. The resulting powder was obtained by centrifugation, and dried in an oven at 80 °C.

DFT Calculations. The DFT calculations were performed using the Vienna ab initio simulation package (VASP) with the projector augmented wave (PAW) pseudopotentials.[100-103] The exchange-correlation energy of interacting electrons was

treated by the Perdew, Burke, and Ernzerhof (PBE) GGA functional.[104] The energy cut off for the plane-wave basis set was 500 eV. The efficient conjugate gradient algorithm based on Hellmann-Feynman forces was used to relax the ions into their equilibrium positions. All considered structures were fully optimized with the force on each atom less than 0.01 eV/Å. Brillouin-zone integration was performed with a Gaussian broadening of 0.2 eV during all relaxations. Since we are dealing with a large cell system, the G-point alone was sufficient for sampling the Brillouin zone.

For UiO series, each Zr_6 cluster is coordinated to 12 organic ligands to form a face-centered cubic unit cell. The cell contains four Zr_6 clusters and 456, 696, and 728 atoms for UiO-66, UiO-67, and compound **5**, respectively. By contrast, with each Zr_6 cluster coordinated to eight TCPP ligands, the cell of PCN-222 has hexagonal symmetry, containing three Zr_6 clusters and 624 atoms. The initial structures used for calculation were obtained by hydroxylating the experimental structures determined from PXRD data.[45, 73, 95] The theoretical structures are optimized firstly by relaxing the atomic positions by keeping the lattice constant and cell volume fixed to experimental values. Then the ground-state volume was determined from total energy minimization by varying the cell volume with the atom positions relaxed for each volume step. The theoretical ground-state lattice parameters were calculated to be 20.96 Å (UiO-66), 27.14 Å (UiO-67), 30.20 Å (compound **5**), and a=b=41.93 Å, c=17.156 Å (PCN-222), respectively, which are within 2% discrepancy with the experiments and in consistent with previous calculations.[105-106]

Essentially, the MOF crystal growth process is ligand substitution on metal ions or clusters. Equilibrium of the formation of MOF and Gibbs free energy of the reaction can be expressed as below:

$$Zr_6(C_6H_5COO)_{12} + 6\ H_2L \rightleftharpoons \{Zr_6L_6\} + 12\ C_6H_5COOH \quad (1)$$

$$\Delta G = \Delta G^{\emptyset} + RT \ln \frac{[C_6H_5COOH]^{12}}{[Zr_6(C_6H_5COO)_{12}][H_2L]^6} \quad (2)$$

$$\Delta G = \Delta H - T\Delta S \quad (3)$$

Scheme III-4. Equilibrium of the formation of MOF and Gibbs free energy of the reaction.

To begin with, we constructed a Zr_6 cluster coordinated to 12 BA (named for **R**), which has a formula of $Zr_6O_4(OH)_4(C_6H_5COO)_{12}$. The DFT total energy method was applied to calculate the enthalpy of the reaction. During the reaction process, terminal BA were substituted by BDC/BPDC/EDDB/NiTCPP ligand to form corresponding MOFs. The enthalpies of these ligand exchange processes were calculated on a unit cell for each MOF according to the following equations:

$$4Zr_6O_4(OH)_4(C_6H_5COO)_{12} + 24H_2BDC \xrightarrow[R]{} UiO\text{-}66 + 48BA \quad (\mathbf{4})$$

$$4Zr_6O_4(OH)_4(C_6H_5COO)_{12} + 24H_2BPDC \xrightarrow[R]{} UiO\text{-}67 + 48BA \quad (\mathbf{5})$$

$$4Zr_6O_4(OH)_4(C_6H_5COO)_{12} + 24H_2EDDB \xrightarrow[R]{} Compound\ \mathbf{5} + 48BA \quad (\mathbf{6})$$

$$3Zr_6O_4(OH)_4(C_6H_5COO)_{12} + 6H_4TCPP(Ni) + 24H_2O \xrightarrow[R]{} PCN\text{-}222 + 36BA \quad (\mathbf{7})$$

Scheme III-5. Equations of the formation of MOFs used for DFT calculations.

In order to make these results comparable, we divided the calculated enthalpies by a factor of 4 for UiO series (equation (1) to (3)) and 3 for PCN-222 (equation (4)) to obtain the enthalpies assigned to each Zr_6 cluster for each MOF.

The bond length (Å) and cell parameters (Å) of the structures used in DFT calculations were summarized in Table III-1. And the atoms used for bond length calculations were assigned according to Figure III-1.

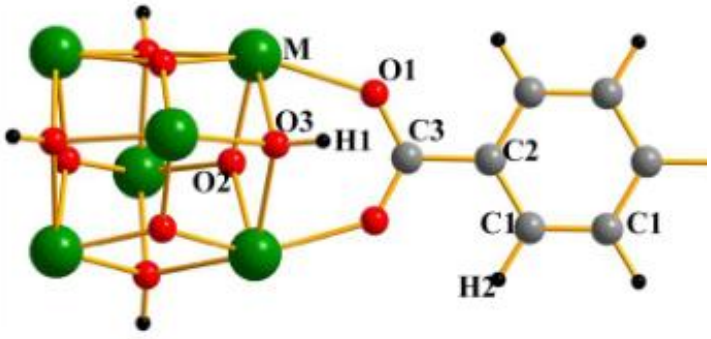

Figure III-1. Schematic illustration of Zr_6 cluster coordinated to the benzoate part of the organic ligands used for DFT calculations.

Table III-1. Bond length (Å) and cell parameters (Å) of the structures used in DFT calculations

Structure	Bond length and cell parameters / Å				
R	Zr-O1	Zr-O2	Zr-O3	O3-H1	C3-O1
	2.247	2.087	2.275	0.969	1.28
	C3-C2	C2-C1	C1-H2	Cell parameters	Ref.
	1.497	1.406	1.096	-	This work
UiO-66	Zr-O1	Zr-O2	Zr-O3	O3-H1	C3-O1
	2.245	2.086	2.276	0.97	1.279
	C3-C2	C2-C1	C1-H2	Cell parameters	Ref.
	1.497	1.403	1.09	20.96	This work
UiO-66	Zr-O1	Zr-O2	Zr-O3	O3-H1	C3-O1
	2.245	2.086	2.277	0.971	1.278
	C3-C2	C2-C1	C1-H2	Cell parameters	Ref.
	1.498	1.404	1.089	20.962	[106]
UiO-66	Zr-O1	Zr-O2	Zr-O3	O3-H1	C3-O1
	2.248	2.09	2.286	0.963	1.273
	C3-C2	C2-C1	C1-H2	Cell parameters	Ref.
	1.499	1.402	1.084	20.9784	[107]
UiO-67	Zr-O1	Zr-O2	Zr-O3	O3-H1	C3-O1
	2.249	2.086	2.275	0.971	1.282

Table III-1. Continued

Structure	Bond length and cell parameters / Å				
	C3-C2	C2-C1	C1-H2	Cell parameters	Ref.
	1.492	1.401	1.091	27.14	This work
UiO-67	Zr-O1	Zr-O2	Zr-O3	O3-H1	C3-O1
	2.249	2.087	2.277	0.971	1.282
	C3-C2	C2-C1	C1-H2	Cell parameters	Ref.
	1.493	1.401	1.09	27.14	[106]
UiO-67	Zr-O1	Zr-O2	Zr-O3	O3-H1	C3-O1
	2.252	2.089	2.285	0.963	1.273
	C3-C2	C2-C1	C1-H2	Cell parameters	Ref.
	1.496	1.401	1.085	27.094	[108]
Compound **5**	Zr-O1	Zr-O2	Zr-O3	O3-H1	C3-O1
	2.203	2.108	2.277	0.97	1.279
	C3-C2	C2-C1	C1-H2	Cell parameters	Ref.
	1.496	1.404	1.09	30.2	This work
Compound **5**	Zr-O1	Zr-O2	Zr-O3	O3-H1	C3-O1
	2.207	2.11	-	-	1.3
	C3-C2	C2-C1	C1-H2	Cell parameters	Ref.
	1.467	1.414	0.951	30.203	[95]

Table III-1. Continued

Structure	Bond length and cell parameters / Å				
PCN-222	Zr-O1	Zr-O2	Zr-O3	O3-H1	C3-O1
	2.21/2.238	2.178	2.277	0.971	1.244/1.253
	C3-C2	C2-C1	C1-H2	Cell parameters	Ref.
	1.513	1.381	1.083	a=b=41.928 c=17.156	This work
PCN-222	Zr-O1	Zr-O2	Zr-O3	O3-H1	C3-O1
	2.21/2.24	2.179	-	-	1.245/1.253
	C3-C2	C2-C1	C1-H2	Cell parameters	Ref.
	1.515	1.382	1.083	a=b=41.968 c=17.143	[73]

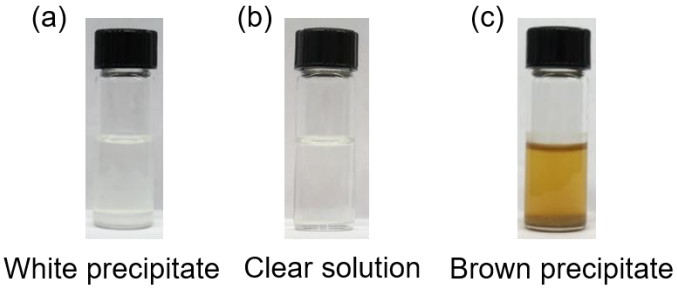

Figure III-2. Photographs of the products obtained with different amounts of BA used for the synthesis of UiO series of MOFs. (a) UiO-66 (BA 600 mg), (b) UiO-67 (BA 600 mg), (c) compound 5 (BA 300 mg).

According to the expression of ΔG, when the amount of BA added increases up to a certain value, ΔG becomes positive, and the formation of the MOF can be totally inhibited since the reaction is nonspontaneous. For example, only a clear solution was obtained with 600 mg (4.9 mmol) BA added during the synthesis of UiO-67 (Figure III-2b). However, UiO-66 can still be obtained with the same amount of BA used for the synthesis (Figure III-2a). The highest amount of BA used to synthesize compound **5** is 300 mg (2.5 mmol), which is the lowest among these three MOFs (Figure III-2c). Therefore, the amount of BA required to fully inhibit the formation of the MOF may indicate the relative value of ΔH and thus $\Delta G^{\emptyset}$ to some degree.

ICP Analyses. Samples were prepared in duplicate with weights of around 3 mg. Each sample was dissolved in J.T. Baker Ultrex® II Ultrapure 70% nitric acid at 70 °C for 12 hours. Samples were then diluted to 150x in 1% nitric acid and 18.2 MΩ water from a Millipore Milli-Q® water purification system. Calibration standards were prepared from certified reference standards from RICCA Chemical Company. Samples were further analyzed with a Perkin Elmer Optima 8000 ICP spectrometer. Resulting calibration curves have minimum R^2 = 0.9999. Additionally, to maintain accuracy, quality control samples from certified reference standards and internal standards were utilized. The individual results of the duplicate samples were averaged to determine the metal ratios.

Table III-2. Ni to Zr atomic ratio in NiTCPP⊂UiO-67 samples when using different amounts of porphyrin ligand for the synthesis

TCPP / mg	2	3	4
Trial 1	0.017	0.023	0.028
Trial 2	0.019	0.024	0.028
Average	0.018	0.024	0.028

Table III-3. Ni to Zr atomic ratio in NiTCPP⊂compounds 1-6 and Mn to Zr atomic ratio in the sample of UiO-67 after PSM with porphyrin

Compound	**1**	**2**	**3**	**4**	**5**	**6**	PSM sample
Trial 1	0.022	0.028	0.023	0.016	0.020	0.027	0.001
Trial 2	0.023	0.025	0.024	0.019	0.026	0.029	0.001
Average	0.023	0.027	0.024	0.018	0.023	0.028	0.001

TGA Analyses. About 10.0 mg of the MOF samples were heated on the Shimadzu TGA-50 instrument from room temperature to 900 °C at a ramp rate of 2 °C/min under nitrogen flow of 25 mL/min. The decomposition temperature of each material was obtained according to corresponding TGA data, which suggested the excellent thermal stability of these MOF samples.

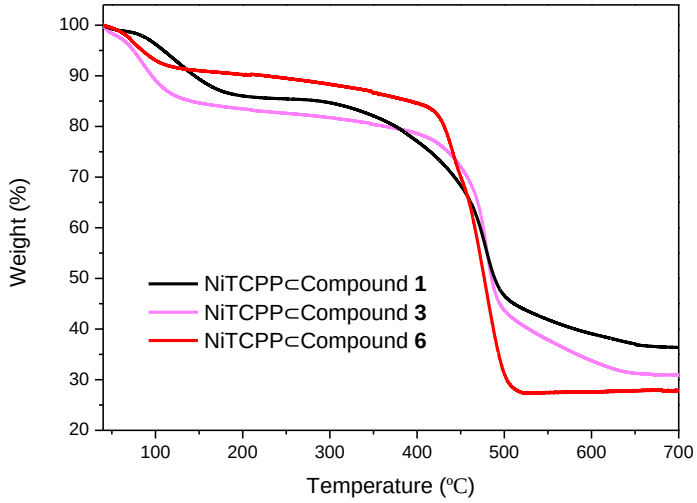

Figure III-3. Thermogravimetric analysis of NiTCPP⊂Compound **1**, NiTCPP⊂Compound **3**, and NiTCPP⊂Compound **6**.

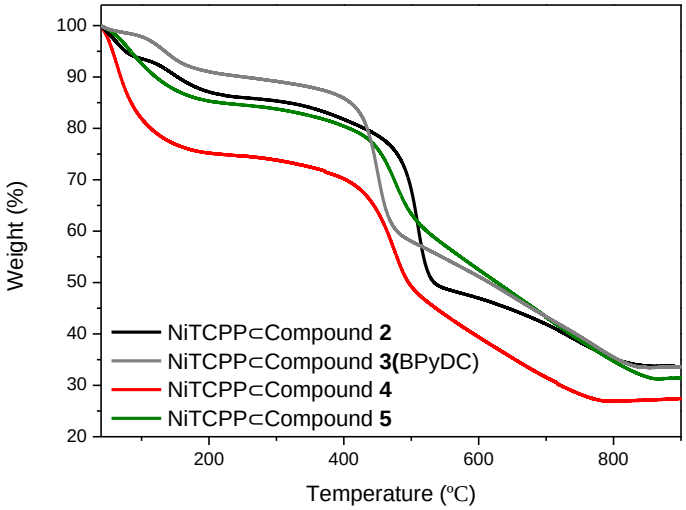

Figure III-4. Thermogravimetric analysis of NiTCPP⊂Compound **2**, NiTCPP⊂Compound **3**(BPyDC), NiTCPP⊂Compound **4**, and NiTCPP⊂Compound **5**.

3.3 Results and Discussion

Functionalization of UiO-67 through ISLI. As an example of UiO-66 analogues, UiO-67 was firstly selected as the parent MOF to implement the in situ secondary ligand incorporation (ISLI) strategy. Solvothermal reaction of $ZrOCl_2 \cdot 8H_2O$, H_2BPDC, and benzoic acid (BA) in N,N-dimethylformamide (DMF) at 120 ℃ for 22 hours yielded white powders of UiO-67 (Figure III-5a). And solvothermal reaction of $ZrOCl_2 \cdot 8H_2O$, H_2BDC, [5,10,15,20-tetrakis(4-carboxyphenyl)porphyrinato]-Ni(II) (NiTCPP), and BA in DMF at 120 ℃ for 22 hours yielded red powders of NiTCPP⊂UiO-67. After washing with DMF and acetone, the product remained red, suggesting the presence of porphyrin (Figure III-5b). Moreover, the PXRD pattern of the product was identical to that of UiO-67 (Figure III-5c), indicating that the framework of UiO-67 was well maintained after functionalization of UiO-67 with porphyrin.

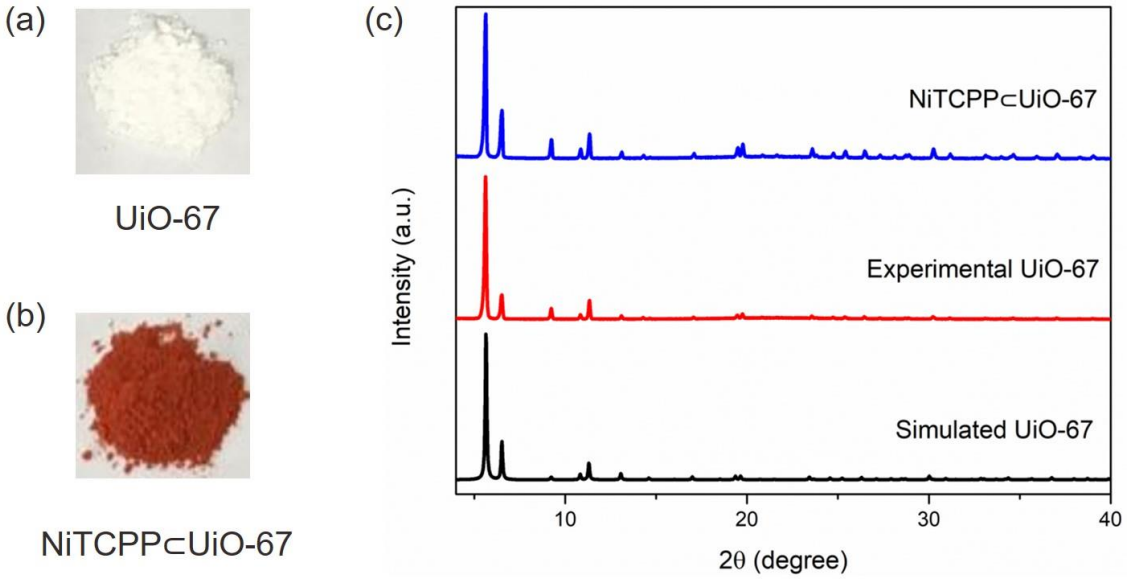

Figure III-5. Photographs of (a) UiO-67 (white) and (b) NiTCPP⊂UiO-67 (red). (c) The PXRD patterns for UiO-67 and NiTCPP⊂UiO-67.

The morphology and phase purity of the product NiTCPP⊂UiO-67 were tested by SEM. The SEM image showed that the obtained powders were octahedral microcrystals with the size of about 2 μm (Figure III-6a). Moreover, the elemental mappings of a single crystal by energy dispersive X-ray spectroscopy (EDS) demonstrated an even distribution of all the elements (Figure III-6b), especially Zr and Ni, implying that porphyrin was incorporated into UiO-67 homogeneously.

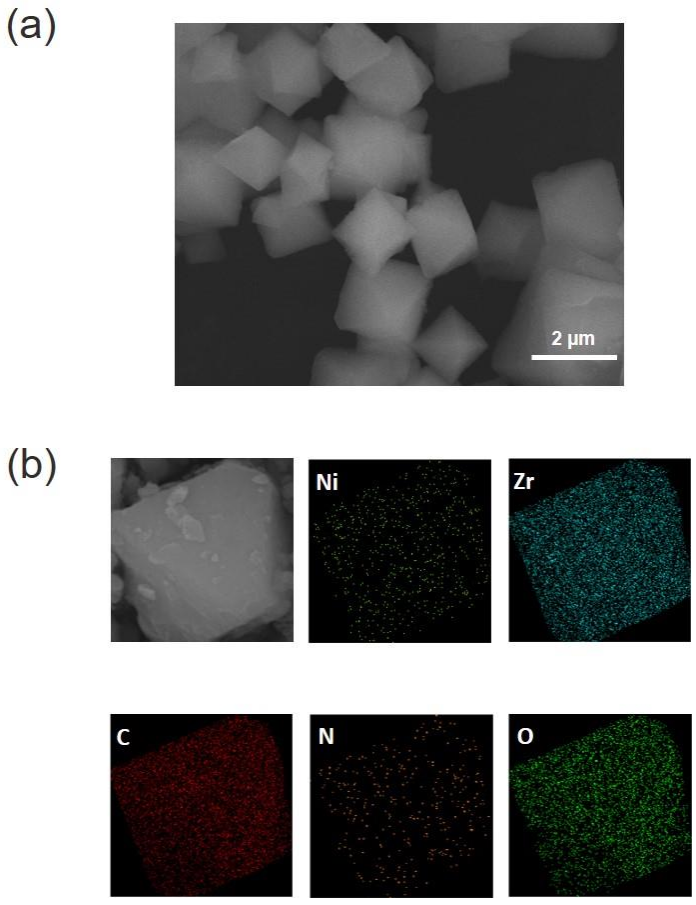

Figure III-6. (a) SEM image of NiTCPP⊂UiO-67. Scale bar: 2 μm. (b) SEM image of a NiTCPP⊂UiO-67 single crystal and the corresponding elemental EDS-mappings.

In order to assess the permanent porosity of the product, we directly activated the sample by removing the solvent and then carried out N2 uptake test at 77 K (Figure III-7). Type I isotherms that are typical for microporous solids were acquired. Compared with pristine UiO-67 (600 cm^3 g^{-1}), NiTCPP⊂UiO-67 exhibited lower N2 uptake at 1 bar (520 cm^3 g^{-1}) (Figure III-7), suggesting the incorporation of porphyrin ligand into the framework of UiO-67.

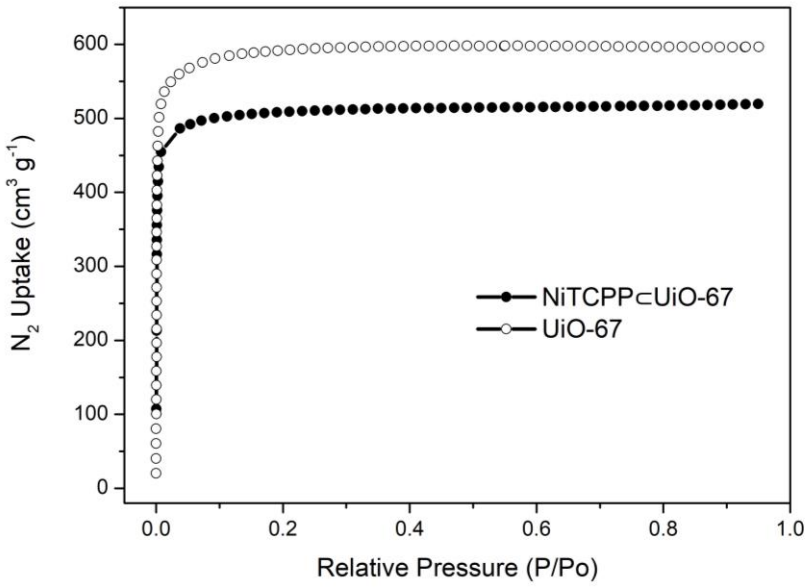

Figure III-7. N_2 adsorption isotherms of UiO-67 and NiTCPP⊂UiO-67 at 77 K.

The amount of incorporated porphyrin ligand was tested by ICP experiments. When increasing the amount of NiTCPP ligand added into the reaction system, the amount of porphyrin incorporated into UiO-67 increased accordingly (Table III-2). Therefore, by adjusting the reaction conditions, different amounts of porphyrin species can be introduced into UiO-67.

Stability Test. In the next step, the chemical stability of NiTCPP⊂UiO-67 was tested by immersing the sample (100 mg) into a series of aqueous solutions (50 mL), including 1 M HCl, deionized water, 0.1 mM NaOH, and 1 mM NaOH aqueous solutions. After 24 h, all the samples were centrifuged and then washed with water, DMF, and acetone three times. These samples were dried in oven and characterized by PXRD. The PXRD patterns of all the samples were identical to that of the product before the chemical stability test (Figure III-8), implying that the framework of UiO-67 was maintained very well after treatment with acid and base solutions.

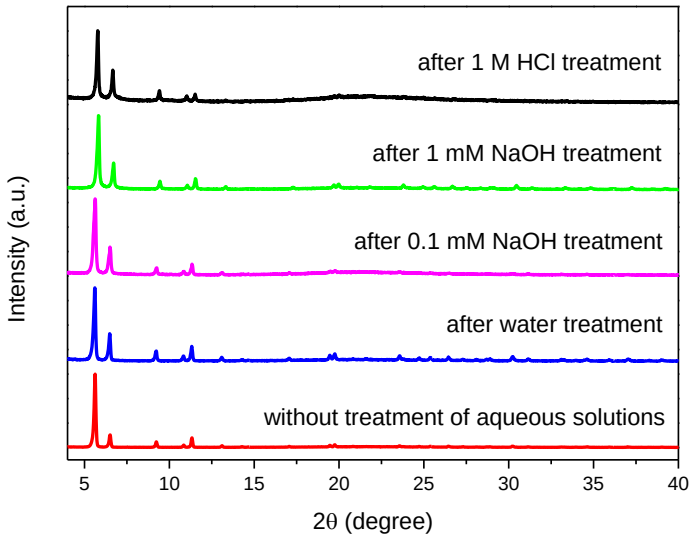

Figure III-8. PXRD patterns for NiTCPP⊂UiO-67 without treatment of any aqueous solutions and the samples treated with deionized water, 1 M HCl, 0.1 mM NaOH and 1 mM NaOH aqueous solutions for 24 h.

To further confirm that NiTCPP⊂UiO-67 was stable under the selected chemical conditions, the samples after the treatment were tested by N_2 uptake experiments at 77 K.

All the samples were degassed on ASAP 2020 adsorption system at 100 °C for 5 h prior to N_2 adsorption measurement at 77 K. According to Figure III-9, N_2 uptake experiments further proved that the framework of all these samples were preserved during the chemical stability test.

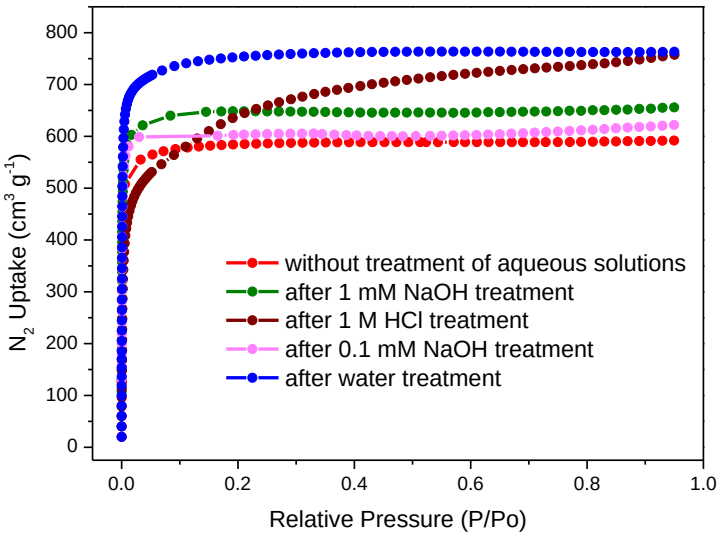

Figure III-9. N_2 adsorption isotherms of NiTCPP⊂UiO-67 at 77 K after treatment with different aqueous solutions.

In addition to the chemical stability, the thermal stability of the sample (about 10.0 mg) was tested by Shimadzu TGA-50 instrument. According to Figure III-3, the decomposition of material was observed at around 420 °C, showing high thermal stability of NiTCPP⊂UiO-67.

Phase Purity Control. A challenge encountered to synthesize UiO-67 functionalized with porphyrin is the formation of competing phases (e.g. porphyrin-based Zr-MOF) along with the desired product. Impure products were obtained under

some reaction conditions. For example, increasing the amount of MnTCPPCl promotes the formation of impurity phase PCN-222 (Figure III-10). Therefore, judicious control of the reaction conditions plays an importane role to force the system towards phase-pure MnTCPPCl⊂UiO-67.

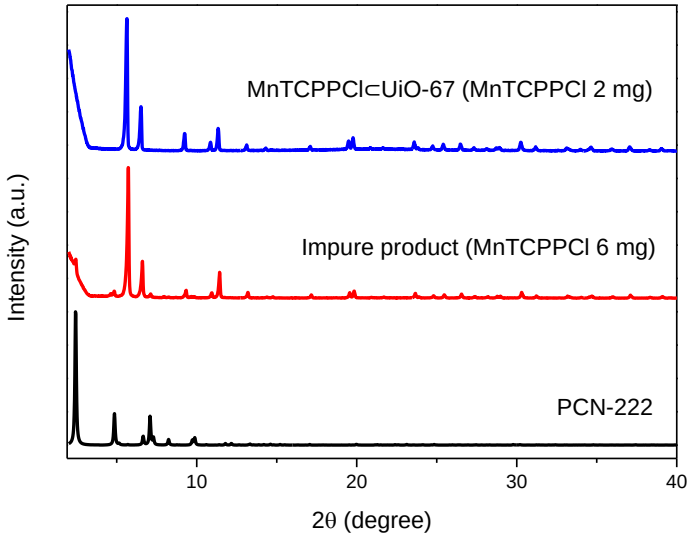

Figure III-10. PXRD patterns for PCN-222 and the products obtained with different amounts of MnTCPPCl used for the synthesis.

Under our synthetic condition, the incorporation of porphyrinic species is mainly achieved by the connectivity reduction of ideally 12-connected Zr_6 clusters in UiO-67, which generates unsaturated coordination sites for the carboxylate groups on porphyrin ligands to coordinate. Owing to high symmetry and connectivity of the Zr_6 clusters, UiO-67 can preserve its three-dimensional (3-D) framework even when the Zr_6 cluster is partially coordinated to TCPP species, which might interrupt the connection between Zr_6 clusters in a 3-D space and create defects (Figure III-11). On the other hand, lower

concentration of porphyrin ligands in the system as well as faster nucleation of UiO-67 hinder the nucleation of PCN-222. Consequently, formation of phase-pure UiO-67 with the incorporation of porphyrinic functionality can be controlled.

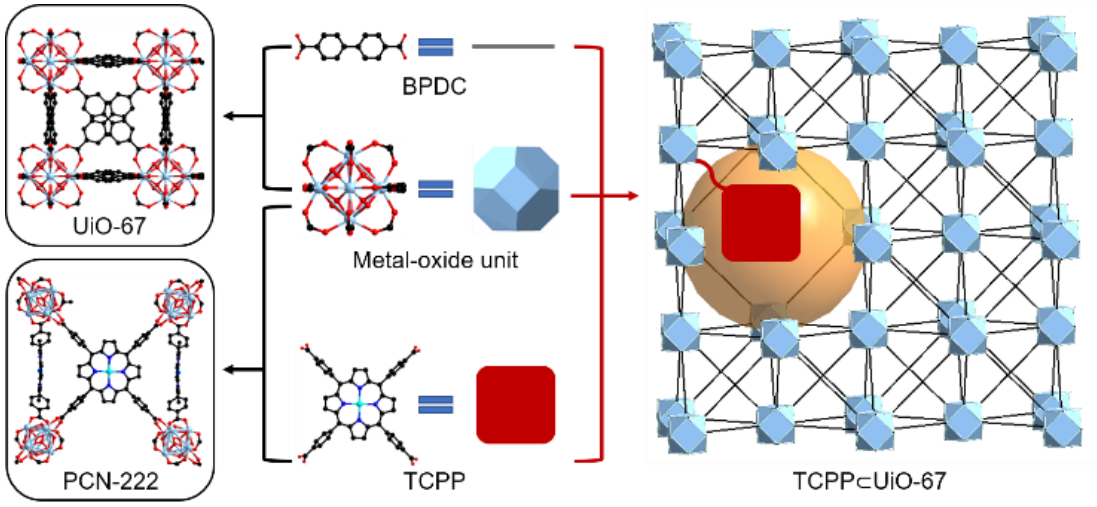

Figure III-11. Schematic illustration of TCPP⊂UiO-67 generated by ISLI strategy and possible competing phases. Yellow sphere indicates the pore cavity.

Comparison of ISLI with PSM. In order to compare the ISLI strategy with widely studied post-synthetic modification (PSM) method,[76, 109-111] we attempted to post-synthetically functionalize UiO-67 by immersing it in the DMF solution of MnTCPPCl. The PXRD pattern of the PSM product suggested that the framework was maintained well after the modification (Figure III-12). However, the small window size of UiO-67 impedes the incorporation of the bulky porphyrinic species. Consequently, porphyrin is more likely to attach on the outer surface of UiO-67 than incorporate into the framework, which is verified by highly reduced content of Mn in the post-synthetically modified product from the ICP test (Table III-3). This control experiment demonstrated that

increased variety of functionalities can be introduced into the MOF through our ISLI strategy, which cannot be achieved by PSM method due to size limitation.

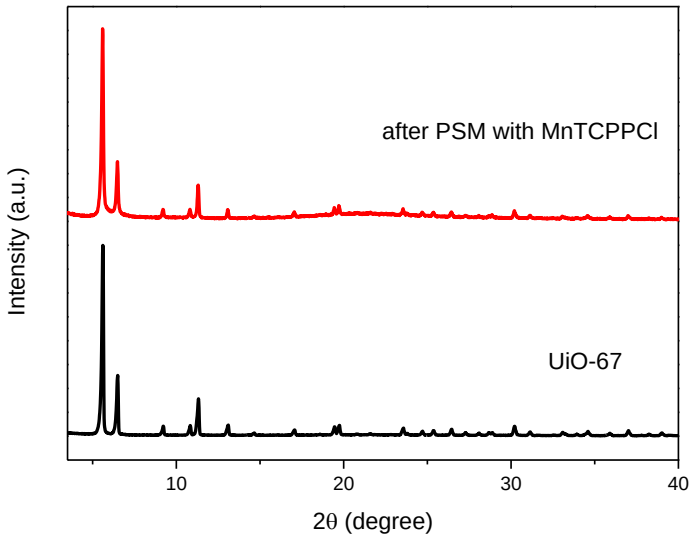

Figure III-12. PXRD patterns for UiO-67 before and after PSM with MnTCPPCl.

Construction of UiO-67 with Multiple Functionalities. A series of functionalities were then selected to introduce into UiO-67 by ISLI strategy, taking advantage of the synthetic versatility of designing diverse organic ligands. By mixing BPDC or its derivatives and porphyrin ligands with different metals in the center, a series of multifunctional UiO-67 were synthesized successfully, including X⊂UiO-67, X⊂UiO-67-2NO_2, X⊂UiO-67-2OH, X⊂UiO-67-2I, X⊂UiO-67-2OMe and X⊂UiO-67(BPyDC) (X = NiTCPP, FeTCPPCl, MnTCPPCl, CuTCPP, H_2TCPP, ZnTCPP, and CoTCPP) (Figure III-13 and Figure III-14). Hence, introducing porphyrin ligands into

UiO-67 adds another dimension to the synthetic flexibility and expand the scope of functionality for MOF modification.

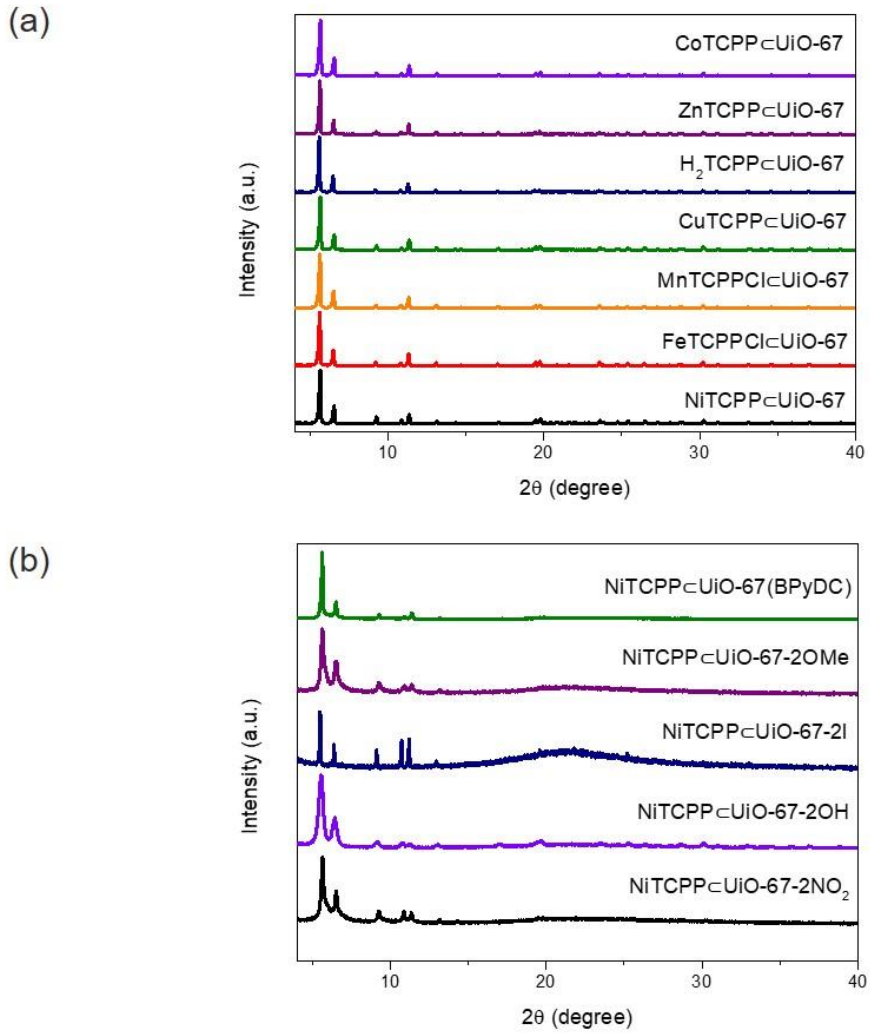

Figure III-13. PXRD patterns for (a) X⊂UiO-67 (X = NiTCPP, FeTCPPCl, MnTCPPCl, CuTCPP, H_2TCPP, ZnTCPP, and CoTCPP) and (b) NiTCPP⊂UiO-67-2NO_2, NiTCPP⊂UiO-67-2OH, NiTCPP⊂UiO-67-2I, NiTCPP⊂UiO-67-2OMe and NiTCPP⊂UiO-67(BPyDC).

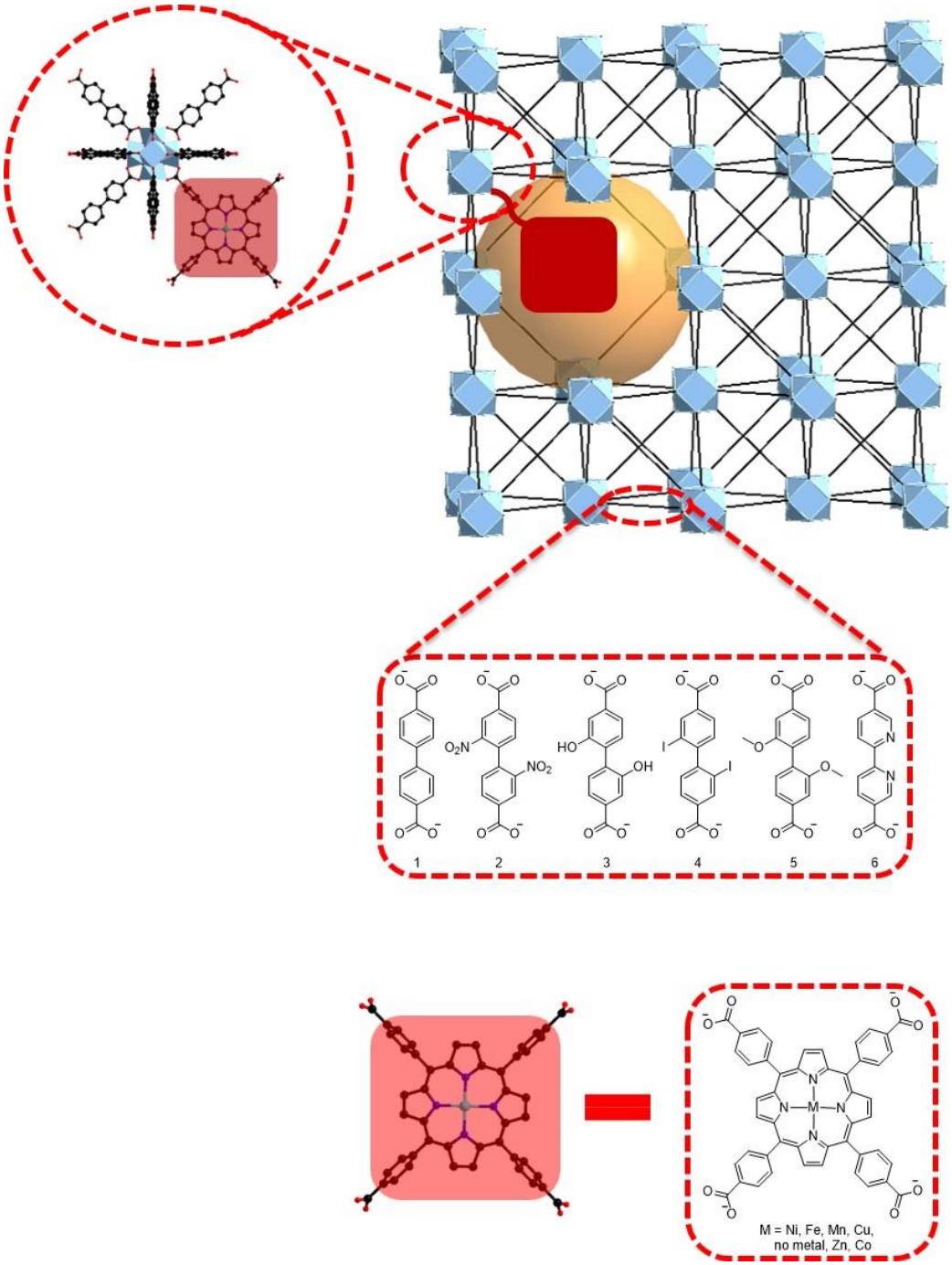

Figure III-14. Schematic illustration of constructing multifunctional UiO-67 by ISLI strategy.

Functionalization of UiO Series of MOFs through ISLI. The above studies showed that multifunctional UiO-67 can be successfully synthesized by ISLI strategy, taking advantage of the available coordination sites of Zr_6 clusters. And the the original crystal structure, morphology and high stability of the parent MOF were well preserved. In light of the ubiquity of unsaturated coordination sites in UiO series of MOFs, we then attempted to extend the ISLI strategy to these Zr-MOFs. A series of linear ditopic organic ligands were selected as the strut of the MOF (Figure III-15).

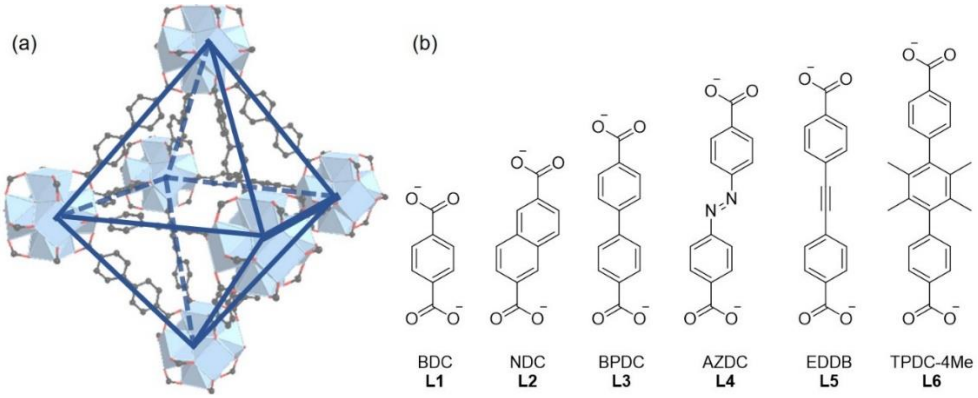

Figure III-15. (a) Schematic illustration of the octahedral cage in UiO series of MOFs. (b) Chemical structures of linear ditopic ligands used for ISLI.

Through ISLI strategy, a series of functionalized UiO series of MOFs were obtained. Compounds **1** to **6** represent Zr-MOFs with ditopic 1,4-benzenedicarboxylate (BDC), 2,6-naphthalene dicarbox-ylate (NDC), BPDC, azobenzene-4,4’-dicarboxylate (AZDC), 4,4’-(ethyne-1,2-diyl) dibenzene dicarboxylate (EDDB), and 2',3',5',6'-tetramethyl-(1,1':4',1''-terphenyl)-4,4''-dicarboxylate (TPDC-4Me) serving as the strut of the framework, respectively. The PXRD patterns of each product remained consistent with that of the corresponding parent MOF (Figure III-5c and Figure III-16), indicating

that the crystal structure of the parent MOF was well preserved after introducing a secondary functionality through our ISLI strategy.

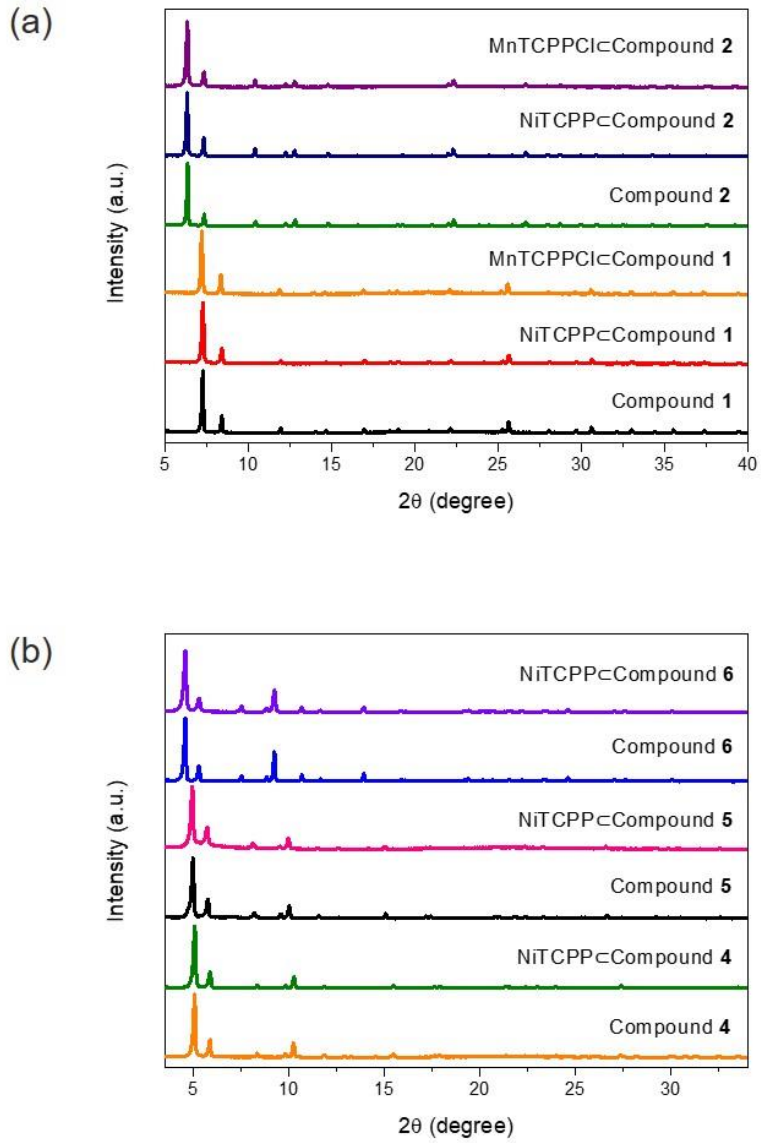

Figure III-16. (a) and (b) represent selected PXRD patterns of functionalized UiO series of MOFs obtained by ISLI strategy.

The morphology of each MOF was observed under SEM. And SEM images showed that these MOFs were octahedral microcrystals (Figure III-17).

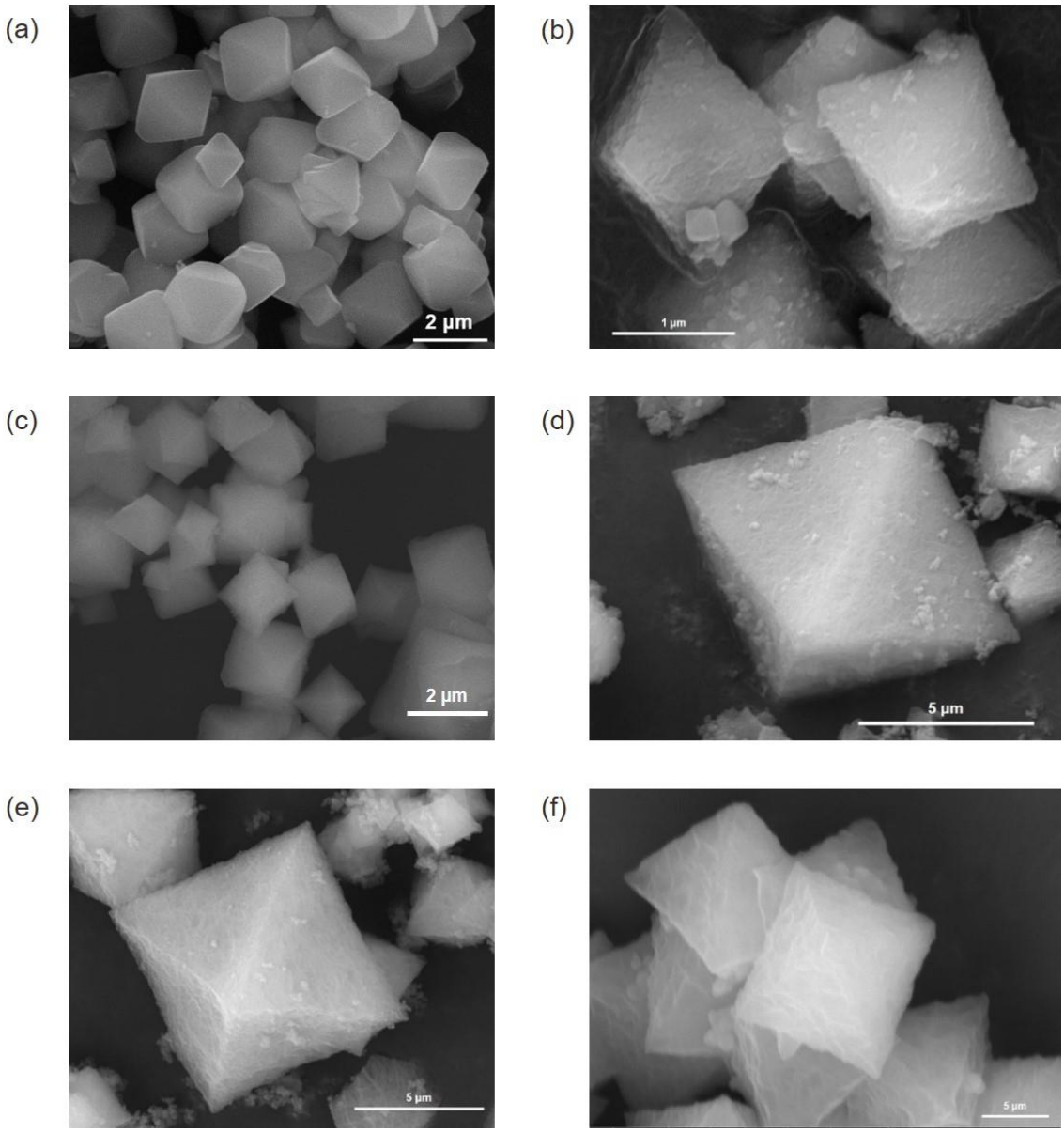

Figure III-17. SEM images of (a) compound **1**, (b) compound **2**, (c) compound **3**, (d) compound **4**, (e) compound **5**, and (f) compound **6**.

In addition, the permanent porosity of each sample was assessed by N_2 adsorption experiments at 77 K (Figure III-18). According to the reticular chemistry, the MOF synthesized from a longer organic strut possesses larger pores and thus shows higher N_2 uptake. As expected, when the parent UiO series of MOF was constructed from longer ditopic linear ligands, its functionalized product also exhibited higher N_2 uptake.

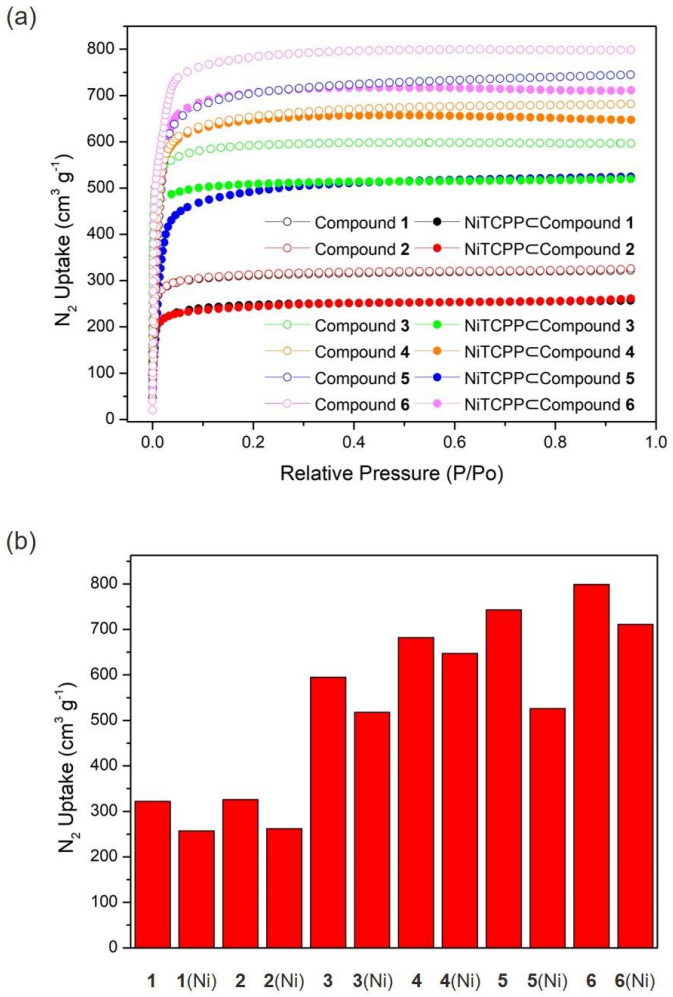

Figure III-18. (a) N_2 adsorption isotherms of parent and NiTCPP-functionalized UiO series of MOFs at 77 K. (b) Comparison of total N_2 uptake of these MOFs.

Moreover, ICP tests were conducted to determine the amount of incorporated porphyrin in the synthesized MOFs (Table III-3). These results showed that the structure of MOF as well as the variety and amount of incorporated functionality can be adjusted at the same time by the ISLI strategy without destructing the original framework integrity. Consequently, this ISLI strategy is of great value to synthesize MOFs with desired functionality for a wide range of applications.

Mechanism Studies of ISLI. Having applied ISLI strategy to synthesize UiO series of MOFs successfully, we attempted to understand the thermodynamics and kinetics aspects of this strategy from both experimental and computational studies.

Essentially, the crystal growth of MOF is ligand substitution on metal ions or clusters.[30] Since the concentration of BA is much higher than the ditopic ligand and tetratopic ligand in the reaction system, Zr_6 clusters are most likely connected by BA at the beginning, and then gradually substituted by the ditopic or tetratopic ligand to form UiO phase or PCN phase in the end.

Taking into consideration of the above reaction processes, we carried out DFT calculations to measure the enthalpy of formation (ΔH) of a series of MOFs, including UiO-66 (Compound **1**), UiO-67 (Compound **3**), Compound **5**, and PCN-222. The Zr_6 cluster coordinated to 12 BA with the formula of $Zr_6O_4(OH)_4(C_6H_5COO)_{12}$ (**R**) was selected as the initial structure for calculation to compare the ΔH value of our selected MOFs. After the reaction process, all the terminal BA were substituted by BDC/BPDC/EDDB/NiTCPP ligands to form the corresponding MOFs. The ΔH value of

these MOFs were calculated on a unit cell for each MOF (Figure III-19) according to the equations shown in Scheme III-5.

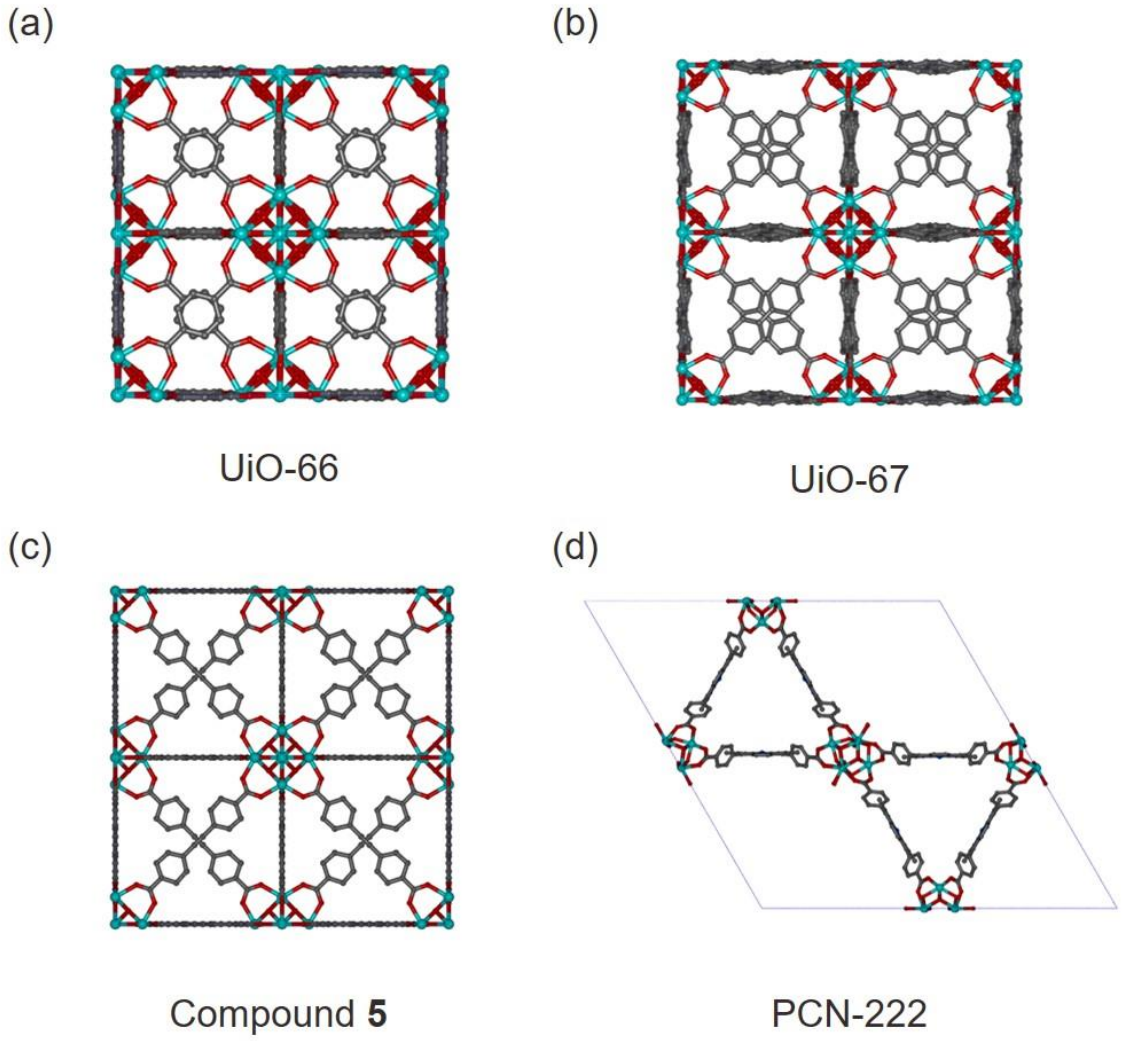

Figure III-19. The structures of MOFs used for DFT calculations. (a) UiO-66; (b) UiO-67; (c) Compound **5**; and (d) PCN-222.

In order to make results comparable, we divided the calculated enthalpies by a factor of 4 for UiO series and 3 for PCN-222 to obtain the enthalpies assigned to each Zr_6 cluster for each MOF (Table III-4).

Table III-4. Calculated enthalpies of formation of the selected MOFs

MOF	UiO-66	UiO-67	Compound **5**	PCN-222
ΔH (kJ mol^{-1})	-51.1	-36.2	-33.4	-62.6

Influence of BA. Since many parameters could influence the product obtained, we firstly examined the effect of BA on the formation of MOF. According to Scheme III-4, if the MOF formation is expressed as an equilibrium reaction of ligand substitution (Equation 1), adding BA into the system increases Gibbs free energy (ΔG) of the reaction (Equation 2) and shifts the reaction equilibrium to the left (starting materials). As a result, the formation of MOF can be significantly suppressed with an increasing amount of BA in the system. In addition, BA could slow down the ligand substitution process by inhibiting deprotonation of the ligands, and thus improve the crystallinity of the obtained products. Given this, we carried out some experiments to demonstrate our hypothesis. For example, different amounts of BA was used to synthesize NiTCPP⊂UiO-66. These products were then tested under SEM. The SEM images showed that the morphology of NiTCPP⊂UiO-66 altered from intergrown aggregates to octahedral microcrystals with increasing amount of BA used for the synthesis (Figure III-20).

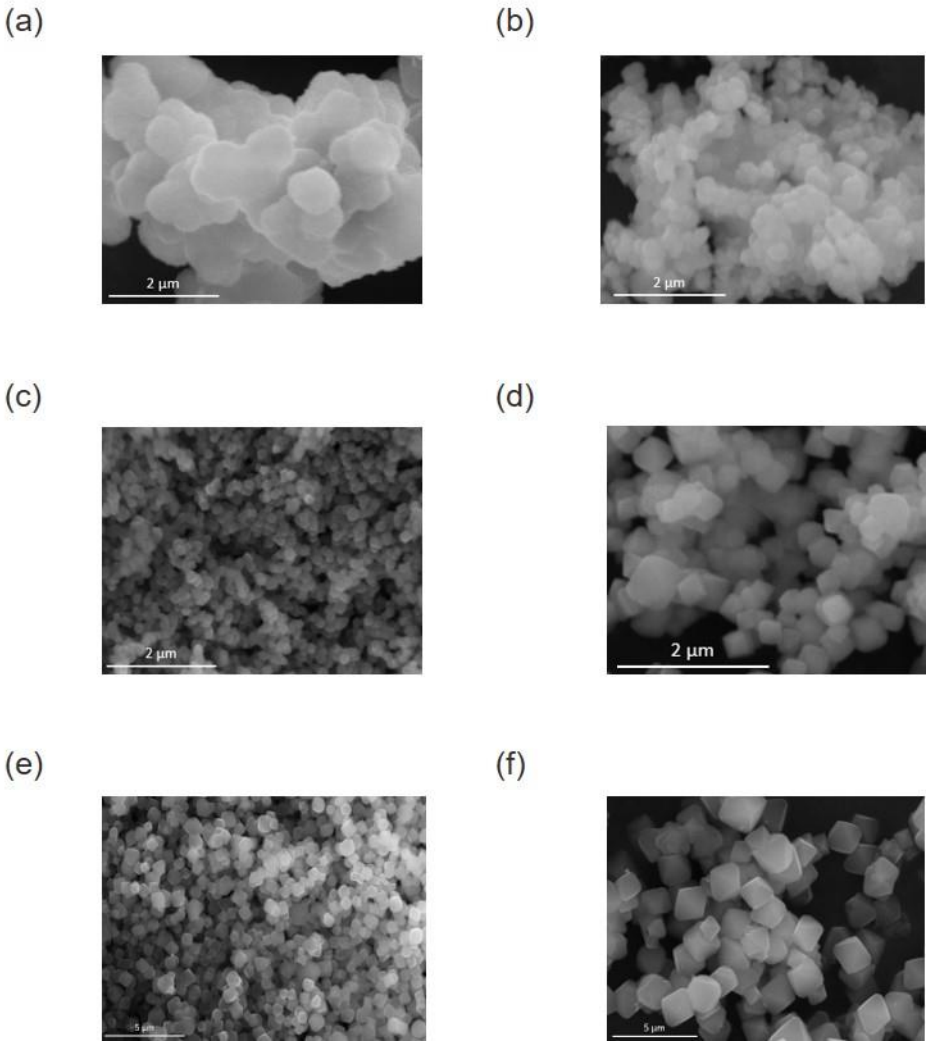

Figure III-20. Representative SEM images of NiTCPP⊂UiO-66 with (a) no BA; (b) 100 mg BA; (c) 200 mg BA; (d) 300 mg BA; (e) 400 mg BA; and (f) 600 mg BA used for the synthesis.

Our hypothesis also suggested that when the amount of BA added increases up to a certain value, the formation of the MOF can be totally inhibited since the reaction becomes nonspontaneous ($\Delta G > 0$). Indeed, when an increased amount of BA (600 mg, 4.9 mmol) did not fully suppress the growth of UiO-66 (Figure III-21c), the growth of UiO-67 was completely inhibited (Figure III-21c). In addition, even less amount of BA

was enough to fully inhibit the growth of compound **5** (Figure III-2c). Interestingly, the tolerance of BA for each MOF is correlated to the ΔH value determined by calculation (Table III-4). This correlation may suggest that the difference of the entropy of formation (ΔS) value between our selected UiO series of MOFs are neglectable, and thus their relative ΔG value can be reflected by ΔH value.

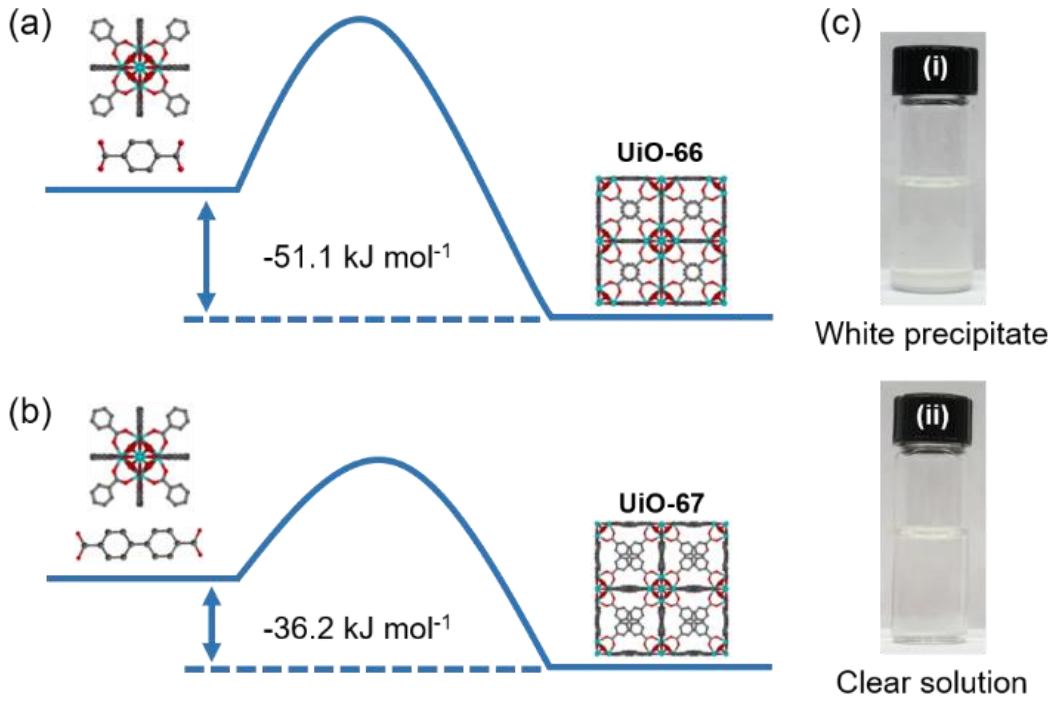

Figure III-21. Energy diagrams of the reaction towards (a) UiO-66 and (b) UiO-67. (c) Photographs of the products obtained with 600 mg BA used for the synthesis of (i) UiO-66 (white precipitate); and (ii) UiO-67 (clear solution).

Furthermore, formation of impurity phase (PCN-222) was observed with 500 mg (4.1 mmol) BA used for the synthesis of MnTCPPCl⊂UiO-67 (Figure III-22). This is most likely because large amount of BA greatly suppressed the formation of UiO-67 thermodynamically, leaving more available Zr species in the system. Despite low

concentration of porphyrin ligands, PCN-222 can still be generated probably due to more favorable thermodynamic driving force.

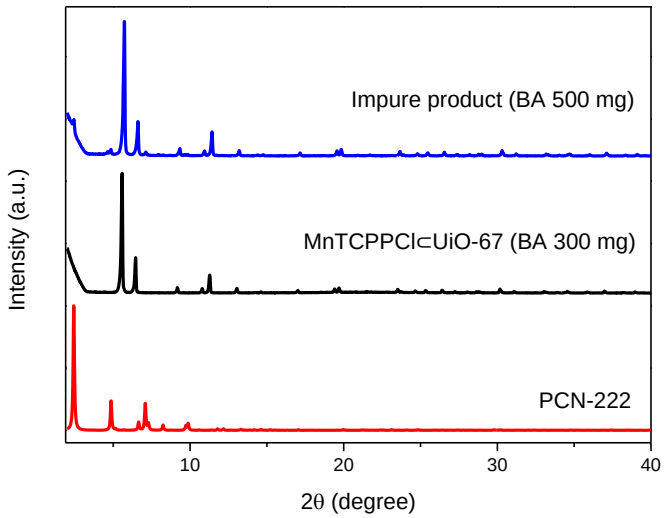

Figure III-22. PXRD patterns for PCN-222 and the products obtained with different amount of BA used for the synthesis of MnTCPPCl⊂UiO-67.

Influence of TCPP. In addition to the modulating reagent (BA), the effect of porphyrin ligand was investigated. During the reaction, TCPP ligand can compete with the ditopic ligand to coordinate to the Zr_6 cluster due to comparable coordination ability (Figure III-23). As we mentioned above, formation of impurity was observed with increased amount of TCPP used for the synthesis (Figure III-10). One possible reason is that with higher concentration of the porphyrin ligand, the rate of ligand substitution on Zr_6 cluster is faster and the nucleation process of the impurity phase can be accelerated. In addition, the impure phase is thermodynamically more favorable to form with more TCPP due to decreased ΔG. Therefore, to prevent the formation of impurities, we

judiciously adjust the amount of mixed ligands used for the synthesis. By increasing the amount of ditopic ligand and decreasing the amount of TCPP ligand, the reaction system can be both kinetically and thermodynamically driven towards porphyrin-functionalized UiO phase and away from the competing PCN-222 phase.

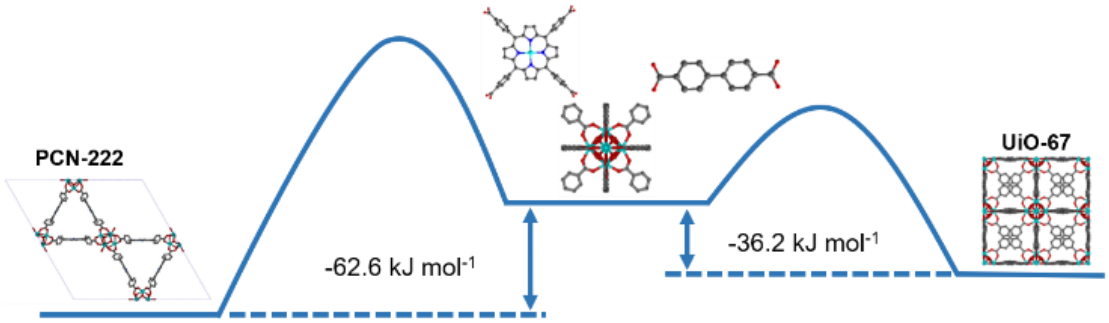

Figure III-23. The energy diagram of the formation of competing phases in the reaction system.

The above computational and experimental results showed that the modulating reagent BA can be used to improve the crystallinity of the product. However, when the concentration of BA increased to a certain amount, impurity phases began to form in the system. Therefore, the concentration of BA should be adjusted in a cerain range to achieve the balance between high crystallinity and purity of the MOF product. Secondly, for different UiO series of MOFs, different amounts of BA can be tolerated in the reaction system while preserving the phase purity of the obtained product. Moreover, the generation of impurity phases was observed with increasing amount of TCPP ligand added in the system. Consequently, it is very important to adjust the concentration of BA, ditopic ligands and tetratopic ligands to both thermodynamically and kinetically control

the reaction system towards the formation of phase-pure UiO series of MOFs with the incorporation of desired porphyrin functionality.

3.4 Conclusions

A comprehensive study of the in situ secondary ligand incorporation (ISLI) strategy was presented in this chapter to construct highly stable UiO series of MOFs (e.g. UiO-66, UiO-67, and UiO-68) with the incorporation of multiple functionalities. Firstly, UiO-67 functionalized with porphyrin was synthesized by mixing ditopic BPDC ligands and tetratopic TCPP ligands in a one-pot synthesis, while maintaining the original crystal structure, morphology, and stability of the parent MOF (UiO-67). By combining diverse porphyrin ligands with different metals in the center as well as BPDC ligand or its derivatives, UiO-67 was successfully modified with multiple functionalities. In addition, the amount of incorporated porphyrin can be gradually adjusted by adding different amounts of porphyrin ligand into the reaction system. Then, the ISLI strategy was successfully applied to functionalize many UiO series of MOFs (e.g. compounds **1**-**6**). Moreover, both computational and experimental studies were carried out to understand the mechanism aspect of our ISLI strategy. Firstly, adding the modulating reagent (BA) could slow down the growth of the MOF and thus improve its crystallinity. However, when the amount of BA increased to a certain value, ΔG of the MOF formation turns to positive and thus the reaction becomes nonspontaneous. Given this, theoretically MOF with lower ΔG could tolerate more BA, which was further confirmed by experimental studies. Secondly, due to the competition of mixed ligands to connect to the metal

clusters, the formation of impurity phases (e.g. PCN-222) can be eliminated with lower concentration of porphyrin ligands. Consequently, the reaction conditions (e.g. the concentration of mixed ligands and BA) should be carefully adjusted to thermodynamically and kinetically drive our reaction system towards phase-pure UiO series of MOFs incorporated with porphyrin.

CHAPTER IV

IN SITU SECONDARY LIGAND INCORPORATION STRATEGY TOWARDS ZIRCONIUM MOFS CONSTRUCTED FROM MULTITOPIC LIGANDS

4.1 Introduction

So far, many studies have shown that the structural features (e.g. pore size and window size) of MOFs could influence their performance in various applications, such as gas storage and separation,[4, 112] catalysis,[113-114] and enzyme immobilization.[115] For example, Feng's group reported the generation of new pores inside the framework through a ligand insertion pore space partition strategy.[112] After fine tailoring of the framework structure, the MOF exhibited superior CO_2 uptake capacity. Although there were no open metal sites in the framework, the MOF still showed CO_2 uptake capacity comparable to MOF-74 at 298 K and 1 bar.

For highly stable Zr-MOFs, depending on their structural features, their applications in many fields have also been investigated. For instance, MOF-808 is constructed from tritopic benzene-1,3,5-tricarboxylate (BTC) ligands and 6-connected Zr_6 clusters to form a 6,3-connected 3-D framework with a **spn** topology, which contains tetrahedral cages (4.8 Å) and larger adamantane cages (18.4 Å).[116] MOF-808 has been studied for water adsorption in recent years, and its sulfated analogue shows superacidity.[117] On the other hand, NU-1000, in which each Zr_6 cluster is coordinated to eight tetratopic 1,3,6,8-tetrakis(p-benzoate)pyrene (TBAPy) ligands, exhibits large pores of 31 Å and high BET surface area of 2320 m^2g^{-1}.[118] Taking advantage of the available

coordination sites of Zr_6 clusters in the framework, NU-1000 has been widely investigated for various applications, such as CO_2 capture[118] and destruction of chemical warfare agents.[119-120]

Therefore, exploring more Zr-MOF platforms suitable for introducing multifunctionality is crucial to broaden the potential applications of MOFs. Previously, we have demonstrated the construction of multifunctional UiO series of MOFs through an in situ secondary ligand incorporation strategy. Taking advantage of the ubiquity of available coordination sites in Zr-MOFs, this strategy was further applied to a series of Zr-MOFs constructed from multitopic ligands (e.g. MOF-808 and NU-1000). The synthesized MOFs were characterized by many techniques, such as PXRD, N_2 uptake, SEM, EDS mappings, TGA, and ICP. Studies showed that ISLI is a very general strategy to construct highly stable Zr-MOFs with multiple functionalities, which provides a useful tool to investigate advanced applications of MOFs.

4.2 Experimental Section

Materials and Instrumentation. Commercially available reagents and solvents were used as received without further purification. Tetrakis(4-carboxyphenyl)porphyrin (H_2TCPP), [5,10,15,20-tetrakis(4-carboxyphenyl)porphyrinato]-Mn(III) chloride (MnTCPPCl), [5,10,15,20-tetrakis(4-carboxyphenyl)porphyrinato]-Fe(III) chloride (FeTCPPCl), [5,10,15,20-tetrakis(4-carboxyphenyl)porphyrinato]-Zn(II) (ZnTCPP), [5,10,15,20-tetrakis(4-carboxyphenyl)porphyrinato]-Ni(II) (NiTCPP), [5,10,15,20-tetrakis(4-carboxyphenyl)porphyrinato]-Co(II) (CoTCPP), [5,10,15,20-tetrakis(4-

carboxyphenyl)porphyrinato]-Cu(II) (CuTCPP) were synthesized according to the procedure in previous reports with slight modifications.[73]

Powder X-ray diffraction (PXRD) experiment was carried out with a BRUKER D8-Focus Bragg−Brentano X-ray powder diffractometer equipped with a Cu-sealed tube (λ = 1.54178) at 40 kV and 40 mA. Thermogravimetric analysis (TGA) were conducted on a Shimadzu TGA-50 thermogravimetric analyzer at a ramp rate of 2 °C/min in a flowing nitrogen atmosphere. Nuclear magnetic resonance (NMR) spectra were collected on a Mercury 300 spectrometer. Inductively coupled plasma (ICP) tests were conducted on a Perkin Elmer Optima 8000 ICP spectrometer. N_2 adsorption/desorption isotherms were measured on a Micrometritics ASAP 2020 system at 77 K. The sample was activated by solvent exchange (in several cycles using fresh acetone), followed by degassing at elevated temperature (100 °C) for 5 h. Scanning electron microscope (SEM) analysis was performed on QUANTA 450 FEG and energy dispersive X-ray spectroscopy (EDS) analysis was carried out by X-Max20 with Oxford EDS system equipped with X-ray mapping.

Synthesis of 1,3,6,8-Tetrakis(p-Benzoic Acid)pyrene (H_4TBAPy). As shown in Scheme IV-1, 1,3,6,8-tetrakis(p-benzoic acid)pyrene (H_4TBAPy) was synthesized according to the reference.[121]

Synthesis of 1,3,6,8-tetrakis(4-(methoxycarbonyl)phenyl)pyrene: to a mixture of (4-(methoxycarbonyl)phenyl)boronic acid (5.200 g, 29.00 mmol), 1,3,6,8-tetrabromopyrene (2.500 g, 4.85 mmol), tetrakis(triphenylphosphine) palladium(0) (0.150 g 0.130 mmol), and potassium phosphate tribasic (5.500 g, 26.50 mmol) was

added dry dioxane (100 mL). Then, the mixture was stirred under nitrogen atmosphere for 72 h at 130 °C in an oil bath. The reaction mixture was evaporated to dryness and the solid residue was washed with water to remove inorganic salts. The insoluble material was extracted with chloroform (three times by 50 mL). Next, the extract was dried over magnesium sulfate, and the solvent volume was reduced under vacuum. The residue was boiled in tetrahydrofuran for 2h and filtered. The resulting filtrate contained majority of the impurities. Finally, 2.90 g of 1,3,6,8-tetrakis(4-(methoxycarbonyl)phenyl)pyrene was obtained (82% yield). ^{1}H NMR ($CDCl_3$, 300 MHz): δ 3.99 (s, 12H), 7.75 (d, 8H), 8.01 (s, 2H), 8.15 (s, 4H), 8.23 (d, 8H).

Synthesis of 1,3,6,8-tetrakis(p-benzoic acid)pyrene (H_4TBAPy): 1.16 g (1.56 mmol) of solid 1,3,6,8-tetrakis(4-(methoxycarbonyl)phenyl)pyrene, 3.0 g (75.0 mmol) NaOH, and 150 mL of a THF/water (ratio 1:1) mixture was added to a 250 mL round bottom flask. Then, the resultant suspension was vigorously stirred under reflux overnight. The solvents were removed under vacuum and water was added to the residue, which formed a clear yellow solution. The clear yellow solution was stirred at room temperature for 2 h and the pH value was adjusted to 1 by adding concentrated HCl. The resulting yellow solid was collected by filtration and then washed with water several times. The crude product was recrystallized from DMF, filtered, washed with chloroform and dried under vacuum. Finally, 0.98 g of the pure product H_4TBAPy was obtained (91% yield). ^{1}H NMR (DMSO, 300 MHz): δ 7.86 (d, 8H), 8.09 (s, 2H), 8.17 (d, 8H), 8.21 (s, 4H), 13.12 (s, 4H).

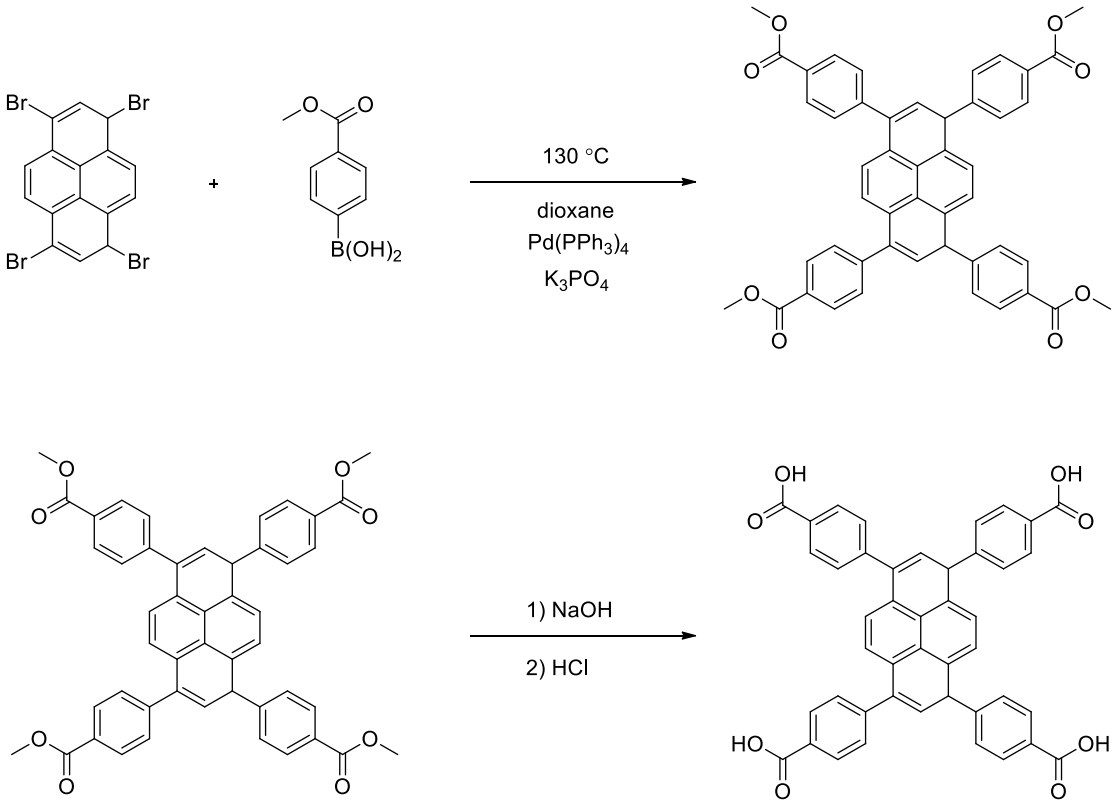

Scheme IV-1. Synthesis of H_4TBAPy ligand.

Synthesis of 4',4''',4''''',4'''''''-(Ethene-1,1,2,2-Tetrayl)tetrakis(([1,1'-Biphenyl]-4-Carboxylic Acid)) (H_4ETTC). As shown in Scheme IV-2, 4',4''',4''''',4'''''''-(ethene-1,1,2,2-tetrayl)tetrakis(([1,1'-biphenyl]-4-carboxylic acid)) (H_4ETTC) was synthesized according to the reference.[122-123]

Synthesis of tetrakis(4-bromophenyl)ethylene: powder tetraphenylethylene (15.00 g, 45.2 mmol) was grinded carefully and reacted with bromine (15.0 mL, 0.3 mol) vapor at room temperature for two weeks. The resulting solid was then recrystallized in methanol and dichloromethane to yield white product (26.2 g, 40.8 mmol, 90% yield). ^{1}H NMR ($CDCl_3$, 300 MHz): δ 6.85 (d, 8H), 7.28 (d, 8H).

Synthesis of tetramethyl 4',4''',4'''',4'''''-(ethene-1,1,2,2-tetrayl)tetrakis([1,1'-biphenyl]-4-carboxylate): tetrakis(4-bromophenyl)ethylene (2.0 g, 3.1 mmol), 4-methoxycarbonylphenylboronic acid (2.8 g, 15.5 mmol), cesium fluoride (6.0 g, 39.5 mmol) and tetrakis(triphenylphosphine)palladium (0.4 g, 0.3 mmol) were added to a 500 mL round bottom flask equipped with a condenser and a stir bar. Then 250 mL degassed dioxane solvent was transferred carefully to the flask through cannula, and the solution was refluxed for 48 h. After the reaction mixture was cooled to room temperature. Then, the solvent was removed under vacuum, and the residue was dissolved in dichloromethane and washed with water three times. The organic layer was dried with magnesium sulfate. After removing the dichloromethane under vacuum, the solid was recrystallized from acetone to yield light yellow product. (1.6 g, 1.8 mmol, 80% yield). ^{1}H NMR ($CDCl_3$, 300 MHz): δ 3.93 (s, 12H), 7.19 (d, 8H), 7.44 (d, 8H), 7.62 (d, 8H), 8.05(d, 8H).

Synthesis of 4',4''',4'''',4'''''-(ethene-1,1,2,2-tetrayl)tetrakis(([1,1'-biphenyl]-4-carboxylic acid)) (H_4ETTC). 4',4''',4'''',4'''''-(ethene-1,1,2,2-tetrayl)tetrakis([1,1'-biphenyl]-4-carboxylate) (1.6 g, 1.8 mmol) and sodium hydroxide (1.7 g, 42.5 mmol) were added into a solvent mixture of THF, methanol and water (v/v/v=1:1:1). The solution was stirred and refluxed overnight. After removing the organic solvent, the aqueous phase was acidified with 6M HCl to yield yellow precipitate of 4',4''',4'''',4'''''-(ethene-1,1,2,2-tetrayl)tetrakis(([1,1'-biphenyl]-3-carboxylic acid)) (H_4ETTC), which was filtered, washed with water, and dried under vacuum. Finally, 1.4 g (1.7 mmol)

product was obtained (95% yield). ^{1}H NMR (DMSO-d_6, 300 MHz): δ, 7.19 (d, 8H), 7.61 (m, 8H), 7.75 (d, 8H), 7.95 (s, 8H).

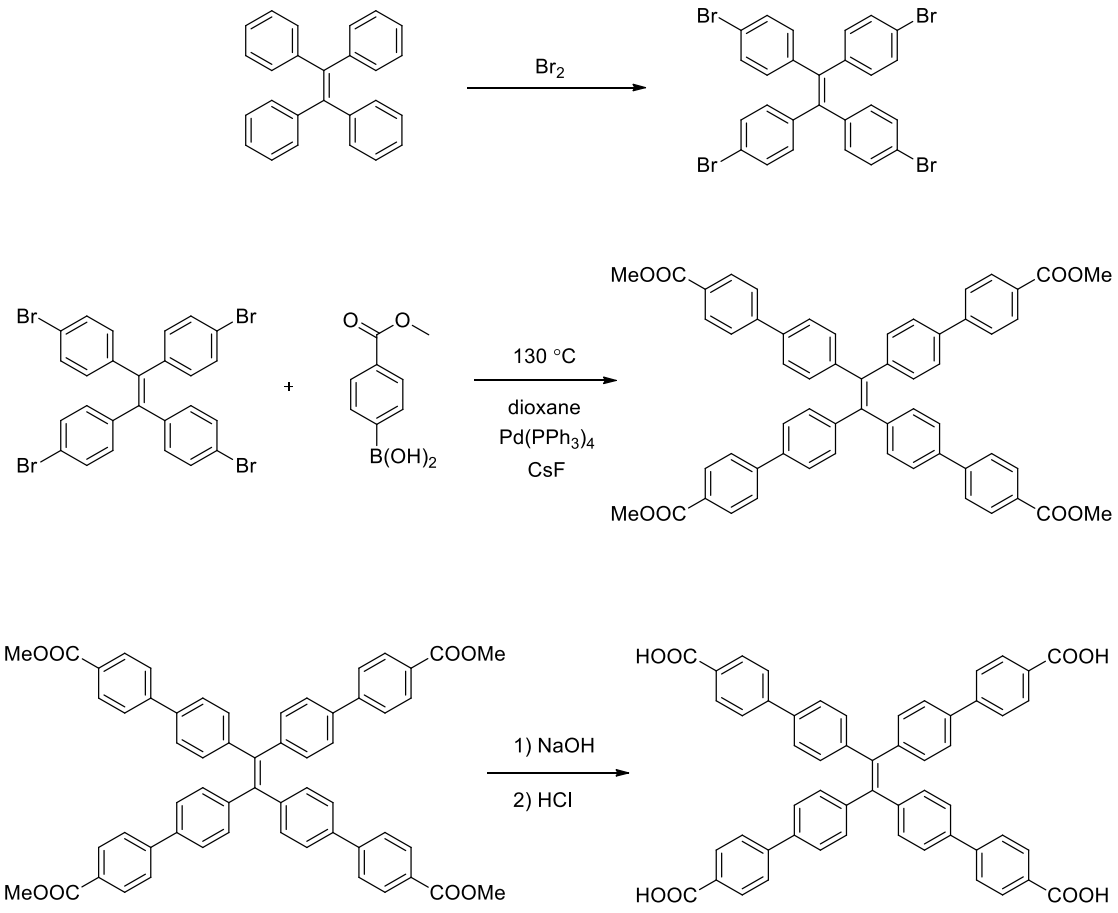

Scheme IV-2. Synthesis of H_4ETTC ligand.

Synthesis of 1,2,4,5-Tetrakis(4-Carboxyphenyl)benzene (H_4TCPB). As shown in Scheme IV-3, 1,2,4,5-tetrakis(4-carboxyphenyl)benzene (H_4TCPB) was synthesized according to the reference by Suzuki coupling of 1,2,4,5-tetrabromobenzene and 4-ethoxycarbonylphenylboronic acid.[124] Firstly, to mixture of 1,2,4,5-tetrabromobenzene (1.01 g, 2.54 mmol), 4-ethoxycarbonylphenylboronic acid (2.42 g, 11.5 mol) and K_3PO_4 (2.70 g, 12.70 mmol) were added degassed 1,4-dioxane (100 mL)

under nitrogen. Then, $Pd(PPh_3)_4$ (0.09 g, 0.08 mmol) was added to the mixture and heated to 85 °C for 4 days under nitrogen atmosphere. The solution was evaporated to dryness and extracted with $CHCl_3$. The $CHCl_3$ was removed by evaporation under vacuum, and the final product H_4TCPB was obtained by hydrolysis of the crude product under reflux overnight with 2M NaOH aqueous solution (200 mL) followed by acidification with concentrated HCl (1.23 g, 86% yield).^{1}H NMR (DMSO-d_6, 300 MHz): δ, 8.08 (d, 8H), 7.83 (d, 8H), 7.80 (s, 2H).

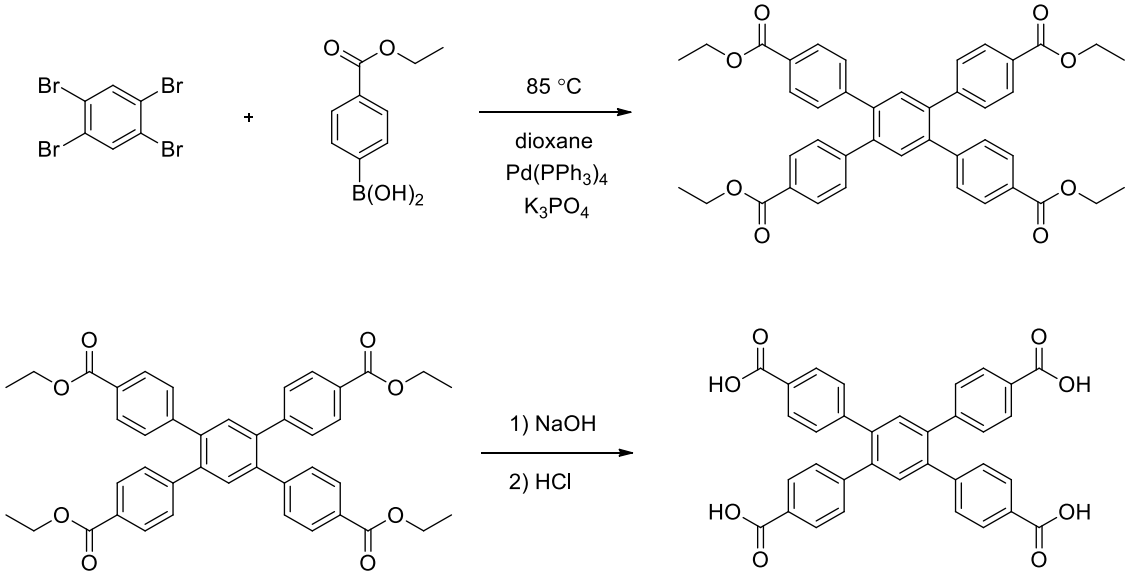

Scheme IV-3. Synthesis of H_4TCPB ligand.

Synthesis of Compound 7 (MOF-808). $ZrOCl_2 \cdot 8H_2O$ (8.0 mg, 0.025 mmol), H_3BTC (5.5 mg, 0.026 mmol), and formic acid (1 mL) in 1 mL of DMF were ultrasonically dissolved in a Pyrex vial. The mixture was heated in an oven at 120 °C for 22 h. After cooling down to room temperature, the precipitates were collected by centrifugation. The solids were washed with DMF three times to remove unreacted

precursors, and then solvent-exchanged with acetone three times. The resulting powder was obtained by centrifugation, and dried in an oven at 80 °C.

Synthesis of NiTCPP⊂Compound 7 (NiTCPP⊂MOF-808). $ZrOCl_2 \cdot 8H_2O$ (8.0 mg, 0.025 mmol), H_3BTC (5.5 mg, 0.026 mmol), NiTCPP (5 mg, 0.006 mmol) and formic acid (1 mL) in 1 mL of DMF were ultrasonically dissolved in a Pyrex vial. The mixture was heated in an oven at 120 °C for 22 h. After cooling down to room temperature, the precipitates were collected by centrifugation. The solids were washed with DMF three times to remove unreacted precursors, and then solvent-exchanged with acetone three times. The resulting powder was obtained by centrifugation, and dried in an oven at 80 °C.

Synthesis of FeTCPPCl⊂Compound 7 (FeTCPPCl⊂MOF-808). $ZrOCl_2 \cdot 8H_2O$ (8.0 mg, 0.025 mmol), H_3BTC (5.5 mg, 0.026 mmol), FeTCPPCl (5 mg, 0.006 mmol) and formic acid (1 mL) in 1 mL of DMF were ultrasonically dissolved in a Pyrex vial. The mixture was heated in an oven at 120 °C for 22 h. After cooling down to room temperature, the precipitates were collected by centrifugation. The solids were washed with DMF three times to remove unreacted precursors, and then solvent-exchanged with acetone three times. The resulting powder was obtained by centrifugation, and dried in an oven at 80 °C.

Synthesis of MnTCPPCl⊂Compound 7 (MnTCPPCl⊂MOF-808). $ZrOCl_2 \cdot 8H_2O$ (8.0 mg, 0.025 mmol), H_3BTC (5.5 mg, 0.026 mmol), MnTCPPCl (5 mg, 0.006 mmol) and formic acid (1 mL) in 1 mL of DMF were ultrasonically dissolved in a Pyrex vial. The mixture was heated in an oven at 120 °C for 22 h. After cooling down to

room temperature, the precipitates were collected by centrifugation. The solids were washed with DMF three times to remove unreacted precursors, and then solvent-exchanged with acetone three times. The resulting powder was obtained by centrifugation, and dried in an oven at 80 °C.

Synthesis of CuTCPP⊂Compound 7 (CuTCPP⊂MOF-808). $ZrOCl_2 \cdot 8H_2O$ (8.0 mg, 0.025 mmol), H_3BTC (5.5 mg, 0.026 mmol), CuTCPP (5 mg, 0.006 mmol) and formic acid (1 mL) in 1 mL of DMF were ultrasonically dissolved in a Pyrex vial. The mixture was heated in an oven at 120 °C for 22 h. After cooling down to room temperature, the precipitates were collected by centrifugation. The solids were washed with DMF three times to remove unreacted precursors, and then solvent-exchanged with acetone three times. The resulting powder was obtained by centrifugation, and dried in an oven at 80 °C.

Synthesis of H_2TCPP⊂Compound 7 (H_2TCPP⊂MOF-808). $ZrOCl_2 \cdot 8H_2O$ (8.0 mg, 0.025 mmol), H_3BTC (5.5 mg, 0.026 mmol), H_2TCPP (5 mg, 0.006 mmol) and formic acid (1 mL) in 1 mL of DMF were ultrasonically dissolved in a Pyrex vial. The mixture was heated in an oven at 120 °C for 22 h. After cooling down to room temperature, the precipitates were collected by centrifugation. The solids were washed with DMF three times to remove unreacted precursors, and then solvent-exchanged with acetone three times. The resulting powder was obtained by centrifugation, and dried in an oven at 80 °C.

Synthesis of ZnTCPP⊂Compound 7 (ZnTCPP⊂MOF-808). $ZrOCl_2 \cdot 8H_2O$ (8.0 mg, 0.025 mmol), H_3BTC (5.5 mg, 0.026 mmol), ZnTCPP (5 mg, 0.006 mmol) and

formic acid (1 mL) in 1 mL of DMF were ultrasonically dissolved in a Pyrex vial. The mixture was heated in an oven at 120 °C for 22 h. After cooling down to room temperature, the precipitates were collected by centrifugation. The solids were washed with DMF three times to remove unreacted precursors, and then solvent-exchanged with acetone three times. The resulting powder was obtained by centrifugation, and dried in an oven at 80 °C.

Synthesis of CoTCPP⊂Compound 7 (CoTCPP⊂MOF-808). $ZrOCl_2 \cdot 8H_2O$ (8.0 mg, 0.025 mmol), H_3BTC (5.5 mg, 0.026 mmol), CoTCPP (5 mg, 0.006 mmol) and formic acid (1 mL) in 1 mL of DMF were ultrasonically dissolved in a Pyrex vial. The mixture was heated in an oven at 120 °C for 22 h. After cooling down to room temperature, the precipitates were collected by centrifugation. The solids were washed with DMF three times to remove unreacted precursors, and then solvent-exchanged with acetone three times. The resulting powder was obtained by centrifugation, and dried in an oven at 80 °C.

Synthesis of Compound 8 (NU-1000). $ZrOCl_2 \cdot 8H_2O$ (24.2 mg, 0.075 mmol), H_4TBAPy (17.1 mg, 0.025 mmol), and benzoic acid (800 mg, 6.551 mmol) in 2 mL of DMF were ultrasonically dissolved in a Pyrex vial. The mixture was heated in an oven at 120 °C for 22 h. After cooling down to room temperature, the precipitates were collected by centrifugation. The solids were washed with DMF three times to remove unreacted precursors, and then solvent-exchanged with acetone three times. The resulting powder was obtained by centrifugation, and dried in an oven at 80 °C.

Synthesis of NiTCPP⊂Compound 8 (NiTCPP⊂NU-1000). $ZrOCl_2 \cdot 8H_2O$ (24.2 mg, 0.075 mmol), H_4TBAPy (17.1 mg, 0.025 mmol), NiTCPP (10 mg, 0.012 mmol) and benzoic acid (800 mg, 6.551 mmol) in 2 mL of DMF were ultrasonically dissolved in a Pyrex vial. The mixture was heated in an oven at 120 °C for 22 h. After cooling down to room temperature, the precipitates were collected by centrifugation. The solids were washed with DMF three times to remove unreacted precursors, and then solvent-exchanged with acetone three times. The resulting powder was obtained by centrifugation, and dried in an oven at 80 °C.

Synthesis of FeTCPPCl⊂Compound 8 (FeTCPPCl⊂NU-1000). $ZrOCl_2 \cdot 8H_2O$ (24.2 mg, 0.075 mmol), H_4TBAPy (17.1 mg, 0.025 mmol), FeTCPPCl (5 mg, 0.006 mmol) and benzoic acid (800 mg, 6.551 mmol) in 2 mL of DMF were ultrasonically dissolved in a Pyrex vial. The mixture was heated in an oven at 120 °C for 22 h. After cooling down to room temperature, the precipitates were collected by centrifugation. The solids were washed with DMF three times to remove unreacted precursors, and then solvent-exchanged with acetone three times. The resulting powder was obtained by centrifugation, and dried in an oven at 80 °C.

Synthesis of MnTCPPCl⊂Compound 8 (MnTCPPCl⊂NU-1000). $ZrOCl_2 \cdot 8H_2O$ (24.2 mg, 0.075 mmol), H_4TBAPy (17.1 mg, 0.025 mmol), MnTCPPCl (5 mg, 0.006 mmol) and benzoic acid (800 mg, 6.551 mmol) in 2 mL of DMF were ultrasonically dissolved in a Pyrex vial. The mixture was heated in an oven at 120 °C for 22 h. After cooling down to room temperature, the precipitates were collected by centrifugation. The solids were washed with DMF three times to remove unreacted

precursors, and then solvent-exchanged with acetone three times. The resulting powder was obtained by centrifugation, and dried in an oven at 80 °C.

Synthesis of Compound 9. $ZrOCl_2 \cdot 8H_2O$ (21.5 mg, 0.067 mmol), H_4TCPB (18.6 mg, 0.033 mmol), and benzoic acid (400 mg, 3.275 mmol) in 2 mL of DMF were ultrasonically dissolved in a Pyrex vial. The mixture was heated in an oven at 120 °C for 22 h. After cooling down to room temperature, the precipitates were collected by centrifugation. The solids were washed with DMF three times to remove unreacted precursors, and then solvent-exchanged with acetone three times. The resulting powder was obtained by centrifugation, and dried in an oven at 80 °C.

Synthesis of NiTCPP⊂Compound 9. $ZrOCl_2 \cdot 8H_2O$ (21.5 mg, 0.067 mmol), H_4TCPB (18.6 mg, 0.033 mmol), NiTCPP (5 mg, 0.006 mmol) and benzoic acid (400 mg, 3.275 mmol) in 2 mL of DMF were ultrasonically dissolved in a Pyrex vial. The mixture was heated in an oven at 120 °C for 22 h. After cooling down to room temperature, the precipitates were collected by centrifugation. The solids were washed with DMF three times to remove unreacted precursors, and then solvent-exchanged with acetone three times. The resulting powder was obtained by centrifugation, and dried in an oven at 80 °C.

Synthesis of MnTCPPCl⊂Compound 9. $ZrOCl_2 \cdot 8H_2O$ (21.5 mg, 0.067 mmol), H_4TCPB (18.6 mg, 0.033 mmol), MnTCPPCl (5 mg, 0.006 mmol) and benzoic acid (400 mg, 3.275 mmol) in 2 mL of DMF were ultrasonically dissolved in a Pyrex vial. The mixture was heated in an oven at 120 °C for 22 h. After cooling down to room temperature, the precipitates were collected by centrifugation. The solids were washed

with DMF three times to remove unreacted precursors, and then solvent-exchanged with acetone three times. The resulting powder was obtained by centrifugation, and dried in an oven at 80 °C.

Synthesis of Compound 10. $ZrOCl_2 \cdot 8H_2O$ (24.2 mg, 0.075 mmol), H_4ETTC (20.3 mg, 0.025 mmol), and TFA (0.2 mL) in 2 mL of DMF were ultrasonically dissolved in a Pyrex vial. The mixture was heated in an oven at 120 °C for 22 h. After cooling down to room temperature, the precipitates were collected by centrifugation. The solids were washed with DMF three times to remove unreacted precursors, and then solvent-exchanged with acetone three times. The resulting powder was obtained by centrifugation, and dried in an oven at 80 °C.

Synthesis of NiTCPP⊂Compound 10. $ZrOCl_2 \cdot 8H_2O$ (24.2 mg, 0.075 mmol), H_4ETTC (20.3 mg, 0.025 mmol), NiTCPP (5 mg, 0.006 mmol) and TFA (0.2 mL) in 2 mL of DMF were ultrasonically dissolved in a Pyrex vial. The mixture was heated in an oven at 120 °C for 22 h. After cooling down to room temperature, the precipitates were collected by centrifugation. The solids were washed with DMF three times to remove unreacted precursors, and then solvent-exchanged with acetone three times. The resulting powder was obtained by centrifugation, and dried in an oven at 80 °C.

Synthesis of X⊂NU-1000 (X = NiTCPP, FeTCPPCl, MnTCPPCl, CuTCPP, ZnTCPP, and CoTCPP). $ZrOCl_2 \cdot 8H_2O$ (24.2 mg, 0.075 mmol), H_4TBAPy (17.1 mg, 0.025 mmol), NiTCPP (1.0 mg, 0.001 mmol), FeTCPPCl (1.0 mg, 0.001 mmol), MnTCPPCl (1.0 mg, 0.001 mmol), CuTCPP (1.0 mg, 0.001 mmol), ZnTCPP (1.0 mg, 0.001 mmol), CoTCPP (1.0 mg, 0.001 mmol) and benzoic acid (700 mg, 5.732 mmol) in

2 mL of DMF were ultrasonically dissolved in a Pyrex vial. The mixture was heated in an oven at 120 °C for 22 h. After cooling down to room temperature, the precipitates were collected by centrifugation. The solids were washed with DMF three times to remove unreacted precursors, and then solvent-exchanged with acetone three times. The resulting powder was obtained by centrifugation, and dried in an oven at 80 °C.

ICP Analyses. Samples were prepared in duplicate with weights of around 3 mg. Each sample was dissolved in J.T. Baker Ultrex® II Ultrapure 70% nitric acid at 70 °C for 12 hours. Samples were then diluted to 150x in 1% nitric acid and 18.2 MΩ water from a Millipore Milli-Q® water purification system. Calibration standards were prepared from certified reference standards from RICCA Chemical Company. Samples were further analyzed with a Perkin Elmer Optima 8000 ICP spectrometer. Resulting calibration curves have minimum R^2 = 0.9999. Additionally, to maintain accuracy, quality control samples from certified reference standards and internal standards were utilized. The individual results of the duplicate samples were averaged to determine the metal ratios.

Table IV-1. Mn to Zr atomic ratio in MnTCPPCl⊂NU-1000 with different amounts of porphyrin ligand used for the synthesis

TCPP / mg	3	4	5
Trial 1	0.019	0.034	0.045
Trial 2	0.020	0.034	0.045
Average	0.020	0.034	0.045

Table IV-2. Ni to Zr atomic ratio in NiTCPP⊂compounds 7-10

Compound	**7**	**8**	**9**	**10**
Trial 1	0.015	0.050	0.018	0.062
Trial 2	0.015	0.050	0.025	0.062
Average	0.015	0.050	0.022	0.062

Phase Diagram Determination. High-throughput screening is applied to plot the phase diagram of Compound **9**. The reactions were carried out under the conditions shown in Table IV-3 (DMF 2 mL at 120 °C). The product obtained was characterized by PXRD to determine the phase purity. Figure IV-1 shows an example of impurity product, the composition of which can be determined by comparing with the simulated one.

Table IV-3. The reaction conditions carried out to determine the phase diagram

Entry	$ZrOCl_2 \cdot 8H_2O$ / mg	TCPB / mg	TCPP /mg	BA / mg
1	21.5	18.6	5	250
2	21.5	18.6	10	250
3	21.5	18.6	15	250
4	21.5	18.6	20	250
5	21.5	18.6	25	250
6	21.5	18.6	30	250
7	21.5	18.6	35	250
8	21.5	18.6	5	370
9	21.5	18.6	10	370
10	21.5	18.6	15	370
11	21.5	18.6	20	370

Table IV-3. Continued

Entry	$ZrOCl_2 \cdot 8H_2O$ / mg	TCPB / mg	TCPP /mg	BA / mg
12	21.5	18.6	25	370
13	21.5	18.6	30	370
14	21.5	18.6	35	370
15	21.5	18.6	5	490
16	21.5	18.6	10	490
17	21.5	18.6	15	490
18	21.5	18.6	20	490
19	21.5	18.6	25	490
20	21.5	18.6	30	490
21	21.5	18.6	35	490
22	21.5	18.6	5	610
23	21.5	18.6	10	610
24	21.5	18.6	15	610
25	21.5	18.6	20	610
26	21.5	18.6	25	610
27	21.5	18.6	30	610
28	21.5	18.6	35	610
29	21.5	18.6	5	730
30	21.5	18.6	10	730
31	21.5	18.6	15	730
32	21.5	18.6	20	730
33	21.5	18.6	25	730
34	21.5	18.6	30	730
35	21.5	18.6	35	730
36	21.5	18.6	5	850
37	21.5	18.6	10	850
38	21.5	18.6	15	850
39	21.5	18.6	20	850

Table IV-3. Continued

Entry	$ZrOCl_2 \cdot 8H_2O$ / mg	TCPB / mg	TCPP /mg	BA / mg
40	21.5	18.6	25	850
41	21.5	18.6	30	850
42	21.5	18.6	35	850
43	21.5	18.6	5	970
44	21.5	18.6	10	970
45	21.5	18.6	15	970
46	21.5	18.6	20	970
47	21.5	18.6	25	970
48	21.5	18.6	30	970
49	21.5	18.6	35	970
50	21.5	18.6	5	1090
51	21.5	18.6	10	1090
52	21.5	18.6	15	1090
53	21.5	18.6	20	1090
54	21.5	18.6	25	1090
55	21.5	18.6	30	1090
56	21.5	18.6	35	1090
57	21.5	18.6	5	1210
58	21.5	18.6	10	1210
59	21.5	18.6	15	1210
60	21.5	18.6	20	1210
61	21.5	18.6	25	1210
62	21.5	18.6	30	1210
63	21.5	18.6	35	1210

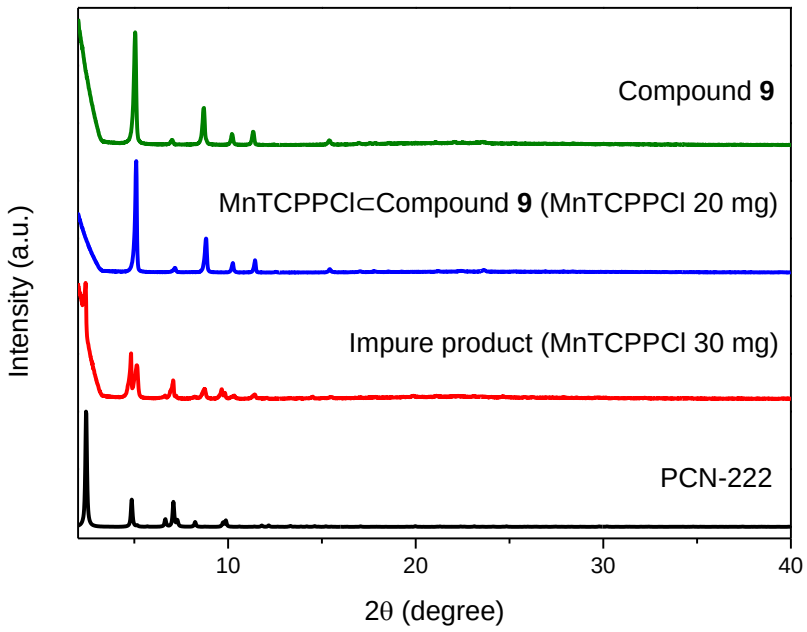

Figure IV-1. PXRD patterns for PCN-222, compound **9** and the products obtained with different amount of MnTCPPCl added in the system.

TGA Analyses. About 10.0 mg of the MOF samples were heated on the Shimadzu TGA-50 instrument from room temperature to 800 °C at a ramp rate of 2 °C/min under nitrogen flow of 25 mL/min. The decomposition temperature of each material was obtained according to corresponding TGA data, which suggested the excellent thermal stability of these MOF samples.

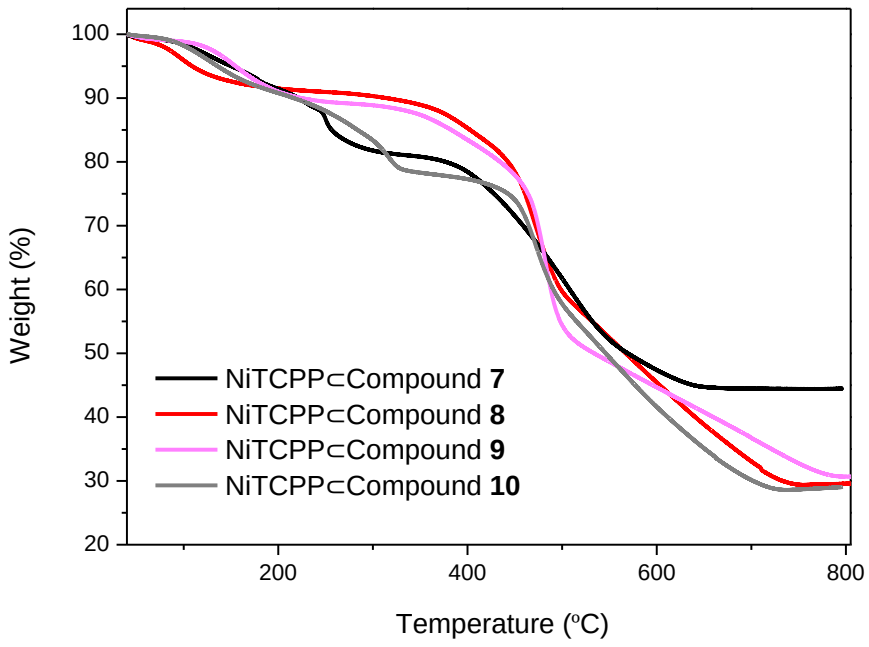

Figure IV-2. TGA analyses of NiTCPP⊂compound **7**, NiTCPP⊂compound **8**, NiTCPP⊂compound **9**, and NiTCPP⊂compound **10**.

4.3 Results and Discussion

Functionalization of MOF-808 through ISLI. In order to extend the ISLI strategy, we firstly selected MOF-808 (compound **7**) as an example of Zr-MOFs constructed from tritopic ligands. Solvothermal reaction of $ZrOCl_2 \cdot 8H_2O$, H_3BTC, and formic acid in N,N-dimethylformamide (DMF) at 120 °C for 22 hours yielded white powders of MOF-808 (Figure IV-3a). And solvothermal reaction of $ZrOCl_2 \cdot 8H_2O$, H_3BTC, [5,10,15,20-tetrakis(4-carboxyphenyl)porphyrinato]-Ni(II) (NiTCPP), and formic acid in DMF at 120 °C for 22 hours yielded red powders of NiTCPP⊂MOF-808. After washing with DMF and acetone, the product remained red, indicating the presence

of porphyrin (Figure IV-3b). In addition, the PXRD pattern of the red powder was in consistent to that of MOF-808 (Figure IV-3c), suggesting that the framework of MOF-808 was well preserved after functionalization of MOF-808 with porphyrin.

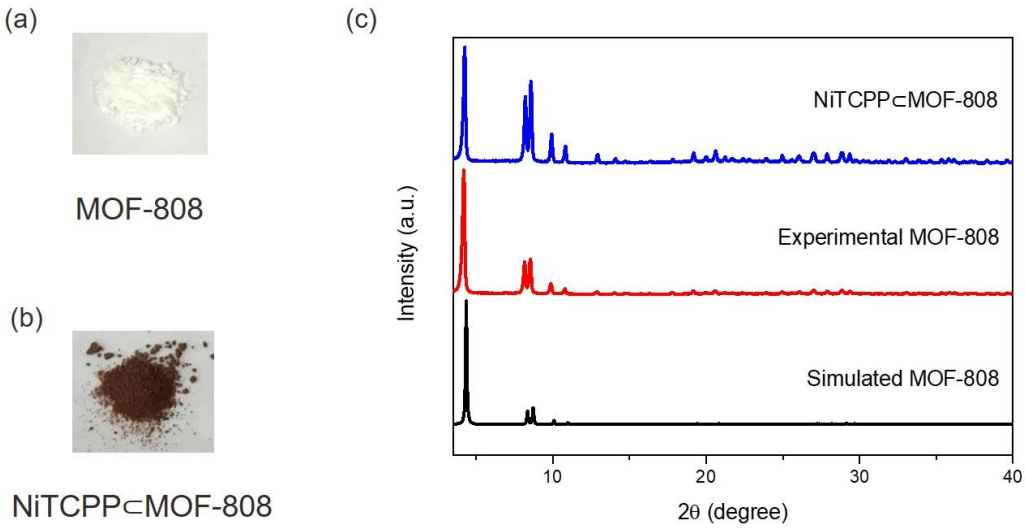

Figure IV-3. Photographs of (a) MOF-808 and (b) NiTCPP⊂MOF-808. (c) PXRD patterns for MOF-808 and NiTCPP⊂MOF-808.

In order to assess the permanent porosity of the product, we directly activated the sample by removing the solvent and then carried out N_2 uptake test at 77 K. Type I isotherms that are typical for microporous solids were acquired. Compared with pristine MOF-808 (537 cm3 g-1), NiTCPP⊂NOF-808 exhibited lower N_2 uptake at 1 bar (437 cm^3 g^{-1}) (Figure IV-4a), indicating the incorporation of porphyrin ligand into the framework of MOF-808. In addition, the morphology and phase purity of the product NiTCPP⊂MOF-808 were tested by SEM. The SEM image showed that the obtained powders were octahedral microcrystals with the size of about 1 μm (Figure IV-4b).

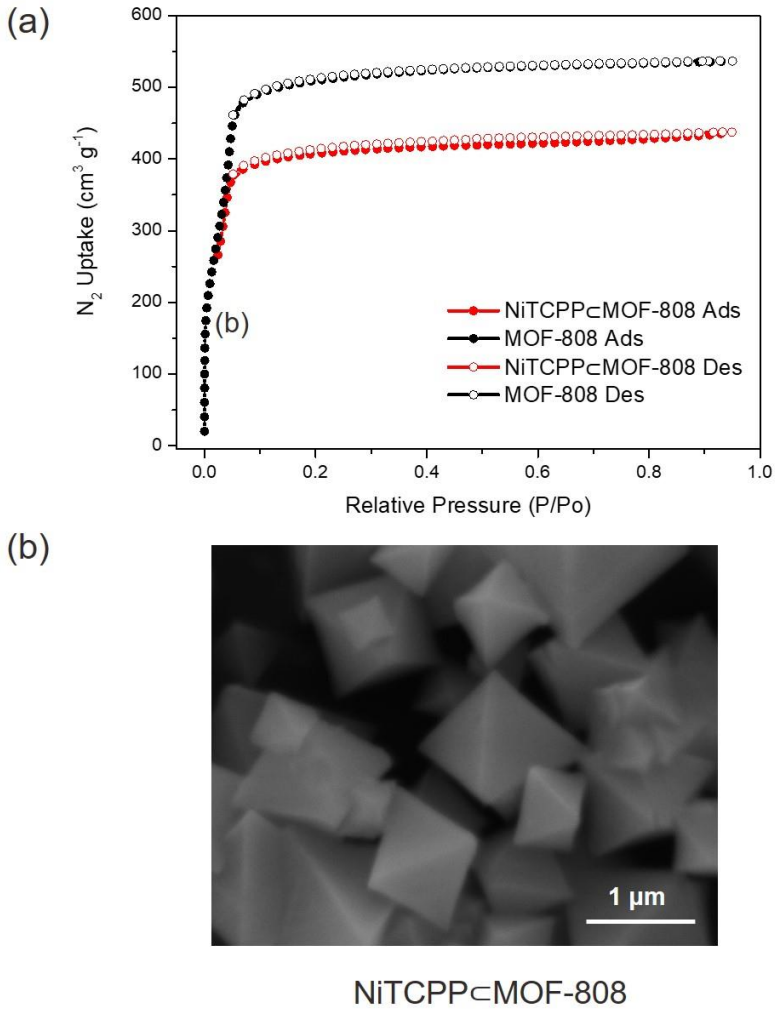

Figure IV-4. (a) N_2 adsorption/desorption isotherms of MOF-808 and NiTCPP⊂MOF-808. (b) SEM image of NiTCPP⊂MOF-808.

Taking advantages of the synthetic versatility by designing organic ligands in this system, a series of functionalities were incorporated into MOF-808 through ISLI strategy. Porphyrin ligands with different metals in the center were utilized to functionalize MO-808. And the phase purity of these products was verified by their

PXRD patterns, which were identical to that of the pristine MOF-808 (Figure IV-5). These functionalized MOF-808 were promising for a series of applications (e.g. CO_2 reduction[125-128] and oxidative cyclization[129]).

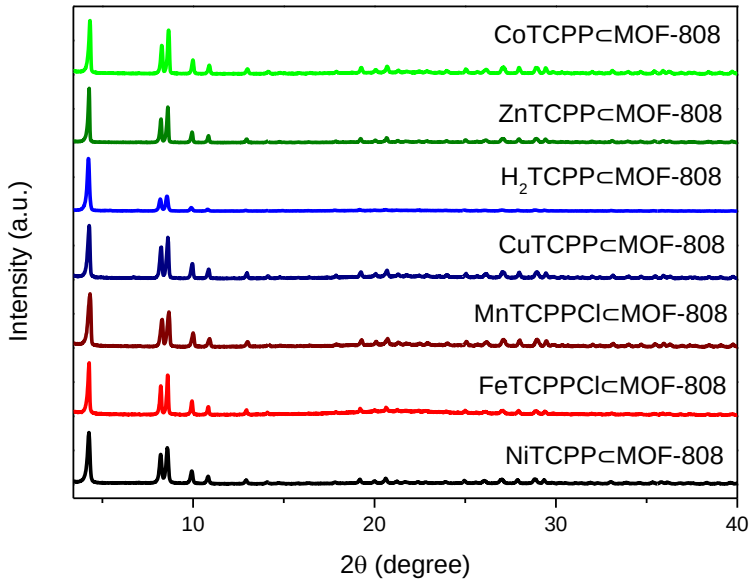

Figure IV-5. PXRD patterns for X⊂MOF-808 (X = NiTCPP, FeTCPPCl, MnTCPPCl, CuTCPP, H_2TCPP, ZnTCPP, and CoTCPP).

Functionalization of NU-1000 through ISLI. In the next step, we tried to extend the ISLI strategy to Zr-MOFs constructed from tetratopic ligands. Firstly, NU-1000 (compound **8**) was selected as an example. Solvothermal reaction of $ZrOCl_2 \cdot 8H_2O$, H_4TBAPy, and benzoic acid in N,N-dimethylformamide (DMF) at 120 ℃ for 22 hours yielded yellow powders of NU-1000 (Figure IV-6a). And solvothermal reaction of $ZrOCl_2 \cdot 8H_2O$, H_4TBAPy, [5,10,15,20-tetrakis(4-carboxyphenyl)porphyrinato]-Ni(II) (NiTCPP), and benzoic acid in DMF at 120 ℃ for 22 hours yielded red powders of

NiTCPP⊂NU-1000. After washing with DMF and acetone, the product remained red, indicating the presence of porphyrin (Figure IV-6b). Moreover, the PXRD pattern of the red powder was in consistent to that of simulated and experimental NU-1000 (Figure IV-6c), suggesting that the framework of NU-1000 was well preserved after functionalization of MOF-808 with porphyrin.

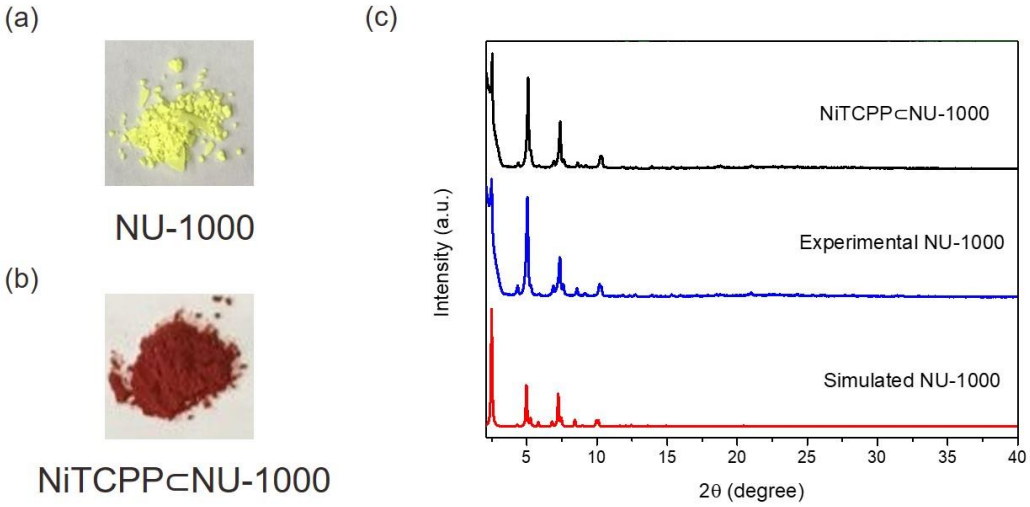

Figure IV-6. Photographs of (a) NU-1000 and (b) NiTCPP⊂NU-1000. (c) PXRD patterns for NU-1000 and NiTCPP⊂NU-1000.

Next, the samples were activated directly by removal of the solvent. And N_2 uptake experiment at 77 K was conducted to assess the permanent porosity of the products. Type IV isotherms that are typical for mesoporous solids were acquired from ASAP 2020 instrument. Compared with the parent MOF (NU-1000) (943 cm^3 g^{-1}), NiTCPP⊂NU-1000 exhibited lower N_2 uptake at 1 bar (777 cm^3 g^{-1}) (Figure IV-7a), suggesting the integration of NiTCPP ligands into the framework of NU-1000. In addition, the morphology and phase purity of the product NiTCPP⊂NU-1000 were

tested by SEM. Its SEM image showed that the obtained powders were rods with a uniform length of about 10 μm (Figure IV-7b).

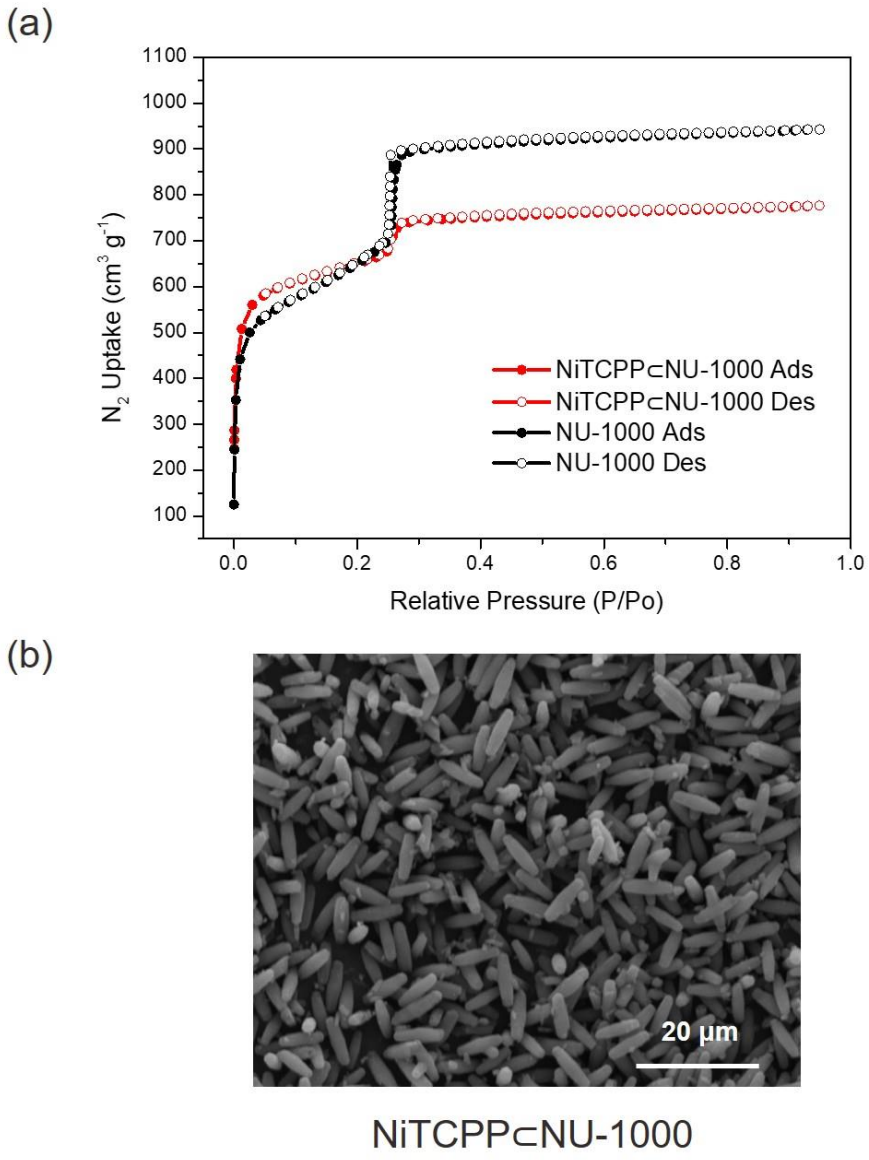

Figure IV-7. (a) N_2 adsorption/desorption isotherms of NU-1000 and NiTCPP⊂NU-1000. (b) SEM image of NiTCPP⊂NU-1000.

So far, many studies have investigated the application of NU-1000 for CO_2 capture and destruction of chemical warfare agents.[118-119] Moreover, since NU-1000 has high stability and contains mesopores, introducing multiple functionalities into NU-1000 is of great significance to broaden the scope of its applications (e.g. separation, enzyme immobilization, and drug delivery). By adjusting the amount of TCPP ligands used for the synthesis, different amounts of porphyrin can be incorporated into the framework of NU-1000 (Table IV-1), which is very important for the applications where the concentration of functionality matters.

Synthesis of Multivariate NU-1000. Through ISLI strategy, up to seven functionalities can be incorporated into NU-1000 (Figure IV-8). It is worth noting that the pore size of NU-1000 is larger than the porphyrin ligand, which further confirms that porphyrin ligands are coordinated to the Zr_6 clusters of NU-1000 instead of purely encapsulated in the framework.

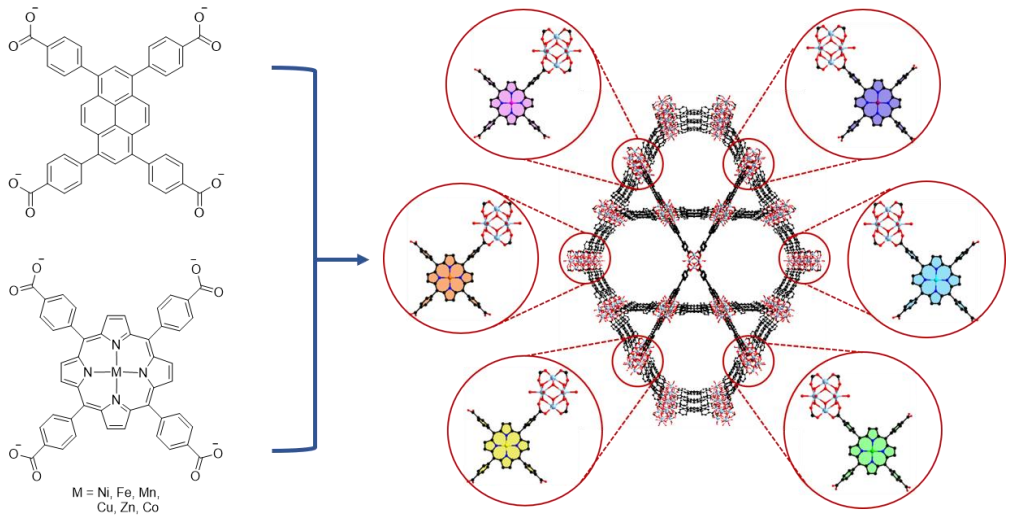

Figure IV-8. Schematic illustration of multifunctional NU-1000 synthesized through ISLI by mixing up to seven organic ligands.

Functionalization of Compound 9 through ISLI. After successfully applied ISLI strategy to functionalize MOF-808 and NU-1000, we further expand this strategy to incorporate multiple functionalities into other Zr-MOFs (compound **9** and compound **10**). Solvothermal reaction of $ZrOCl_2 \cdot 8H_2O$, H_4TCPB, and benzoic acid in N,N-dimethylformamide (DMF) at 120 ℃ for 22 hours yielded yellow powders of compound **9** (Figure IV-9a). And solvothermal reaction of $ZrOCl_2 \cdot 8H_2O$, H_4TCPB, [5,10,15,20-tetrakis(4-carboxyphenyl)porphyrinato]-Ni(II) (NiTCPP), and benzoic acid in DMF at 120 ℃ for 22 hours yielded red powders of NiTCPP⊂compound **9**. After washing with DMF and acetone, the product remained red, indicating the presence of porphyrin (Figure IV-9b). Moreover, the PXRD pattern of the red powder was in consistent to that of the parent MOF (compound **9**) (Figure IV-10c), suggesting that the framework of compound **9** was well preserved after functionalization with porphyrin.

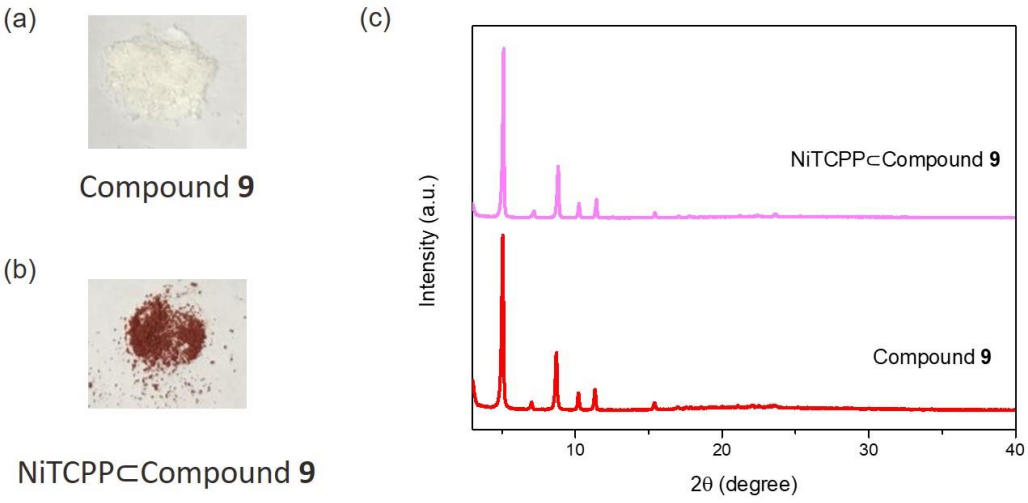

Figure IV-9. Photographs of (a) compound **9** and (b) NiTCPP⊂compound **9**. (c) PXRD patterns for compound **9** and NiTCPP⊂compound **9**.

Next, the samples were activated directly by removal of the solvent. And N_2 uptake experiment at 77 K was conducted to assess the permanent porosity of the products. Type II isotherms that are typical for microporous solids were acquired from ASAP 2020 instrument. Compared with the parent MOF (compound **9**) (444 cm^3 g^{-1}), NiTCPP⊂compound **9** exhibited decreased N_2 uptake at 1 bar (411 cm^3 g^{-1}) (Figure IV-10a), suggesting the integration of NiTCPP ligands into the framework of compound **9**. In addition, the morphology and phase purity of the product NiTCPP⊂compound **9** were tested by SEM. Its SEM image showed that the obtained powders were octahedral microcrystals with the size of about 150 nm (Figure IV-10b).

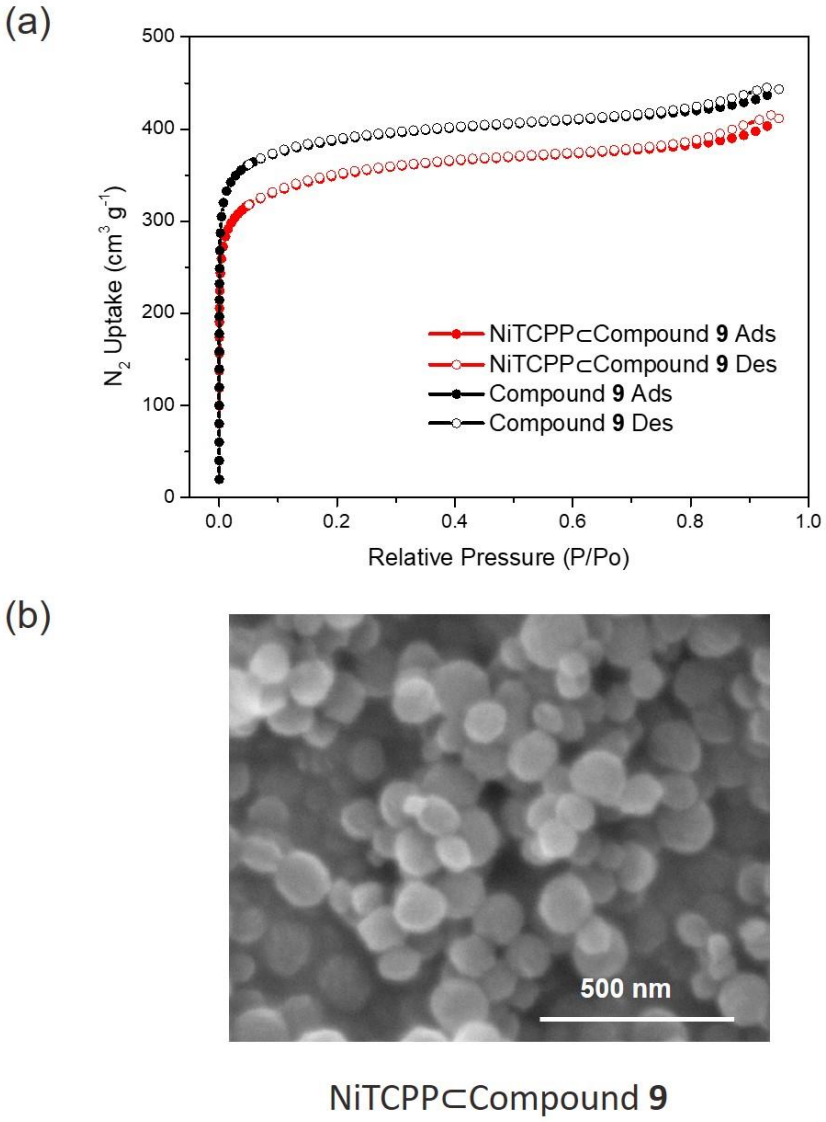

Figure IV-10. (a) N_2 adsorption/desorption isotherms of compound **9** and NiTCPP⊂compound **9**. (b) SEM image of NiTCPP⊂compound **9**.

Phase Diagram Determination. Take compound **9** as an example, in order to investigate appropriate synthetic conditions, we tested the product obtained with different amounts of BA and TCPP used for the synthesis and summarized the results in

a phase diagram (Figure IV-11). In consistent with our previous studies, impurity phases appeared with higher concentration of BA and TCPP.

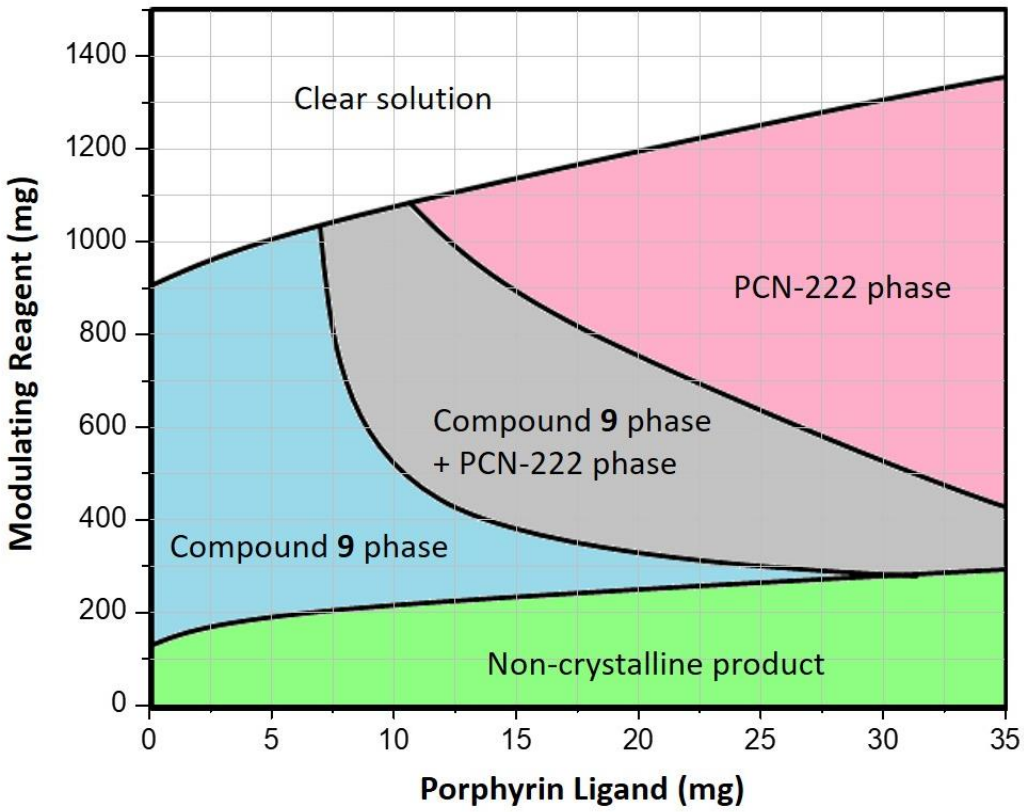

Figure IV-11. The phase diagram showing the product obtained with different amounts of TCPP and BA used for the synthesis.

Functionalization of Compound 10 through ISLI. To further extend the ISLI strategy, solvothermal reaction of $ZrOCl_2 \cdot 8H_2O$, H_4ETTC, and TFA in N,N-dimethylformamide (DMF) at 120 ℃ for 22 hours yielded yellow powders of compound **10**. And solvothermal reaction of $ZrOCl_2 \cdot 8H_2O$, H_4ETTC, [5,10,15,20-tetrakis(4-

carboxyphenyl)porphyrinato]-Ni(II) (NiTCPP), and TFA in DMF at 120 ℃ for 22 hours yielded red powders of NiTCPP⊂compound **10**. After washing with DMF and acetone, the product remained red, indicating the presence of porphyrin. Moreover, the PXRD pattern of the red powder was in consistent to that of the parent MOF (compound **10**) (Figure IV-12), suggesting that the framework of compound **10** was well preserved after functionalization with porphyrin.

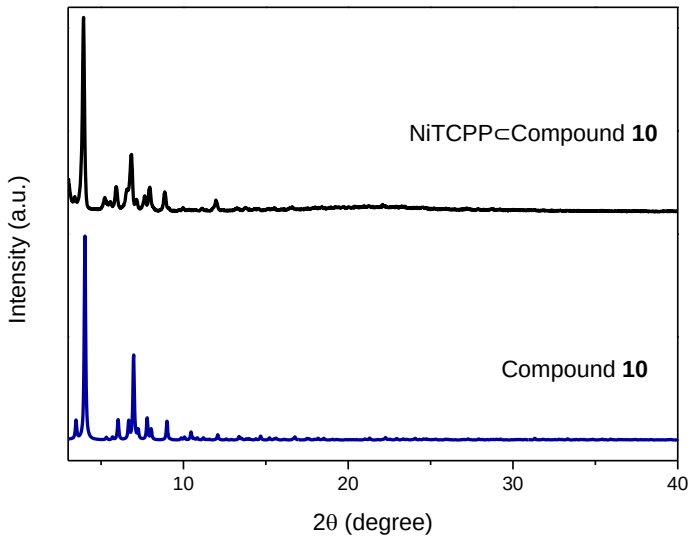

Figure IV-12. The PXRD patterns for compound **10** and NiTCPP⊂compound **10**.

In order to assess the permanent porosity of the products, the samples were activated directly by removal of the solvent. Then, they were tested by N_2 uptake experiment at 77 K. Type IV isotherms that are typical for mesoporous solids were acquired from ASAP 2020 instrument. Compared with the parent MOF (compound **10**) (1092 $cm^3\ g^{-1}$), NiTCPP⊂compound **10** exhibited lower N_2 uptake at 1 bar (730 $cm^3\ g^{-1}$)

(Figure IV-13), suggesting the introduction of NiTCPP ligands into the framework of compound **10**.

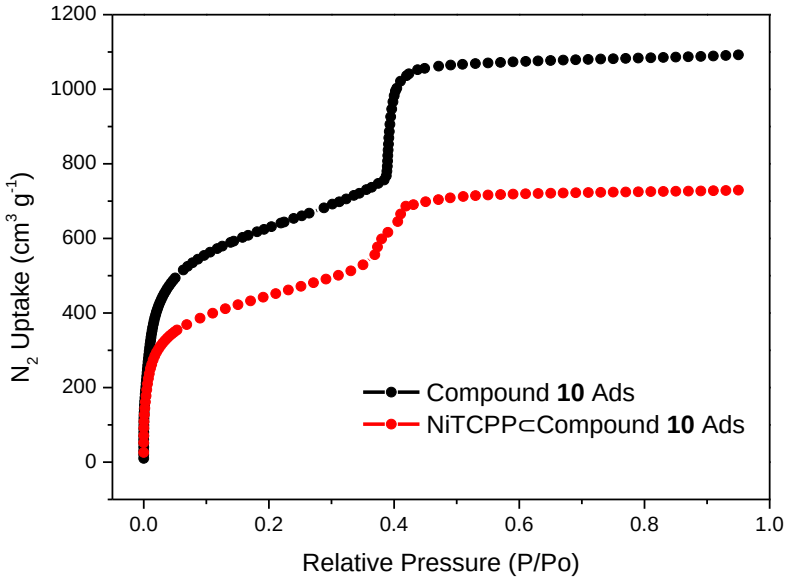

Figure IV-13. N_2 adsorption isotherms for compound **10** and NiTCPP⊂compound **10**.

ISLI towards Multifunctional Zr-MOFs. As a brief summary, the ISLI strategy has been applied to a series of Zr-MOFs constructed from multitopic organic ligands (Figure IV-14). For example, L7 and L8 represent the organic structs for the construction of MOF-808 and NU-1000, respectively.

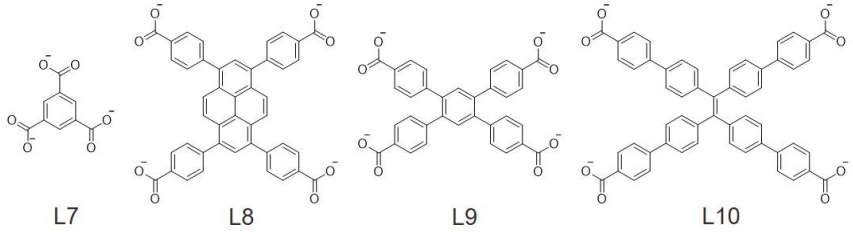

Figure IV-14. Chemical structures of multitopic ligands used for ISLI.

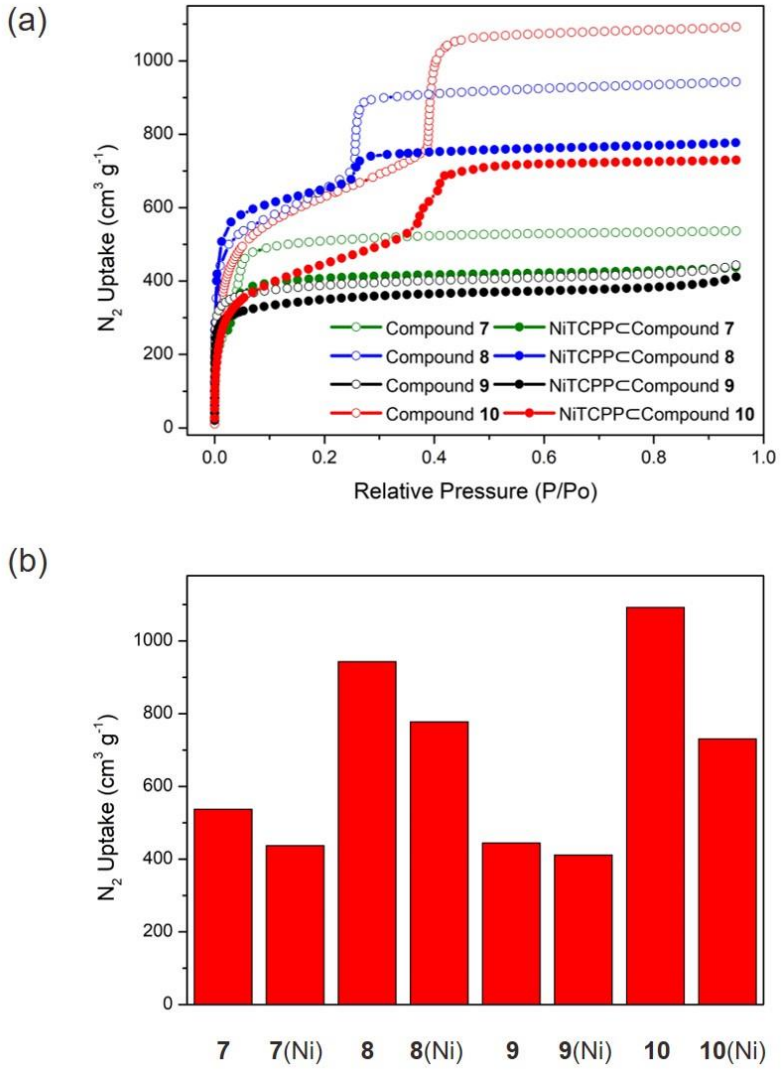

Figure IV-15. (a) N_2 adsorption isotherms and (b) total N_2 uptake of compounds **7**-**10** and NiTCPP⊂compounds **7**-**10**.

The N_2 adsorption isotherms and total N_2 uptake of all the parent Zr-MOFs and their functionalized products obtained through ISLI were summarized in Figure IV-15. After functionalization, the MOFs exhibited decreased N_2 uptake compared with that of their corresponding parent MOFs.

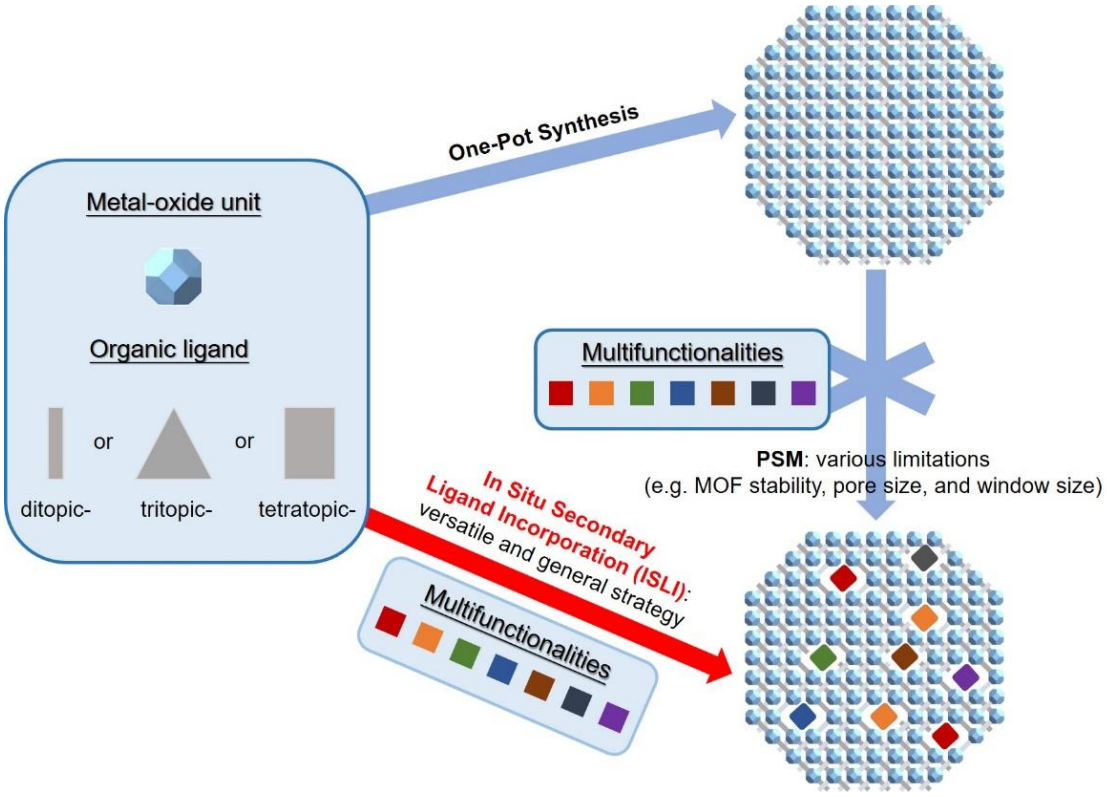

Figure IV-16. Schematic illustration of the construction of multifunctional Zr-MOFs through ISLI.

Construction of highly stable Zr-MOFs with multiple functionalities through versatile and general ISLI strategy was summarized in Figure IV-16. Compared with ISLI strategy, PSM strategy has several disadvantages for functionalization of MOFs, such as damaging the framework integrity, and impeding the access of interior framework because of small pore size and window size. By mixing ligands of different size, shape and connectivity to synthesize phase-pure MOFs, ISLI strategy also overcomes the limitations of conventional mixed-ligand strategy. Therefore, this ISLI strategy provides a very useful tool to synthesize Zr-MOFs with multifunctionalities and investigate their potential applications.

4.4 Conclusions

In this chapter, the ISLI strategy was further extended to synthesize Zr-MOFs constructed from multitopic organic ligands (compounds **7**-**10**). By mixing tritopic/tetratopic ligands and tetratopic porphyrin ligands, a series of Zr-MOFs incorporated with multiple functionalities have been successfully synthesized. And the crystal structure and morphology of their corresponding parent MOFs were well preserved after applying ISLI strategy. Depending on the synthetic conditions, the porphyrin ligands can be introduced into the framework homogeneously with a tunable amount. Interestingly, up to seven functionalities have been integrated into NU-1000 through ISLI strategy. Moreover, taking compound **9** as an example, the product obtained under different synthetic conditions were investigated and summarized in a phase diagram, which demonstrated the importance of ISLI to thermodynamically and kinetically tune the reaction system towards the formation of phase-pure product with desired functionality. Therefore, ISLI has been proved to be a versatile and general strategy to construct highly stable Zr-MOFs with multiple functionalities, which is challenging for PSM strategy due to several limitations (e.g. MOF stability, small pore size, and small window size). In addition, since ligands of different size, shape and connectivity can be used for the synthesis without generating mixed phases, the ISLI strategy overcomes the limitations of conventional mixed-ligand strategy. Consequently, this ISLI strategy provides a feasible route to synthesize highly stable Zr-MOFs with multiple functionalities for a wide range of potential applications.

CHAPTER V

THERMODYNAMICALLY GUIDED SYNTHESIS OF MIXED-LIGAND MOFS WITH MULTIFUNCTIONALITY

5.1 Introduction

In recent years, tremendous efforts have been made to synthesize multifunctional MOFs through a one-pot synthesis, taking advantage of the retained framework integrity and straightforward synthesis. One of the most commonly used methods is to mix inorganic metal salts with organic ligands of the same backbone connected to different functional groups (e.g. organic ligand derivatives) that cannot be distinguished during the synthesis.[130-133] Although this method can effectively eliminate the formation of mixed phases, it is very difficult to located the position of each organic ligand precisely at the molecular level since these ligands are distributed randomly inside the framework. So far, solid-state nuclear magnetic resonance (NMR) measurements combined with molecular simulations have been applied to determine the heterogeneous mesoscale spatial arrangement of functional groups in a series of multivariate metal-organic frameworks (MTV-MOF-5).[134] However, it remains quite challenging to map different functional groups that are integrated in a disordered manner in ordered materials.

To address this issue, attempts were made to functionalize MOFs by mixing organic ligands of different size, shape, or connectivity that can be differentiated.[135-142] In this way, each of the ligand can be located accurately by solving the MOF structure based on crystallography. One of the most typical examples are the synthesis of pillar-

layered MOFs by mixing a ditopic ligand and a tetratopic ligand.[44, 143] Generally, the tetratopic ligands coordinate to the metal clusters to form 2-D layers, which are pillared by the ditopic ligands to form 3-D networks. However, most of the reported pillar-layered MOFs are constructed from low-valent metal ions or clusters. Therefore, they are unstable under many conditions, including moisture, acid, and base.

Given this, it is of great significance to synthesize highly stable Zr-MOFs with multiple functionalities by mixing distinguishable organic ligands via a one-pot reaction. However, most of the reported Zr-MOFs only contain a single-typed organic ligand, which limits the varitey of functional groups that can be introduced into the framework.[45, 144-146] One possible reason is that when a Zr-MOF can be constructed from a single organic ligand, mixed phases tend to form in general when additional organic ligands are added for the synthesis, unless the mixed-ligand MOF product is thermodynamically more favorable. In addition to the difficulty in synthesizing mixed-ligand Zr-MOFs, even using the same inorganic salt and organic ligand could generate different products.[29, 51, 147-150]

In this chapter, through a thermodynamically guided synthesis, a series of highly stable mixed-ligand Zr/Hf-based MOFs (PCN-555) with a novel topology have been synthesized by mixing tetratopic tetrakis(4-carboxyphenyl)porphyrin (TCPP) and 1,3,6,8-tetrakis(p-benzoate)pyrene (TBAPy) ligands. By solving the crystal structure of PCN-555, the positions of porphyrin and pyrene functionalities were precisely located inside the framework. Moreover, with the presence of coordinatively available sites on Zr_6 clusters, additional functionalities (e.g. amino group, hydroxyl group, and carboxylic

group) were incorporated into PCN-555 through a solvent-assisted ligand incorporation (SALI) strategy. Therefore, this mixed-ligand MOF (PCN-555) provides an ideal platform for further functionalization and exploration of new structures.

5.2 Experimental Section

Materials and Instrumentation. Commercially available reagents and solvents were used as received without further purification. Tetrakis(4-carboxyphenyl)porphyrin (H_2TCPP), [5,10,15,20-tetrakis(4-carboxyphenyl)porphyrinato]-Mn(III) chloride (MnTCPPCl), [5,10,15,20-tetrakis(4-carboxyphenyl)porphyrinato]-Fe(III) chloride (FeTCPPCl), [5,10,15,20-tetrakis(4-carboxyphenyl)porphyrinato]-Zn(II) (ZnTCPP), [5,10,15,20-tetrakis(4-carboxyphenyl)porphyrinato]-Ni(II) (NiTCPP), [5,10,15,20-tetrakis(4-carboxyphenyl)porphyrinato]-Co(II) (CoTCPP), [5,10,15,20-tetrakis(4-carboxyphenyl)porphyrinato]-Cu(II) (CuTCPP) were synthesized according to the procedure in previous reports with slight modifications.[73] 2-Azido terephthalic acid was synthesized according to the procedure in the literature.[74]

Powder X-ray diffraction (PXRD) experiment was carried out with a BRUKER D8-Focus Bragg−Brentano X-ray powder diffractometer equipped with a Cu-sealed tube (λ = 1.54178) at 40 kV and 40 mA. Thermogravimetric analysis (TGA) were conducted on a Shimadzu TGA-50 thermogravimetric analyzer at a ramp rate of 2 °C/min in a flowing nitrogen atmosphere. Nuclear magnetic resonance (NMR) spectra were collected on a Mercury 300 spectrometer. N_2 adsorption/desorption isotherms were measured on a Micrometritics ASAP 2020 system at 77 K. The sample was activated by solvent exchange (in several cycles using fresh acetone), followed by degassing at

elevated temperature (100 °C) for 5 h. Scanning electron microscope (SEM) analysis was performed on QUANTA 450 FEG and energy dispersive X-ray spectroscopy (EDS) analysis was carried out by X-Max20 with Oxford EDS system equipped with X-ray mapping. Transmission electron microscope (TEM) analysis was performed on a JEOL JEM2100 microscope.

Synthesis of 1,3,6,8-Tetrakis(p-Benzoic Acid)pyrene (H_4TBAPy). As shown in Scheme V-1, 1,3,6,8-tetrakis(p-benzoic acid)pyrene (H_4TBAPy) was synthesized according to the reference.[121]

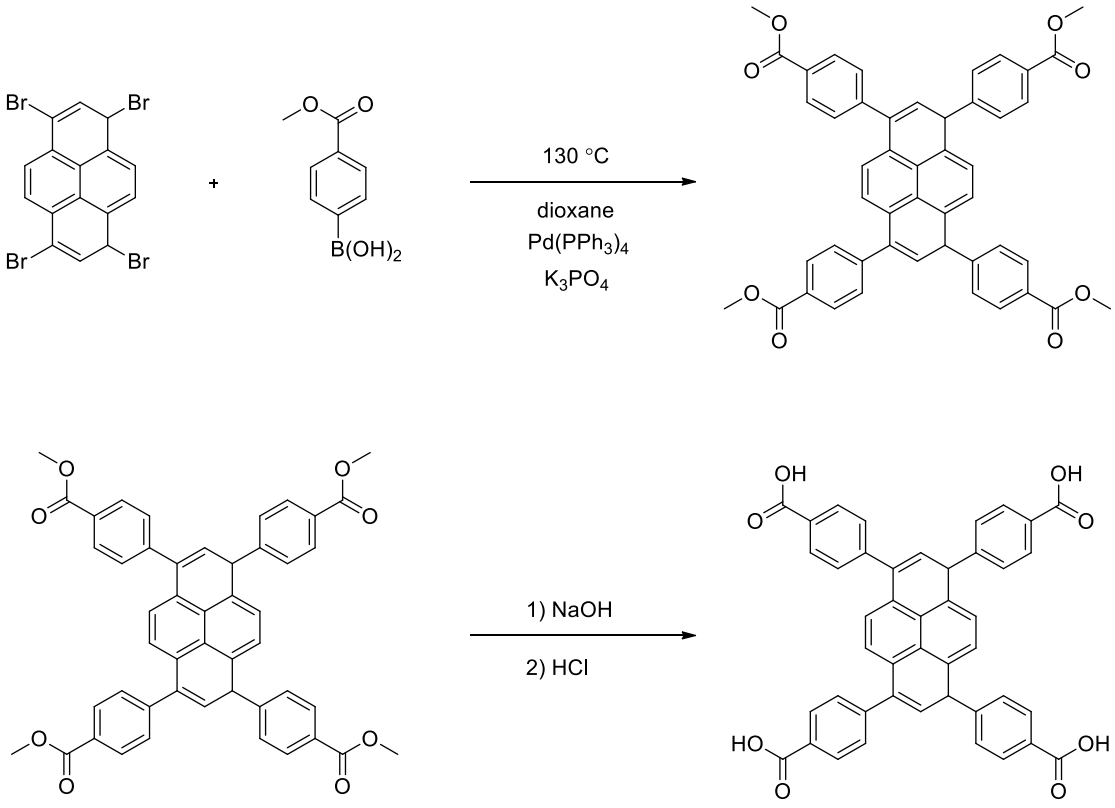

Scheme V-1. Synthesis of H_4TBAPy ligand.

Synthesis of 1,3,6,8-tetrakis(4-(methoxycarbonyl)phenyl)pyrene: to a mixture of (4-(methoxycarbonyl)phenyl)boronic acid (5.200 g, 29.00 mmol), 1,3,6,8-tetrabromopyrene (2.500 g, 4.85 mmol), tetrakis(triphenylphosphine) palladium(0) (0.150 g 0.130 mmol), and potassium phosphate tribasic (5.500 g, 26.50 mmol) was added dry dioxane (100 mL). Then, the mixture was stirred under nitrogen atmosphere for 72 h at 130 °C in an oil bath. The reaction mixture was evaporated to dryness and the solid residue was washed with water to remove inorganic salts. The insoluble material was extracted with chloroform (three times by 50 mL). Next, the extract was dried over magnesium sulfate, and the solvent volume was reduced under vacuum. The residue was boiled in tetrahydrofuran for 2h and filtered. The resulting filtrate contained majority of the impurities. Finally, 2.90 g of 1,3,6,8-tetrakis(4-(methoxycarbonyl)phenyl)pyrene was obtained (82% yield). ^{1}H NMR ($CDCl_3$, 300 MHz): δ 3.99 (s, 12H), 7.75 (d, 8H), 8.01 (s, 2H), 8.15 (s, 4H), 8.23 (d, 8H).

Synthesis of 1,3,6,8-tetrakis(p-benzoic acid)pyrene (H_4TBAPy): 1.16 g (1.56 mmol) of solid 1,3,6,8-tetrakis(4-(methoxycarbonyl)phenyl)pyrene, 3.0 g (75.0 mmol) NaOH, and 150 mL of a THF/water (ratio 1:1) mixture was added to a 250 mL round bottom flask. Then, the resultant suspension was vigorously stirred under reflux overnight. The solvents were removed under vacuum and water was added to the residue, which formed a clear yellow solution. The clear yellow solution was stirred at room temperature for 2 h and the pH value was adjusted to 1 by adding concentrated HCl. The resulting yellow solid was collected by filtration and then washed with water several times. The crude product was recrystallized from DMF, filtered, washed with

chloroform and dried under vacuum. Finally, 0.98 g of the pure product H_4TBAPy was obtained (91% yield). ^{1}H NMR (DMSO, 300 MHz): δ 7.86 (d, 8H), 8.09 (s, 2H), 8.17 (d, 8H), 8.21 (s, 4H), 13.12 (s, 4H).

Synthesis of Porphyrin Ligands (MTCPP). Porphyrin ligands with different metals in the center (MTCPP) were synthesized according to the synthetic routes shown in Scheme V-2.

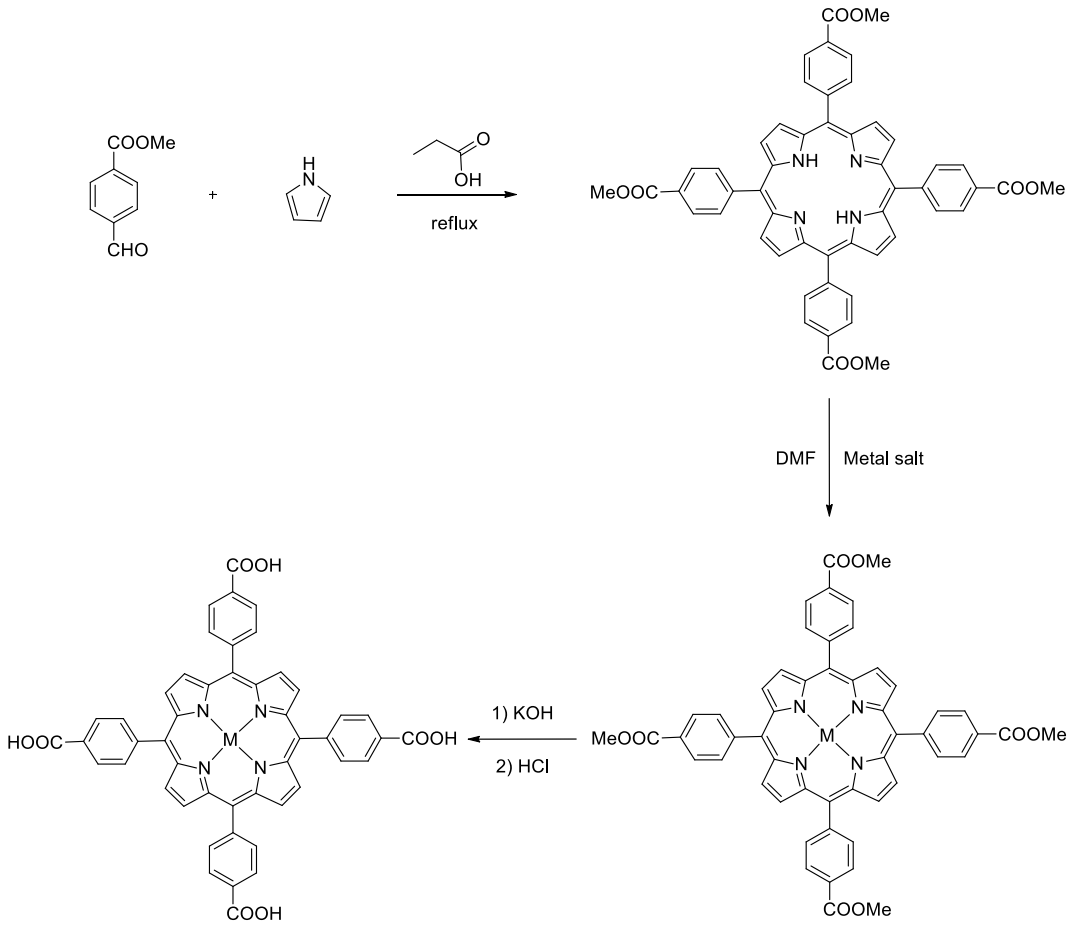

Scheme V-2. Synthetic routes for MTCPP ligands.

Synthesis of 5,10,15,20-Tetrakis(4-Methoxycarbonylphenyl)porphyrin (TPPCOOMe). To propionic acid (100 mL) in a 500 mL three-necked flask were added pyrrole (3.0 g, 0.043 mol) and methyl p-formylbenzoate (6.9 g, 0.042 mol). Then the solution was refluxed for 12 h in darkness. After the reaction mixture was cooled to room temperature, crystals were collected by suction-filtration to afford purple crystals (1.9 g, 2.24 mmol, 21%). ^{1}H NMR (300 MHz, $CDCl_3$), δ 8.81 (s, 8H), 8.43 (d, 8H), 8.28 (d, 8H), 4.11 (s, 12H), 2.83 (s, 2H).

Synthesis of [5,10,15,20-Tetrakis(4-Methoxycarbonylphenyl)porphyrinato]-Ni(II). A solution of TPPCOOMe (0.854 g, 1.0 mmol) and $NiCl_2 \cdot 6H_2O$ (3.1 g, 12.8 mmol) in 100 mL of DMF was refluxed for 6 h. After the mixture was cooled to room temperature, 150 mL of H_2O was added. The resultant precipitate was filtered and washed with 50 mL of H_2O for two times. The obtained solid was dissolved in $CHCl_3$, followed by washing three times with 1 M HCl and twice with water. The organic layer was dried over anhydrous magnesium sulfate and evaporated to afford quantitative crimson crystals.

Synthesis of [5,10,15,20-Tetrakis(4-Methoxycarbonylphenyl)porphyrinato]-Fe(III) Chloride. A solution of TPPCOOMe (0.854 g, 1.0 mmol) and $FeCl_2 \cdot 4H_2O$ (2.5 g, 12.8 mmol) in 100 mL of DMF was refluxed for 6 h. After the mixture was cooled to room temperature, 150 mL of H_2O was added. The resultant precipitate was filtered and washed with 50 mL of H_2O for two times. The obtained solid was dissolved in $CHCl_3$, followed by washing three times with 1 M HCl and twice with water. The organic layer was dried over anhydrous magnesium sulfate and evaporated to afford quantitative dark

brown crystals.

Synthesis of [5,10,15,20-Tetrakis(4-Methoxycarbonylphenyl)porphyrinato]-Mn(III) Chloride. A solution of TPPCOOMe (0.854 g, 1.0 mmol) and $MnCl_2 \cdot 4H_2O$ (2.5 g, 12.8 mmol) in 100 mL of DMF was refluxed for 6 h. After the mixture was cooled to room temperature, 150 mL of H_2O was added. The resultant precipitate was filtered and washed with 50 mL of H_2O for two times. The obtained solid was dissolved in $CHCl_3$, followed by washing three times with water. The organic layer was dried over anhydrous magnesium sulfate and evaporated to afford quantitative dark green crystals.

Synthesis of [5,10,15,20-Tetrakis(4-Methoxycarbonylphenyl)porphyrinato]-Cu(II). A solution of TPPCOOMe (0.854 g, 1.0 mmol) and $CuCl_2 \cdot 2H_2O$ (2.2g, 12.8 mmol) in 100 mL of DMF was refluxed for 6 h. After the mixture was cooled to room temperature, 150 mL of H_2O was added. The resultant precipitate was filtered and washed with 50 mL of H_2O for two times. The obtained solid was dissolved in $CHCl_3$, followed by washing three times with water. The organic layer was dried over anhydrous magnesium sulfate and evaporated to afford quantitative dark red crystals.

Synthesis of [5,10,15,20-Tetrakis(4-Methoxycarbonylphenyl)porphyrinato]-Zn(II). A solution of TPPCOOMe (0.854 g, 1.0 mmol) and $ZnCl_2$ (1.75 g, 12.8 mmol) in 100 mL of DMF was refluxed for 6 h. After the mixture was cooled to room temperature, 150 mL of H_2O was added. The resultant precipitate was filtered and washed with 50 mL of H_2O for two times. The obtained solid was dissolved in $CHCl_3$, followed by washing three times with water. The organic layer was dried over anhydrous magnesium sulfate and evaporated to afford quantitative violet crystals.

Synthesis of [5,10,15,20-Tetrakis(4-Methoxycarbonylphenyl)porphyrinato]-Co(II). A solution of TPPCOOMe (0.854 g, 1.0 mmol) and $CoCl_2 \cdot 6H_2O$ (3.1 g, 12.8 mmol) in 100 mL of DMF was refluxed for 6 h. After the mixture was cooled to room temperature, 150 mL of H_2O was added. The resultant precipitate was filtered and washed with 50 mL of H_2O for two times. The obtained solid was dissolved in $CHCl_3$, followed by washing three times with water. The organic layer was dried over anhydrous magnesium sulfate and evaporated to afford quantitative red crystals.

Synthesis of [5,10,15,20-Tetrakis(4-Carboxyphenyl)porphyrinato]-Ni(II) (NiTCPP). The obtained corresponding ester (0.75 g) was stirred in THF (25 mL) and MeOH (25 mL) mixed solvent, to which a solution of KOH (2.63 g, 46.95 mmol) in H_2O (25 mL) was added. The mixture was then refluxed for 12 h. After cooling down to room temperature, THF and MeOH were evaporated under vacuum. Additional water was added to the resulting water phase and the mixture was heated until the solid was fully dissolved, then the homogeneous solution was acidified with 1 M HCl until no further precipitate was detected. The crimson solid was collected by filtration, washed with water and dried in vacuum.

Synthesis of [5,10,15,20-Tetrakis(4-Carboxyphenyl)porphyrinato]-Fe(III) Chloride (FeTCPPCl). The obtained corresponding ester (0.75 g) was stirred in THF (25 mL) and MeOH (25 mL) mixed solvent, to which a solution of KOH (2.63 g, 46.95 mmol) in H_2O (25 mL) was added. The mixture was then refluxed for 12 h. After cooling down to room temperature, THF and MeOH were evaporated under vacuum. Additional water was added to the resulting water phase and the mixture was heated

until the solid was fully dissolved, then the homogeneous solution was acidified with 1 M HCl until no further precipitate was detected. The brown solid was collected by filtration, washed with water and dried in vacuum.

Synthesis of [5,10,15,20-Tetrakis(4-Carboxyphenyl)porphyrinato]-Mn (III) Chloride (MnTCPPCl). The obtained corresponding ester (0.75 g) was stirred in THF (25 mL) and MeOH (25 mL) mixed solvent, to which a solution of KOH (2.63 g, 46.95 mmol) in H_2O (25 mL) was added. The mixture was then refluxed for 12 h. After cooling down to room temperature, THF and MeOH were evaporated under vacuum. Additional water was added to the resulting water phase and the mixture was heated until the solid was fully dissolved, then the homogeneous solution was acidified with 1 M HCl until no further precipitate was detected. The dark green solid was collected by filtration, washed with water and dried in vacuum.

Synthesis of [5,10,15,20-Tetrakis(4-Carboxyphenyl)porphyrinato]-Cu(II) (CuTCPP). The obtained corresponding ester (0.75 g) was stirred in THF (25 mL) and MeOH (25 mL) mixed solvent, to which a solution of KOH (2.63 g, 46.95 mmol) in H_2O (25 mL) was added. The mixture was then refluxed for 12 h. After cooling down to room temperature, THF and MeOH were evaporated under vacuum. Additional water was added to the resulting water phase and the mixture was heated until the solid was fully dissolved, then the homogeneous solution was acidified with 1 M HCl until no further precipitate was detected. The dark red solid was collected by filtration, washed with water and dried in vacuum.

Synthesis of [5,10,15,20-Tetrakis(4-Carboxyphenyl)porphyrinato]-Zn(II)

(ZnTCPP). The obtained corresponding ester (0.75 g) was stirred in THF (25 mL) and MeOH (25 mL) mixed solvent, to which a solution of KOH (2.63 g, 46.95 mmol) in H_2O (25 mL) was added. The mixture was then refluxed for 12 h. After cooling down to room temperature, THF and MeOH were evaporated under vacuum. Additional water was added to the resulting water phase and the mixture was heated until the solid was fully dissolved, then the homogeneous solution was acidified with 1 M HCl until no further precipitate was detected. The violet solid was collected by filtration, washed with water and dried in vacuum.

Synthesis of [5,10,15,20-Tetrakis(4-Carboxyphenyl)porphyrinato]-Co(II) (CoTCPP). The obtained corresponding ester (0.75 g) was stirred in THF (25 mL) and MeOH (25 mL) mixed solvent, to which a solution of KOH (2.63 g, 46.95 mmol) in H_2O (25 mL) was added. The mixture was then refluxed for 12 h. After cooling down to room temperature, THF and MeOH were evaporated under vacuum. Additional water was added to the resulting water phase and the mixture was heated until the solid was fully dissolved, then the homogeneous solution was acidified with 1 M HCl until no further precipitate was detected. The red solid was collected by filtration, washed with water and dried in vacuum.

Synthesis of Zr-based PCN-555(Ni). $ZrOCl_2 \cdot 8H_2O$ (24.2 mg, 0.075 mmol), H_4TBAPy (11.5 mg, 0.017 mmol), NiTCPP (20 mg, 0.024 mmol) and benzoic acid (850 mg, 6.960 mmol) in 2 mL of DMF were ultrasonically dissolved in a Pyrex vial. The mixture was heated in an oven at 160 °C for 22 h. After cooling down to room temperature, the precipitates were collected by centrifugation. The solids were washed

with DMF three times to remove unreacted precursors, and then solvent-exchanged with acetone three times. The resulting powder was obtained by centrifugation, and dried in an oven at 80 °C.

Synthesis of Zr-based PCN-555(Fe). $ZrOCl_2 \cdot 8H_2O$ (24.2 mg, 0.075 mmol), H_4TBAPy (11.5 mg, 0.017 mmol), FeTCPPCl (20 mg, 0.024 mmol) and benzoic acid (850 mg, 6.960 mmol) in 2 mL of DMF were ultrasonically dissolved in a Pyrex vial. The mixture was heated in an oven at 160 °C for 22 h. After cooling down to room temperature, the precipitates were collected by centrifugation. The solids were washed with DMF three times to remove unreacted precursors, and then solvent-exchanged with acetone three times. The resulting powder was obtained by centrifugation, and dried in an oven at 80 °C.

Synthesis of Zr-based PCN-555(Mn). $ZrOCl_2 \cdot 8H_2O$ (24.2 mg, 0.075 mmol), H_4TBAPy (11.5 mg, 0.017 mmol), MnTCPPCl (20 mg, 0.024 mmol) and benzoic acid (850 mg, 6.960 mmol) in 2 mL of DMF were ultrasonically dissolved in a Pyrex vial. The mixture was heated in an oven at 160 °C for 22 h. After cooling down to room temperature, the precipitates were collected by centrifugation. The solids were washed with DMF three times to remove unreacted precursors, and then solvent-exchanged with acetone three times. The resulting powder was obtained by centrifugation, and dried in an oven at 80 °C.

Synthesis of Zr-based PCN-555(Cu). $ZrOCl_2 \cdot 8H_2O$ (24.2 mg, 0.075 mmol), H_4TBAPy (11.5 mg, 0.017 mmol), CuTCPP (20 mg, 0.023 mmol) and benzoic acid (850 mg, 6.960 mmol) in 2 mL of DMF were ultrasonically dissolved in a Pyrex vial. The

mixture was heated in an oven at 160 °C for 22 h. After cooling down to room temperature, the precipitates were collected by centrifugation. The solids were washed with DMF three times to remove unreacted precursors, and then solvent-exchanged with acetone three times. The resulting powder was obtained by centrifugation, and dried in an oven at 80 °C.

Synthesis of Zr-based PCN-555(no). $ZrOCl_2 \cdot 8H_2O$ (24.2 mg, 0.075 mmol), H_4TBAPy (11.5 mg, 0.017 mmol), H_2TCPP (20 mg, 0.025 mmol) and benzoic acid (850 mg, 6.960 mmol) in 2 mL of DMF were ultrasonically dissolved in a Pyrex vial. The mixture was heated in an oven at 160 °C for 22 h. After cooling down to room temperature, the precipitates were collected by centrifugation. The solids were washed with DMF three times to remove unreacted precursors, and then solvent-exchanged with acetone three times. The resulting powder was obtained by centrifugation, and dried in an oven at 80 °C.

Synthesis of Zr-based PCN-555(Zn). $ZrOCl_2 \cdot 8H_2O$ (24.2 mg, 0.075 mmol), H_4TBAPy (11.5 mg, 0.017 mmol), ZnTCPP (20 mg, 0.023 mmol) and benzoic acid (850 mg, 6.960 mmol) in 2 mL of DMF were ultrasonically dissolved in a Pyrex vial. The mixture was heated in an oven at 160 °C for 22 h. After cooling down to room temperature, the precipitates were collected by centrifugation. The solids were washed with DMF three times to remove unreacted precursors, and then solvent-exchanged with acetone three times. The resulting powder was obtained by centrifugation, and dried in an oven at 80 °C.

Synthesis of Zr-based PCN-555(Co). $ZrOCl_2 \cdot 8H_2O$ (24.2 mg, 0.075 mmol), H_4TBAPy (11.5 mg, 0.017 mmol), CoTCPP (20 mg, 0.024 mmol) and benzoic acid (850 mg, 6.960 mmol) in 2 mL of DMF were ultrasonically dissolved in a Pyrex vial. The mixture was heated in an oven at 160 °C for 22 h. After cooling down to room temperature, the precipitates were collected by centrifugation. The solids were washed with DMF three times to remove unreacted precursors, and then solvent-exchanged with acetone three times. The resulting powder was obtained by centrifugation, and dried in an oven at 80 °C.

Synthesis of Hf-based PCN-555(Ni). $HfOCl_2 \cdot 8H_2O$ (30.7 mg, 0.075 mmol), H_4TBAPy (11.5 mg, 0.017 mmol), NiTCPP (20 mg, 0.024 mmol) and benzoic acid (850 mg, 6.960 mmol) in 2 mL of DMF were ultrasonically dissolved in a Pyrex vial. The mixture was heated in an oven at 160 °C for 22 h. After cooling down to room temperature, the precipitates were collected by centrifugation. The solids were washed with DMF three times to remove unreacted precursors, and then solvent-exchanged with acetone three times. The resulting powder was obtained by centrifugation, and dried in an oven at 80 °C.

Synthesis of Hf-based PCN-555(Fe). $HfOCl_2 \cdot 8H_2O$ (30.7 mg, 0.075 mmol), H_4TBAPy (11.5 mg, 0.017 mmol), FeTCPPCl (20 mg, 0.024 mmol) and benzoic acid (850 mg, 6.960 mmol) in 2 mL of DMF were ultrasonically dissolved in a Pyrex vial. The mixture was heated in an oven at 160 °C for 22 h. After cooling down to room temperature, the precipitates were collected by centrifugation. The solids were washed with DMF three times to remove unreacted precursors, and then solvent-exchanged with

acetone three times. The resulting powder was obtained by centrifugation, and dried in an oven at 80 °C.

Synthesis of Hf-based PCN-555(Mn). $HfOCl_2 \cdot 8H_2O$ (30.7 mg, 0.075 mmol), H_4TBAPy (11.5 mg, 0.017 mmol), MnTCPPCl (20 mg, 0.024 mmol) and benzoic acid (850 mg, 6.960 mmol) in 2 mL of DMF were ultrasonically dissolved in a Pyrex vial. The mixture was heated in an oven at 160 °C for 22 h. After cooling down to room temperature, the precipitates were collected by centrifugation. The solids were washed with DMF three times to remove unreacted precursors, and then solvent-exchanged with acetone three times. The resulting powder was obtained by centrifugation, and dried in an oven at 80 °C.

Synthesis of Hf-based PCN-555(Cu). $HfOCl_2 \cdot 8H_2O$ (30.7 mg, 0.075 mmol), H_4TBAPy (11.5 mg, 0.017 mmol), CuTCPP (20 mg, 0.023 mmol) and benzoic acid (850 mg, 6.960 mmol) in 2 mL of DMF were ultrasonically dissolved in a Pyrex vial. The mixture was heated in an oven at 160 °C for 22 h. After cooling down to room temperature, the precipitates were collected by centrifugation. The solids were washed with DMF three times to remove unreacted precursors, and then solvent-exchanged with acetone three times. The resulting powder was obtained by centrifugation, and dried in an oven at 80 °C.

Synthesis of Hf-based PCN-555(no). $HfOCl_2 \cdot 8H_2O$ (30.7 mg, 0.075 mmol), H_4TBAPy (11.5 mg, 0.017 mmol), H_2TCPP (20 mg, 0.025 mmol) and benzoic acid (850 mg, 6.960 mmol) in 2 mL of DMF were ultrasonically dissolved in a Pyrex vial. The mixture was heated in an oven at 160 °C for 22 h. After cooling down to room

temperature, the precipitates were collected by centrifugation. The solids were washed with DMF three times to remove unreacted precursors, and then solvent-exchanged with acetone three times. The resulting powder was obtained by centrifugation, and dried in an oven at 80 °C.

Synthesis of Hf-based PCN-555(Zn). $HfOCl_2 \cdot 8H_2O$ (30.7 mg, 0.075 mmol), H_4TBAPy (11.5 mg, 0.017 mmol), ZnTCPP (20 mg, 0.023 mmol) and benzoic acid (850 mg, 6.960 mmol) in 2 mL of DMF were ultrasonically dissolved in a Pyrex vial. The mixture was heated in an oven at 160 °C for 22 h. After cooling down to room temperature, the precipitates were collected by centrifugation. The solids were washed with DMF three times to remove unreacted precursors, and then solvent-exchanged with acetone three times. The resulting powder was obtained by centrifugation, and dried in an oven at 80 °C.

Synthesis of Hf-based PCN-555(Co). $HfOCl_2 \cdot 8H_2O$ (30.7 mg, 0.075 mmol), H_4TBAPy (11.5 mg, 0.017 mmol), CoTCPP (20 mg, 0.024 mmol) and benzoic acid (850 mg, 6.960 mmol) in 2 mL of DMF were ultrasonically dissolved in a Pyrex vial. The mixture was heated in an oven at 160 °C for 22 h. After cooling down to room temperature, the precipitates were collected by centrifugation. The solids were washed with DMF three times to remove unreacted precursors, and then solvent-exchanged with acetone three times. The resulting powder was obtained by centrifugation, and dried in an oven at 80 °C.

Activation of PCN-555. PCN-555 (50 mg) was immersed in 15 mL of 0.3 M HCl solution in DMF, and heated in an oven at 100 °C for 12 h. After cooling down to

room temperature, the precipitates were collected by centrifugation. The solids were washed with water and DMF three times, and then solvent-exchanged with acetone three times. The resulting powder was obtained by centrifugation, and dried in an oven at 80 °C.

SALI of NH_2-BDC into PCN-555(Ni). A 50 mg of activated PCN-555 was loaded in a Pyrex vial. Then, 10 mL of 0.1 M solution of 2-aminoterephthalic acid (1 mmol) in DMF was added to the reaction vial, which was sealed and heated at 65 °C for 24 h. After cooling down to room temperature, the precipitates were collected by centrifugation. The solids were washed with DMF three times, and then solvent-exchanged with acetone three times. The resulting powder was obtained by centrifugation, and dried in an oven at 80 °C.

SALI of DOBDC into PCN-555(Ni). A 50 mg of activated PCN-555 was loaded in a Pyrex vial. Then, 10 mL of 0.1 M solution of 2,5-dihydroxyterephthalic acid (1 mmol) in DMF was added to the reaction vial, which was sealed and heated at 65 °C for 24 h. After cooling down to room temperature, the precipitates were collected by centrifugation. The solids were washed with DMF three times, and then solvent-exchanged with acetone three times. The resulting powder was obtained by centrifugation, and dried in an oven at 80 °C.

SALI of 2Me-BDC into PCN-555(Ni). A 50 mg of activated PCN-555 was loaded in a Pyrex vial. Then, 10 mL of 0.1 M solution of 2,5-dimethylterephthalic acid (1 mmol) in DMF was added to the reaction vial, which was sealed and heated at 65 °C for 24 h. After cooling down to room temperature, the precipitates were collected by

centrifugation. The solids were washed with DMF three times, and then solvent-exchanged with acetone three times. The resulting powder was obtained by centrifugation, and dried in an oven at 80 °C.

SALI of Monosodium Salt of 2-Sulfonyl Terephthalic Acid into PCN-555(Ni). A 50 mg of activated PCN-555 was loaded in a Pyrex vial. Then, 10 mL of 0.1 M solution of monosodium salt of 2-sulfonyl terephthalic acid (1 mmol) in DMF was added to the reaction vial, which was sealed and heated at 65 °C for 24 h. After cooling down to room temperature, the precipitates were collected by centrifugation. The solids were washed with DMF three times, and then solvent-exchanged with acetone three times. The resulting powder was obtained by centrifugation, and dried in an oven at 80 °C.

SALI of H_4BTeC into PCN-555(Ni). A 50 mg of activated PCN-555 was loaded in a Pyrex vial. Then, 10 mL of 0.1 M solution of 1,2,4,5-benzenetetracarboxylic acid (1 mmol) in DMF was added to the reaction vial, which was sealed and heated at 65 °C for 24 h. After cooling down to room temperature, the precipitates were collected by centrifugation. The solids were washed with DMF three times, and then solvent-exchanged with acetone three times. The resulting powder was obtained by centrifugation, and dried in an oven at 80 °C.

SALI of N_3-BDC into PCN-555(Ni). A 50 mg of activated PCN-555 was loaded in a Pyrex vial. Then, 10 mL of 0.1 M solution of 2-azido terephthalic acid (1 mmol) in DMF was added to the reaction vial, which was sealed and heated at 65 °C for 24 h. After cooling down to room temperature, the precipitates were collected by centrifugation. The solids were washed with DMF three times, and then solvent-

exchanged with acetone three times. The resulting powder was obtained by centrifugation, and dried in an oven at 80 °C.

Transmission Electron Microscopic (TEM) Analysis. Samples for transmission electron microscopy observation were dispersed in acetone. A droplet of the suspension was transferred onto a carbon-coated copper grid. Observation was performed on a JEOL JEM2100 microscope, and operated at 200 kV (Cs 1.0 mm, point resolution 0.23 nm). Images were recorded with a Gatan Orius 833 CCD camera (resolution 2048 x 2048 pixels, pixel size 7.4 µm) under low dose conditions. Electron diffraction patterns were recorded with a Timepix pixel detector QTPX-262k (512 x 512 pixels, pixel size 55 µm, Amsterdam Sci. Ins.).

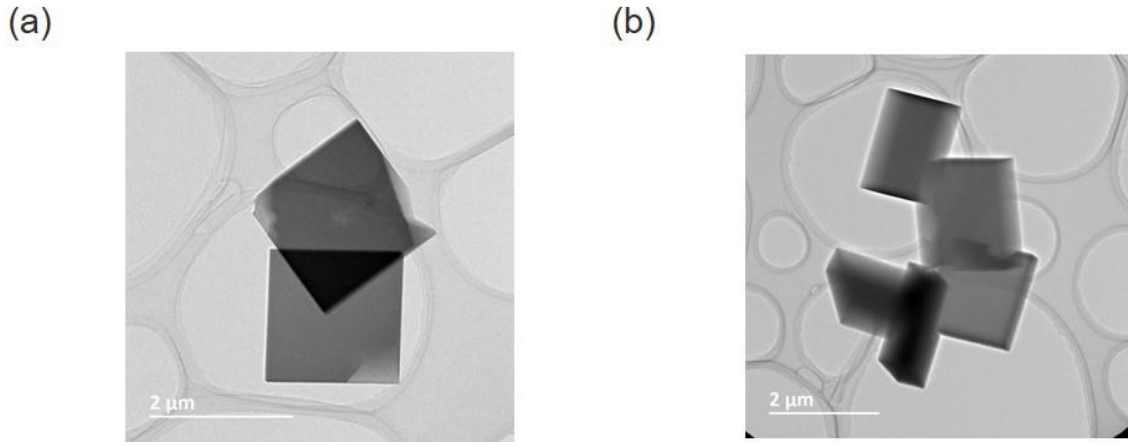

Figure V-1. TEM images of PCN-555.

Continuous Rotation Electron Diffraction (cRED) Collection. The crystal size of PCN-555 is too small to be solved by single crystal X-ray diffraction. Therefore, continuous rotation electron diffraction (cRED) was applied for solving and refining their structures. Samples of as-made PCN-555 for TEM investigations were dispersed in

acetone. A droplet of the suspension was transferred onto a carbon-coated copper grid. cRED data collection was performed on a JEOL JEM2100 microscope and operated at 200 kV (Cs 1.0 mm, point resolution 0.23 nm). Images were recorded with a Gatan Orius 833 CCD camera (resolution 2048 x 2048 pixels, pixel size 7.4 μm) under low dose conditions. Electron diffraction patterns were recorded with a Timepix pixel detector QTPX-262k (512 x 512 pixels, pixel size 55 μm, Amsterdam Sci. Ins.). The data were collected using the software *cREDCollection*. A single-tilt tomography sample holder was used for the data collection, which could tilt from -70° to +70° in the TEM. The aperture used for cRED data collection was about 1.0 μm in diameter. The speed of goniometer tilt was 0.45° s^{-1}, and the exposure time was 0.5 s per frame. Data was collected within 3 min to minimize the beam damage and to maximize the data quality. The covered tilt angle is 91.26°.

Structure Solution and Refinement from cRED. Figure V-2 presents the reconstructed 3D reciprocal lattice from the cRED data that PCN-555 has a primitive unit cell with the parameters of a = 27.25 Å, b = 26.74 Å, c = 16.46 Å, α = 89.64°, β = 90.37°, γ = 91.54°. As the lattice parameters a and b are close, and α, β, γ are near 90°, it indicates that the possible crystal system could be tetragonal. Figures V-2a-c show the two-dimensional (2D) slices cut of the 3D reciprocal lattice reconstructed from the cRED data. No special reflection condition can be deduced. This indicates several possible space groups for PCN-555: *P*4 (No. 75), *P*-4 (No. 81), *P*4/*m* (No. 83), *P*422 (No. 89), *P*4*mm* (No. 99), *P*-4*m*2 (No. 115), *P*-42*m* (No. 111) and *P*4/mmm (No. 123). The

space group *P*4/*mmm* with the highest symmetry was chosen for further structure determination.

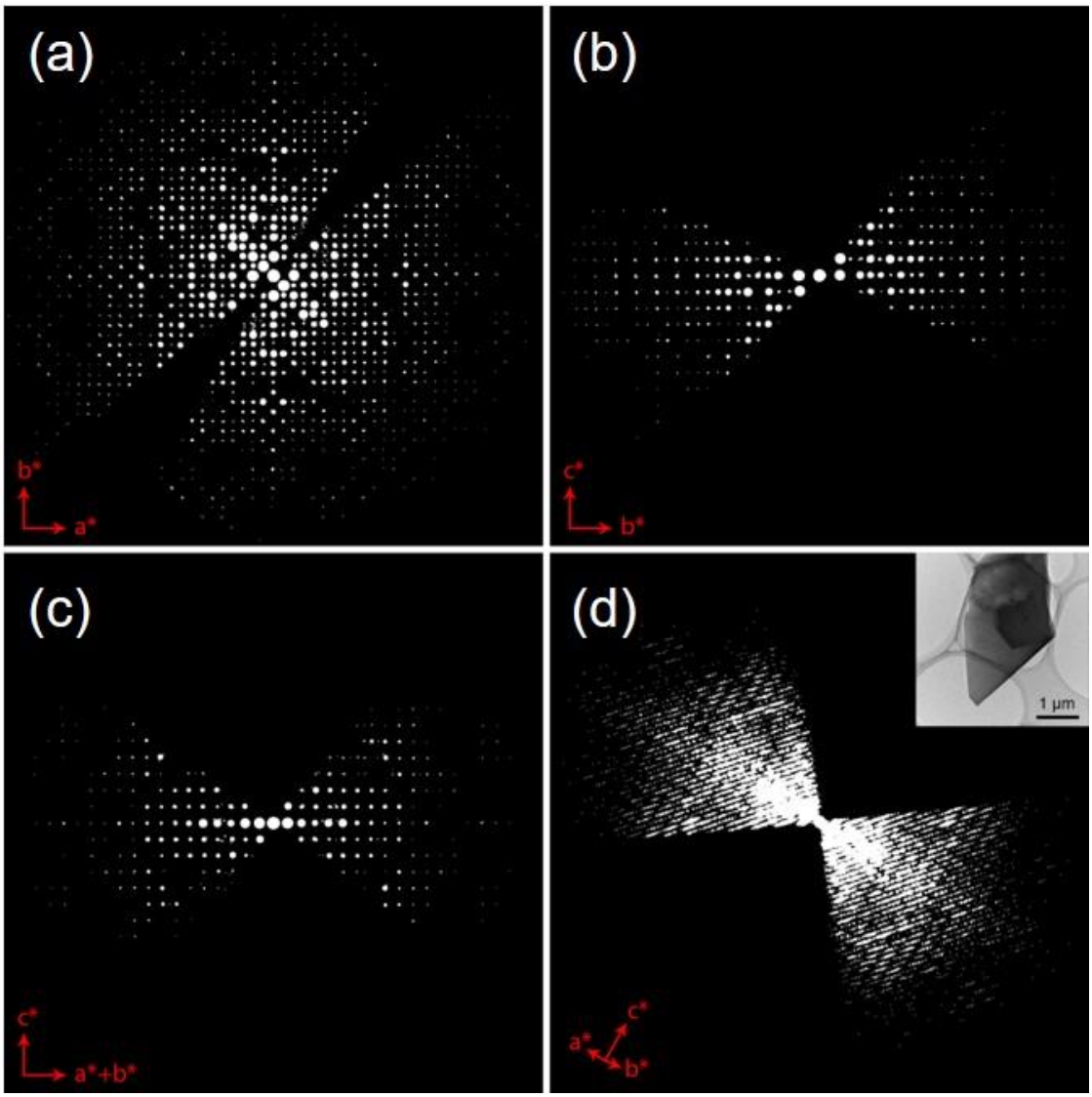

Figure V-2. 2D slices cut from the reconstructed 3D reciprocal lattice of PCN-555 show the (a) *hk*0, (b) 0*kl* and (c) *hhl* plane. (d) Reconstructed 3D reciprocal lattice of PCN-555 from cRED data. Insert is the crystal from which the cRED data was collected.

The ED dataset was collected by the cRED method with an improved resolution of 1.10 Å for structure solution. The data was processed by using XDS package. The

completeness is 78.9% and the Rint value is 0.173. The framework structure of PCN-555 was determined by direct methods using the program Shelx-2014. All of the framework atoms were found directly. The final refinement was done by using Shelxl-2014, and data converged to R1 = 0.261. The high Rint and R1 value are mainly caused by the dynamical effects. In the refinement, the structure factor was calculated in a kinematic way, while the electron diffraction data is dynamic. The details of data collection and refinement were summarized in Table V-1.

Table V-1. Experimental parameters for cRED data collection and crystallographic data for PCN-555 (λ = 0.0251 Å)

Tilt range (^{o})	-57.0° to 34.3°
Tilt rate (^{o}/s)	0.45
Exposure time/frame (s)	0.5
Total number of frames	380
Data collection time (min)	3
Crystal system	Tetragonal
Possible space group	*P*4/*mmm* (No. 123)
Unit cell parameter	*a*= 27.7 Å, *c*= 16.7 Å
Volume (Å^3)	12791
Resolution (Å)	1.10
Completeness	0.789
No. unique reflections	2297

Table V-1. Continued

No. observed reflections (I > 2 sigma(I))	1347
R1 (I > 2 sigma(I))	0.261
R1 (all reflections)	0.295
Goof	1.96

* Hydrogen atoms were not included in the refinement.

Rietveld Refinement. The structures of PCN-555 obtained from cRED method were further refined against synchrotron powder X-ray diffraction (PXRD, Figure V-3). High resolution PXRD data of PCN-555 was collected at room temperature at beamline (X-ray wavelength 0.45220 Å). Rietveld refinement was performed using TOPAS Academic V4.1. The background was fitted with a 16th order Chebychev polynomial. The refinement was conducted using a modified Thompson-Cox-Hastings pseudo-Voigt type peak profile function, followed by refinement of unit cells and zero-shift. The Zr-O distances were soft-restrained to 2.18 Å. Rigid bodies were applied on ligands. Terminal benzoic acid that bonded to the Zr clusters was located from difference Fourier maps. The guest species in the cages could not be located due to their partial occupancies and low symmetry. Instead, several oxygen atoms were added at random positions inside the cages to compensate for the contributions of the guest species, and refined subsequently. Finally, R-value was converged to R_p= 0.04416, R_{wp}= 0.06132, R_{exp}= 0.04418, and GOF= 1.389. The details of PXRD data collection and refinement were summarized in Table V-2.

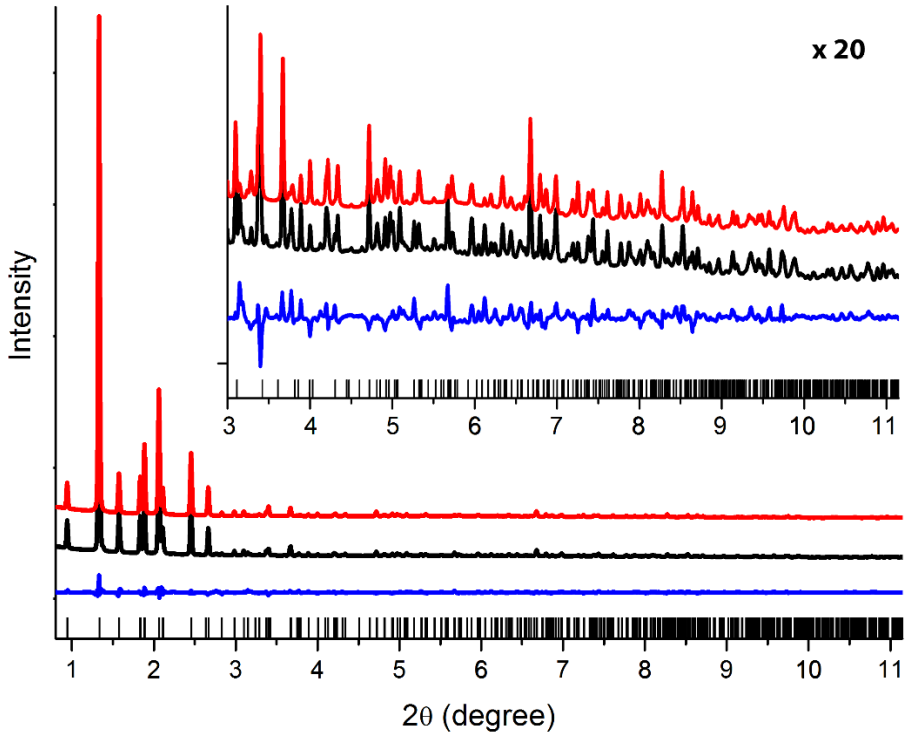

Figure V-3. Rietveld refinement of powder X-ray diffraction (wavelength 0.45220 Å) for PCN-555. The curves are simulated (red), observed (black), and difference profiles (blue), respectively; the bars below curves indicate peak positions.

Table V-2. Crystallographic data, powder X-ray collection conditions, and Rietveld refinement results of PCN-555

Name	**PCN-555**
Chemical formula	$C_{58.10}H_{29.20}Cu_{0.25}NO_{42.73}Zr_3$
Formula weight	1714.50
Crystal system	Tetragonal
Space group	*P*4/*mmm*

Table V-2. Continued

Name	**PCN-555**
a/Å	27.459(5)
c/Å	16.450(3)
Z	4
Temperature/K	298(2)
Wavelength/Å	0.45220
2θ range/°	0.79 – 11.15
Number of reflections	130
Number of structural variables	70
R_p	0.04108
R_{wp}	0.06132
R_{exp}	0.04418
GOF	1.389

As shown in Figure V-4, the structure of PCN-555 is consisted by Zr_6O_8 clusters, TCPP and TBAPy ligands. The benzoic acid acts as a modulator that competitively coordinates with the metals and slows down the crystal growth process to help generate highly crystalline products. Some of the BA were bonded to the Zr_6 cluster, replacing hydroxyl groups as terminals.

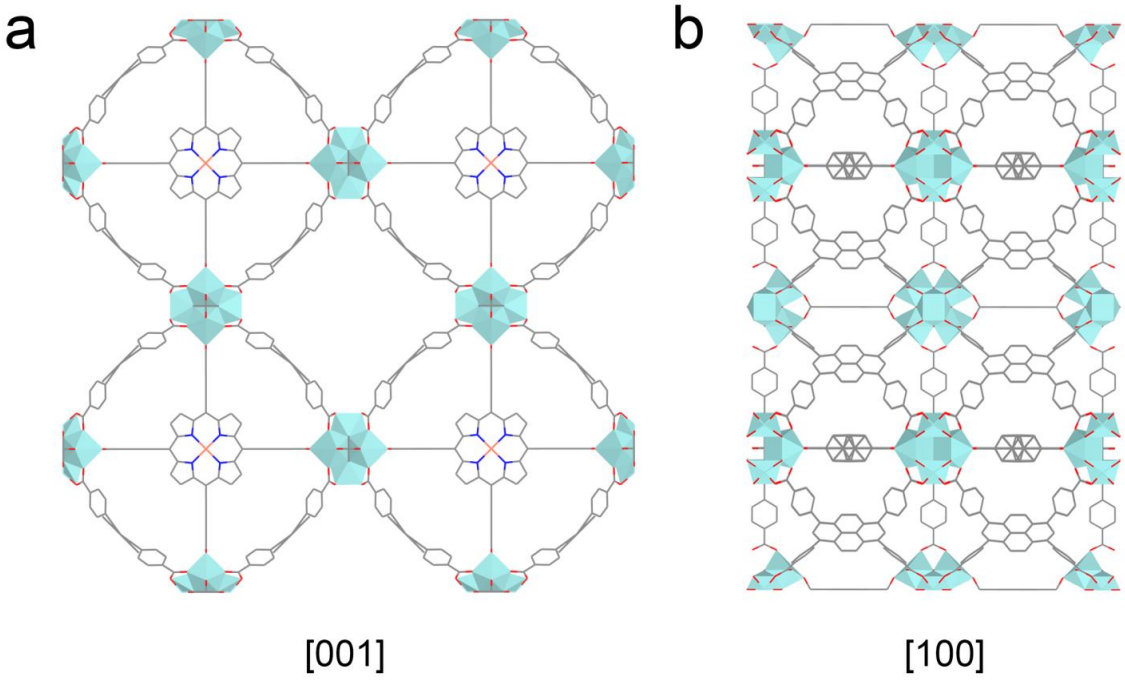

Figure V-4. Structural model of PCN-555 showing along [001] (a) and [100] (b) directions.

5.4 Results and Discussion

Thermodynamically Guided Synthesis of PCN-555. Although huge numbers of MOFs have been synthesized in recent years, reports on the synthesis of mixed-ligand Zr-MOFs are still very rare. Generally, mixing inorganic metal salts and distinguishable organic ligands tends to generate mixtures of Zr-MOFs containing a single organic ligand, unless the mixed-ligand Zr-MOF product is thermodynamically more favorable. Moreover, many studies have shown that Zr-MOFs with different structures can be obtained even when using the same starting materials (metal salt and organic ligand). For example, PCN-222 and PCN-224 are both synthesized from $ZrCl_4$ and TCPP ligand,[29, 73] while NU-901 and NU-1000 are both synthesized from $ZrCl_4$ and TBAPy

ligand.[150] One possible reason is that the Zr_6 cluster has versatile symmetry and connectivity (Figure V-5a). In addition, the conformation of the organic ligand can be altered upon bond rotation (Figure V-5b).

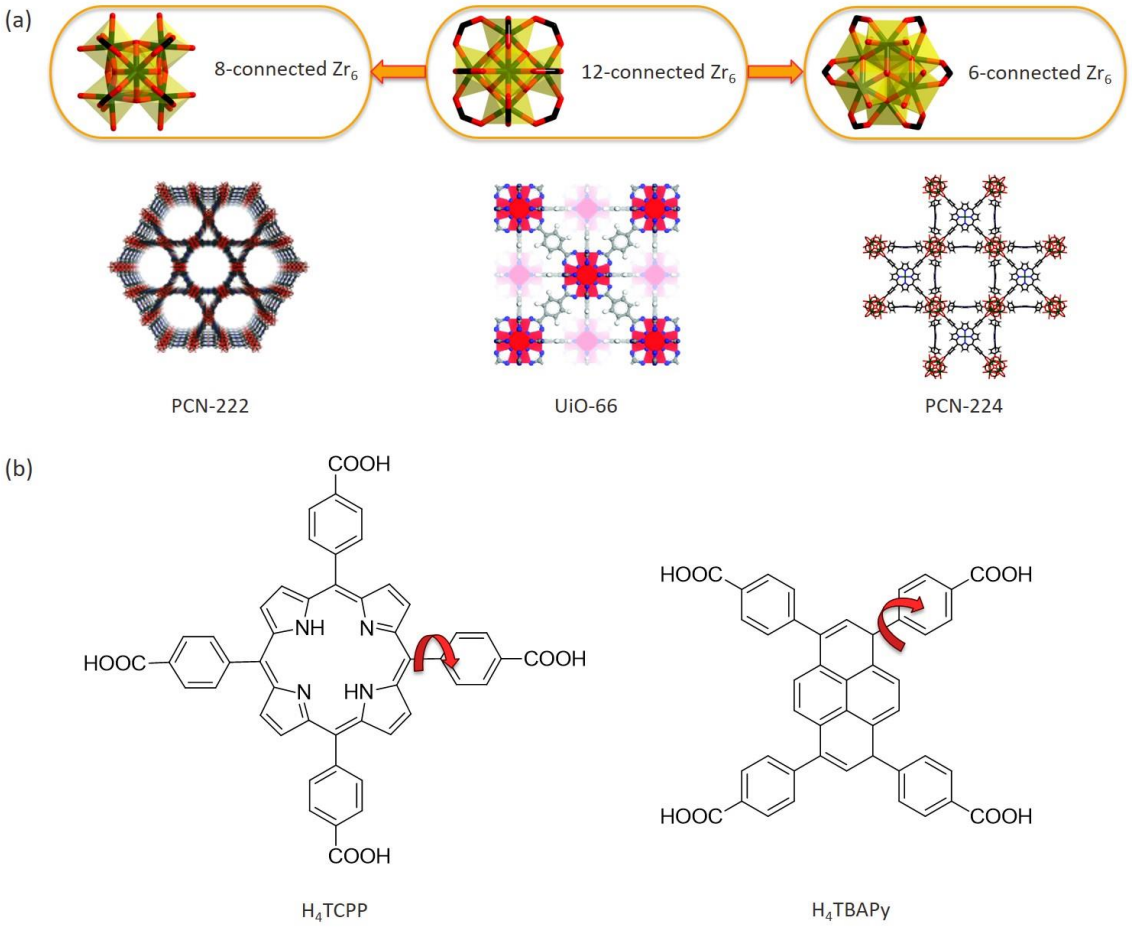

Figure V-5. (a) Versatile symmetry and connectivity of Zr_6 cluster. (b) Conformation change of TCPP and TBAPy ligand upon bond rotation.

Although it is very difficult to control the product obtained from a one-pot reaction, the flexibility of the Zr_6 cluster as well as the TCPP and TBAPy ligands makes it topologically possible to construct a mixed-ligand Zr-MOF based on these compositions. Given this, a mixed-ligand Zr-MOF (PCN-555) has been obtained

successfully through a thermodynamically guided synthesis. Solvothermal reaction of $ZrOCl_2 \cdot 8H_2O$, 1,3,6,8-tetrakis(p-benzoic acid)pyrene (H_4TBAPy), [5,10,15,20-tetrakis(4-carboxyphenyl)porphyrinato]-Ni(II) (NiTCPP), and benzoic acid (BA) in DMF at 160 °C for 22 hours yielded red powders of PCN-555.

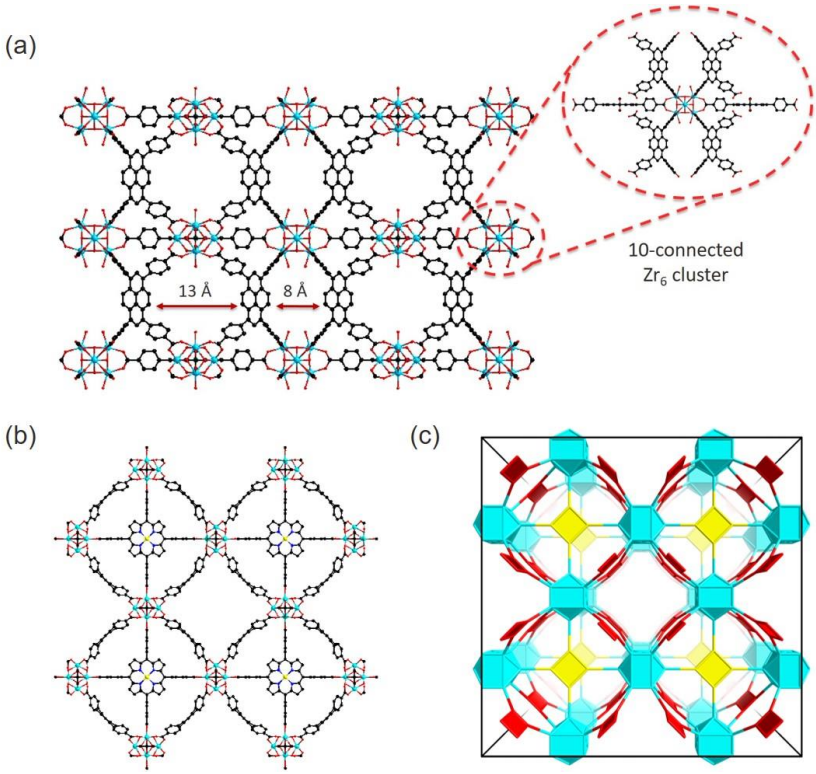

Figure V-6. Structure of PCN-555 viewing along (a) b axis, and (b) c axis. (c) Novel **zpp** topology of PCN-555. PCN-555 contains porphyrin planes (yellow), pyrene planes (red), and Zr_6 clusters (cyan) in the framework.

The structure of PCN-555 was solved from cRED data, followed by Rietveld refinement. As shown in Figure V-6, PCN-555 is constructed from 10-connected Zr_6 clusters, tetratopic NiTCPP ligands, and tetratopic TBAPy ligands. Each Zr_6 cluster is

coordinated to eight TBAPy ligands and two TCPP ligands. Moreover, PCN-555 exhibits a novel topology (**zpp**) (Figure V-6c).

The conformation of TCPP and TBAPy ligands in PCN-555 are shown in Figure V-7. The TBAPy ligand has a symmetry of C_{2v}, and the dihedral angle between the pyrene plane and the plane of outer benzene ring is about 50° (Figure V-7a). On the other hand, TCPP ligand in PCN-555 adopts D_{4h} symmetry, and the outer benzene ring is perpendicular to the plane of porphyrin center (Figure V-7b).

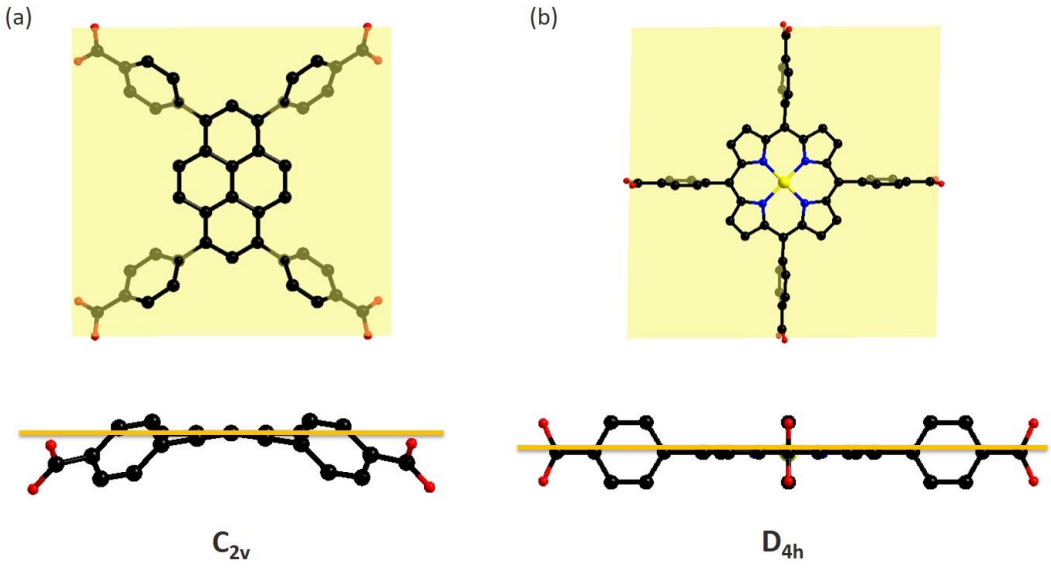

Figure V-7. The conformation and symmetry of (a) TBAPy ligand and (b) TCPP ligand in PCN-555.

Characterization of PCN-555. Firstly, PXRD analysis was carried out to characterize PCN-555. Its diffraction pattern was shown in Figure V-8, which matched very well with the simulated one.

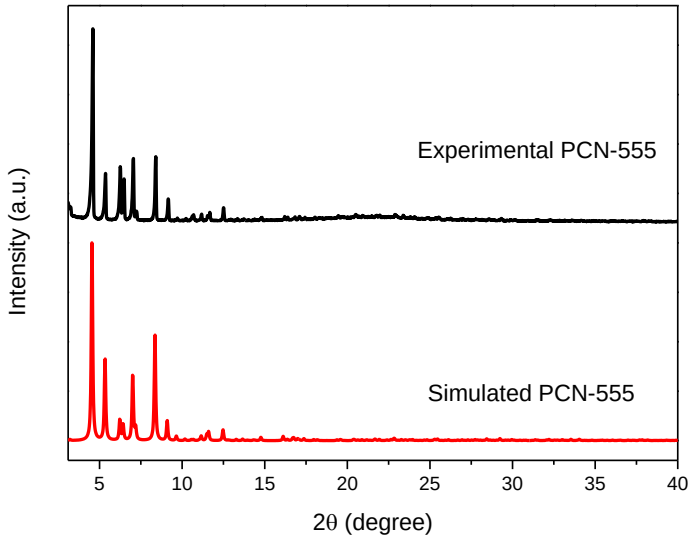

Figure V-8. The PXRD patterns for simulated and experimental PCN-555.

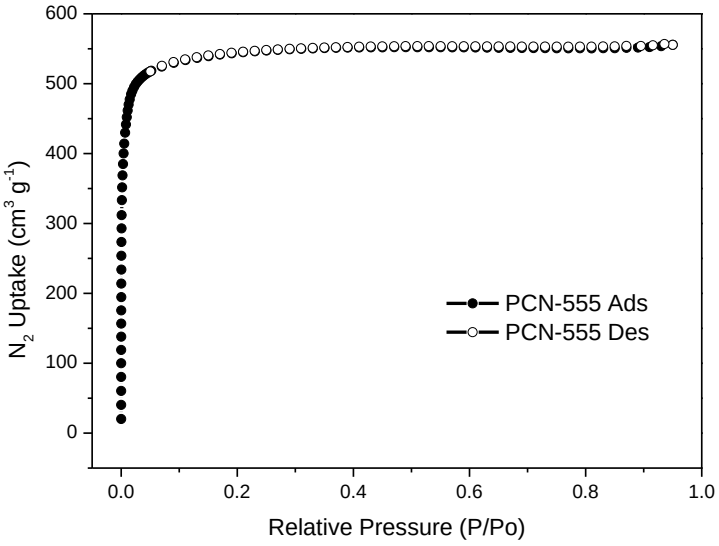

Figure V-9. N_2 adsorption isotherms for PCN-555 at 77 K.

To assess the permanent porosity of the material, PCN-555 was directly activated by removal of the solvent and tested by ASAP 2020 instrument. Type I isotherms that are typical for microporous solids were acquired. PCN-555 exhibited N_2 uptake of 555 $cm^3\ g^{-1}$ at 77 K and 1 bar (Figure V-9).

The morphology of PCN-555 was observed under SEM to be square slices (Figure V-10a). And all of the elements (e.g. Zr and Ni) were distributed evenly in the material, which was confirmed by EDS mappings (Figure V-10b-d).

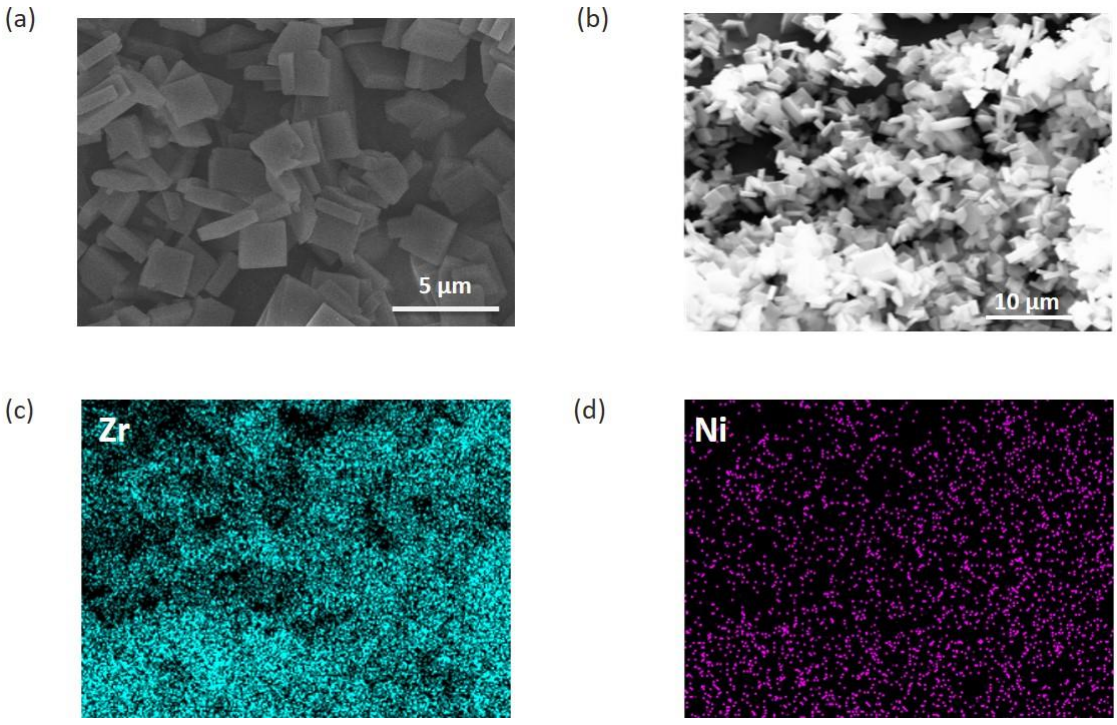

Figure V-10. (a) The SEM image of PCN-555. (b) The SEM image of PCN-555 showing the region used for EDS mappings. (c) EDS mapping of Zr. (d) EDS mapping of Ni.

Stability Tests. The thermal stability of PCN-555 was tested by TGA analysis. About 10.0 mg of the sample was heated on the Shimadzu TGA-50 instrument from

room temperature to 750 °C at a ramp rate of 2 °C/min under nitrogen flow of 25 mL/min. The decomposition of material was observed at around 450 °C (Figure V-11), showing high thermal stability of the material.

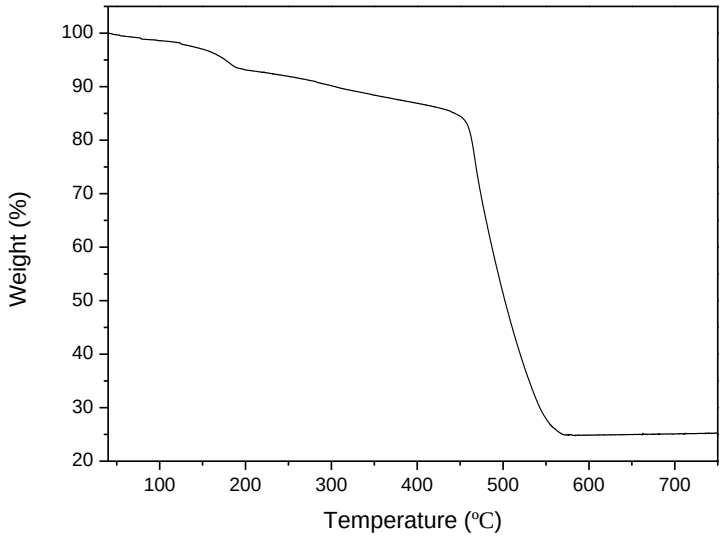

Figure V-11. TGA analysis of PCN-555.

In the next step, the chemical stability of PCN-555 was tested by immersing the sample (100 mg) into a series of aqueous solutions (50 mL), including 1 M HCl, 6 M HCl, deionized water, 0.1 mM NaOH, and 1 mM NaOH aqueous solutions. After 24 h, all the samples were centrifuged and then washed with water, DMF, and acetone three times. These samples were dried in oven and characterized by PXRD. The PXRD patterns of all the samples were identical to that of PCN-555 before the chemical stability test (Figure V-12), implying that the framework of PCN-555 was maintained very well after treatment with these acid and base solutions.

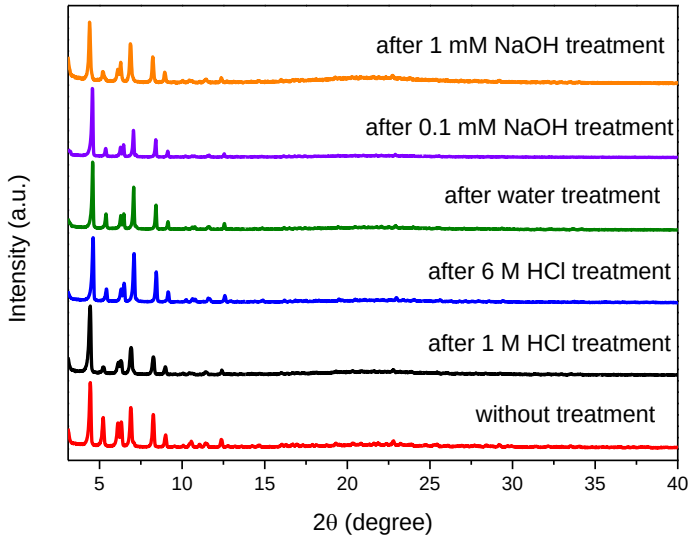

Figure V-12. PXRD patterns for PCN-555 before and after treatment with different aqueous solutions.

To further confirm that PCN-555 was stable under the selected chemical conditions, the samples after the treatment were tested by N_2 uptake experiments at 77 K. All the samples were degassed on ASAP 2020 adsorption system at 100 °C for 5 h prior to N_2 adsorption measurement at 77 K. According to Figure V-13, N_2 uptake experiments further proved that the framework of all these samples were preserved during the chemical stability test.

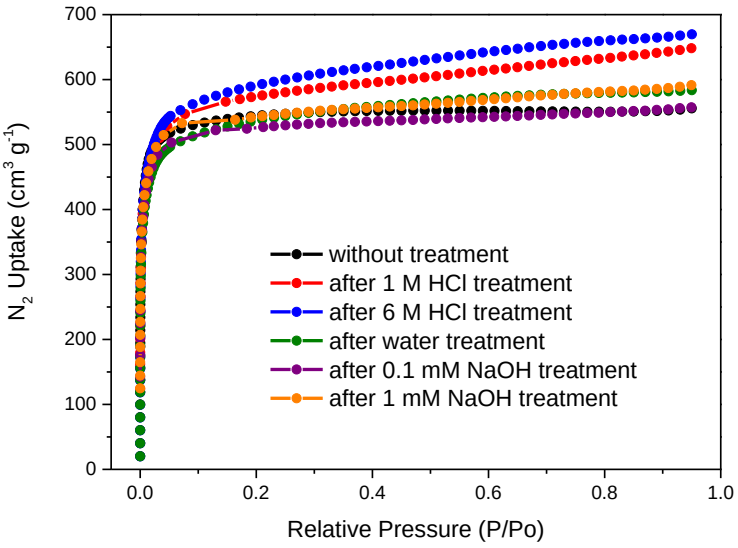

Figure V-13. N_2 adsorption isotherms for PCN-555 before and after treatment with different aqueous solutions.

Construction of PCN-555 with Multiple Functionalities. Taking advantage of the synthetic versatility of PCN-555, we attempted to incorporate various functionalities into PCN-555.

Firstly, different functionalities can be introduced into the framework through the organic ligand moiety. Given this, porphyrin ligands with different metals in the center were used for the synthesis, including NiTCPP, FeTCPPCl, MnTCPP, CuTCPP, H_2TCPP, ZnTCPP, and CoTCPP. And a series of functional mixed-ligand Zr-MOFs were obtained. These products exhibited PXRD patterns identical to that of the simulated PCN-555 (Figure V-14).

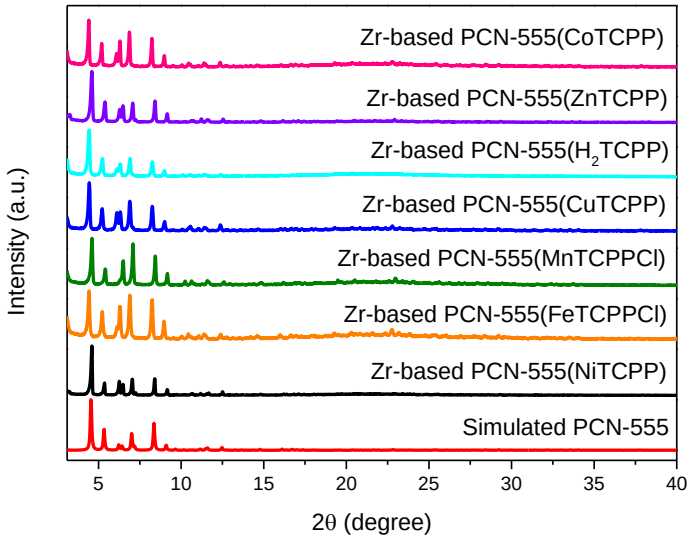

Figure V-14. PXRD patterns for Zr-based PCN-555 containing various porphyrin ligands, including NiTCPP, FeTCPPCl, MnTCPPCl, CuTCPP, H_2TCPP, ZnTCPP, and CoTCPP.

Secondly, a series of Hf-based PCN-555 were synthesized by replacing the secondary building block of Zr_6 cluster with Hf_6 cluster. In recent years, many studies have shown that Hf_6 cluster can adopt the same symmetry and connectivity compared with Zr_6 cluster.[151-157] Therefore, Hf-based MOFs with the structure similar to Zr-based MOFs can be obtained under similar synthetic conditions. With that in mind, we synthesized Hf-based PCN-555 by adding Hf salt instead of Zr salt. In addition, by mixing TBAPy ligand and various TCPP ligands with different metals in the center, multiple functionalities were incorporated into Hf-based PCN-555. Their PXRD patterns were shown in Figure V-15, which were in consistent with that of the simulated PCN-555.

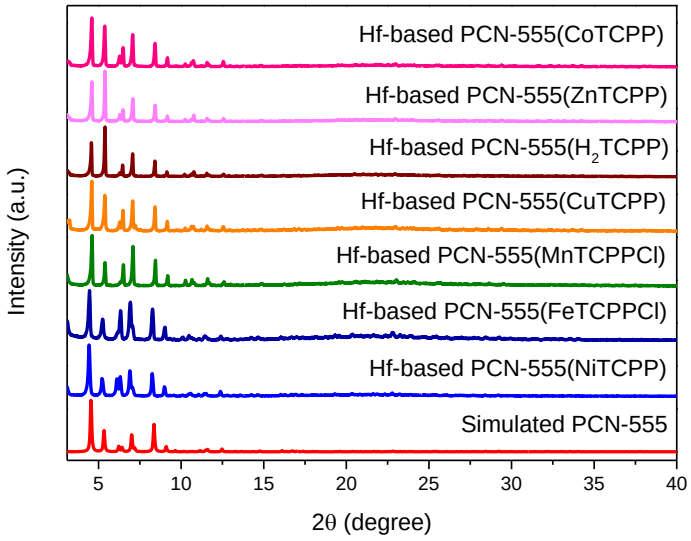

Figure V-15. PXRD patterns for Hf-based PCN-555 containing various porphyrin ligands, including NiTCPP, FeTCPPCl, MnTCPPCl, CuTCPP, H_2TCPP, ZnTCPP, and CoTCPP.

In addition to functionalization through the organic ligand moiety and replacement of the secondary building block, the available coordination sites on the Zr_6 cluster can be utilized for introducing additional functionalities. For example, solvent-assisted ligand incorporation (SALI) strategy has been widely applied to post-synthetically functionalize MOFs.[149, 158-161] For PCN-555, each Zr_6 cluster is coordinated to eight TBAPy ligands and two TCPP ligands, leaving two available coordination sites for further modification of the framework (Figure V-16a). Therefore, it is possible to incorporate additional ligands into PCN-555 through the post-synthetic modification method.

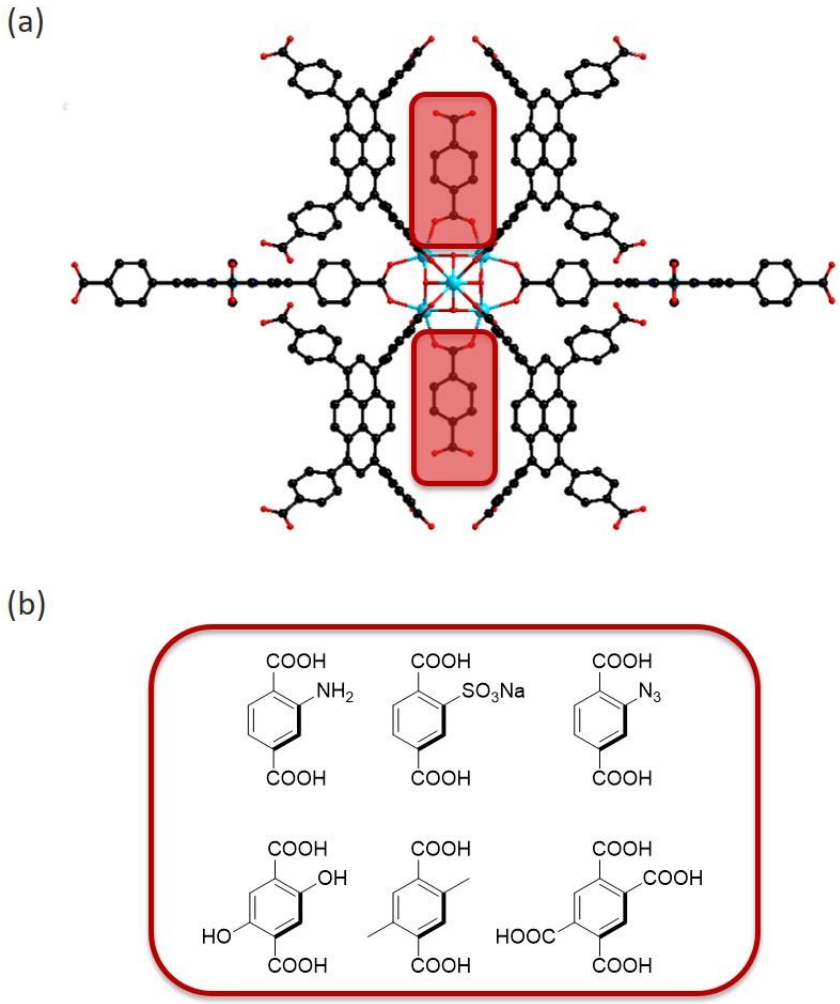

Figure V-16. (a) The structure of PCN-555 containing two coordinatively available sites for PSM. (b) Ligands of BDC derivatives used for SALI.

In the next step, SALI of BDC derivatives (Figure V-16b) were carried out on PCN-555. After immersing PCN-555 in the DMF solution of each BDC derivative, a series of secondary functionalities were introduced into the framework of PCN-555. Their PXRD patterns were in consistent with that of the pristine PCN-555 (Figure V-17a), confirming that the framework integrity was maintained very well after the SALI

process. In addition, the N_2 adsorption isotherms of these products were summarized in Figure V-17b. The N_2 uptake of these materials decreased after incorporation of additional functionalities.

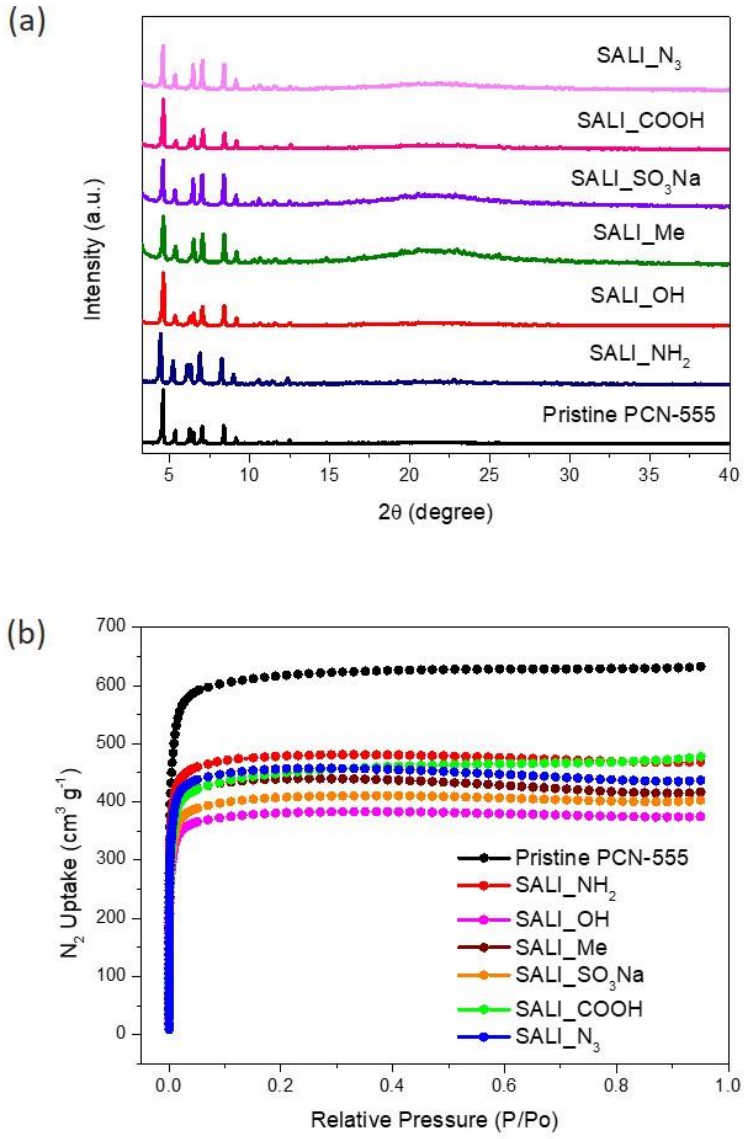

Figure V-17. (a) The PXRD patterns of the samples after SALI. (b) N_2 adsorption isotherms of the samples after SALI.

5.5 Conclusions

Through a thermodynamically guided synthesis, a series of highly stable mixed-ligand Zr/Hf-based MOFs (PCN-555) have been successfully synthesized by mixing tetratopic TCPP ligands and TBAPy ligands. In PCN-555, each of the Zr_6 cluster is coordinated to eight TBAPy ligands and two TCPP ligands. The position of both porphyrin and pyrene functionalities can be precisely located in the framework. PCN-555 exhibited very high thermal and chemical stability. Through mixing organic ligands of different functionalities (e.g. NiTCPP, FeTCPPCl, MnTCPPCl, CuTCPP, H_2TCPP, ZnTCPP, and CoTCPP) and replacement of the secondary building units (inorganic metal clusters), a series of Zr/Hf-based PCN-555 with multiple functionalities have been synthesized. Moreover, taking advantage of the available coordination sites on the metal clusters, SALI strategy was applied to post-synthetically introduce multiple functionalities into PCN-555. Therefore, PCN-555 provides an ideal platform for further functionalization and exploration of new structures.

CHAPTER VI

SUMMARY

In this dissertation, different strategies to construct highly stable MOFs with multiple functionalities have been presented.

In the first project, a facile one-pot synthetic strategy was developed to introduce porphyrin into highly stable UiO-66 homogeneously. The amount of incorporated porphyrin can be tuned gradually. In addition, the crystal structure, morphology, and ultrahigh chemical stability of UiO-66 were all well maintained after functionalization of UiO-66. By mixing ditopic BDC ligand and/or its derivatives and various tetratopic porphyrin ligands, 49 MOFs with multiple functionalities were obtained. This synthetic strategy combines the framework robustness of UiO-66 as well as the desired functionalities.

In the second project, a comprehensive study of the in situ secondary ligand incorporation (ISLI) strategy was presented to construct highly stable UiO series of MOFs (e.g. UiO-66, UiO-67, and UiO-68) with the incorporation of multiple functionalities with a tunable amount. The crystal structure, morphology, and stability of the parent MOF were well preserved. Moreover, both computational and experimental studies were carried out to understand the mechanism aspect of the ISLI strategy. The influence of the modulating reagent (BA) and the porphyrin ligand were discussed, demonstrating the importance of adjusting the reaction conditions to thermodynamically

and kinetically drive the reaction system towards phase-pure UiO series of MOFs integrated with multiple functionalities.

In the third project, the ISLI strategy was further extended to synthesize Zr-MOFs constructed from multitopic organic ligands (compounds **7**-**10**). Depending on the synthetic conditions, tunable amount of porphyrin ligands can be incorporated into the parent MOF homogeneously. Significantly, up to seven functionalities have been introduced into NU-1000 through ISLI strategy. In addition, taking compound **9** as an example, the product obtained under different synthetic conditions were studied and summarized in a phase diagram. Generation of phase-pure product with desired functionality can be achieved by ISLI strategy to thermodynamically and kinetically tune the reaction system. Overall, ISLI strategy overcomes the limitations of PSM and traditional mixed-ligand strategy, providing a feasible route to construct highly stable Zr-MOFs with multiple functionalities for advanced applications.

In the last project, a series of highly stable mixed-ligand Zr/Hf-based MOFs (PCN-555) have been synthesized through a thermodynamically guided synthesis. Both porphyrin and pyrene functionalities can be located precisely. Various functionalities were introduced into PCN-555 through the organic ligand moiety and the inorganic metal clusters. Moreover, additional functional groups were incorporated post-synthetically via SALI strategy. Therefore, PCN-555 provides an ideal scaffold for further functionalization and exploration of new structures.

In summary, different strategies to synthesize highly stable MOFs with multifunctionality have been presented in this dissertation. Firstly, ISLI demonstrates a

facile and general strategy for doping multiple functionalities into Zr-MOFs homogeneously with a tunable amount, while maintaining the original structural features of the parent MOF. ISLI strategy overcomes the limitations of PSM strategy and conventional mixed-ligand strategy (Figure VI-1a). Secondly, unlike ISLI strategy that introduces porphyrin in a disordered manner, through a thermodynamic control, porphyrin can be introduced into a pyrene-based MOF periodically through a *de novo* synthesis, resulting in the formation of a mixed-ligand structure with a novel topology (Figure VI-1b). Consequently, these strategies provide useful tools to investigate highly stable MOFs with desired multifunctionality for a wide range of potential applications.

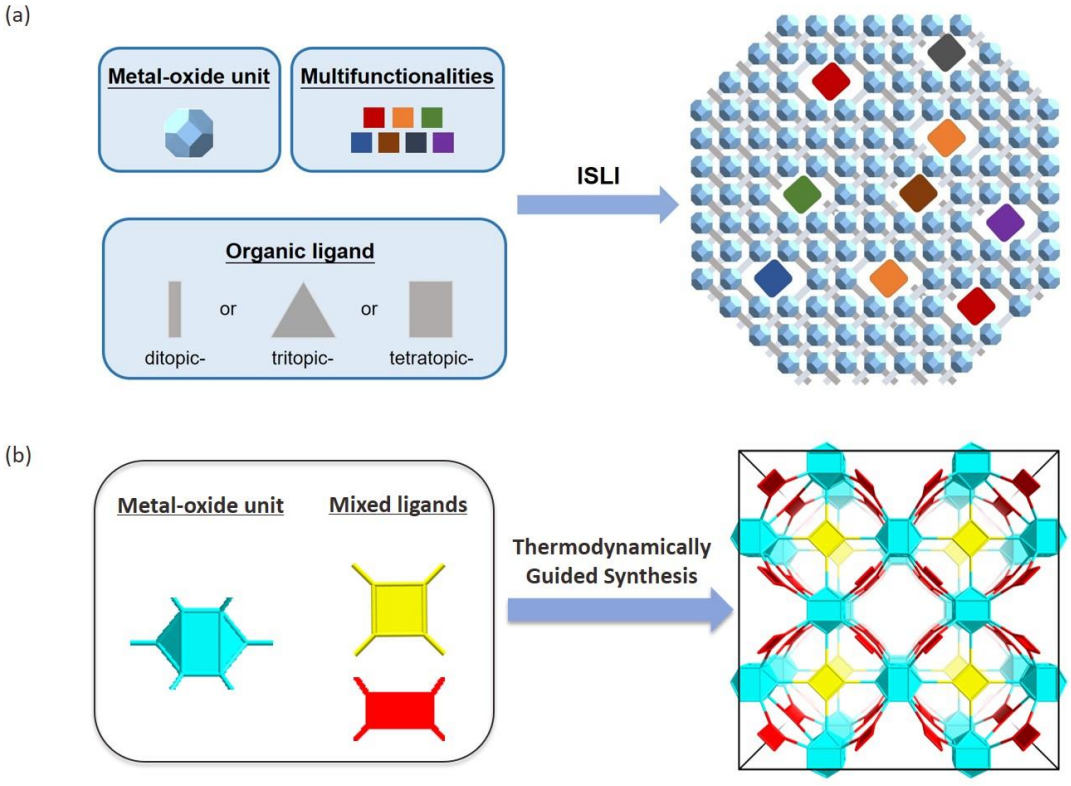

Figure VI-1. Strategies to construct highly stable MOFs with multiple functionalities. (a) ISLI strategy; (b) thermodynamically guided synthesis.

REFERENCES

1. Long, J. R.; Yaghi, O. M., The pervasive chemistry of metal-organic frameworks. *Chem. Soc. Rev.* **2009,** *38* (5), 1213-1214.

2. Zhou, H.-C.; Long, J. R.; Yaghi, O. M., Introduction to Metal–Organic Frameworks. *Chem. Rev.* **2012,** *112* (2), 673-674.

3. Lu, W.; Wei, Z.; Gu, Z.-Y.; Liu, T.-F.; Park, J.; Park, J.; Tian, J.; Zhang, M.; Zhang, Q.; Gentle Iii, T.; Bosch, M.; Zhou, H.-C., Tuning the structure and function of metal-organic frameworks via linker design. *Chem. Soc. Rev.* **2014,** *43* (16), 5561-5593.

4. Eddaoudi, M.; Kim, J.; Rosi, N.; Vodak, D.; Wachter, J.; O'Keeffe, M.; Yaghi, O. M., Systematic Design of Pore Size and Functionality in Isoreticular MOFs and Their Application in Methane Storage. *Science* **2002,** *295* (5554), 469-472.

5. Murray, L. J.; Dinca, M.; Long, J. R., Hydrogen storage in metal-organic frameworks. *Chem. Soc. Rev.* **2009,** *38* (5), 1294-1314.

6. D'Alessandro, D. M.; Smit, B.; Long, J. R., Carbon Dioxide Capture: Prospects for New Materials. *Angew. Chem. Int. Ed.* **2010,** *49* (35), 6058-6082.

7. Sumida, K.; Rogow, D. L.; Mason, J. A.; McDonald, T. M.; Bloch, E. D.; Herm, Z. R.; Bae, T.-H.; Long, J. R., Carbon Dioxide Capture in Metal–Organic Frameworks. *Chem. Rev.* **2012,** *112* (2), 724-781.

8. Li, J.-R.; Kuppler, R. J.; Zhou, H.-C., Selective gas adsorption and separation in metal-organic frameworks. *Chem. Soc. Rev.* **2009,** *38* (5), 1477-1504.

9. Bae, Y.-S.; Snurr, R. Q., Development and Evaluation of Porous Materials for Carbon Dioxide Separation and Capture. *Angew. Chem. Int. Ed.* **2011,** *50* (49), 11586-11596.

10. Seo, J. S.; Whang, D.; Lee, H.; Jun, S. I.; Oh, J.; Jeon, Y. J.; Kim, K., A homochiral metal-organic porous material for enantioselective separation and catalysis. *Nature* **2000,** *404* (6781), 982-986.

11. Lee, J.; Farha, O. K.; Roberts, J.; Scheidt, K. A.; Nguyen, S. T.; Hupp, J. T., Metal-organic framework materials as catalysts. *Chem. Soc. Rev.* **2009,** *38* (5), 1450-1459.

12. Ma, L.; Abney, C.; Lin, W., Enantioselective catalysis with homochiral metal-organic frameworks. *Chem. Soc. Rev.* **2009,** *38* (5), 1248-1256.

13. Liu, J.; Chen, L.; Cui, H.; Zhang, J.; Zhang, L.; Su, C.-Y., Applications of metal-organic frameworks in heterogeneous supramolecular catalysis. *Chem. Soc. Rev.* **2014,** *43* (16), 6011-6061.

14. Zhang, T.; Lin, W., Metal-organic frameworks for artificial photosynthesis and photocatalysis. *Chem. Soc. Rev.* **2014,** *43* (16), 5982-5993.

15. Allendorf, M. D.; Bauer, C. A.; Bhakta, R. K.; Houk, R. J. T., Luminescent metal-organic frameworks. *Chem. Soc. Rev.* **2009,** *38* (5), 1330-1352.

16. Kreno, L. E.; Leong, K.; Farha, O. K.; Allendorf, M.; Van Duyne, R. P.; Hupp, J. T., Metal–Organic Framework Materials as Chemical Sensors. *Chem. Rev.* **2012,** *112* (2), 1105-1125.

17. Heine, J.; Muller-Buschbaum, K., Engineering metal-based luminescence in coordination polymers and metal-organic frameworks. *Chem. Soc. Rev.* **2013,** *42* (24), 9232-9242.

18. Hu, Z.; Deibert, B. J.; Li, J., Luminescent metal-organic frameworks for chemical sensing and explosive detection. *Chem. Soc. Rev.* **2014,** *43* (16), 5815-5840.

19. Zhang, X.; Wang, W.; Hu, Z.; Wang, G.; Uvdal, K., Coordination polymers for energy transfer: Preparations, properties, sensing applications, and perspectives. *Coord. Chem. Rev.* **2015,** *284*, 206-235.

20. Celli, J. P.; Spring, B. Q.; Rizvi, I.; Evans, C. L.; Samkoe, K. S.; Verma, S.; Pogue, B. W.; Hasan, T., Imaging and Photodynamic Therapy: Mechanisms, Monitoring, and Optimization. *Chem. Rev.* **2010,** *110* (5), 2795-2838.

21. Horcajada, P.; Gref, R.; Baati, T.; Allan, P. K.; Maurin, G.; Couvreur, P.; Férey, G.; Morris, R. E.; Serre, C., Metal–Organic Frameworks in Biomedicine. *Chem. Rev.* **2012,** *112* (2), 1232-1268.

22. Howarth, A. J.; Liu, Y.; Li, P.; Li, Z.; Wang, T. C.; Hupp, J. T.; Farha, O. K., Chemical, thermal and mechanical stabilities of metal–organic frameworks. *Nat. Rev. Mater.* **2016,** *1*, 15018.

23. Chui, S. S.-Y.; Lo, S. M.-F.; Charmant, J. P. H.; Orpen, A. G.; Williams, I. D., A Chemically Functionalizable Nanoporous Material $[Cu_3(TMA)_2(H_2O)_3]_n$. *Science* **1999,** *283* (5405), 1148-1150.

24. Li, H.; Eddaoudi, M.; O'Keeffe, M.; Yaghi, O. M., Design and synthesis of an exceptionally stable and highly porous metal-organic framework. *Nature* **1999,** *402*, 276.

25. Helm, L.; Merbach, A. E., Applications of advanced experimental techniques: high pressure NMR and computer simulations. *J. Chem. Soc., Dalton Trans.* **2002,** (5), 633-641.

26. Thierry, L.; Christian, S.; Clarisse, H.; Gerhard, F.; Francis, T.; Marc, H.; Thierry, B.; Gérard, F., A Rationale for the Large Breathing of the Porous Aluminum Terephthalate (MIL‐53) Upon Hydration. *Chem. - Eur. J.* **2004,** *10* (6), 1373-1382.

27. Llewellyn, P. L.; Bourrelly, S.; Serre, C.; Vimont, A.; Daturi, M.; Hamon, L.; De Weireld, G.; Chang, J.-S.; Hong, D.-Y.; Kyu Hwang, Y.; Hwa Jhung, S.; Férey, G., High Uptakes of CO2 and CH4 in Mesoporous Metal—Organic Frameworks MIL-100 and MIL-101. *Langmuir* **2008,** *24* (14), 7245-7250.

28. Kandiah, M.; Nilsen, M. H.; Usseglio, S.; Jakobsen, S.; Olsbye, U.; Tilset, M.; Larabi, C.; Quadrelli, E. A.; Bonino, F.; Lillerud, K. P., Synthesis and Stability of Tagged UiO-66 Zr-MOFs. *Chem. Mater.* **2010,** *22* (24), 6632-6640.

29. Feng, D.; Chung, W.-C.; Wei, Z.; Gu, Z.-Y.; Jiang, H.-L.; Chen, Y.-P.; Darensbourg, D. J.; Zhou, H.-C., Construction of Ultrastable Porphyrin Zr Metal–Organic Frameworks through Linker Elimination. *J. Am. Chem. Soc* **2013,** *135* (45), 17105-17110.

30. Feng, D.; Wang, K.; Wei, Z.; Chen, Y.-P.; Simon, C. M.; Arvapally, R. K.; Martin, R. L.; Bosch, M.; Liu, T.-F.; Fordham, S.; Yuan, D.; Omary, M. A.;

Haranczyk, M.; Smit, B.; Zhou, H.-C., Kinetically tuned dimensional augmentation as a versatile synthetic route towards robust metal–organic frameworks. *Nat. Commun.* **2014,** *5*, 5723.

31. Fracaroli, A. M.; Furukawa, H.; Suzuki, M.; Dodd, M.; Okajima, S.; Gándara, F.; Reimer, J. A.; Yaghi, O. M., Metal–Organic Frameworks with Precisely Designed Interior for Carbon Dioxide Capture in the Presence of Water. *J. Am. Chem. Soc* **2014,** *136* (25), 8863-8866.

32. Manna, K.; Zhang, T.; Lin, W., Postsynthetic Metalation of Bipyridyl-Containing Metal–Organic Frameworks for Highly Efficient Catalytic Organic Transformations. *J. Am. Chem. Soc* **2014,** *136* (18), 6566-6569.

33. Hu, Z.; Lustig, W. P.; Zhang, J.; Zheng, C.; Wang, H.; Teat, S. J.; Gong, Q.; Rudd, N. D.; Li, J., Effective Detection of Mycotoxins by a Highly Luminescent Metal–Organic Framework. *J. Am. Chem. Soc* **2015,** *137* (51), 16209-16215.

34. Lee, C. Y.; Farha, O. K.; Hong, B. J.; Sarjeant, A. A.; Nguyen, S. T.; Hupp, J. T., Light-Harvesting Metal–Organic Frameworks (MOFs): Efficient Strut-to-Strut Energy Transfer in Bodipy and Porphyrin-Based MOFs. *J. Am. Chem. Soc* **2011,** *133* (40), 15858-15861.

35. Gu, X.; Lu, Z.-H.; Jiang, H.-L.; Akita, T.; Xu, Q., Synergistic Catalysis of Metal–Organic Framework-Immobilized Au–Pd Nanoparticles in Dehydrogenation of Formic Acid for Chemical Hydrogen Storage. *J. Am. Chem. Soc* **2011,** *133* (31), 11822-11825.

36. Zhu, Q.-L.; Xu, Q., Metal-organic framework composites. *Chem. Soc. Rev.* **2014,** *43* (16), 5468-5512.

37. Huang, Y.-B.; Liang, J.; Wang, X.-S.; Cao, R., Multifunctional metal-organic framework catalysts: synergistic catalysis and tandem reactions. *Chem. Soc. Rev.* **2017,** *46* (1), 126-157.

38. Wang, Z.; Cohen, S. M., Postsynthetic modification of metal-organic frameworks. *Chem. Soc. Rev.* **2009,** *38* (5), 1315-1329.

39. Stock, N.; Biswas, S., Synthesis of Metal-Organic Frameworks (MOFs): Routes to Various MOF Topologies, Morphologies, and Composites. *Chem. Rev.* **2012,** *112* (2), 933-969.

40. Deria, P.; Mondloch, J. E.; Karagiaridi, O.; Bury, W.; Hupp, J. T.; Farha, O. K., Beyond post-synthesis modification: evolution of metal-organic frameworks via building block replacement. *Chem. Soc. Rev.* **2014,** *43* (16), 5896-5912.

41. Furukawa, H.; Müller, U.; Yaghi, O. M., "Heterogeneity within Order" in Metal–Organic Frameworks. *Angew. Chem. Int. Ed.* **2015,** *54* (11), 3417-3430.

42. Cui, Y.; Li, B.; He, H.; Zhou, W.; Chen, B.; Qian, G., Metal–Organic Frameworks as Platforms for Functional Materials. *Acc. Chem. Res.* **2016,** *49* (3), 483-493.

43. Deng, H.; Doonan, C. J.; Furukawa, H.; Ferreira, R. B.; Towne, J.; Knobler, C. B.; Wang, B.; Yaghi, O. M., Multiple Functional Groups of Varying Ratios in Metal-Organic Frameworks. *Science* **2010,** *327* (5967), 846-850.

44. Choi, E.-Y.; Barron, P. M.; Novotny, R. W.; Son, H.-T.; Hu, C.; Choe, W., Pillared Porphyrin Homologous Series: Intergrowth in Metal−Organic Frameworks. *Inorg. Chem.* **2009,** *48* (2), 426-428.

45. Cavka, J. H.; Jakobsen, S.; Olsbye, U.; Guillou, N.; Lamberti, C.; Bordiga, S.; Lillerud, K. P., A New Zirconium Inorganic Building Brick Forming Metal Organic Frameworks with Exceptional Stability. *J. Am. Chem. Soc* **2008,** *130* (42), 13850-13851.

46. Schaate, A.; Roy, P.; Godt, A.; Lippke, J.; Waltz, F.; Wiebcke, M.; Behrens, P., Modulated Synthesis of Zr-Based Metal–Organic Frameworks: From Nano to Single Crystals. *Chem. - Eur. J.* **2011,** *17* (24), 6643-6651.

47. Schaate, A.; Roy, P.; Preuße, T.; Lohmeier, S. J.; Godt, A.; Behrens, P., Porous Interpenetrated Zirconium–Organic Frameworks (PIZOFs): A Chemically Versatile Family of Metal–Organic Frameworks. *Chem. - Eur. J.* **2011,** *17* (34), 9320-9325.

48. Bon, V.; Senkovskyy, V.; Senkovska, I.; Kaskel, S., Zr(iv) and Hf(iv) based metal-organic frameworks with reo-topology. *Chem. Commun.* **2012,** *48* (67), 8407-8409.

49. Guillerm, V.; Ragon, F.; Dan-Hardi, M.; Devic, T.; Vishnuvarthan, M.; Campo, B.; Vimont, A.; Clet, G.; Yang, Q.; Maurin, G.; Férey, G.; Vittadini, A.; Gross, S.; Serre, C., A Series of Isoreticular, Highly Stable, Porous Zirconium Oxide Based Metal–Organic Frameworks. *Angew. Chem. Int. Ed.* **2012,** *51* (37), 9267-9271.

50. Morris, W.; Volosskiy, B.; Demir, S.; Gándara, F.; McGrier, P. L.; Furukawa, H.; Cascio, D.; Stoddart, J. F.; Yaghi, O. M., Synthesis, Structure, and Metalation of Two New Highly Porous Zirconium Metal–Organic Frameworks. *Inorg. Chem.* **2012,** *51* (12), 6443-6445.

51. Feng, D.; Jiang, H.-L.; Chen, Y.-P.; Gu, Z.-Y.; Wei, Z.; Zhou, H.-C., Metal–Organic Frameworks Based on Previously Unknown Zr8/Hf8 Cubic Clusters. *Inorg. Chem.* **2013,** *52* (21), 12661-12667.

52. Valenzano, L.; Civalleri, B.; Chavan, S.; Bordiga, S.; Nilsen, M. H.; Jakobsen, S.; Lillerud, K. P.; Lamberti, C., Disclosing the Complex Structure of UiO-66 Metal Organic Framework: A Synergic Combination of Experiment and Theory. *Chem. Mater.* **2011,** *23* (7), 1700-1718.

53. Delgado Friedrichs, O.; O'Keeffe, M.; Yaghi, O. M., Three-periodic nets and tilings: semiregular nets. *Acta Crystallogr. A* **2003,** *59* (6), 515-525.

54. Wu, H.; Chua, Y. S.; Krungleviciute, V.; Tyagi, M.; Chen, P.; Yildirim, T.; Zhou, W., Unusual and Highly Tunable Missing-Linker Defects in Zirconium Metal–Organic Framework UiO-66 and Their Important Effects on Gas Adsorption. *J. Am. Chem. Soc* **2013,** *135* (28), 10525-10532.

55. Cliffe, M. J.; Wan, W.; Zou, X.; Chater, P. A.; Kleppe, A. K.; Tucker, M. G.; Wilhelm, H.; Funnell, N. P.; Coudert, F.-X.; Goodwin, A. L., Correlated defect nanoregions in a metal–organic framework. *Nat. Commun.* **2014,** *5*.

56. Shearer, G. C.; Chavan, S.; Ethiraj, J.; Vitillo, J. G.; Svelle, S.; Olsbye, U.; Lamberti, C.; Bordiga, S.; Lillerud, K. P., Tuned to Perfection: Ironing Out the Defects in Metal–Organic Framework UiO-66. *Chem. Mater.* **2014,** *26* (14), 4068-4071.

57. Stich, M. I. J.; Fischer, L. H.; Wolfbeis, O. S., Multiple fluorescent chemical sensing and imaging. *Chem. Soc. Rev.* **2010,** *39* (8), 3102-3114.

58. Wolf, C.; Bentley, K. W., Chirality sensing using stereodynamic probes with distinct electronic circular dichroism output. *Chem. Soc. Rev.* **2013,** *42* (12), 5408-5424.

59. Ding, Y.; Tang, Y.; Zhu, W.; Xie, Y., Fluorescent and colorimetric ion probes based on conjugated oligopyrroles. *Chem. Soc. Rev.* **2015,** *44* (5), 1101-1112.

60. Gust, D.; Moore, T. A.; Moore, A. L., Solar Fuels via Artificial Photosynthesis. *Acc. Chem. Res.* **2009,** *42* (12), 1890-1898.

61. Imahori, H.; Umeyama, T.; Ito, S., Large π-Aromatic Molecules as Potential Sensitizers for Highly Efficient Dye-Sensitized Solar Cells. *Acc. Chem. Res.* **2009,** *42* (11), 1809-1818.

62. Li, L.-L.; Diau, E. W.-G., Porphyrin-sensitized solar cells. *Chem. Soc. Rev.* **2013,** *42* (1), 291-304.

63. Urbani, M.; Grätzel, M.; Nazeeruddin, M. K.; Torres, T., Meso-Substituted Porphyrins for Dye-Sensitized Solar Cells. *Chem. Rev.* **2014,** *114* (24), 12330-12396.

64. Astruc, D., Electron-transfer processes in dendrimers and their implication in biology, catalysis, sensing and nanotechnology. *Nat. Chem.* **2012,** *4* (4), 255-267.

65. Wei, H.; Wang, E., Nanomaterials with enzyme-like characteristics (nanozymes): next-generation artificial enzymes. *Chem. Soc. Rev.* **2013,** *42* (14), 6060-6093.

66. Zhao, M.; Ou, S.; Wu, C.-D., Porous Metal–Organic Frameworks for Heterogeneous Biomimetic Catalysis. *Acc. Chem. Res.* **2014,** *47* (4), 1199-1207.

67. Bonnett, R., Photosensitizers of the porphyrin and phthalocyanine series for photodynamic therapy. *Chem. Soc. Rev.* **1995,** *24* (1), 19-33.

68. Ethirajan, M.; Chen, Y.; Joshi, P.; Pandey, R. K., The role of porphyrin chemistry in tumor imaging and photodynamic therapy. *Chem. Soc. Rev.* **2011,** *40* (1), 340-362.

69. Auwarter, W.; Ecija, D.; Klappenberger, F.; Barth, J. V., Porphyrins at interfaces. *Nat. Chem.* **2015,** *7* (2), 105-120.

70. Son, H.-J.; Jin, S.; Patwardhan, S.; Wezenberg, S. J.; Jeong, N. C.; So, M.; Wilmer, C. E.; Sarjeant, A. A.; Schatz, G. C.; Snurr, R. Q.; Farha, O. K.; Wiederrecht, G. P.; Hupp, J. T., Light-Harvesting and Ultrafast Energy Migration in Porphyrin-Based Metal–Organic Frameworks. *J. Am. Chem. Soc* **2013,** *135* (2), 862-869.

71. Xie, M.-H.; Yang, X.-L.; He, Y.; Zhang, J.; Chen, B.; Wu, C.-D., Highly Efficient C H Oxidative Activation by a Porous MnIII–Porphyrin Metal–Organic Framework under Mild Conditions. *Chem. - Eur. J.* **2013,** *19* (42), 14316-14321.

72. Lu, K.; He, C.; Lin, W., Nanoscale Metal–Organic Framework for Highly Effective Photodynamic Therapy of Resistant Head and Neck Cancer. *J. Am. Chem. Soc* **2014,** *136* (48), 16712-16715.

73. Feng, D.; Gu, Z.-Y.; Li, J.-R.; Jiang, H.-L.; Wei, Z.; Zhou, H.-C., Zirconium-Metalloporphyrin PCN-222: Mesoporous Metal–Organic Frameworks with Ultrahigh Stability as Biomimetic Catalysts. *Angew. Chem. Int. Ed.* **2012,** *51* (41), 10307-10310.

74. Kim, M.; Cahill, J. F.; Su, Y.; Prather, K. A.; Cohen, S. M., Postsynthetic ligand exchange as a route to functionalization of 'inert' metal-organic frameworks. *Chem. Sci.* **2012,** *3* (1), 126-130.

75. Trickett, C. A.; Gagnon, K. J.; Lee, S.; Gándara, F.; Bürgi, H.-B.; Yaghi, O. M., Definitive Molecular Level Characterization of Defects in UiO-66 Crystals. *Angew. Chem. Int. Ed.* **2015,** *54* (38), 11162-11167.

76. Cohen, S. M., Postsynthetic Methods for the Functionalization of Metal–Organic Frameworks. *Chem. Rev.* **2012,** *112* (2), 970-1000.

77. Millward, A. R.; Yaghi, O. M., Metal−Organic Frameworks with Exceptionally High Capacity for Storage of Carbon Dioxide at Room Temperature. *J. Am. Chem. Soc* **2005,** *127* (51), 17998-17999.

78. Arstad, B.; Fjellvåg, H.; Kongshaug, K.; Swang, O.; Blom, R., Amine functionalised metal organic frameworks (MOFs) as adsorbents for carbon dioxide. *Adsorption* **2008,** *14* (6), 755-762.

79. Banerjee, R.; Furukawa, H.; Britt, D.; Knobler, C.; O'Keeffe, M.; Yaghi, O. M., Control of Pore Size and Functionality in Isoreticular Zeolitic Imidazolate Frameworks and their Carbon Dioxide Selective Capture Properties. *J. Am. Chem. Soc* **2009,** *131* (11), 3875-3877.

80. Couck, S.; Denayer, J. F. M.; Baron, G. V.; Rémy, T.; Gascon, J.; Kapteijn, F., An Amine-Functionalized MIL-53 Metal−Organic Framework with Large Separation Power for CO2 and CH4. *J. Am. Chem. Soc* **2009,** *131* (18), 6326-6327.

81. An, J.; Geib, S. J.; Rosi, N. L., High and Selective CO2 Uptake in a Cobalt Adeninate Metal−Organic Framework Exhibiting Pyrimidine- and Amino-Decorated Pores. *J. Am. Chem. Soc* **2010,** *132* (1), 38-39.

82. Si, X.; Jiao, C.; Li, F.; Zhang, J.; Wang, S.; Liu, S.; Li, Z.; Sun, L.; Xu, F.; Gabelica, Z.; Schick, C., High and selective CO2 uptake, H2storage and methanol sensing on the amine-decorated 12-connected MOF CAU-1. *Energy Environ. Sci.* **2011,** *4* (11), 4522-4527.

83. Gascon, J.; Aktay, U.; Hernandez-Alonso, M. D.; van Klink, G. P. M.; Kapteijn, F., Amino-based metal-organic frameworks as stable, highly active basic catalysts. *J. Catal.* **2009,** *261* (1), 75-87.

84. Garibay, S. J.; Cohen, S. M., Isoreticular synthesis and modification of frameworks with the UiO-66 topology. *Chem. Commun.* **2010,** *46* (41), 7700-7702.

85. Savonnet, M.; Bazer-Bachi, D.; Bats, N.; Perez-Pellitero, J.; Jeanneau, E.; Lecocq, V.; Pinel, C.; Farrusseng, D., Generic Postfunctionalization Route from Amino-Derived Metal−Organic Frameworks. *J. Am. Chem. Soc* **2010,** *132* (13), 4518-4519.

86. Yujia, S.; Hong-Cai, Z., Recent progress in the synthesis of metal–organic frameworks. *Science and Technology of Advanced Materials* **2015,** *16* (5), 054202.

87. Ferey, G., Hybrid porous solids: past, present, future. *Chem. Soc. Rev.* **2008,** *37* (1), 191-214.

88. Yaghi, O. M.; O'Keeffe, M.; Ockwig, N. W.; Chae, H. K.; Eddaoudi, M.; Kim, J., Reticular synthesis and the design of new materials. *Nature* **2003,** *423*, 705.

89. Ockwig, N. W.; Delgado-Friedrichs, O.; O'Keeffe, M.; Yaghi, O. M., Reticular Chemistry: Occurrence and Taxonomy of Nets and Grammar for the Design of Frameworks. *Acc. Chem. Res.* **2005,** *38* (3), 176-182.

90. Furukawa, H.; Kim, J.; Ockwig, N. W.; O'Keeffe, M.; Yaghi, O. M., Control of Vertex Geometry, Structure Dimensionality, Functionality, and Pore Metrics in the Reticular Synthesis of Crystalline Metal−Organic Frameworks and Polyhedra. *J. Am. Chem. Soc* **2008,** *130* (35), 11650-11661.

91. O'Keeffe, M., Design of MOFs and intellectual content in reticular chemistry: a personal view. *Chem. Soc. Rev.* **2009,** *38* (5), 1215-1217.

92. Schaate, A.; Dühnen, S.; Platz, G.; Lilienthal, S.; Schneider, A. M.; Behrens, P., A Novel Zr ‐ Based Porous Coordination Polymer Containing Azobenzenedicarboxylate as a Linker. *Eur. J. Inorg. Chem.* **2012,** *2012* (5), 790-796.

93. Katz, M. J.; Brown, Z. J.; Colon, Y. J.; Siu, P. W.; Scheidt, K. A.; Snurr, R. Q.; Hupp, J. T.; Farha, O. K., A facile synthesis of UiO-66, UiO-67 and their derivatives. *Chem. Commun.* **2013,** *49* (82), 9449-9451.

94. Bon, V.; Senkovska, I.; Weiss, M. S.; Kaskel, S., Tailoring of network dimensionality and porosity adjustment in Zr- and Hf-based MOFs. *CrystEngComm* **2013,** *15* (45), 9572-9577.

95. Lv, X.-L.; Tong, M.; Huang, H.; Wang, B.; Gan, L.; Yang, Q.; Zhong, C.; Li, J.-R., A high surface area Zr(IV)-based metal–organic framework showing stepwise gas adsorption and selective dye uptake. *J. Solid State Chem.* **2015,** *223*, 104-108.

96. Marshall, R. J.; Griffin, S. L.; Wilson, C.; Forgan, R. S., Single-Crystal to Single-Crystal Mechanical Contraction of Metal–Organic Frameworks through Stereoselective Postsynthetic Bromination. *J. Am. Chem. Soc* **2015,** *137* (30), 9527-9530.

97. Zhao, J. S.; Wang, J. H.; He, W. B.; Ruan, Y. B.; Jiang, Y. B., Isolable Chiral Aggregates of Achiral π - Conjugated Carboxylic Acids. *Chem. - Eur. J.* **2012,** *18* (12), 3631-3636.

98. Tranchemontagne, D. J.; Park, K. S.; Furukawa, H.; Eckert, J.; Knobler, C. B.; Yaghi, O. M., Hydrogen Storage in New Metal–Organic Frameworks. *J. Phys. Chem. C* **2012,** *116* (24), 13143-13151.

99. Jiang, H.-L.; Feng, D.; Liu, T.-F.; Li, J.-R.; Zhou, H.-C., Pore Surface Engineering with Controlled Loadings of Functional Groups via Click Chemistry in Highly Stable Metal–Organic Frameworks. *J. Am. Chem. Soc* **2012,** *134* (36), 14690-14693.

100. Blöchl, P. E., Projector augmented-wave method. *Phys. Rev. B* **1994,** *50* (24), 17953-17979.

101. Kresse, G.; Furthmüller, J., Efficiency of ab-initio total energy calculations for metals and semiconductors using a plane-wave basis set. *Comput. Mater. Sci.* **1996,** *6* (1), 15-50.

102. Kresse, G.; Furthmüller, J., Efficient iterative schemes for ab initio total-energy calculations using a plane-wave basis set. *Phys. Rev. B* **1996,** *54* (16), 11169-11186.

103. Kresse, G.; Joubert, D., From ultrasoft pseudopotentials to the projector augmented-wave method. *Phys. Rev. B* **1999,** *59* (3), 1758-1775.

104. Perdew, J. P.; Burke, K.; Ernzerhof, M., Generalized Gradient Approximation Made Simple. *Phys. Rev. Lett.* **1996,** *77* (18), 3865-3868.

105. Wu, H.; Yildirim, T.; Zhou, W., Exceptional Mechanical Stability of Highly Porous Zirconium Metal–Organic Framework UiO-66 and Its Important Implications. *The Journal of Physical Chemistry Letters* **2013,** *4* (6), 925-930.

106. Yang, L.-M.; Ganz, E.; Svelle, S.; Tilset, M., Computational exploration of newly synthesized zirconium metal-organic frameworks UiO-66, -67, -68 and analogues. *J. Mater. Chem. C* **2014,** *2* (34), 7111-7125.

107. Øien, S.; Wragg, D.; Reinsch, H.; Svelle, S.; Bordiga, S.; Lamberti, C.; Lillerud, K. P., Detailed Structure Analysis of Atomic Positions and Defects in Zirconium Metal–Organic Frameworks. *Cryst. Growth Des.* **2014,** *14* (11), 5370-5372.

108. Yang, Q.; Guillerm, V.; Ragon, F.; Wiersum, A. D.; Llewellyn, P. L.; Zhong, C.; Devic, T.; Serre, C.; Maurin, G., CH4 storage and CO2 capture in highly

porous zirconium oxide based metal-organic frameworks. *Chem. Commun.* **2012,** *48* (79), 9831-9833.

109. Kandiah, M.; Usseglio, S.; Svelle, S.; Olsbye, U.; Lillerud, K. P.; Tilset, M., Post-synthetic modification of the metal-organic framework compound UiO-66. *J. Mater. Chem.* **2010,** *20* (44), 9848-9851.

110. Evans, J. D.; Sumby, C. J.; Doonan, C. J., Post-synthetic metalation of metal-organic frameworks. *Chem. Soc. Rev.* **2014,** *43* (16), 5933-5951.

111. Marshall, R. J.; Forgan, R. S., Postsynthetic Modification of Zirconium Metal‐Organic Frameworks. *Eur. J. Inorg. Chem.* **2016,** *2016* (27), 4310-4331.

112. Zhao, X.; Bu, X.; Zhai, Q.-G.; Tran, H.; Feng, P., Pore Space Partition by Symmetry-Matching Regulated Ligand Insertion and Dramatic Tuning on Carbon Dioxide Uptake. *J. Am. Chem. Soc* **2015,** *137* (4), 1396-1399.

113. Deria, P.; Gómez-Gualdrón, D. A.; Hod, I.; Snurr, R. Q.; Hupp, J. T.; Farha, O. K., Framework-Topology-Dependent Catalytic Activity of Zirconium-Based (Porphinato)zinc(II) MOFs. *J. Am. Chem. Soc* **2016,** *138* (43), 14449-14457.

114. Diercks, C. S.; Liu, Y.; Cordova, K. E.; Yaghi, O. M., The role of reticular chemistry in the design of CO2 reduction catalysts. *Nat. Mater.* **2018,** *17* (4), 301-307.

115. Li, P.; Modica, J.; Howarth, A.; Vargas, E.; Moghadam, P.; Snurr, R.; Mrksich, M.; Hupp, J.; Farha, O., Toward Design Rules for Enzyme Immobilization in Hierarchical Mesoporous Metal-Organic Frameworks. *Chem* **2016,** *1* (1), 154-169.

116. Furukawa, H.; Gándara, F.; Zhang, Y.-B.; Jiang, J.; Queen, W. L.; Hudson, M. R.; Yaghi, O. M., Water Adsorption in Porous Metal–Organic Frameworks and Related Materials. *J. Am. Chem. Soc* **2014,** *136* (11), 4369-4381.

117. Jiang, J.; Gándara, F.; Zhang, Y.-B.; Na, K.; Yaghi, O. M.; Klemperer, W. G., Superacidity in Sulfated Metal–Organic Framework-808. *J. Am. Chem. Soc* **2014,** *136* (37), 12844-12847.

118. Deria, P.; Mondloch, J. E.; Tylianakis, E.; Ghosh, P.; Bury, W.; Snurr, R. Q.; Hupp, J. T.; Farha, O. K., Perfluoroalkane Functionalization of NU-1000 via Solvent-Assisted Ligand Incorporation: Synthesis and CO2 Adsorption Studies. *J. Am. Chem. Soc* **2013,** *135* (45), 16801-16804.

119. Mondloch, J. E.; Katz, M. J.; Isley Iii, W. C.; Ghosh, P.; Liao, P.; Bury, W.; Wagner, G. W.; Hall, M. G.; DeCoste, J. B.; Peterson, G. W.; Snurr, R. Q.; Cramer, C. J.; Hupp, J. T.; Farha, O. K., Destruction of chemical warfare agents using metal–organic frameworks. *Nat. Mater.* **2015,** *14*, 512.

120. Bobbitt, N. S.; Mendonca, M. L.; Howarth, A. J.; Islamoglu, T.; Hupp, J. T.; Farha, O. K.; Snurr, R. Q., Metal-organic frameworks for the removal of toxic industrial chemicals and chemical warfare agents. *Chem. Soc. Rev.* **2017,** *46* (11), 3357-3385.

121. Mondloch, J. E.; Bury, W.; Fairen-Jimenez, D.; Kwon, S.; DeMarco, E. J.; Weston, M. H.; Sarjeant, A. A.; Nguyen, S. T.; Stair, P. C.; Snurr, R. Q.; Farha, O. K.; Hupp, J. T., Vapor-Phase Metalation by Atomic Layer Deposition in a Metal–Organic Framework. *J. Am. Chem. Soc* **2013,** *135* (28), 10294-10297.

122. Wei, Z.; Gu, Z.-Y.; Arvapally, R. K.; Chen, Y.-P.; McDougald, R. N.; Ivy, J. F.; Yakovenko, A. A.; Feng, D.; Omary, M. A.; Zhou, H.-C., Rigidifying Fluorescent Linkers by Metal–Organic Framework Formation for Fluorescence Blue Shift and Quantum Yield Enhancement. *J. Am. Chem. Soc* **2014,** *136* (23), 8269-8276.

123. Zhang, Q.; Su, J.; Feng, D.; Wei, Z.; Zou, X.; Zhou, H.-C., Piezofluorochromic Metal–Organic Framework: A Microscissor Lift. *J. Am. Chem. Soc* **2015,** *137* (32), 10064-10067.

124. Ibarra, I. A.; Bayliss, P. A.; Perez, E.; Yang, S.; Blake, A. J.; Nowell, H.; Allan, D. R.; Poliakoff, M.; Schroder, M., Near-critical water, a cleaner solvent for the synthesis of a metal-organic framework. *Green Chem.* **2012,** *14* (1), 117-122.

125. Lin, S.; Diercks, C. S.; Zhang, Y.-B.; Kornienko, N.; Nichols, E. M.; Zhao, Y.; Paris, A. R.; Kim, D.; Yang, P.; Yaghi, O. M.; Chang, C. J., Covalent organic frameworks comprising cobalt porphyrins for catalytic CO_2 reduction in water. *Science* **2015,** *349* (6253), 1208-1213.

126. Kornienko, N.; Zhao, Y.; Kley, C. S.; Zhu, C.; Kim, D.; Lin, S.; Chang, C. J.; Yaghi, O. M.; Yang, P., Metal–Organic Frameworks for Electrocatalytic Reduction of Carbon Dioxide. *J. Am. Chem. Soc* **2015,** *137* (44), 14129-14135.

127. Xu, H.-Q.; Hu, J.; Wang, D.; Li, Z.; Zhang, Q.; Luo, Y.; Yu, S.-H.; Jiang, H.-L., Visible-Light Photoreduction of CO2 in a Metal–Organic Framework: Boosting Electron–Hole Separation via Electron Trap States. *J. Am. Chem. Soc* **2015,** *137* (42), 13440-13443.

128. Zhang, H.; Wei, J.; Dong, J.; Liu, G.; Shi, L.; An, P.; Zhao, G.; Kong, J.; Wang, X.; Meng, X.; Zhang, J.; Ye, J., Efficient Visible‐Light‐Driven Carbon Dioxide Reduction by a Single‐Atom Implanted Metal–Organic Framework. *Angew. Chem. Int. Ed.* **2016,** *55* (46), 14310-14314.

129. Farha, O. K.; Shultz, A. M.; Sarjeant, A. A.; Nguyen, S. T.; Hupp, J. T., Active-Site-Accessible, Porphyrinic Metal−Organic Framework Materials. *J. Am. Chem. Soc.* **2011,** *133* (15), 5652-5655.

130. Kim, M.; Cohen, S. M., Discovery, development, and functionalization of Zr(iv)-based metal-organic frameworks. *CrystEngComm* **2012,** *14* (12), 4096-4104.

131. Du, M.; Li, C.-P.; Liu, C.-S.; Fang, S.-M., Design and construction of coordination polymers with mixed-ligand synthetic strategy. *Coord. Chem. Rev.* **2013,** *257* (7), 1282-1305.

132. Hu, Z.; Zhao, D., De facto methodologies toward the synthesis and scale-up production of UiO-66-type metal-organic frameworks and membrane materials. *Dalton Trans.* **2015,** *44* (44), 19018-19040.

133. Lee, Y.; Kim, S.; Kang, J. K.; Cohen, S. M., Photocatalytic CO2 reduction by a mixed metal (Zr/Ti), mixed ligand metal-organic framework under visible light irradiation. *Chem. Commun.* **2015,** *51* (26), 5735-5738.

134. Kong, X.; Deng, H.; Yan, F.; Kim, J.; Swisher, J. A.; Smit, B.; Yaghi, O. M.; Reimer, J. A., Mapping of Functional Groups in Metal-Organic Frameworks. *Science* **2013**.

135. Ma, B.-Q.; Mulfort, K. L.; Hupp, J. T., Microporous Pillared Paddle-Wheel Frameworks Based on Mixed-Ligand Coordination of Zinc Ions. *Inorg. Chem.* **2005,** *44* (14), 4912-4914.

136. Bae, Y.-S.; Mulfort, K. L.; Frost, H.; Ryan, P.; Punnathanam, S.; Broadbelt, L. J.; Hupp, J. T.; Snurr, R. Q., Separation of CO2 from CH4 Using Mixed-Ligand Metal−Organic Frameworks. *Langmuir* **2008,** *24* (16), 8592-8598.

137. Shultz, A. M.; Farha, O. K.; Hupp, J. T.; Nguyen, S. T., A Catalytically Active, Permanently Microporous MOF with Metalloporphyrin Struts. *J. Am. Chem. Soc* **2009,** *131* (12), 4204-4205.

138. Eubank, J. F.; Wojtas, L.; Hight, M. R.; Bousquet, T.; Kravtsov, V. C.; Eddaoudi, M., The Next Chapter in MOF Pillaring Strategies: Trigonal Heterofunctional Ligands To Access Targeted High-Connected Three Dimensional Nets, Isoreticular Platforms. *J. Am. Chem. Soc* **2011,** *133* (44), 17532-17535.

139. Wang, H.-N.; Meng, X.; Qin, C.; Wang, X.-L.; Yang, G.-S.; Su, Z.-M., A series of pillar-layer metal-organic frameworks based on 5-aminoisophthalic acid and 4,4[prime or minute]-bipyridine. *Dalton Trans.* **2012,** *41* (3), 1047-1053.

140. Zhao, X.-L.; Sun, W.-Y., The organic ligands with mixed N-/O-donors used in construction of functional metal-organic frameworks. *CrystEngComm* **2014,** *16* (16), 3247-3258.

141. Chen, D.-M.; Xu, N.; Qiu, X.-H.; Cheng, P., Functionalization of Metal–Organic Framework via Mixed-Ligand Strategy for Selective CO2 Sorption at Ambient Conditions. *Cryst. Growth Des.* **2015,** *15* (2), 961-965.

142. Huh, S.; Kim, S.-J.; Kim, Y., Porphyrinic metal-organic frameworks from custom-designed porphyrins. *CrystEngComm* **2016,** *18* (3), 345-368.

143. Xuan, Z.-H.; Zhang, D.-S.; Chang, Z.; Hu, T.-L.; Bu, X.-H., Targeted Structure Modulation of "Pillar-Layered" Metal–Organic Frameworks for CO2 Capture. *Inorg. Chem.* **2014,** *53* (17), 8985-8990.

144. Wang, T. C.; Bury, W.; Gómez-Gualdrón, D. A.; Vermeulen, N. A.; Mondloch, J. E.; Deria, P.; Zhang, K.; Moghadam, P. Z.; Sarjeant, A. A.; Snurr, R. Q.; Stoddart, J. F.; Hupp, J. T.; Farha, O. K., Ultrahigh Surface Area Zirconium MOFs and Insights into the Applicability of the BET Theory. *J. Am. Chem. Soc* **2015,** *137* (10), 3585-3591.

145. Fei, H.; Cohen, S. M., Metalation of a Thiocatechol-Functionalized Zr(IV)-Based Metal–Organic Framework for Selective C–H Functionalization. *J. Am. Chem. Soc* **2015,** *137* (6), 2191-2194.

146. Bai, Y.; Dou, Y.; Xie, L.-H.; Rutledge, W.; Li, J.-R.; Zhou, H.-C., Zr-based metal-organic frameworks: design, synthesis, structure, and applications. *Chem. Soc. Rev.* **2016,** *45* (8), 2327-2367.

147. Kung, C.-W.; Wang, T. C.; Mondloch, J. E.; Fairen-Jimenez, D.; Gardner, D. M.; Bury, W.; Klingsporn, J. M.; Barnes, J. C.; Van Duyne, R.; Stoddart, J. F.; Wasielewski, M. R.; Farha, O. K.; Hupp, J. T., Metal–Organic Framework Thin Films Composed of Free-Standing Acicular Nanorods Exhibiting Reversible Electrochromism. *Chem. Mater.* **2013,** *25* (24), 5012-5017.

148. Feng, D.; Gu, Z.-Y.; Chen, Y.-P.; Park, J.; Wei, Z.; Sun, Y.; Bosch, M.; Yuan, S.; Zhou, H.-C., A Highly Stable Porphyrinic Zirconium Metal–Organic Framework with shp-a Topology. *J. Am. Chem. Soc* **2014,** *136* (51), 17714-17717.

149. Deria, P.; Bury, W.; Hupp, J. T.; Farha, O. K., Versatile functionalization of the NU-1000 platform by solvent-assisted ligand incorporation. *Chem. Commun.* **2014,** *50* (16), 1965-1968.

150. Webber, T. E.; Liu, W.-G.; Desai, S. P.; Lu, C. C.; Truhlar, D. G.; Penn, R. L., Role of a Modulator in the Synthesis of Phase-Pure NU-1000. *ACS Applied Materials & Interfaces* **2017,** *9* (45), 39342-39346.

151. Bon, V.; Senkovska, I.; Baburin, I. A.; Kaskel, S., Zr- and Hf-Based Metal–Organic Frameworks: Tracking Down the Polymorphism. *Cryst. Growth Des.* **2013,** *13* (3), 1231-1237.

152. Cliffe, M. J.; Hill, J. A.; Murray, C. A.; Coudert, F.-X.; Goodwin, A. L., Defect-dependent colossal negative thermal expansion in UiO-66(Hf) metal-organic framework. *Phys. Chem. Chem. Phys.* **2015,** *17* (17), 11586-11592.

153. Beyzavi, M. H.; Vermeulen, N. A.; Howarth, A. J.; Tussupbayev, S.; League, A. B.; Schweitzer, N. M.; Gallagher, J. R.; Platero-Prats, A. E.; Hafezi, N.; Sarjeant, A. A.; Miller, J. T.; Chapman, K. W.; Stoddart, J. F.; Cramer, C. J.; Hupp, J. T.; Farha, O. K., A Hafnium-Based Metal–Organic Framework as a Nature-Inspired Tandem Reaction Catalyst. *J. Am. Chem. Soc* **2015,** *137* (42), 13624-13631.

154. Klet, R. C.; Tussupbayev, S.; Borycz, J.; Gallagher, J. R.; Stalzer, M. M.; Miller, J. T.; Gagliardi, L.; Hupp, J. T.; Marks, T. J.; Cramer, C. J.; Delferro, M.; Farha,

O. K., Single-Site Organozirconium Catalyst Embedded in a Metal–Organic Framework. *J. Am. Chem. Soc* **2015,** *137* (50), 15680-15683.

155. Nasalevich, M. A.; Hendon, C. H.; Santaclara, J. G.; Svane, K.; van der Linden, B.; Veber, S. L.; Fedin, M. V.; Houtepen, A. J.; van der Veen, M. A.; Kapteijn, F.; Walsh, A.; Gascon, J., Electronic origins of photocatalytic activity in d0 metal organic frameworks. *Sci. Rep.* **2016,** *6*, 23676.

156. Hu, Z.; Mahdi, E. M.; Peng, Y.; Qian, Y.; Zhang, B.; Yan, N.; Yuan, D.; Tan, J.-C.; Zhao, D., Kinetically controlled synthesis of two-dimensional Zr/Hf metal-organic framework nanosheets via a modulated hydrothermal approach. *J. Mater. Chem. A* **2017,** *5* (19), 8954-8963.

157. Nguyen, L. H. T.; Nguyen, T. T.; Nguyen, H. L.; Doan, T. L. H.; Tran, P. H., A new superacid hafnium-based metal-organic framework as a highly active heterogeneous catalyst for the synthesis of benzoxazoles under solvent-free conditions. *Catal. Sci. Technol.* **2017,** *7* (19), 4346-4350.

158. McGonigal, P. R.; Deria, P.; Hod, I.; Moghadam, P. Z.; Avestro, A.-J.; Horwitz, N. E.; Gibbs-Hall, I. C.; Blackburn, A. K.; Chen, D.; Botros, Y. Y.; Wasielewski, M. R.; Snurr, R. Q.; Hupp, J. T.; Farha, O. K.; Stoddart, J. F., Electrochemically addressable trisradical rotaxanes organized within a metal–organic framework. *Proc. Natl. Acad. Sci.* **2015,** *112* (36), 11161-11168.

159. Deria, P.; Chung, Y. G.; Snurr, R. Q.; Hupp, J. T.; Farha, O. K., Water stabilization of Zr6-based metal-organic frameworks via solvent-assisted ligand incorporation. *Chem. Sci.* **2015,** *6* (9), 5172-5176.

160. Hod, I.; Farha, O. K.; Hupp, J. T., Modulating the rate of charge transport in a metal-organic framework thin film using host:guest chemistry. *Chem. Commun.* **2016,** *52* (8), 1705-1708.

161. Rimoldi, M.; Howarth, A. J.; DeStefano, M. R.; Lin, L.; Goswami, S.; Li, P.; Hupp, J. T.; Farha, O. K., Catalytic Zirconium/Hafnium-Based Metal–Organic Frameworks. *ACS Catalysis* **2017,** *7* (2), 997-1014.